Wissenschaftszentrum Weihenstephan für Ernährung, Landnutzung und Umwelt

Fachgebiet für Peptidbiochemie

**Synthesis and study of conformationally constrained peptides
as inhibitors of amyloid self-assembly**

Anna Spanopoulou

Vollständiger Abdruck der von der Fakultät Wissenschaftszentrum Weihenstephan, für Ernährung, Landnutzung und Umwelt der Technischen Universität München zur Erlangung des akademischen Grades eines
        Doktors der Naturwissenschaften (Dr.rer.nat.)
genehmigten Dissertation.

Vorsitzende: Prof. Dr. Iris Antes

Prüfer der Dissertation: 1. Prof. Dr. Aphrodite Kapurniotu
                            2. Prof. Dr. Dr.h.c. Horst Kessler

Die Dissertation wurde am 18.01.2019 bei der Technischen Universität München eingereicht und durch die Fakultät Wissenschaftszentrum Weihenstephan für Ernährung, Landnutzung und Umwelt am.07.06.2019 angenommen.

Abstract

Protein aggregation is linked to many cell degenerative diseases such as Alzheimer's disease (AD) and type 2 diabetes (T2D). AD is associated with the self-assembly of the 40-42 residue β-amyloid peptide (Aβ) whereas T2D is linked to the aggregation of the 37-residue long islet amyloid polypeptide (IAPP). Both polypeptides Aβ and IAPP share in addition to their amyloidogenicity 50% of sequence similarity. It has been previously shown that non-fibrillar and non-toxic Aβ and IAPP species bind to each other with low nanomolar affinity and that Aβ-IAPP hetero-association suppresses cytotoxic self-association and amyloidogenesis by both peptides. In addition, clinical and pathophysiological studies suggest that the two diseases AD and T2D might be linked to each other.

Earlier work has identified IAPP segments IAPP(8-18) and IAPP(22-28) as "hot segments" in both IAPP self- and its cross-interaction with Aβ. More recently, these segments were linked to each via different linkers and a series of linear IAPP-derived peptides were synthesized. These peptides, termed cross-amyloid interaction surface mimics (ISMs), have been shown to be potent inhibitors of amyloid self-assembly of Aβ, IAPP, or both polypeptides. Notably, the nature of the linker has been shown to determine ISM structure and inhibitory function, including both potency and target (Aβ versus IAPP) selectivity.

In the first part of the thesis, three cyclic analogues of R3-GI (1), one of the above mentioned ISMs which is a potent inhibitor of amyloid self-assembly of Aβ, were synthesized and studied. These peptides comprised the Cys-bridged cc-R3-GI (1a) and the two "Cys-stapled" (via aromatic linker moieties) peptides cc-L1-R3-GI and cc-L2-R3-GI. The aim was to find out whether cyclization would be (a) compatible with inhibitor function and (b) confer stability toward proteolytic degradation in human plasma. In fact, all three peptides were found to be nanomolar inhibitors of amyloid self-assembly of both Aβ and IAPP. Thus, cyclization via Cys-bridges and "Cys-stapling" likely stabilized a peptide conformation which is important for amyloid inhibitor function. However, only slight improvements were observed regarding the resistance of all three cyclic analogues toward proteolytic degradation in human plasma as compared to the linear precursor.

In the second part of the thesis, cyclization via flanking cysteines of N-terminal truncated analogues of the three ISMs L3-GI, R3-GI and G3-GI was first performed; its effects on their structures and inhibitory effects were studied. The cyclic 17-residue long cc-R3-GIsh (2a) containing three Arg residues in the linker tripeptide was thus identified. 2a was a nanomolar inhibitor of amyloid self-assembly of both Aβ and IAPP; by contrast, its linear precursor was unable to do so.

The cyclic cc-R3-GIsh (2a) was then used as a template for the development of a next generation of cyclic peptides. Their design was based on recent findings which suggested that IAPP residues F15, L16, F23 and I26 are key residues of IAPP self-assembly and its interaction with Aβ. The question was whether these four residues together with the linker tripeptide RRR and the cyclic structure via the two flanking cysteines would be sufficient for inhibitory activity. To investigate this hypothesis, all other amino acids of 2a were substituted with Gly resulting in cc-ALLG-R3-GIsh (2b). In fact, 2b turned out to be a nanomolar inhibitor of amyloid self-assembly of both Aβ and IAPP. In addition, six "2b-linker" analogues were also synthesized and studied; the results suggest that all three arginines of the linker tripeptide are required for inhibitory function.

Furthermore, detailed studies on the effects of systematic substitutions of L-amino acid residues in 2b with D-ones were performed. Toward this aim, the three cyclic 2b analogues cc-ALLG-r3-GI (2c), cc-ALLG-(f15,l16,f23)-r3-GIsh (2d), and cc-ALLD-ALLG-r3-GIsh (2e) were synthesized and studied. Here, the focus was on both inhibitory function and proteolytic stability. Analogue 2e was identified as a selective nanomolar inhibitor of Aβ amyloid self-assembly. Most importantly, 2e was found to exhibit a highly improved proteolytic stability in human plasma in comparison to other analogues being >30-

fold more resistant than R3-GI (1) and >15-fold more resistant than its L-precursor 2b. 2e is thus a promising candidate for further development as an anti-amyloid drug in AD.

In the third part of my thesis, I studied the effects of the previously developed ISMs on insulin amyloid self-assembly. These studies were done based on the facts that IAPP is able to bind insulin and inhibit its amyloidogenesis and that IAPP-GI, an earlier designed soluble IAPP analogue, is a potent inhibitor of amyloid self-assembly of insulin. My results show that all ISMs containing hydrophobic linkers can inhibit insulin oligomerization and amyloid self-assembly whereas all but two of the ISM$_S$ containing polar amino acids in the linker were unable to do so. Together with previous results, my studies on 14 different ISMs revealed the following amyloid inhibitor selectivities: L3-GI, Nle3-GI and Cha3-GI are able to inhibit all three polypeptides Aβ, IAPP and insulin; V3-GI, I3-GI and F3-GI inhibit Aβ and insulin but not IAPP, 2-Aoc3-GI inhibits IAPP and insulin but not Aβ, and KAc3-GI and SpG-GI inhibit only insulin while R3-GI inhibits only Aβ. Based on their selectivity profiles, some of these ISMs could be suitable leads for the design of anti-amyloid drugs in AD and/or T2D likely also in combination with insulin-based treatments.

Taken together, the results of my studies should contribute in both understanding how cross-interactions between different amyloidogenic polypeptides may affect amyloid self-assembly and the development of novel highly potent inhibitors of amyloid self-assembly of Aβ, IAPP and/or insulin as promising leads for anti-amyloid drugs in AD and/or T2D.

Zusammenfassung

Die Proteinaggregation wird mit zelldegenerativen Erkrankungen wie der Alzheimer-Krankheit (AD) und dem Typ-2-Diabetes (T2D) in Verbindung gebracht. AD ist mit der Selbstassoziation des β-Amyloid-Peptids (Aβ) assoziiert, während die Aggregation des Islet-Amyloid-Polypeptids (IAPP) T2D begünstigt. Die beiden Polypeptide Aβ und IAPP weisen zusätzlich zu ihrer ähnlichen Amyloidogenität 50% Sequenzähnlichkeit auf. Es wurde bereits gezeigt, dass nicht-fibrilläre und nicht-toxische Aβ- und IAPP-Spezies mit nanomolarer Affinität aneinanderbinden; dadurch wird die zytotoxische Selbstassoziation und die Amyloidogenese beider Peptide unterdrückt. Darüber hinaus deuten klinische und pathophysiologische Studien darauf hin, dass die beiden Erkrankungen AD und T2D im Zusammenhang stehen könnten.

Frühere Studien haben die IAPP-Segmente IAPP(8-18) und IAPP(22-28) als "Hot-Segmente", sowohl in der IAPP-Selbst-, als auch in seiner Kreuz-Interaktion mit Aβ, identifiziert. Vor kurzem wurden diese Segmente über verschiedene Linker miteinander verknüpft und eine Reihe von linearen, von IAPP abgeleiteten, Peptiden wurde entworfen. Es zeigte sich, dass diese Peptide, die auch als Cross-Amyloid-Interaktionsoberflächen-Mimetika (ISMs) bezeichnet werden, hochpotente Inhibitoren der Amyloid-Selbstassemblierung von Aβ, IAPP oder beiden Polypeptiden sind. Dabei bestimmt die Zusammensetzung des Linkers die ISM-Struktur, ihre inhibitorische Funktion und ihre Zielselektivität (Aβ versus IAPP).

Im ersten Teil der Arbeit wurden drei zyklische Analoga von R3-GI (1), einem der oben genannten ISMs, der ein potenter Inhibitor der amyloiden Selbstassoziation von Aβ ist, synthetisiert und untersucht. Diese Peptide bestehen aus dem Cys-verbrückten cc-R3-GI (1a) und den zwei „Cys-gestapelten" Analoga cc-L1-R3-GI und cc-L2-R3-GI. Letztere sind über aromatische Linker-Einheiten verbrückt. Ziel war es, herauszufinden, ob die Zyklisierung (a) mit der inhibitorischen Funktion kompatibel wäre, und (b) Stabilität gegenüber der Proteolyseanfälligkeit im humanen Plasma verleihen würde. Es stellte sich heraus, dass alle drei Peptide Inhibitoren im nanomolaren Konzentrationsbereich der amyloiden Selbstassoziation von sowohl Aβ als auch IAPP sind. Diese Ergebnisse deuten darauf hin, dass die Zyklisierung über eine Cys-Brücke und das "Cys-Stapeln" eine Peptidkonformation, stabilisiert hat, die für die Inhibitor-Funktion wichtig ist. Allerdings war die Proteolysestabilität der drei Analoga nicht stark verbessert im Vergleich zum linearen Vorläuferpeptid.

Im zweiten Teil der Arbeit wurden zunächst N-terminal verkürzte Analoga der drei ISMs L3-GI, R3-GI und G3-GI über flankierende Cysteine zyklisiert; die Analoga wurden dann im Bezug auf ihre Strukturen und die Amyloidinhibitor-Funktion untersucht. Das zyklische cc-R3-GIsh (2a), welches aus 17 Aminosäureresten besteht und drei Argininreste im Linker-Tripeptid enthält, wurde auf diese Weise identifiziert. Im Gegensatz zum linearen Vorläuferpeptid war 2a in der Tat ein hochpotenter Inhibitor der amyloiden Selbstassoziation von Aβ und IAPP.

Daher wurde cc-R3-GIsh (2a) als Templat für die Entwicklung der nächsten Generation von zyklischen Peptiden verwendet. Das Design dieser Peptide basierte auf dem Befund, dass die IAPP-Aminosäurereste F15, L16, F23 und I26 eine sehr wichtige Rolle bei der IAPP-Selbstassoziation und seiner Wechselwirkung mit Aβ spielen. Es wurde daher die Frage verfolgt, ob die obigen vier Aminosäuren, zusammen mit dem Linker-Tripeptid RRR und der über die beiden Cysteine zyklisierten Struktur vom 2a für die Amyloidinhibitor-Funktion ausreichend wären. Um diese Frage zu beantworten, wurden alle übrigen Aminosäuren in 2a durch Glycin ausgetauscht und das Analog cc-ALLG-R3-GIsh (2b) synthetisiert und untersucht. In der Tat erwies sich 2b als hochpotenter Inhibitor (im nanomolaren Konzentrationsbereich) der amyloiden Selbstassoziation von Aβ und IAPP. In addition, six "2b-linker" analogues were also synthesized and studied; the results suggest that all three arginines of the linker tripeptide are required for inhibitory function.

Darüber hinaus wurden noch sechs 2b-Linker Analoga synthetisiert und untersucht; die Ergebnisse deuten darauf hin, dass alle drei Arg-Reste für die amyloid inhibitorische Funktion von 2b notwendig sind.

Zum Schluß wurden detaillierte Untersuchungen zur Wirkung des Austausches von L- durch D-Aminosäuren im Analog 2b durchgeführt. Die drei 2b-Analoga cc-ALLG-r3-GIsh (2c), cc-ALLG-(f15,l16,f23)-r3-GIsh (2d), cc-ALLD-ALLG-r3-GIsh (2e) wurden synthetisiert und untersucht. Der Schwerpunkt lag auf sowohl ihrer Inhibitor-Funktion als auch ihrer proteolytischen Stabilität. Das Analog 2e wurde als ein hochpotenter und selektiver (Aβ versus IAPP) Inhibitor der amyloiden Selbstassoziation von Aβ identifiziert. Fernerhin weist 2e eine stark verbesserte proteolytische Stabilität auf; im Vergleich zu den anderen Peptiden ist 2e >30-mal Proteolyse-resistenter als R3-GI (1) und >15-mal stabiler als das aus L-Aminosäuren bestehende Vorläuferpeptid 2b. Obige Befunde deuten darauf hin, dass das zyklische Peptid 2e ein guter Kandidat für die Entwicklung von Anti-Amyloid-Molekülen für die Behandlung von AD sein könnte.

Im dritten Teil meiner Arbeit wurde die Wirkung der vorher entwickelten ISMs auf die amyloide Selbstassoziation von Insulin erforscht. Die hier durchgeführten Untersuchungen basierten auf vorherigen Befunden, die gezeigt hatten, dass IAPP Insulin binden und seine Fibrillogenese unterdrücken kann und dass IAPP-GI, ein lösliches IAPP-Analog, die Insulin-Amyloidogenese mit einer IC_{50} im nanomolaren Konzentrationsbereich inhibieren kann.

Die gewonnenen Ergebnisse zeigten, dass alle ISMs, die hydrophobe Linker-Tripeptide enthalten, die Insulinaggregation unterdrücken können, während, bis auf zwei Ausnahmen, solche ISMs, die polare Aminosäuren im Linker enthalten -, nicht in der Lage sind, die Insulinaggregation zu beeinflussen.

In Verbindung mit früheren Ergebnissen zeigen die Untersuchungen an 14 verschiedenen ISMs die folgenden Selektivitäten im Bezug auf ihre Amyloidinhibitor-Funktion gegenüber Aβ, IAPP und Insulin: L3-GI, Nle3-GI und Cha3-GI sind fähig, die amyloide Selbstassoziation aller drei Polypeptide zu hemmen; V3-GI, I3-GI und F3-GI inhibieren die Amyloidogenese von Aβ und Insulin, aber nicht die von IAPP; Aoc3-GI inhibiert die Amyloidogenese von IAPP und Insulin, aber nicht die von Aβ; KAc3-GI und SpG-GI inhibieren nur Insulin während R3-GI nur die Aβ-Amyloidogenese inhibiert. Auf Grund dieser „Target-Selektivitäten" könnten einige der ISMs Leitstrukturen für das Design von Anti-Amyloid-Molekülen werden, die bei der Behandlung von AD und/oder T2D (evt. auch zusammen mit Insulin) Anwendung finden könnten.

Insgesamt sollten die Ergebnisse dieser Dissertationsarbeit zur Aufklärung des molekularen Mechanismus der Wirkung von Kreuz-Amyloid-Wechselwirkungen auf die amyloide Selbstassemblierung beitragen und gleichzeitig dabei helfen, neue hochwirksame Inhibitoren der Selbstassemblierung von Aβ, IAPP und/oder Insulin als Leitstrukturen für Anti-Amyloid-Moleküle zu entwickeln. Diese könnten zukünftig bei der Behandlung von AD und/oder T2D Anwendung finden.

Abbreviations

α	Alpha
A	Absorbance
Å	Angstrom
AA	Aminoacid
Aβ	β-amyloid peptide
Aβ40	β-amyloid peptide (sequence [1-40])
Aβ42	β-amyloid peptide (sequence [1-42])
ACN	Acetonitrile
Ac_2O	Acetic anhydride
AD	Alzheimer's disease
AFM	Atomic force microscopy
APP	Amyloid precursor protein
β	Beta
BCA	Bicinchoninic acid
BSA	Bovine serum albumin
c	Concentration
CD	Circular dichroism
CR	Congo red
CSF	Cerebrospinal fluid
cISM(s)	"cyclic interaction surface mimics" peptides
cISM(s).sh	"cyclic N-terminally truncated interaction surface mimics" peptides
cALLG.sh	"cyclic N-terminally truncated with glycine substitution" peptides
Dac	7-Diethylaminocoumarine-3-carboxylic acid
DCM	Dichlormethane
DIC	Diisopropylcarbodiimide
DIEA	Diisopropylethylamine
DMF	Dimethylformamid
DMS	Dimethysulfide
DMSO	Dimethylsulfoxide
EDT	1,2-ethanedithiol
EDTA	Ethylenediaminetetraacetic acid
ER	Endoplasmic reticulum
Eq	Equivalent
FCS	Fetal calf serum
Fitc	Fluorescein isothiocyanate
Fluos	5(6)-Carboxyfluorescein
Fmoc	9-fluorenylmethoxycarbonyl
FTIR	Fourier transform infrared spectroscopy
Gdn-HCl	Guanidinium-HCl
h	hour
HCl	Hydrochloric acid
HFIP	1,1,1,3,3,3-Hexafluoro-2-propanol

HATU	2-(7-Aza-1H-benzotriazole-1-yl)-1,1,3,3-tetramethyluroniumhexafluorophosphate
HOBt	1-Hydroxybenzotriazole
H₂O₂	Hydrogen peroxide
IC₅₀	Half maximal inhibitory concentration
ISM(s)	"Interaction surface mimics" peptides
ISM(s).sh	"N-terminally truncated interaction surface mimics" peptides
IAPP	Islet amyloid polypeptide (human)
IAPP-GI	[(N-Me)G24, (N-Me)I26]-IAPP
IDE	Insulin-degrading enzyme
M	Molar
MALDI	Matrix-assisted laser desorption ionization mass spectrometry
mg	Milligram
min	Minutes
mM	Millimolar
ml	Milliliter
μg	Microgram
μM	Micromolar
μl	Microliter
MTT	3-(4,5-dimethylthiazol-2-yl)-2,5-diphenyltetrazolium bromide
MW	Molecular weight
nm	Nanometer
nM	Nanomolar
NMR	Nuclear magnetic resonance
NSAID's	Nonsteroidal anti-inflammatory drugs
OBt-ester	1-hydroxybenzotriazole ester
PC-12	Rat pheochromocytoma cell line
POD	Peroxidase
prg.	HPLC Program
rIAPP	Rat IAPP
RP-HPLC	Reverse phase high performance liquid chromatography
t_R	Retention time
t_{1/2}	Half life time
SD	Standard deviation
SPPS	Solid phase peptide synthesis
SDS	Sodium dodecyl sulfate
SS-NMR	Solid state nuclear magnetic resonance
TBS	Tris buffered saline
TBTU	N,N,N′,N′-Tetramethyl-O-(benzotriazol-1-yl)uronium tetrafluoroborate
tBu	tert-butyl
TEM	Transmission electron microscopy
TFA	Trifluoroacetic acid

ThT	Thioflavin T
TIS	Triisopropylsilan
Tris-HCl	2-Amino-2-(hydroxymethyl)-1,3-propanediol hydrochloride
Trt	Trityl
T2D	Type 2 diabetes
UV	Ultraviolet

Index

1.   Introduction

1.1   Protein aggregation and amyloid formation

The term amyloid was introduced in 1854 by the German physician Rudolph Virchow[1]. Amyloids are aggregates of a peptide or a protein which are mainly formed of β-structured fibrils. The denaturation of peptides (or proteins) and the formation of insoluble aggregates changes the properties of the peptide and affects its biological function. Misfolding and aggregation of peptides and proteins seems to be responsible for various chronic diseases. Neurodegenerative diseases such as Alzheimer's disease (AD), Parkinson's disease (PD) and Huntington's disease (HD) seem to have common cellular and molecular mechanisms including protein aggregation[2].

1.1.1   Cross β-sheet structure

Each amyloid disease involves predominately the aggregation of specific protein, although a range of other proteins and carbohydrates are incorporated into the deposits when they form *in vivo*. In neurodegenerative diseases the quantities of aggregates involved can sometimes be so small as to almost undetectable, whereas in some systemic diseases literally kilograms of proteins can be found in one or more organs[3]. The characteristics of the soluble forms of the 20 or so proteins involved in the well-defined amyloidosis varied from intact globular proteins to largely unstructured peptide molecules, but the aggregated forms have many characteristics in common. Amyloid deposits all show specific optical properties (such as birefringence) on binding certain dye molecules, notably Congo Red, these properties have been used in diagnosis for over a century. The fibrillar structures that are characteristic of many aggregates have similar morphology (long, unbranched and often twisted structures a few nm in diameters) and a characteristic "cross-beta" X-ray fiber diffraction pattern, that caused by the β-sheet motif when irradiated with X-rays[4]. The motif is composed of tightly interacting intermolecular β-sheets and each β-sheet comprises thousands of identical copies of the same β-strand that stack through hydrogen bonding. The backbone amide hydrogen bonds maintain the β-strands at a spacing of 4.8 Å in the direction of the fibril. Two or more such β-sheets lie in parallel 6-12 Å apart[5].
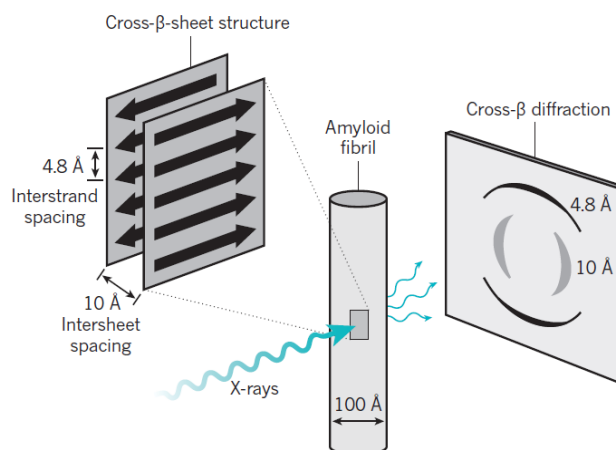
Figure 1. Amyloids are composed of an ordered, repetitive arrangement of many copies of a peptide or protein. The cross-β-sheet motif generates characteristic X-ray fiber diffraction patterns with a meridional reflection at about 4.8 Å, which corresponds to the spacing between β-strands, and a protein-dependent equatorial reflection at 6–12 Å, which corresponds to the distance between stacked β-sheets (picture taken from Riek et al. ref.[5]).

All amyloid-segment microcrystals show that the cross β-sheet motif is composed of two β-sheet structures with a steric-zipper chain interface. The various cross-β-sheet structures can be categorized according to several criteria: Whether their β-strands are parallel or antiparallel; whether their β-sheets pack with the same surfaces (face-to-face packing) or different surfaces (face-to-back packing) adjacent

to one another and whether the two closely packed β-sheets are oriented in the same direction (up-up) or opposite direction (up-down)[5].

1.1.2 Mechanism of amyloid formation

For aggregation to be initiated, the soluble amyloid proteins or peptides (blue coils) must be partially unfolded, misfolded or intrinsically disordered. Furthermore, several molecules must come together to form a nucleus (star like entity composed of several extended blue coils) from which the fibrils can grow. Because the nucleus is the most energetically unfavorable state, nucleus formation seems to determine the reaction rate. After the nucleus has formed the further addition of monomers becomes faster, favoring growth of the aggregate (arrays of extended blue entities). Evidence from experiments indicates that such nuclei could be oligomers of a different structural nature to that of the final amyloid fibrils (arrays of blue arrows). There might be further intermediates such as protofibrils (array of arrowless, extended blue entities) that finally become amyloid fibrils (arrays of blue arrows)[5].
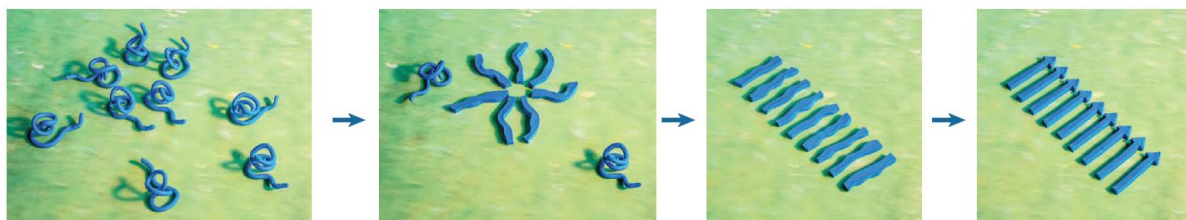
Figure 2. A simplified mechanism of the nucleation-depedent process of amyloid aggregation. The sequence of events along the fibril formation pathway includes: Aggregation of misfolded monomers (blue coils) into small intermediate oligomers; re-arrangement of these oligomers into an organized conformation containing the cross beta structure (star like entity); Association of beta structured oligomers into proto-fibrils (array of arrowless extended blue entities) and finally into fibrils (arrays of blue arrows) (picture taken from Riek et al. ref. [5]

Secondary nucleation processes including fibril fragmentation and nucleus formation induced at the amyloid fibril surface[6] are of relevance to the kinetics of fibril growth. Off-pathway aggregation might also occur.

1.2 Alzheimer's disease (AD)

Dementia is a syndrome which leads to deterioration of memory, thinking, behavior and the ability to perform daily activities[7]. Around 47.5 million people worldwide suffer from dementia with 7.7 million new cases per year. The most common cause for dementia is Alzheimer's disease (AD), which accounts for an estimated 60 to 80% of all cases[7a]. The biggest risk factor of AD is aging because over 95% of all patients develop AD at an age over 65 years and only 4% develop AD below this age[7]. AD is a heterogeneous disease with sporadic and familial forms both of which have a genetic component that increases the risk for developing AD[8]. The familial form is inherited autosomal dominant and involves mutations in one of three genes: amyloid precursor protein (APP), Presenilin-1 (PSEN1) and Presenilin-2 (PSEN2)[8-9]. However, the familial form is very rare[8]. A genetic risk factor for sporadic AD is the apolipoprotein E (APOE)[8-10], specifically the allele ε4 which increases the risk in heterozygotes by three times and in homozygotes by 15 times[11].

The course of disease is accompanied by a progressive loss of neurons and synapses in the cerebral cortex as well as by the formation of neurofibrillary tangles and senile plaques[9, 12]. Neurofibrillary tangles consist of hyper-phosphorylated tau protein, which is why AD is also classified as a tauopathy[8]. Tau is a microtubule-associated cytosolic protein that is usually found in axons where it is involved in axonal transport[13]. Hyper-phosphorylation of tau occurs due to an imbalance between kinases and phosphatases that control tau phosphorylation and a change in tau's conformation that alters the interaction with theses enzymes[14]. This hyper-phosphorylated tau sequesters normal tau causing the disassembly of microtubules and an impaired axonal transport. Additionally, hyper-phosphorylated tau is prone to aggregate and forms insoluble aggregates and fibrils[8, 14]. Ultimately, the toxic hyper-

phosphorylated tau is involved in the progressive neuronal degeneration that is characteristic for AD[8]. The extracellular senile plaques that are found in the brains of AD patients are formed by aggregated amyloid-β (Aβ) proteins which are generated through the cleavage of APP. Aβ was first sequenced and identified as the core protein of the senile plaques in the mid-1980s[15].

1.2.1 Amyloid-β peptide and amyloid-β fibrils

The accumulation of amyloid-β plays an important part in the pathophysiology of AD. Although the physiological functions of amyloid-β remain unknown, decades of research founded in genetic studies of AD continue to suggest a causative role for the peptide, the build-up of amyloid-β in the brain parenchyma probably contributes to the loss of synapses, neurodegeneration and alternations in neuronal activity. Each of these changes disrupts neural circuits, which can also lead to widespread network dysfunction and cognitive decline[16].
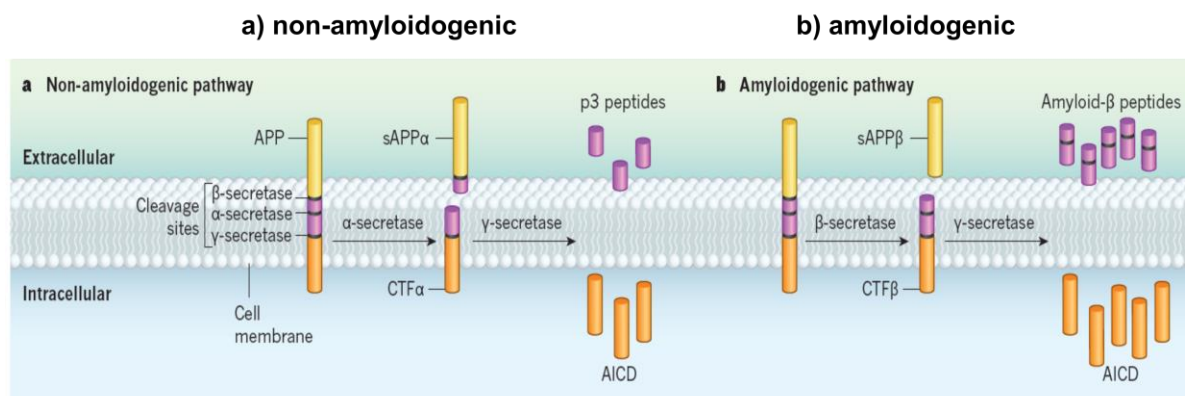
**Figure 3. The structure of APP includes an amyloid-β domain (purple) with the cleavage sites for secretase enzymes.** Two pathways compete for the APP substrate, which leads to either amyloidogenic or non-amyloidogenic processing of the protein[17] (picture taken from Canter et al. ref.[16]).

Amyloid-β peptides result from the sequential cleavage of APP, a type I integral membrane glycoprotein. The structure of APP includes an amyloid-β domain (purple) with cleavage sites for secretase enzymes. Two pathways compete for the APP substrate, which leads to either amyloidogenic or non-amyloidogenic processing of the protein (Figure 3). In the non-amyloidogenic pathway (Figure 3a), the cleavage of APP in the amyloid-β domain by α-secretase, a complex that contains ADAM metalloproteases, releases the soluble ectodomain sAPPα and the C-terminal fragment CTFα. The subsequent cleavage of CTFα by γ-secretase produces a soluble extracellular p3 peptide and the APP intracellular domain (AICD)[18]. The amyloidogenic pathway (Figure 3b) involves APP cleavage by β-secretase (also known as BACE1), which releases the soluble ectodomain sAPPβ and CTFβ. Cleavage of CTFβ by γ-secretase yields amyloid-β peptides of varying lengths as well as the AICD fragment. The pathogenic impact of amyloid-β peptides varies in length. The longer amyloid-β (1-42) and amyloid-β (1-43) species are more prone to aggregation and prion-like seeding[19]. Under basal conditions, ~ 90% of Aβ produced is Aβ40, with Aβ42 consisting less than 10%[17]. In general, Aβ40 is less toxic than Aβ42 and has the ability to inhibit Aβ42 oligomerization[20]. Aβ peptides can exert numerous detrimental effects on the neurons and other cell types of the brain (Figure 4)[21]. As peptide species with acute toxicity, oligomeric Aβ directly incites neuronal apoptosis through interactions with cell-surface receptors. The effects of Aβ on synapse activity vary with its extracellular concentration: low levels of Aβ promote excitatory activity and higher levels depress it. Small increases in Aβ levels promote activity through presynaptic acetylcholine receptors, which elevate internal calcium concentrations to increase probability of glutamate release[22]. Acute increases in synaptic Aβ can impair the long term potentiation of synaptic strength and promote the depression of synaptic activity (known as log-term depression)[23], chronic elevations can weaken connectivity alter the dynamics of dendric

spines, promote synapse loss[23-24]. Loss of synaptic inhibition occurs through numerous pathways, including the downregulation of cell-surface voltage-gated sodium channels[25]. Moreover, long term accumulation of toxic Aβ species in the parenchyma also leads to oxidative damage of DNA and proteins, to physical injury of cellular organelles and to dysregulation of intracellular calcium levels-each of which can provoke cell death[26].
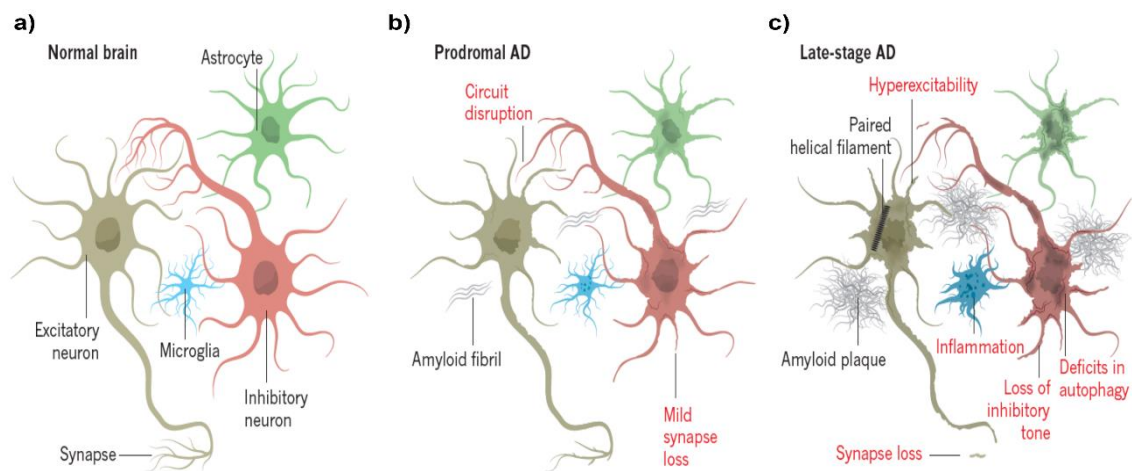
Figure 4. Neural circuits and synapses during the progression of AD. (a) Subpopulations of neurons and glia cells form functional circuits through synaptic connections, (b) in prodromal AD, Aβ fibrils begin to form in the extracellular space, possibly contributing to early circuit disfunction that stimulates the inhibitory spouting and the initiation of inflammatory processes, (c) in the late stage AD, Aβ plaques grow as production of the peptide outpaces its clearance. Deficits in autophagy and other quality control pathways contribute to the dysfunctions of neurons and glia. Despite loss of synapses, excitatory neurons become hyperexcitable, compromising the fidelity of synaptic network connections for long-range communications (picture taken from Canter et al. ref.[16]).

The most compelling property of Aβ is the formation of insoluble fibrils that accumulate extracellularly as amyloid deposits in the brains of AD patients. Scientists are engaged in finding out what the Aβ fibril looks like and how Aβ forms β-sheet structures that are typical for amyloid fibrils. Petkova et al. have suggested a structure for one Aβ40 cross-β unit with the help of solid state NMR as displayed in Figure 5[27]. According to this model, the residues 1-8 are fully disordered and the residues 12-24 and 30-40 are responsible for the formation of in-register parallel β-sheets. Residues 25-29 form a loop that brings the two β-sheets in close contact through sidechain interactions (Figure 5)[27]. This leads to a double-layered cross-β unit with and hydrophobic core and one hydrophobic side (Figure 5b)[27]. The only charged sidechains in the core, residues 23 and 28, form a salt bridge (Figure 5b) and a protofibril consists of two cross-β units with the hydrophobic sides facing each other (Figure 5c)[27]. These findings are supported by further studies[28] that also form the u-form structure although the quaternary structure of the protofibrils differs[28a, 28b]. A similar structure was found by Luhrs et al[29] for Aβ42 (Figure 6a,b) with the help of NMR studies. However, they used a recombinant peptide that contains a methionine sulfoxide at position 35[29]. In this model, residues 1-17 at the N-terminus are disordered and residues 18-26 and 31-42 form two parallel in-register β-sheets along the fibril axis[29]. A comparison to the findings of Petkova et al. however, showed that the packing of the hydrophobic core of Aβ42 is entirely different to the one of Aβ40[29].
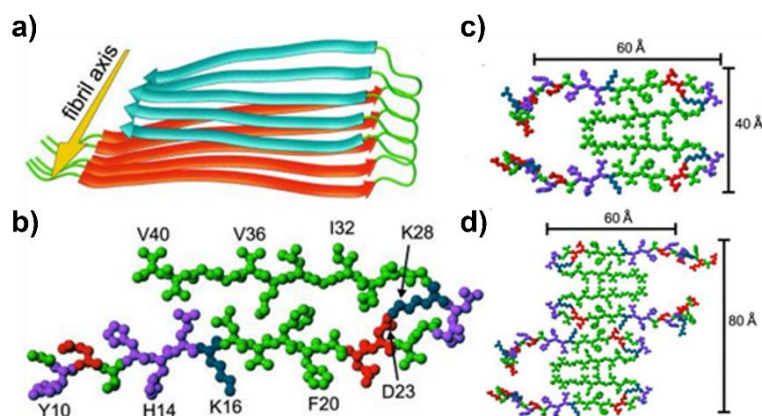
Figure 5. Structural model of Aβ40 fibrils. (a) Model of a cross-β unit of Aβ40 with two parallel in-register β-sheets formed by the residues 12-24 and 30-40 (orange and blue). Residues 1-8 are disordered and a loop from residue 25 to 29 (green) connects the two β-sheets that run along the fibril axis (yellow), (b) one Aβ40 monomer in its fibril conformation viewed down the fibril axis. The short loop brings the two β-strands in close contact generating a hydrophobic core and one hydrophobic side, (c) proposed interaction of two Aβ40 monomers in a protofibril, (d) interaction of two protofibrils. Residues are colored according to their sidechains as hydrophobic (green), polar (magenta), positive (blue), or negative (red) (picture taken from Petkova et al. ref.[27]).

A more recent study contradicts these findings for Aβ42 (Figure 6)[30]. This model of Xiao et al.[30], based on NMR data, postulates a triple-β motif with 3 parallel in-register β-sheets formed by the residues 12–18, 24–33 and 36–40[30]. Furthermore, they identified a salt bridge between the side chains Lys28 and Ala42 (Figure 6c, d). These findings suggest a protofibril formed by Aβ42 that is very distinct to the models of Aβ40. But, according to Xiao et al.[30], this would explain the selective misfolding of Aβ42 at an early stage AD as well as the lack of cross-propagation of Aβ40 fibrils from Aβ42 fibrils[30].
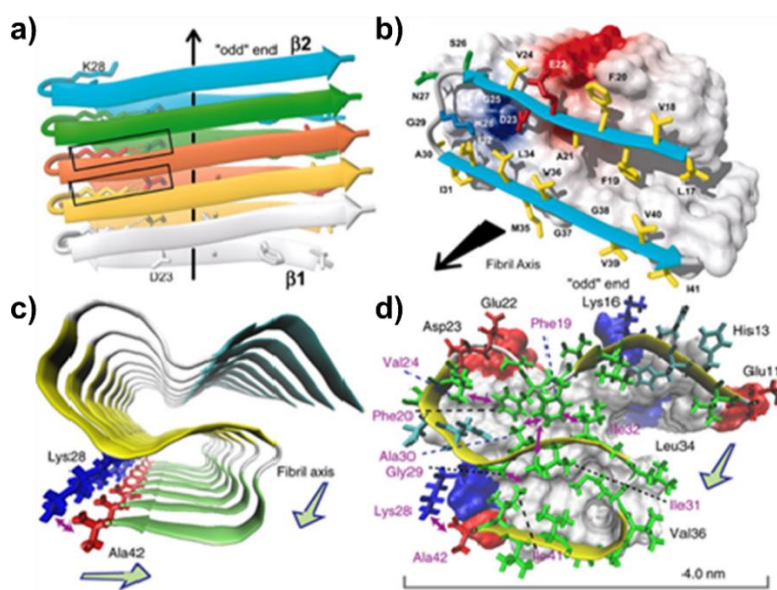
Figure 6. Two structural models of Aβ42 protofibrils. (a,b) Structural model of Aβ42 fibrils according to the findings of Luhrs et al. (taken from Reference[29]). Aβ42 monomers contain two β-strands leading to protofibrils with two β-sheets that form a steric zipper in between, (c,d) structural model of Aβ42 fibrils according to the findings of Xiao et al. This model shows three β-strands (cyan, yellow and green) resulting in a protofibril with three parallel in-register β-sheets and a salt bridge between Lys28 and Ala42 (picture taken from Xiao et al. ref.[30]).

1.2.2 Drug development in AD

The global impact of Alzheimer's disease (AD) continues to increase, and focused efforts are needed to address this immense public health challenge. National leaders have set a goal to prevent or effectively

treat AD by 2025. Under the current conditions, only drugs currently in late Phase 1 or later will have a chance of being approved by 2025. However, there is an opportunity to reduce the time and risk of AD drug development through an improvement in trial design; better trial infrastructure; validated biomarkers to better detect disease; determine risk and monitor disease progression as well as predict disease response; more sensitive clinical assessment tools. Improved mechanistic understanding of disease onset and progression is central to more efficient AD drug development and will lead to improved therapeutic approaches and targets[31].

1.2.3 Peptide-based inhibitors of amyloid formation in AD

The development of inhibitors of amyloid formation is an important scientific and therapeutic task. The design of inhibitors of amyloid formation has been described in depth in several reviews[32] (small molecules, peptides, other proteins, antibodies, chaperones).

The key pathogenic event on the onset of Alzheimer's disease (AD) is believed to be the aggregation of the β-amyloid (Aβ) peptide into amyloid fibrils. First in the peptide-based inhibitors field was Tjenberg et al.[33] , who reported a small fragment Aβ(16-20) or (KLVFF) that binds to full length Aβ and prevents its assembly into amyloid fibrils, with K16, L17, F20 to be critical for binding to Aβ. Peptides targeting the central hydrophobic region of Aβ became leads fragments for optimizing of Aβ amyloid inhibitors[34]. In 2004, Datki et al.[35] presented a pentapeptide LPYFD-NH$_2$ derived from Aβ, which significantly decreased neurite degeneration and cell viability reduction induced by Aβ42. In 2014, Minicozzi et al.[36] reported a related peptide Ac-LPFFN-NH$_2$ as an effective inhibitor of Aβ40 aggregation.

Another class of peptide inhibitors have been designed to interfere with β-sheet formation by preventing propagation of hydrogen bonds along the long axes of β-sheets. In most cases modification of the amide bonds has been performed by alkylating the amide nitrogen (e.g. N-methylation) or substituting of the amide nitrogen (e.g.by oxygen resulting in an ester bond). Doig and co-workers synthesized Aβ(25-35) peptides containing single N-methyl amino acids[37]. In some cases, these peptides were found either to alter the morphology or to prevent aggregation and neurotoxicity (as measured by MTT assays on PC-12 cells) of Aβ partial segment Aβ(25-35). [NMe-Gly25]-Aβ(25-35) had properties like the non-methylated peptide, but [NMe-Gly33]-Aβ(25-35) prevented fibril assembly and reduced the toxicity of preformed amyloid, whereas [NMe-Leu34]-Aβ(25-35) altered fibril morphology and reduced toxicity[37]. Thus, the location of the N-methyl groups was critical in determining the efficacy of inhibition of fibril formation and toxicity[37].

Further development of the N-methylation strategy was to incorporate N-methyl amino acids into alternate positions in the putative fibrillogenic region of the peptide[38]. Using this concept Gordon et al.[34b] synthesized inhibitors targeted against Aβ as well as peptide from human prion protein (residues 106-126). Furthermore, Gordon and Meredith (2003) synthesized fibrillogenesis inhibitors with essentially the same design as their earlier inhibitors containing N-methyl amino acids (i.e., with ester bonds at alternate residues within the Aβ(16–20) peptide)[34c]. Like the N-methylated peptides, the ester containing peptides remained water soluble, did not form fibrils and were effective inhibitors of Aβ fibrillogenesis. In 2004, Giralt et al.[39] studied the reduction in cytotoxicity of Aβ in PC12 cell culture by peptides having single N-methyl amino acid in the designed sequence (based on the central hydrophobic core of Aβ). They designed a peptide inhibitor "inL" having two motifs: an additional amino acid Lys at N-terminus to enhance the solubility and an N-methy-Phe29 residue to block Aβ aggregation. Later, a corresponding D-peptide (inD) and its retro –inverse variant (inrD) were designed and investigated for their ability to inhibit Aβ aggregation. Both peptides (inL) and (inD) were stable to proteases[40]. PPI-1019 also known as Apan was another effective N-methylated contained D amino acids inhibitor of Aβ aggregation and toxicity[41].

Other classes of inhibitors included β-Wrapins, which are engineered binding proteins obtained from phage–display libraries based on the Aβ-binding affibody protein ZAβ3. ZAβ3 stabilizes the β-sheet by extending it intermolecular and by bearing both mostly nonpolar faces of the Aβ hairpin within a large hydrophobic tunnel-like cavity. Consequently, ZAβ3 acts as a stoichiometric inhibitor of Aβ fibrillation[42]. Moreover, it is reported that random mutagenesis of ZAβ3 resulted in a single β-wrapin AS10, which through binding to Aβ, α-Syn, IAPP inhibits the aggregation and toxicity of all of them[43]. Cyclic peptides have been developed as new class of amyloid inhibitor over the past five years. They have been shown to be powerful and specific inhibitors for amyloid formation. Cyclic peptides are metabolized slower than their non-cyclic precursors because of their resistance to enzymatic degradation. It has been shown that sequence and conformational mimics are good starting points for the design of specific inhibitors against amyloid formation[44].

In 2014 Kanai, Sohma et al. reported cyclic derivatives of KLVFF and its all D-enantiomer which showed three times better inhibitory activity than the linear[45]. In a later report they designed a more potent inhibitor by incorporating an additional phenyl group at the β-position of a Phe side chain. Biophysical and biochemical analyses revealed the rapid formation of oligomer species when Aβ42 was mixed with the peptide. The oligomer species is an "off-pathway" species with low affinity for cross-β-sheet-specific dye thioflavin T and oligomer-specific A11 antibodies[46].

In 2009 Teplow and co-workers identified PP-Leu, a tridecapeptide analogues of θ-defensins as potent inhibitors of Aβ oligomer and fibril formation. The proposed mechanism was through colloid-like assemblies[47]. In Rahimipour et al. was reported the synthesis and screening of a self-assembled cyclic D, L,-a-peptide library.The library was constructed based on the hypothesis that the significant similarities between amyloid and the architecture of self-assembled cyclic D,L-a-peptides could play a vital role in making the cyclic peptides efficient binders and inhibitors of Aβ amyloidogenicity. CP-2 showed significant inhibition of Aβ aggregation and protected PC-12 cells from Aβ toxicity[48].

It has been shown that macrocycles amyloid β-sheet mimics (ABMs), which contain heptapeptide β-strands from β-sheet rich amyloid proteins such as Aβ, β2-microglobulin, a-syn, Tau, hIAPP and Prion proteins could inhibit the toxicity of amyloid aggregates[44a]. Side-chain-to-side-chain lactam bridged cyclo (17-21)-[Lys17, Asp21]Aβ(1-28) was found to inhibit the fibrillation of linear peptide Aβ(1-28). Moreover, cyclo(17-21)-[Lys17, Asp21]Aβ(1-28) reduced the toxicity of Aβ40 aggregates, through a formation of a homodimeric complex peptide and Aβ(1-28)[49].

Another cyclic peptide (Cyc[60-70]) derived from ApoII is formed by disulfide crosslinking of cysteine residues. Cyc[60-70])was shown to inhibit the fibril formation of Apoc-II peptide and its ability to inhibit was decreased by reducing the disulfide bond. A mechanism was proposed in which the flexible hydrophobic and hydrophilic surfaces of the cyclic peptide interact transiently with the fibrillogenic peptide[50].

Finally, a different approach was proposed by Murphy et al.[51] for anti-Aβ peptides using as templates proteins that bind natural to Aβ, in this case TTR. They were demonstrated that G16 linear peptide (102-117) TTR residues- PRRYTIAALLSPYSWS, a TTR[52] derived peptide, interacts with Aβ, affects Aβ aggregation and inhibits Aβ toxicity. To enforce proper residue alignment, they transplanted the G16 sequence on to β-hairpin template. Two peptides with 18 and 22 amino-acids were synthesized and cyclized. The cyclized 22-mer CG3 SKVVT[D] PPRYTIAALLSPYSYSQ (but not the non-cyclized 22-mer nor the 18-mer) strongly suppressed Aβ aggregation to fibrils and protected neurons against Aβ toxicity, but not so effective as native TTR[52]. Later, Murphy et al.[53] reported the use of TANGO algorithm to design anti-amyloid molecules with a greater match to the TTR template but having lower propensity to self-associate and thus being more effective inhibitor. There demonstrated that the peptide (CG8) binds to Aβ and redirects Aβ toward protease-sensitive, nonfibrillar aggregates. Cyclic peptides designed using this strategy have attractive solubility, specificity, and stability characteristics[53].

1.3   Type II diabetes (T2D)

Diabetes mellitus is a chronic metabolic disease, 422 million adults suffered from T2D in 2014. This equates to 8.5% of the adult world population. Moreover, the number of cases is estimated to rise up to 642 million in 2040[54]. Three forms are distinguished: type 1, type 2 and gestational diabetes. Type 2 diabetes (T2D) is the most common form and accounts for around 91% of all diabetes cases and it is caused by a combination of lifestyle and genetic factors[55]. T2D is characterized by insulin resistance and progressive β-cell failure and extracellular amyloid deposits[56]. β-cells are a cell type of the pancreas and their task is the synthesis, storage and secretion of insulin[57]. The hormone insulin is produced and released after glucose enters the bloodstream and it controls the blood sugar level by triggering glucose uptake into body cells[57]. During insulin resistance, the cells fail to respond properly to the insulin. The β-cells try to compensate by proliferation and overproduction of insulin but eventually they cannot maintain the homeostasis. This leads to β-cell failure with a reduction in cell mass and function[56] . Another feature of T2D is the pathological extracellular deposition of IAPP in form of islet amyloid[58]. IAPP is a neuropancreatic hormone which is synthesized and secreted by β-cells as well[58a]. It is involved in maintaining energy homeostasis and in regulating i.e. satiety and blood glucose[58a, 59]. However, IAPP is highly amyloidogenic and in the form of pancreatic islet amyloid, it contributes to β-cell dysfunction and death[58a].

1.3.1   IAPP and IAPP derived fibrils

Islet amyloid polypeptide is expressed by the β-cells as a preprohormone with a length of 89 amino acids, including a 22 aa-residue signal peptide and two short flanking sequences (Figure 7)[58c, 59-60]. PreproIAPP is cleaved by a signal peptidase[61] and the cleavage takes place in the endoplasmic reticulum (ER) generating the 67-residue proIAPP[58c, 59]. ProIAPP is further processed in the late Golgi and secretory granules by two prohormone convertases (PC2 and PC1/3) and a carboxypeptidase E (CPE) which remove the flanking sequences[58c, 59]. PC2 cleaves proIAPP after the lysine at position 10 (Lys10) and the arginine at position 11 (Arg11), whereas PC1/3 cleaves after the residues Lys50 and Arg51 (Figure 7)[58c, 62]. However, the C-terminal cleavage can also be performed by PC2 in absence of PC1/3[62]. The remaining C-terminal basic residues are removed by carboxypeptidase E (CPE) and the C-terminus is amidated by peptidyl-glycine alpha-amidating monooxygenase (PAM) upon removal of glycine (Figure 7)[62]. Mature IAPP has a length of 37 amino acids, an amidated C-terminus and an intramolecular disulfide bond between the cysteines at positions 2 and 7 as displayed (Figure 7).
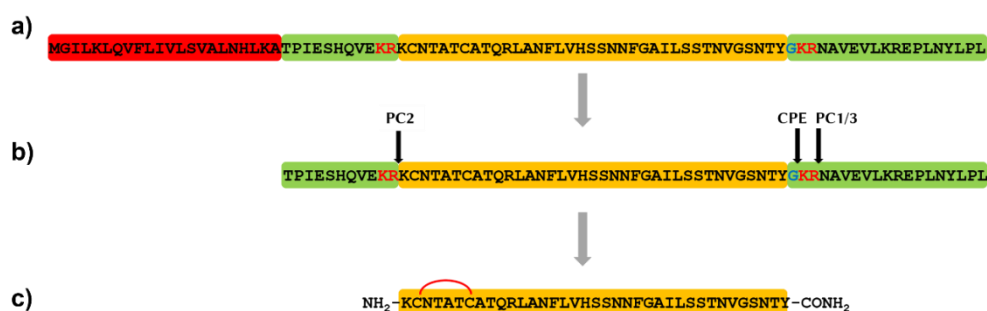
Figure 7. Processing of human islet amyloid polypeptide. (a) IAPP is expressed as 89-residue preproIAPP with a 22-residue signal sequence (highlighted in red), two short flanking sequences (highlighted in green) and the IAPP sequence (highlighted in yellow), (b) the signal sequence is cleaved by a signal peptidase in the endoplasmic reticulum generating the 67-residue proIAPP. Further processing takes place in the Golgi and in secretory granules by prohormone convertases (PC) and carboxypeptidase E (CPE). PC2 cleaves proIAPP at residues Lys10 and Arg11 while PC1/3 cleavse at Lys50 and Arg51. (indicated as red letters). The C-terminal dibasic residues are removed by CPE and the C-terminus is amidated by peptidyl-glycine alpha-amidating monooxygenase (PAM) upon removal of glycine (indicated in blue letters), (c) the mature 37-residue IAPP possesses an amidated C-terminus and an intramolecular disulfide bond (picture taken from Marzban et al. ref.[62]).

In T2D, however, IAPP forms insoluble fibrils that accumulate extracellularly as plaques. The fibrils consist of many IAPP monomers generating the characteristic cross-β structure. In 2005, Kajava et al.[63] proposed a model for the conformation of IAPP monomers in the fibril with three β-strands that are connected by turns (Figure 8a, b)[63]. The monomers are stacked along the fibril axis generating three parallel in-register β-sheets[63]. In this model, the 8 N-terminal amino acids containing the disulfide bond are disordered and do not contribute to the β-sheets (Figure 8a, b)[63]. This is supported by the findings that a fragment of IAPP from residues 8 to 37 forms protofibrils with the same width as full-length IAPP[64]. The β-strands are assigned to the residues (12–17), (22–27) and (31–37), which is confirmed by studies that found the regions (8–20), (20–29) and (30–37) to be amyloidogenic[65]. This model would also explain why IAPP deposits in the context of diabetes occurs in primates and cats but not in rodents[63]. The IAPP sequence of rodents is substituted at the positions 25, 28 and 29 with proline[65b], an amino acid that is known as β-sheet disruptor.
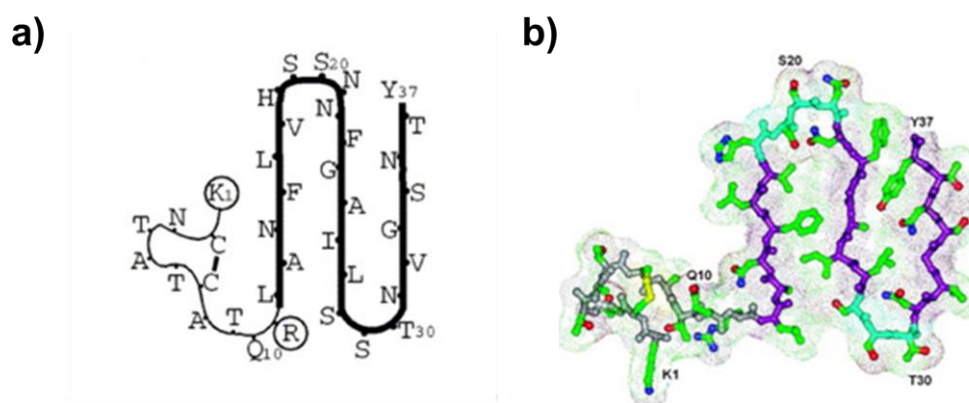
Figure 8. Different models for the conformation of IAPP within a protofibril. (a) Model of the β-serpentines of IAPP with three β-strands and the disulfide bond within the first eleven residues. Charged residues are circled, (b) ball and stick model of the serpentine structure of IAPP[26] (picture taken from Wiltzius et al. ref.[66]).

1.3.2 Peptide-based inhibitors of amyloid formation in T2D

While many different compounds and chemical strategies to inhibit amyloid formation and cytotoxicity of Aβ have been developed, there are not so many reports available about IAPP aggregation inhibitors. A category of IAPP aggregation inhibitors introduces N-methyl amino acids in short peptides corresponding to the amyloid core of the IAPP sequence. The generated peptides do not form β-sheet structure and are very good soluble. Based on the information that IAPP(23-27) and IAPP(22-27) are the shortest IAPP sequences still able to make fibrils, two N-methyl moieties were introduced to those sequences on the same side of the β-strand (Scheme 9)[38, 67]. Based on these findings the double N-methylated full length IAPP analogue [(NMe)G24, (N-Me)I26]IAPP (IAPP-GI) is a highly soluble, nonamyloidogenic analogue, which binds with low nanomolar affinity and blocks IAPP cytotoxic self-assembly and fibrillogenesis in the nanomolar range[68].
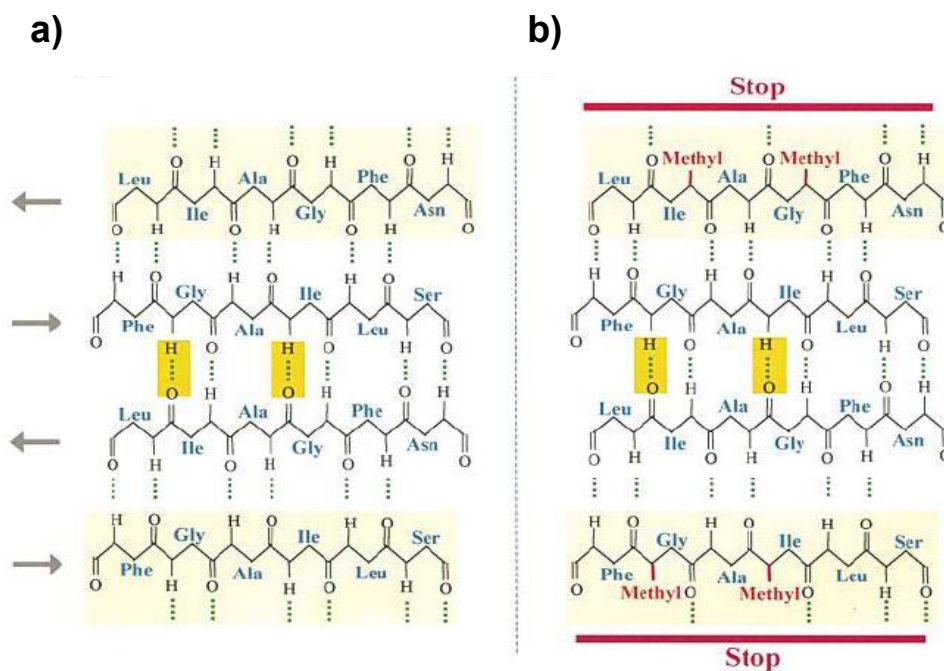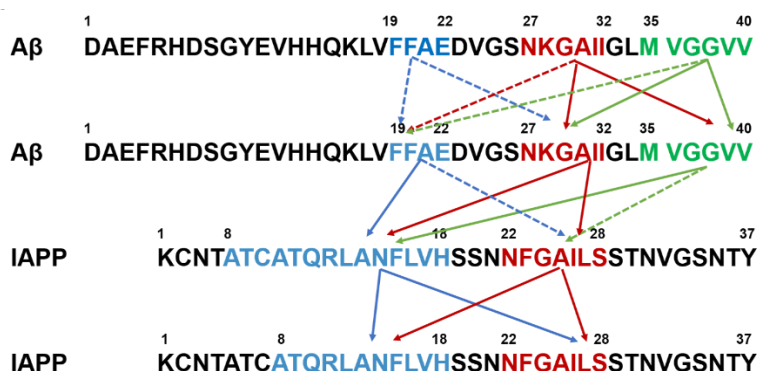
Figure 9.Schematic model of IAPP(22-28) and design of an inhibitor with N-methyl amino acids at alternate residues. (a) Schematic model for IAPP(22-28) antiparallel β-sheet self-assembly based on rotational resonance (R2) solid state NMR of IAPP(20-29)[69]]. (b) Hypothetical mechanism of inhibition of IAPP fibril formation by introducing two N-methyl residues at G24 and I26 (picture was taken from Kapurniotu et al. ref.[38]).

Later, Yan et al.[68, 70] showed that soluble IAPP mimics obtained by N-methylating specific amide bonds within IAPP(22–27) exhibit both IAPP receptor agonism and nanomolar-affinity inhibitory effects on the aggregation and cytotoxicity of both IAPP and Aβ40. They designed analogues with the N-methyl residues present in IAPP-GI and systematically transferred them to other amide bonds within IAPP(22–27). Two other analogues with alternate N-methylations ([(N-Me)A25, (N-Me)L27]-IAPP (IAPP-AL) and [(N-Me)F23, (N-Me)A25]-IAPP (IAPP-FA)) and one with consecutive N-methylations ([(N-Me)I26, (N-Me)L27]-IAPP (IAPP-IL)) were synthesized and studied[71]. The presented multifunctional IAPP mimics constitute a unique class of IAPP analogues in that they are a) soluble, nonamyloidogenic and nontoxic, b) markedly stable toward proteolytic degradation in human plasma, c) potent IAPP receptor agonists, and d) nanomolar-affinity inhibitors of cytotoxic self-assembly and fibrillogenesis of IAPP[72].

Also Mirecka et al. have reported a characterization of a β-hairpin conformation of IAPP in complex with engineered binding protein β-wrapin HI18[73]. The β-strands correspond to two amyloidogenic motifs, IAPP 12-LANFLVH-18 and 22-NFGAILS-28, which are connected by a turn established around Ser20. Besides backbone hydrogen bonds, the IAPP/HI18 interaction surface is dominated by non-polar contacts involving hydrophobic side chains of the IAPP β-strands. Apart from monomers, HI18 binds oligomers and fibrils and inhibits IAPP aggregation and toxicity at low substoichiometric concentrations. These results supported the idea that IAPP β-hairpin can serve as a molecular recognition motif enabling control of IAPP aggregation[73].

Another approach showed that small peptides bearing no similarity to the IAPP sequence, but containing Trp and Tyr residues in the β-strands of a hairpin could inhibit IAPP amyloidogenicity and cytotoxicity: WW2 peptide, (KKLTWVS-IpGK-WITVSA) has been found to be the most potent inhibitor of both, synuclein and hIAPP[74]. Lately based on this idea, the cyclized hairpin, cyclo-WW2 cyclo-(-GKWITVS-IpPK-KLTVWIp) was synthesized and found to display inhibitory activity towards IAPP amyloidogenensis. The results suggested that a β-hairpin -like conformation is involved in the

binding interactions of the WW2-related peptides that are responsible for the inhibition of toxic oligomer formation[75].

Finally, pramlintide (PM) is a peptide drug approved for use as an adjunct to insulin therapy for treatment of diabetes[76]. PM was further developed by introducing the three Pro substitutions found in rIAPP(which was an inhibitor of hIAPP[77] into hIAPP polypeptide[76]. Wang et al. examined and compared the ability of PM, as well as of two mutants His18Arg Pramlintide (h18RPM) and Phe23Leu (F23LPM), to inhibit amyloid formation of hIAPP[78]. The results showed that PM inhibited IAPP fibrillogenesis, however the other two mutants were less effective inhibitors of hIAPP amyloidogenesis.

1.4   Connection between AD and T2D

At first sight, T2D and AD seem to be distinct diseases that have nothing in common. However, individuals with a history of diabetes have a 73% increased risk of dementia and a 56% increased risk of AD[79]. Therefore, it seems likely that there is a link between the two diseases. Studies have been conducted to investigate a possible link; in fact, impaired insulin and insulin-like growth factor expression were found in AD brains. Other studies have suggested that not T2D per se, but hyperinsulinemia is related to AD development[80]. This scenario focuses on the insulin degrading enzyme (IDE) as a key molecule. IDE degrades insulin and more interestingly, Aβ as well[80b, 81]. It is secreted to the extracellular space where it degrades monomeric Aβ and thereby inhibits the formation of oligomers and fibrils[80b, 81]. The hypothesis is that during hyperinsulinemia insulin competes with Aβ for IDE thereby reducing Aβ degradation. This increases the Aβ level which in turn increases the risk of Aβ aggregation[81]. Alternatively, decreased IDE activity, due to i.e. reduced expression, increases Aβ aggregation. Another possible link between T2D and AD involves insulin signalling. Glycogen synthase kinase 3 (GSK3) is an enzyme that phosphorylates serine or threonine residues on its target, one of which is tau, thereby regulating its activity. Inhibition of GSK3 is induced by insulin signalling[81]. Upon binding to its receptor, insulin activates a cascade that leads to the phosphorylation and thereby inhibition of GSK3[81]. In theory, an insulin resistance or a lack of insulin due to pancreatic dysfunction would increase GSK3 activity, because it is not inhibited via insulin signalling[81]. Overactive GSK3 hyperphosphorylates tau, which can then form neurofibrillary tangles characteristic for AD[81]. This theory is supported by the findings that GSK3 activity is deregulated in AD[82]. Overexpression of GSK in mice increases tau phosphorylation[83] and lithium treatment, a weak unspecific GSK3 inhibitor in overexpressing mice, reduces tau phosphorylation[84].

Furthermore, Aβ and IAPP are two short, linear and conformational flexible polypeptides which exhibit high self-association affinities and their aggregates are highly cytotoxic[85]. Importantly, the sequences of Aβ and IAPP are 25% identical and 50% similar (Figure 10)[70]. Moreover, Aβ and IAPP are present in similar concentration in serum and cerebrospinal fluid, therefore the interaction between the two peptides is possible *in vivo*[86].

Figure 10. Primary structures of Aβ and IAPP. Shown are the primary structures of Aβ and IAPP. Identical amino acids between sequences are highlighted in blue and similar amino acids are highlighted in green (picture taken from Yan et al. ref.[70]).

Finally, Andreetto et al. identified the "hot segments" of Aβ and IAPP which are important for their self and cross-interaction, such as Aβ(19-21) and IAPP(8-18) or Aβ(27-32) and IAPP(22-28) (Figure 11)[86b].

Figure 11. "Hot segments" of Aβ and IAPP self- and cross-association. "Hot segments" of Aβ and IAPP self- and cross-interactions highlighted in blue, red and green. Solid arrows indicate interactions between "hot segments". Dashed arrows indicate interactions between segments, which are slightly longer than the "hot segments" (picture taken from Andreetto et al. ref.[86b]).

A recent study by our group has shown that Aβ40 binds IAPP with low nanomolar affinity (app. K_d = 48.5nM) and that pre-fibrillar Aβ40 attenuates IAPP aggregation into IAPP aggregates and fibrils and vice versa (Figure 12)[70].
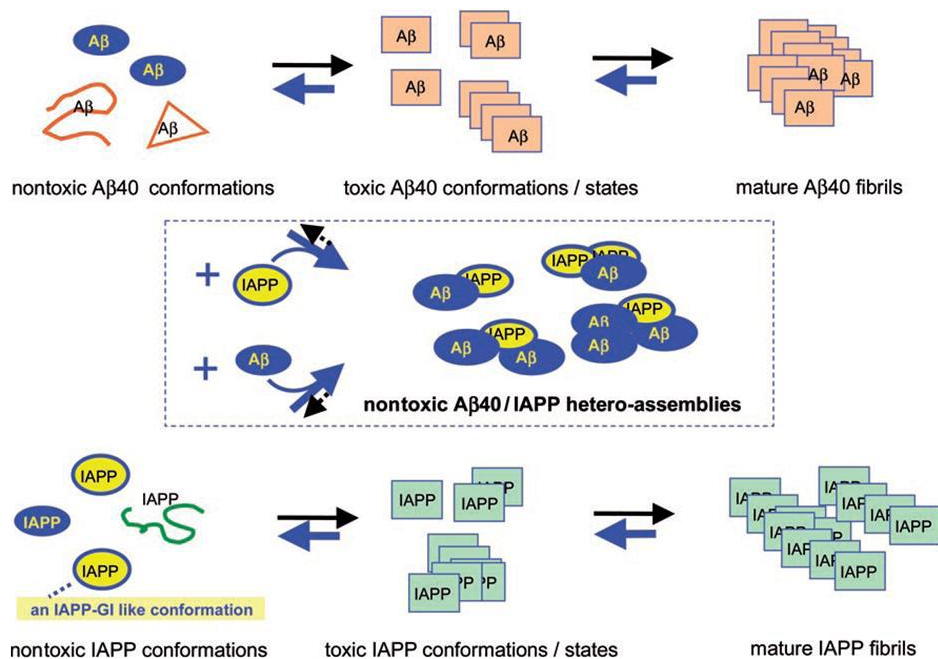
Figure 12. Proposed molecular model of the interaction between pre-fibrillar Aβ40 and IAPP. Molecular model of the interaction of early early prefibrillar Aβ40 and IAPP species resulting in attenuation (blue arrows) of cytotoxic self-assembly and fibrillogenesis of both Aβ40 and IAPP (picture taken from Yan et al. ref. [70]).

The discovery of the Aβ-IAPP interaction was the result of the finding that the IAPP mimic, IAPP-GI, binds with low nanomolar affinity pre-fibrillar Aβ40 (app. K_d= 41.2nM) and as well strongly inhibits Aβ40 cytotoxic self-association and fibrillogenesis[70]. Additionally, IAPP-GI has been shown to redissociate already formed cytotoxic Aβ40 assemblies and fibrils[70]. The hetero-complex between Aβ40 and IAPP-GI is stabilized in a non-fibrillar and non-toxic soluble oligomeric form due to the high affinity of the Aβ-IAPP-GI interaction and the N-methylations in the amyloid core segment of IAPP-GI; the formation of this heterocomplex is consistent with the high potency of the inhibitory effect of IAPP-GI (Figure 13). In conclusion, IAPP-GI can be considered as a high affinity ligand of both pre-fibrillar IAPP and Aβ and a cross-amyloid disease inhibitor[70].

23
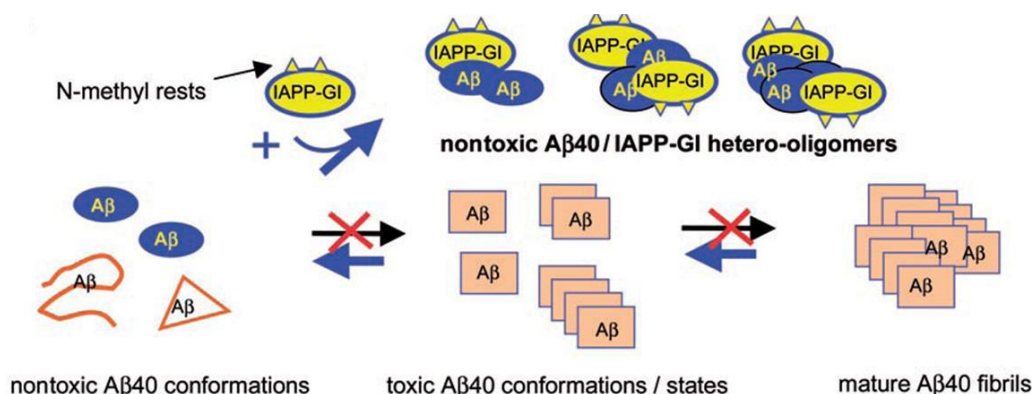
Figure 13. Proposed molecular model of the interaction between IAPP-GI and pre-fibrillar Aβ40. Sequesteration of early prefibrillar and nontoxic precursors of cytotoxic Aβ40 assemblies in the form of soluble and nontoxic hetero-oligomers is suggested to occur through their high-affinity binding to IAPP-GI. Aβ40/IAPP-GI hetero-oligomers will not propagate β-sheet structure and cytotoxic self-association and fibrillogenesis of Aβ40 as a result of the N-methylations in the amyloid core of IAPP-GI, consistent with the high potency of the inhibitory effect of IAPP-GI (picture taken from Yan et al. ref.[70]).

In recent studies by Andreetto et al.[87], a "hot-segment"-linking approach was presented to design a series of IAPP cross-amyloid interaction surface mimics (ISMs) as potent inhibitors of amyloid self-assembly of Aβ, IAPP, or both polypeptides. Figure 13 shows the two "hot segments" that were covalently linked by different tripeptide linker units to produce various ISMs. The unique feature of the approach was that the nature of the linker determines both, inhibitory potency and target selectivity (Aβ versus IAPP).
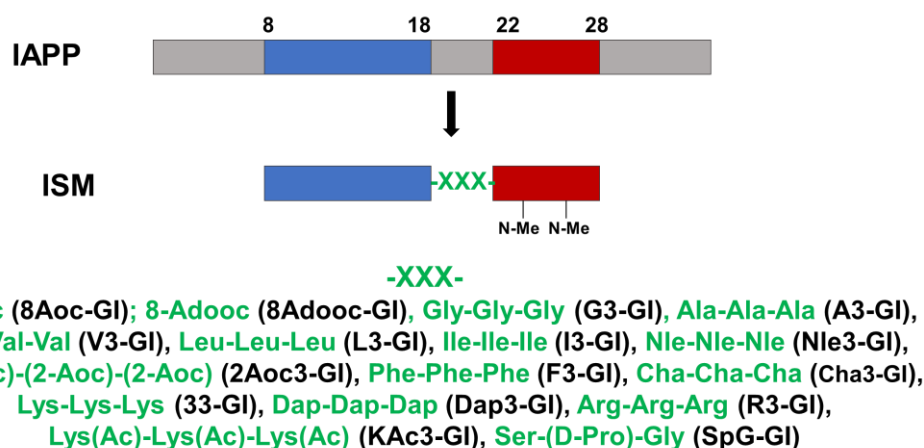
Figure 14. "Hot segments" of IAPP and Aβ self- and cross-interaction and the design of interaction surface mimics. Design of interaction surface mimics (ISM) based on IAPP sequences, IAPP(8-18) and IAPP(22-28) (picture taken from Andreetto et al. ref.[87]).

The above concepts have yielded three nanomolar inhibitors of cytotoxic self-assembly of both Aβ40 and IAPP, four nanomolar inhibitors of Aβ40 cytotoxic self assembly, and one nanomolar IAPP inhibitor. Furthermore, IAPP inhibitors could also inhibit IAPP self-assembly, mediated by Aβ40 seeds, while all seven Aβ40 inhibitors were able to block Aβ42 fibrillogenesis and cytotoxicity as well.

Other studies of our group have recently identified single aromatic/hydrophobic residues within the IAPP segment as hot spots or key residues IAPP(8-28) of its self- and cross-interaction with Aβ40(42)[88].
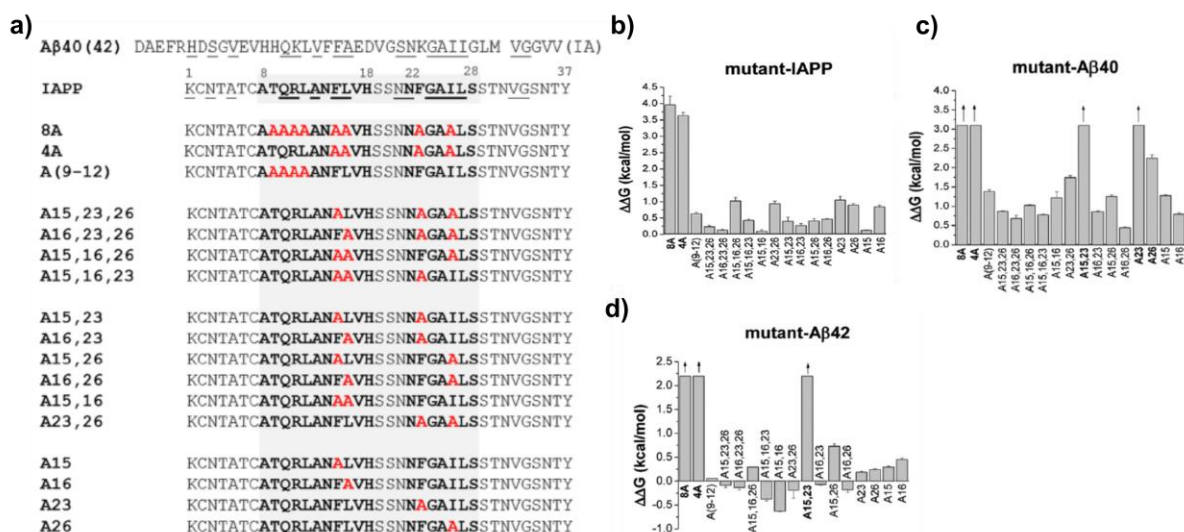
Figure 15. Aβ40(42), IAPP, IAPP mutants and identification of hot spots and key residues of IAPP self-assembly and its hetero-assembly with Aβ40(42) via fluorescence spectroscopic titrations. (a) Similar/identical residues between Aβ and IAPP are *underlined*. Previously identified "hot segments" of IAPP self-assembly and its hetero-assembly with Aβ are in *boldface type*, and introduced Ala substituents are shown in *red* (left, short names). C-terminal amides, Cys2–Cys7 disulfide bridge not shown. (b) Differences in binding free energy of Ala mutants (*mut*) and wild-type (*wt*) IAPP ($\Delta\Delta G_{mut-wt}$ or $\Delta\Delta G$) toward wild-type IAPP, (c) Aβ40, or (d) Aβ42 (means ±SD (*error bars*); n = 3 assays). Mutants in bold are those with strongly diminished binding affinity to IAPP, Aβ40, or Aβ42 as compared with IAPP (pictures taken from Bakou et al. ref.[88]).

Figure 15a presents 17 mutants of full-length IAPP comprising one mutant with substitutions of eight residues with Ala, two quadruple-point mutants, four triple-point mutants, six double-point mutants and four single-point Ala mutants. The affinities of their interactions with IAPP, Aβ40 and Aβ42 were quantified by fluorescence spectroscopy. The determined app. K_d values were used for the calculation of the differences between binding free energies of the Ala mutants and IAPP regarding their interaction with IAPP or Aβ40(42) ($\Delta\Delta G$ values) (Figure 15b-d). In the case of 8A and 4A mutants, the $\Delta\Delta G$ values were higher than 2 or 3 kcal/mol, which showed that simultaneously substitution of the eight residues or of the four residues by Ala caused a strong destabilization of the IAPP-Aβ40(42) and IAPP-IAPP complexes. These and other results, reported in Bakou et al.[88] suggested that the "core region" of both IAPP self- and hetero-assembly with Aβ40(42) lies within IAPP (15-26) and that the four residues Phe[15], Leu[16], Phe[23] and Ile[26] are key residues of these interactions. Moreover, the results identified full-length IAPP analogue, which have a high sequence similarity to IAPP, but distinct profiles regarding their amyloid self-assembly and/or their cross-interactions with Aβ40(42). It has been proposed that the above results will aid in designing novel IAPP analogues as leads for therapeutics in T2D, AD.

1.5 Insulin aggregation

About 230 million people worldwide suffer from diabetes mellitus[89]. There are two major forms of diabetes: type 1 and type 2 diabetes. Approximately 10% of type 1 diabetics have a lifelong, absolute insulin deficiency. In contrast, type 2 diabetes is characterized by two defects: insulin deficiency and insulin[90]. However, in many cases the treatment with insulin is a suitable form of therapy. WHO estimated that 6 tonnes of this hormone are needed every year[91]. Only genetically engineering is a possible way to produce human insulin in amounts required for the therapeutic application. Before that, one had to rely on animal insulin, which was isolated from the pancreas of pigs and cattle. Despite this therapy, diabetics have chronic elevated blood glucose levels. In order to control the blood glucose level in diabetics, different insulin analogues have been developed[92]. Another property of insulin is to form insoluble high molecular weight aggregates, which hinder its therapeutic use, storage as well as its production[93]. Native insulin is characterized by the formation of zinc-containing hexamers with a higher stability to aggregate. During biotechnological processes including insulin isolation and

purification, its aggregation results in a reduction of yield and a loss of its biological activity. Also, during transport and storage protein-based pharmaceutical products can be inactivated by aggregation processes[94]. The insulin aggregation is triggered by physical, chemical and mechanical factors such as elevated temperatures, UV irradiances, low pH values, metal ion contamination or shaking movements. Despite intensive research, the aggregation process of the insulin is not completely discovered. The investigation of the molecular mechanism is not only of economic interest. The development of strategies that lead to the elimination of undesirable aggregation, the applicability of the insulin preparations in their therapeutic application is needed.

1.5.1 Insulin structure and amyloid fibrils

In the insulin synthesis pathway, first preproinsulin is translocated into the endoplasmic reticulum of beta cells of the pancreas with an A-chain, a C-peptide, a B-chain, and a signal sequence[95]. The signal sequence is cleaved from the N-terminus of the peptide by a signal peptidase leaving proinsulin. After proinsulin is packaged into vesicles in the Golgi apparatus (beta-granules), the C-peptide is removed, leaving the A-chain and B-chain bound together by disulfide bonds, that constitute the insulin molecule[95].

The human insulin has a 51-amino acids and a molecular weight of 5805Da and is constituted by two polypeptide chains, an A chain and a B chain, containing 21 and 30 amino acid residues, respectively. The two chains are linked together by two inter-chain disulfide bonds (CysA7-CysB7 and CysA20-CysB19) and an additional intra disulfide bond connects CysA6 and CysA11 within the A chain (Figure 16a). The amino-acids of the two chains are also involved in numerous non-covalent interactions. Moreover, both insulin chains form secondary structural elements. The A-chain consists of two α-helices in the sequence regions (A1-A8) and (A12-A19). The B-chain forms two β-strands, (B1-B5) and (B24-B28), and an α-helix in the region (B8-B19)[95-96] (Figure 16a).

Under physiological conditions there is an equilibrium between the mono-, di-, and tetra- hexameric insulin species. The formation of dimeric structures is mainly the C-terminal β- strands (B24-B28) (blue residues) of the insulin monomers involved in the dimer antiparallel β-sheet (Figure 16a, b). Insulin molecules tend to form dimers in solution due to hydrogen-bonding between the C-termini of B chains. In the presence of zinc ions, insulin dimers associate into hexamers (red residues) (Figure 16a,b). Insulin is stored in the body as a hexamer, whereas the active form is the monomer. Monomers and dimers readily diffuse into blood, while hexamers diffuse poorly. In the case of wild type hexamer; the A chains are shown in black (A1-A21 residues) and the B chain in blue (residues B1-B6) or green (residues B7-B30). Three dimers of insulin are stabilized by two zinc ions, which are bound to six histidines (B10) inside of the oligomer[97] (Figure 16c).
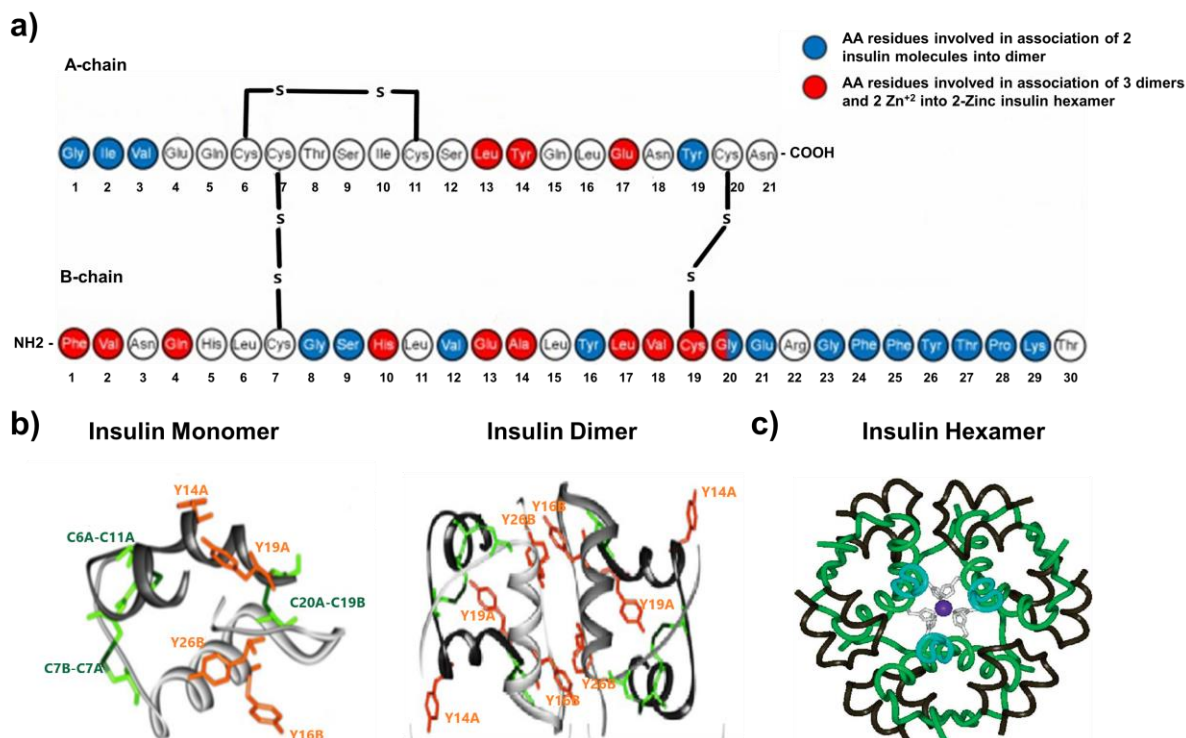
Figure 16. Primary and tertiary structures of insulin, dimer and 2Zn hexamer forms. (a) Primary structure of human insulin; the two chains comprising the insulin structure, A and B, indicating also disulfide bonds between cysteins. The amino acid residues involved in the association of two insulin molecules into a dimer (blue residues) and in the molecular assembly of three dimers into 2Zn insulin hexamer (red residues) are displayed[96]. (b) 3D structures of insulin monomer (left-side) and dimer (right-side) extracted from the crystallized structured of the 2Zn pig insulin hexamer (4INS.pdb). Insulin B chains of insulin are displayed in gray (two different shades in the insulin dimer) and A chains are displayed in black. The four Tyr residues of insulin (Y, orange) and the six Cys (C, green) involved in three disulfide bridges are displayed in green (pictures a, b taken from Correia et al. ref.[96]).(c) Structure of wild-type insulin hexamer. The two naturally occurring zinc ions within each hexamer (overlaid at center; purple) and are coordinated by six His side chains (B10; light gray). The A chain (A1-A21 residues) is shown in black and the B chain in blue (residues B1-B6) or green (B7-B30) (1TRZ.pdb) (picture taken from Phillips et al ref.[98]).

The cross-β structure of insulin fibrils was reported by Burke and Rougvie in 1972[99] and amyloid deposits containing intact insulin molecules, have been reported in a patient with insulin-dependent diabetes undergoing treatment by injection of porcine insulin[100]. Insulin has two amyloidogenic sequences, which show that specific sequences of amino acids can favour fibril formation[101]. One consists of 7 amino acids in the B chain: LVEALYL (B11 to B17). The other one is a 6 amino acid sequence in the A chain: NELQYL (A13 to A18). Ivanova et al.[101a] have discussed the role of the LVEALYL sequence in accelerating and/or retarding insulin fibril formation and shown a concentration dependent behaviour (of extra added LVEALYL in solution). Insulin has become a model peptide for studying fibril formation because it has such a simple structure. Jimenenz et al.[102] have proposed a model for insulin fibrils consisting of a cross-β structure. Several cross-β filaments twist around one another to form the fibril (Figure 17). This model proposes fibril formation after complete unfolding of the native insulin (Figure 17a). A and B chains remain bonded, and stack on top of each other, to further rearrange in a β-like structure (as shown in Figure 17b). Those β-structures further self-assemble in a fibril-like structure[102].
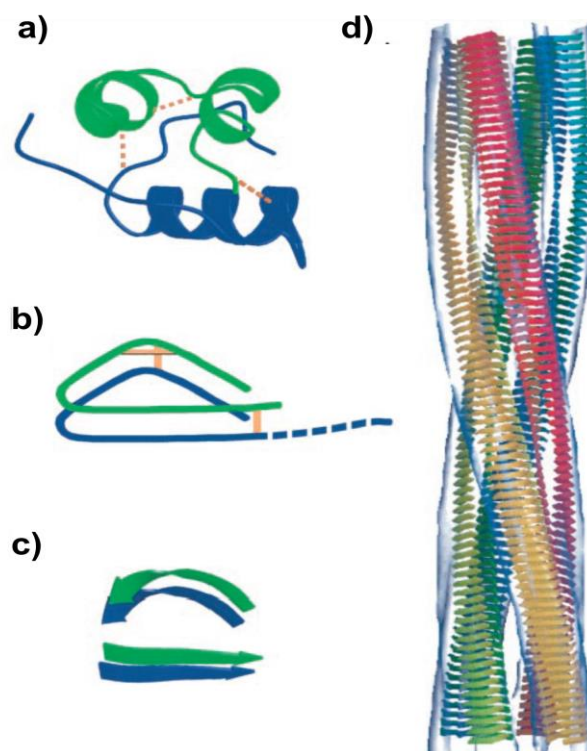
Figure 17. Insulin structure, β-strand model of protofilament and fibril. (a) Insulin native structrue. Disulphide bonds are shown in yellow. A chain is depicted in green and B chain is depicted in blue. (b) Unfolded state of a single insulin monomer. Possible model for an amyloid protoffilament; the C terminus of chain B (dashed) is not required for amyloid fibril formation. (c) β-strand model of a protoffilament. Each insulin occupies two layers. (d) A possible β-strand model docked into the EM density of the compact fibril (transparent gray surface). The four protofilaments are colored separately (picture taken from Jimenez et al ref.[102]).

Jimenez et al. proposed moreover the existence of 4 different types of insulin fibrils of different in thicknesses. They measured cryo-EM images, and their corresponding diffraction patterns and they propose that each insulin fibrils present a common protoffilament structure as shown in Figure17c & d.

1.5.2 Peptide-based inhibitors of insulin

The tendency of insulin to undergo structural transformation resulting in aggregation and formation of insoluble insulin fibrils has been one of the most intriguing and widely studied phenomena[71a].

Many naturally occurring small compounds such as ectoine, betaine, trehalose, and citrulline have been in vitro discovered to inhibit fibrillation of insulin[103]. The drawback of these and other inhibitors is the nonspecific inhibition and the use of relatively high concentrations.

However, few insulin-based inhibitors have been reported towards insulin aggregation. The combination of recognition domain and disrupting domain showed potential in the development of inhibitors of insulin. LVEALYL, was identified as recognition domain, which corresponds to the residues B11-17 of full-length insulin and a hexapeptide consisting of Arg peptides was added to the N-terminus (RRRRRRLVEALYLV) as the disrupting domain and so inhibited insulin aggegration[104]. Moreover, Banerjee et al.[105] developed a nine residue peptide NIVNVSLVK (NK9) constituting mostly with hydrophobic residues, which delayed insulin fibrillization and decreased its cytotoxicity. Recently, Ratha et al.[106] designed a heptapeptide, KR7 (KPWWPRR), which was an effective inhibitor of insulin fibrillization, but less effective inhibitor of insulin cytotoxicity. Finally, one dimensional proton NMR experiments suggested that KR7 primarily targeted the fibril elongation step. More resently, they have designed short peptide sequences and their conjugates, based on some principles implicated for insulin aggregation, and have investigated their ability to interfere and inhibit formation of insulin amyloidogenic fibrils[107]. Optimization of the design of such molecules that may eventually have relevance in pharmaceutical applications, resulted in taurine-containing peptide D4. D4 peptide

was found to prevent the fibrillation of insulin more intensively and has been found to be stable in serum condition even after several hours of incubation[108]. Hydrophobic interactions, aromatic stacking, and hydrogen bonding of peptide D4 with insulin were suggested to inhibit the nucleation phase and slow down the elongation process. MD simulation studies demonstrated that the D4 molecule had a preferred binding site in insulin and it was suggested that residues from the helix and the C-terminal extended segment of chain B of insulin were involved in interactions with D4[108].

Moreover, it is known that IAPP interacts with insulin[109]. Gazit and coworkers used peptide-array methodology to identify the molecular determinants of insulin with IAPP and vice versa. They identified a single domain within insulin that binds to IAPP and inhibits IAPP amyloid formation. This domain located at the center of the B chain of insulin and spans residues 9-20. The B chain of insulin targets the hIAPP monomer in its compact isoform and shifts the equilibrium away from its extended isoform, an aggregation-prone conformation;this interactions has been suggested to inhibit IAPP from forming β-sheets and subsequently amyloid fibrils[110]. Moreover, Gazit et al. identified a single domain within IAPP that binds insulin residues 7-19. It has been proposed that these two domains compose the recognition site that mediates the IAPP/insulin interaction[109a]. Finally, Velkova et al.[71b] proposed another strategy to inhibit non-native aggregation of insulin without affecting its function and therefore suppressing the native cross-amyloid peptide interactions. IAPP-GI, a designed peptide mimic of a non amyloidogenic conformation of IAPP has been found to inhibit non-native amyloidogenesis and toxicity of insulin. It is proposed that IAPP-GI could become a lead compound for development of novel drugs, targeting on both diseases AD and T2D as it inhibits amyloidogenesis of Aβ, IAPP and insulin as well[71b].

2.   Aims of the thesis

Earlier work has identified IAPP segments IAPP(8-18) and IAPP(22-28) as "hot segments" in both IAPP self- and its cross-interaction with Aβ40(42). More recently, these segments (in native or selectively N-methylated form) were linked to each via different linkers and a series of linear IAPP-derived peptides were synthesized. These peptides, termed cross-amyloid interaction surface mimics (ISMs), have been shown to be potent inhibitors of amyloid self-assembly of Aβ40(42), IAPP, or both polypeptides. Notably, the nature of the linker has been shown to determine ISM structure and inhibitory function, including both potency and target (Aβ40(42) versus IAPP) selectivity. One of the above identified ISMs is R3-GI which contains three Arg residues in the linker tripeptide and is a potent inhibitor of Aβ40(42) amyloidogenesis.

Based on these findings, the aims of the first part of my PhD thesis were:

1. Design and synthesis of cyclic analogues of R3-GI as inhibitors of amyloid self-assembly of Aβ40(42) and/or IAPP. Cyclization in the first analogue cc-R3-GI should be achieved via disulfide bridged cysteines introduced in its C- und N- termini. The chemical synthesis of the other two cyclic analogues should be performed using the cysteine crosslinking-based peptide "stapling" strategy[111].

2. Biophysical studies on conformation and aggregation potential of the cyclic peptides.

3. Biochemical and biophysical studies on the interactions and effects of the designed cyclic peptides on Aβ40(42) and or IAPP amyloid self-assembly and cytotoxicity.

4. Studies on the stability of the above cyclic peptides toward proteolytic degradation in human plasma.

The second part of my PhD thesis had the following aims:

1. Rational design, synthesis and biophysical and biochemical studies of cyclic analogues of N-terminally truncated R3-GI as inhibitors of amyloid self-assembly of Aβ40(42) and/or IAPP. This series of analogues were generated by connecting IAPP segments IAPP(14-18) and the double N-methylated analogue of IAPP(22-28) IAPP(22-28)-GI to each other by different tripeptide segments and cyclization via disulphide bond formation between two flanking cysteines.

2. Synthesis and biophysical and biochemical studies on cyclic analogues of N-terminal truncated R3-GI having a minimal sequence identity to IAPP; this study should enable identifying a minimum "pharmacophore" for IAPP-based inhibitors of Aβ40(42), IAPP or both polypeptides. All amino acids within IAPP(14-18) and IAPP(22-28)-GI were substituted with glycine residues except for four potential "hot" residues, i.e. residues which might be crucial for interactions with IAPP and Aβ40(42); peptide cyclization was performed via disulphide bond formation as above. In addition, the effects of each of the Arg residues of the linker tripeptide on inhibitory function should also be investigated.

3. Studies on the effects of substituting L- with D-amino acids on structure, function and inhibitor stability toward proteolytic degradation in human plasma.

Finally, the aim of the third part of my PhD thesis was to investigate whether the previously designed IAPP-derived ISMs[87] could inhibit amyloid self-assembly and related cytotoxicity of insulin as well. The results of my studies should contribute both in devising novel potent IAPP-derived inhibitors of amyloid self-assembly of Aβ, IAPP or insulin and in obtaining more insight into the molecular determinants of their inhibitory function.
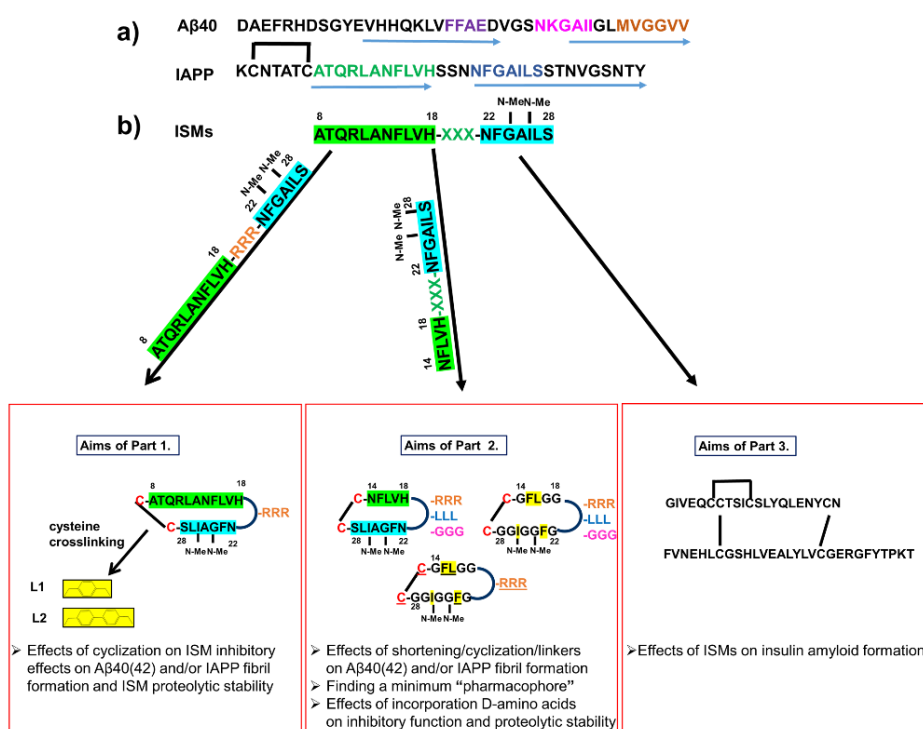
Scheme 1. Schematic representation of the aims of my PhD thesis: (a) Sequences of Aβ40 and IAPP ("hot segments" (IAPP(8-18) and IAPP(22-28) coloured); (b) design concept of IAPP-derived ISMs[87] and aims of the PhD thesis: Aims of Part 1(left side): cyclic analogues of full-length R3-GI generated via cysteine disulfide bond formation or cysteine crosslinking using as linkers p-xylene (L1) and 4,4´Bis(methyl)biphenyl (L2). Studies on the effects of cyclic R3-GI analogues on Aβ40(42)/IAPP fibrillization and proteolytic stability properties of cyclic R3-GI analogues. Aims of Part 2 (center): N-terminal truncated analogues of R3-GI. Studies on the effects of shortening/cyclization/application of different linker units (RRR, LLL, GGG) on Aβ40(42) and/or IAPP fibrillization, importance of the four highlighted (with yellow) amino acid residues, identification of a minimim pharmacophore motif; effects of exchanging specific L-residues of an inhibitor with D-residues (underlined) on inhibitory effects and its resistance toward proteolytic degradation in human plasma. Aims of Part 3 (right side): effects of previously reported IAPP-derived ISMs on insulin fibril formation and cytotoxicity.

3.   Materials

3.1   Materials

3.1.1   Chemicals

Table 1. Chemicals.

Chemicals	Company (city or country)
Protected amino acids (AA)	Iris Biotech (Marktredwitz, DE)
Acetaldheyde	Roth (Karlsruhe, DE)
Acetic anhydride	Sigma-Aldrich (St. Louis, USA)
Acetonitrile (ACN)	VWR (DE)
2-(7-Aza-1H-benzotriazole-1yl)-1,1,3,3-tetramethyluronium (HATU)	Iris Biotech (Marktredwitz, DE)
5(6)-carboxyfluorescein (Fluos)	Sigma-Aldrich (St. Louis, USA)
Chloranil	Fluka (Seelze, DE)
9-Fluorenylmethoxycarbonyl-S-trityl-cysteine-MBHA resin (Fmoc-Cys(Trt)-Rink amide)	Iris Biotech (Marktredwitz, DE)
7-Diethylaminocoumarin-3-carboxylic acid (Dac)	Invitrogen (DE)
Dimethylsulfoxide (DMSO)	Sigma-Aldrich (St. Louis, USA)
N,N-Diisopropylcarbodiimide (DIC)	Fluka (Seelze, DE)
N,N-Diisopropylethylamine (DIEA)	Biosolve (Valkenswaard, NL)
3-(4,5-dimethylthiazol-2-yl)-2,5-diphenyltetrazolium bromide (MTT)	Sigma-Aldrich (St. Louis, USA)
N,N-Dimethylformamide (DMF)	CLN (Niederhummer, DE)
Diethyl ether (Et$_2$O)	Roth (Karlsruhe, DE)
1,2-Ethanedithiol (EDT)	Fluka (Seelze, DE)
Glycin	Fluka (Seelze, DE)
Hellmanex	Hellma Analytics (Müllheim, DE)
Hydrochloric acid (HCl)	Roth (Karlsruhe, DE)
1,1,1,3,3,3-hexafluor-2-propanol (HFIP)	Sigma-Aldrich (St. Louis, USA)
1-Hydroxybenzotriazol (HOBt)	Sigma-Aldrich (St. Louis, USA)
Isopropanol	Roth (Karlsruhe, DE)
Methanol (MeOH)	VWR (DE)
Milk powder (not fat dried)	Applichem (Darmstadt, DE)
Ninhydrin	Fluka (Steinheim, DE)
Phenol	Sigma-Aldrich (St. Louis, USA)
Piperidine	Iris Biotech (Marktredwitz, DE)
Pyridine	Roth (Karlsruhe, DE)
Polylysin	Sigma-Aldrich (St. Louis, USA)
Potassium chloride (KCl)	Merck (Darmstadt, DE)
Proteinmarker-Multimark TM	Invitrogen (DE)
Sodium chloride (NaCl)	Merck (Darmstadt, DE)
Sodium dihydrogen phosphate (NaH$_2$PO4)	Merck (Darmstadt, DE)
Sodium dodecyl sulfate (SDS)	Roth (Karlsruhe, DE)
Sodium hydrogen phosphate dihydrate (Na$_2$HPO$_4$ x 2 H$_2$O)	Merck (Darmstadt, DE)
Sodium hydroxide (NaOH)	Roth (Karlsruhe, DE)
Super signal duration ECL staining solution	Sigma-Aldrich (St. Louis, USA)
2-(1H-Benzotriazole-1-yl)-1,1,3,3-tetramethyluronium-tetrafluoroborate (TBTU)	ThermoFischer Scientific (DE) Iris Biotech (Marktredwitz, DE)
Thioanisol	Fluka (Seelze, DE)
Thioflavin T (ThT)	Sigma-Aldrich (St. Louis, USA)
Trichloracetic acid (TCA)	Roth (Karlsruhe, DE)
Trifluoracetic acid (>99.5%) (TFA for synthesis)	Sigma-Aldrich (St. Louis, USA)
Trifluoracetic acid (>99.5%) (TFA for HPLC)	Sigma-Aldrich (St. Louis, USA)
Triton X-100	Sigma-Aldrich (St. Louis, USA)
Trypsin/EDTA	Invitrogen (DE)
Tween 20	Roth (Karlsruhe, DE)

Chemicals	Company (city or country)
Uranyl acetate	Sigma-Aldrich (St. Louis, USA)

3.1.2 **Peptides**

Table 2. Peptides.

Peptides	Manufacturer/supplier
Aβ(1-40)	Synthesis by the group of Prof. Kapurniotu
Dac-Aβ(1-40)	Synthesis by the group of Prof. Kapurniotu
Aβ(1-42)	Peptide Speciality Laboratories GmbH (DE)
Fitc-Aβ(1-42)	Bachem (Bubendorf, CH)
hIAPP	Synthesis by the group of Prof. Kapurniotu
Fluos-IAPP	Synthesis by the group of Prof. Kapurniotu
Insulin from bovine pancreas	Sigma-Aldrich (DE)

3.1.3 **Assay kits**

Table 3. Assay kits.

Assay kit	Company (city or country)
Micro Bicinchoninic acid (BCA) protein assay kit	ThermoFischer Scientific (DE)
SuperSignal West Dura extended duration substrate	ThermoFischer Scientific (DE)

3.1.4 **Materials and devices**

Table 4. Materials.

Materials	Company (city or country)
96 well plate, Cellstar, sterile, F-bottom	Greiner Bio-One (Frickenhausen, DE)
96 well plate, CellGradeTM plus, sterile	B. Braun (Melsungen, DE)
Cellstar® Tubes, 15 ml	Greiner Bio-One (Frickenhausen, DE)
Cellstar® Tubes, 50ml	Greiner Bio-One (Frickenhausen, DE)
Syringe, BD Discardit II, sterile, 10ml	Becton Dickinson (Franklin Lakes, USA)
Syringe, BD Discardit II, sterile, 20ml	Becton Dickinson (Franklin Lakes, USA)
Syringe, BD Discardit II, sterile, 2ml	Becton Dickinson (Franklin Lakes, USA)
TEM grids, FCF300-Cu, 300 mesh	Electron Microscopy Sciences (Hatfield)
Pipette tips, 2-200µl, yellow	BRAND (Wertheim, DE)
Pipette tips, 100-1000µl, blue	BRAND (Wertheim, DE)
Pipette tips, 0.5-10µl	Axygen (Union City, USA)
Pasteur pipettes, glass, 145mm	BRAND (Wertheim, DE)
Cuvette, quartz	Hellma Analytics (Müllheim, DE)
Microtiter plate, 96 well, F-bottom, black	ThermoFischer Scientific (DE)
Filter, Millex-FG, 0.2µm	Merck (Darmstadt, DE)
Reaction vessel, 1.5ml	Sarstedt (Nümbrecht, DE)
Pasteur pipette	BRAND (Wertheim, DE)

Table 5. Devices.

Devices	Company (city or country)
Analytical balance	Denver Instrument Sartorius (Göttingen, DE)
Centrifuge Labofuge Ae	Heraeus Sepatech (Osterode, DE)
CO_2 Incubator MCO-17AIC	Sanyo Electric Co (J)
Dry freezer Alpha 1-2 LDplus	CHRIST (Osterode, DE)
Heating block neoBlock 1	NeoLab (Heidelberg, DE)
HPLC degassing unit DG-2080-53	Jasco (Gross-Umstadt, DE)
HPLC low pressure gradient unit LG-2080-02S	Jasco (Gross-Umstadt, DE)
HPLC pump PU-2080 Plus	Jasco (Gross-Umstadt, DE)
HPLC UV/Vis detector UV-2077 Plus	Jasco (Gross-Umstadt, DE)
Incubator T6 Heraeus	ThermoFischer scientific (DE)
LAS-4000 mini Fujifilm	FujifilmEurope GmbH (Düsseldorf, DE)
Magnetic stirrer Topolino	Carl Roth (DE)
MALDI-TOF Mass Spectrometer	Bruker Daltonics (Bremen, DE)
Microscope model CKX41	Olympus (Shin juku, J)
Multichannel pipette	BRAND (Wertheim, DE)
Multilabel plate reader 2030 VictorTM X3	PerkinElmer, Life and analytical sciences (FN)
pH-Meter	Mettler Toledo (Greifensee, CH)
Shaker CAT S20	CAT (Staufen, DE)
Spectrofluorometer FP-6500	Jasco (Gross-Umstadt, DE)
Spectropolarimeter J-715	Jasco (Gross-Umstadt, DE)
SDS X cell sure Lock BIO RAD	Invitrogen (Carlsbad, USA)
Ultrapure water unit TKA MikroPure	TKA (Niederelbert, DE)
Ultrasonic bath SONOREX	Bandelin (Berlin, DE)
UV-Vis spectrophotometer V630	Jasco (Gross-Umstadt, DE)
Vortex Mixer Vortex Genie 2	Scientific Industries (New York, USA)
Nucleosil 100 C18, 33mm length, ID 8mm,7µm particle size	Grace, (Columbia, USA)
Nucleosil 100 C18, 250mm length, ID 8mm, 7µm particle size	Grace, (Columbia, USA)
Eppendorf centrifuge 5417C	Netheler-Hinz GmbH (Hamburg, DE)

3.1.5 Cell culture media

Table 6. Cell culture media.

Cell culture	Company (city or country)
Fetal calf serum (FCS)	GIBCO[TM] by Life technologies, ThermoFischer Scientific (DE)
Glutamine	GIBCO[TM] by Life technologies, ThermoFischer Scientific (DE)
Horse serum	GIBCO[TM] by Life technologies, ThermoFischer Scientific (DE)
Penicillin/Streptomycin	GIBCO[TM] by Life technologies, ThermoFischer Scientific (DE)
RPMI-1640	GIBCO[TM] by Life technologies, ThermoFischer Scientific (DE)
Trypsin	GIBCO[TM] by Life technologies, ThermoFischer Scientific (DE)

3.1.6 Antibodies

Table 7. Antibodies.

Antibodies	Company (city or country)
Mouse monoclonal anti-insulin	Sigma-Aldrich (DE)
Goat anti-mouse IgG-POD	Pierce (USA)

3.2 Methods

3.2.1 Solid phase peptide synthesis (SPPS) using Fmoc/tBu-methodology

The synthesis of the peptides was performed according to the Fmoc-strategy and orthogonal protection was applied with the Fmoc-group as temporary protection of the N^a group and tBu- and Trt-based side

34

chain protecting groups (Table 8). Fmoc-cleavage was obtained with a solution of 25% piperidine in DMF according to the protocol shown in Table 9. Couplings were performed using the amino acid (Fmoc and side chain protected) (Fmoc-AA) and TBTU (3-fold molar excess) in the presence of DIEA (4,5-fold molar excess) (Table 9). During the coupling, each amino acid was added to the peptidyl-resin in 3-fold excess compared to the substitution of Fmoc-Cys(Trt)-Rink amide MBHA resin. Coupling efficiencies were checked by the Kaiser test, chloranil test for the N-methylated amino acid[112] [113].

Table 8. Fmoc-amino acids and their side chain protecting groups.

Amino acids (AA)	Protecting groups
Ala	-
Arg	Pbf
Asn	Trt
Cys	Trt
Gln	Trt
Gly	-
(NMe)Gly	-
His	Trt
(NMe)Ile	-
Leu	-
Phe	-
Ser	(tBu)
Thr	(tBu)

Table 9. Protocol for SPPS using Fmoc-chemistry.

Synthesis Step	Reagent	Time
Fmoc cleavage	25% piperidine/DMF	1×5 & 1×10min
Wash	DMF	3×1min
Coupling	Fmoc-AA/TBTU/DIEA (3eq/3eq/4.5eq)	2×40min
Wash	DMF	3×1min
Acetylation	Ac$_2$O/DIEA (10eq/10eq)	15min
Wash	DMF	3×1min

3.2.1.1 Coupling of Cys residues in Fmoc-SPPS

Couplings of Fmoc-Cys(Trt)-OH were performed via the ester formation protocol. This coupling procedure was to avoid racemization of cysteine[114]. More specifically, 3eq of Fmoc-Cys(Trt)-OH, 3eq of HOBt and 4.5eq DIC were dissolved in DMF (0.1M each). Followed by stirring of the reaction mixture at 4°C for 10min and then 10min more at RT. Formation of the Fmoc-Cys(Trt)-OBt ester occurred and the mixture was then added to the N$^\alpha$-deprotected peptide resin. Coupling was performed for 90min. A second activation/coupling cycle was also performed using the same protocol. Coupling efficiency was estimated by Kaiser test and as usual a capping step was performed (Ac$_2$O/DIEA in DMF 10-fold molar excess).

3.2.1.2 Coupling of N-methyl residues and on N-methyl residues

For the coupling of N-methyl (N-Me) residues the standard TBTU protocol was used as described on Table 9. Coupling times were altered and were often longer (60min instead of 40 min) compared to the non-N-methylated amino-acids. Coupling of amino acids on N-methyl residues was more difficult due to the steric hindrance caused by the N-Me residue on the amino group. In these cases, coupling with HATU was performed for 60min. The coupling efficiency was estimated by chloranil test[112], where

secondary amines could be observed. Thereafter, a capping step (Ac$_2$O/DIEA in DMF, 10-fold molar excess) was performed.

3.2.1.3 **Kaiser test**
The Kaiser test is a qualitative colorimetric test for determining the presence or absence of free primary amino groups on a peptide resin (following deprotection and coupling steps)[113].The following three solutions are prepared:
- Ninhydrin in ethanol (5gr in 100ml ethanol)
- Phenol in ethanol (40gr in 10ml ethanol)
- An aqueous solution of potassium cyanide in pyridine (2ml of aqueous 0.001M KCN in 100ml pyridine)

A small sample of resin is placed into a glass test tube and two drops of each of the above solutions are then added to the resin and the mixture is mixed thoroughly and heated at 110°C for 5min. In the case where the solution remains yellow and the resin beads white, then the test is considered as negative for the presence of the free amino group. If the colour of the beads, solution, or both turn to blue-purple, the test is considered positive while it is required a recoupling of free amino groups to the resin. The ninhydrin reacts with the amino acids in a transamination-decarboxylation reaction and gives a blue-purple dye known as Ruhemann's purple[115].

3.2.1.4 **Acetaldehyde/Chloranil test**
Notably, the Kaiser test detects only primary amino groups, which means that in the case of Pro- or N-methylated amino acids it could not be applied. In such cases the acetaldehyde/chloranil test was performed[112]. For the acetaldehyde/chloranil test the following two solutions are prepared:
- 2% acetaldehyde in DMF (A)
- 2% chloranil in DMF (B)

Thereafter, few beads of the peptide resin were added to the small test tube and two drops of saturated solution (B) and two drops of solution (A). After short mixing at room temperature, the beads were inspected. The positive test gave a dark-blue green colour in the beads, which indicated the free amino-group, while colourless beads indicate that the coupling has been accomplished. The detection of secondary amines was important for the synthesis of all peptides, since the successful couplings of AA to N-methylated amino-acids could be controlled only by the acetaldehyde/chloranil test. The sensitivity of both tests decreases with the length of the peptide attached to the resin. Thus for medium to small peptides up to 15 amino acid residues the accuracy is sufficient, but for longer sequences the results are often misleading[116].

3.2.1.5 **Final deprotection of side chain and peptide cleavage from the resin**
In Fmoc-SPPS this step is normally carried out by treating the peptidyl resin with TFA solution. The most popular is reagent K (TFA/water/phenol/thioanisole/EDT, ([82.5:5:5:5:2.5]), which also was used with a slight modification in the cases where EDT was found to be added to a part of the peptides. For these cases the cocktail mixture that used was: TFA/water/phenol/thioanisole, ([85:5:5:5]). Cleavage of the peptide resin was carried out using 20-50mg resin per 1ml reagent K, shaking for 3h at room temperature. When the incubation time is finished the cleavage, solution is transferred into the centrifugation tube, containing water. The aqueous solution was then extracted with cold diethyl-ether (three times for 2min at 4ºC). Thereafter, the aqueous layer was lyophilized.

3.2.1.6 **Side-chain to side-chain cyclization**

The cyclization reactions were performed with two different methods, depending on the peptide and the final cyclic peptide to be obtained. Method (1): Cyclization via disulfide bridge formation (via DMSO or DMSO/H_2O_2)[117]. The formation of disulfide bond of the two cysteines, using DMSO as an oxidant is described in Figure 17. This method has been used in aqueous and aqueous/organic media in the pH range from 1 to 8.
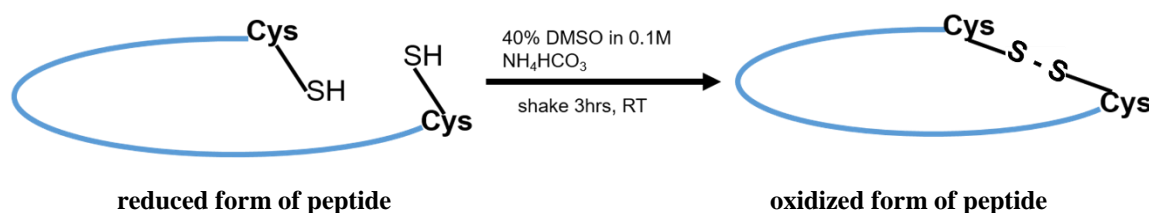
Figure 18. Oxidation of via DMSO. Oxidation of two cysteine molecules to form a disfulfide bond in cc-R3-GI.

Therefore, 1mg of crude peptide is dissolved in a solution containing 400µl of DMSO and 600µl of aqueous 0.1M NH_4HCO_3, pH 8 and the solution was stirred for 3h.

In case of very hydrophobic peptides oxidation was accomplished by a mixture of DMSO, H_2O, H_2O_2. 1mg of crude peptide was dissolved in a mixture of 300µl DMSO, 500µl H_2O and 300µl H_2O_2 (Figure 18). The mixture was immediately subjected to RP-HPLC for purification.
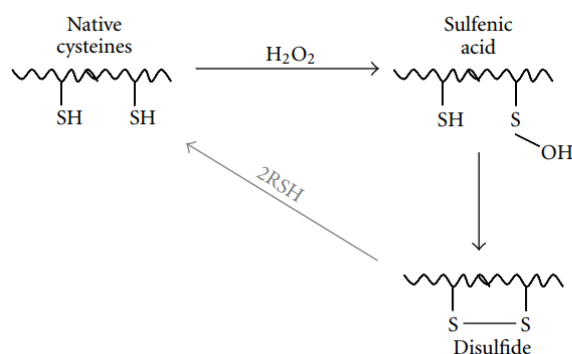
Figure 19. Formation of intramolecular disulfide bonds (S–S) by H_2O_2 mediated oxidation. Oxidation of a cysteine thiol by H_2O_2 yields a sulfenic acid that can undergo a reaction with a neighbouring "back door" cysteine thiol to generate a disulfide linkage (S–S) (picture taken from Sivaramakrishnan et al. ref.[118]).

Cyclization of two analogues was done by the method (2): i.e. a cysteine crosslinking-based "stapling" strategy. Cyclization of biscysteine-containing peptides with bifunctional linkers is usually carried out in solution phase with unprotected peptides[111, 119]. Mechanistically it occurs in two steps: first, one cysteine reacts with the linker to form a linear monothioether intermediate, followed by intramolecular ring closure between the second cysteine and the linker to give the final cyclic bisthioether-linked peptide. In particularly, the side-chains of cysteine residues are covalently connected with two different cross-linkers; Linker 1: dibromo-p-xylene for cc-L1-R3-GI and Linker 2: 4,4´-Bis(bromomethyl)biphenyl) for cc-L2-R3-GI analogues. Figure 19 is shows a general reaction for formation of two "stapled" analogues. For the cc-L1-R3-GI analogue synthesis 500µg pure peptide was dissolved in 500µl solution, consisting of 200µl of 1M NH_4HCO_3 (pH 8) and 300µl DMF and 3eq Linker 1 (in DMF) were added to the solution, which was stirred for 2h. For the synthesis of cc-L2-R3-GI 2mg crude peptide was dissolved in 8ml solution, consisting of 2ml of 10mM NH_4HCO_3 (pH 8), 1eq DTT, 6eq Linker 2 (in DMF) and 6ml DMF. The reaction was stirred for 3h.
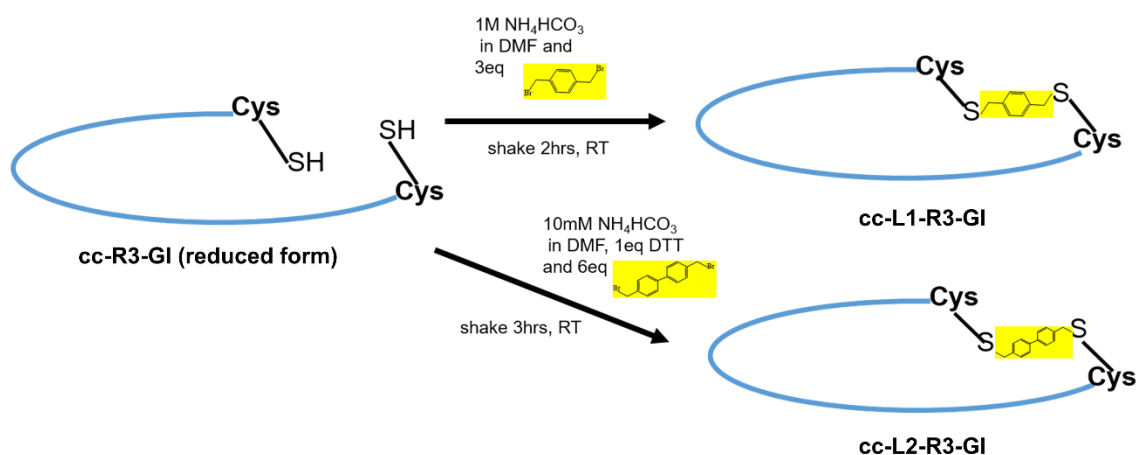
Figure 20. General reaction for the formation of the two "stapled" analogues. Formation of cc-L1-R3-GI and cc-L2-R3-GI, using Linker 1 and Linker 2.

3.2.1.7 N-terminal labeling of peptides with carboxyfluorescein

In order to study the binding properties of the synthesized peptides they were N-terminally linked to carboxyfluorescein (Fluos). Therefore, 20mg of peptide resin were weighed into a 2ml syringe and after Fmoc-deprotection with 25% piperidine in DMF (20min) and subsequent washing with DMF (3 times, 1min each), coupling of 3eq Fluos, 3eq HATU and 4.5eq DIEA in DMF was performed. The coupling mixture was added to the resin and agitated for 2h. Couplings were performed in twice. The cleavage of the fluorescein-peptide was accomplished according to paragraph 3.2.1.5.

3.2.2   Purification and characterization of peptides

3.2.2.1 Reversed-phase HPLC (RP-HPLC)

Reversed-phase HPLC (RP-HPLC) uses a hydrophobic stationary phase to separate the peptides from impurities according to their hydrophobicity. Purification of the products (Aβ40, IAPP analogues and fragments) was carried out by RP-HPLC on a C18 Nucleosil column with a length of 25cm, internal diameter of 8mm and 7μm particle size and a pre-column Nucleosil 100 C18 with a length of 33mm. The flow rate was 2ml/min and eluting buffers were:

- Buffer A: 0.058% (v/v) TFA in water
- Buffer B: 0.05% (v/v) TFA in 90%ACN/water

Peptides were detected at 214nm and the gradient programs that were applied are shown in Table 10. Eluates containing peptide peaks were immediately frozen in dry ice and lyophilized.

Table 10. The usually applied HPLC-gradient programs to purify the synhetic-peptides.

HPLC-programs Number/Name	Time (min)	Buffer A	Buffer B
1. "Fast Aβ"	0	90%	10%
	1	90%	10%
	31	10%	90%
2. "Fast-Fast Aβ"	0	90%	10%
	1	90%	10%
	11	10%	90%
3. "Fast stay at 100%B 10min"	0	90%	10%
	1	90%	10%
	20	0.0	100%
	30	0.0	100%
	31	90%	10%

3.2.2.2 **Laser desorption ionization mass spectroscopy (MALDI-TOF)**

This technique is used to identify the synthesized peptides by detecting the correct mass in the spectrum. A sample of lyophilized peptide was dissolved in a solution of 30% acetonitrile and 0.1% TFA in ddH$_2$O and then mixed (1:1) with a saturated solution of a cyano-4-hydroxycinnamic acid (HCCA) in 30% ACN 0.1% TFA (matrix). 0.5μl of the mixture was placed on the target, dried and then the spot was washed with 10mM NH$_4$H$_2$PO$_4$ in ddH$_2$O with 0.1% TFA to quench the signal of adduct ions (such as Na$^+$, K$^+$ etc.). The mass was recorded on positive ion mode and monoisotopic mass was determined as [M+H$^+$] (M is monoisotopic mass). The fluorescein labeled-peptides were dissolved in 97% acetone and 0.1% TFA in ddH$_2$O and mixed (1:1) with 97% acetone 0.1% TFA matrix solution.

3.2.3 **Preparation of the stocks and concentration determination**

1. Preparation of Aβ40 stock solution

Synthetic Aβ40 was dissolved at 1mg/ml in a mixture of 72% ACN in water containing 0.004% TFA, made aliquots, lyophilized and stored at -20ºC. Concentrations of Aβ40 were determined using the bicinchoninic acid assay (BCA). Aβ40 stocks were freshly made with HFIP (1mg/1ml) on ice, stocks were kept on ice and used within few hours.

2. Preparation of IAPP stock solution

Synthetic IAPP was oxidized, purified and stored at -20ºC. IAPP stocks were made by dissolving IAPP in HFIP (C≤350μM). Solutions were filtered (0.2μm). The absorbance at 274nm was used to determine the exact IAPP concentration with an extinction coefficient in HFIP $\varepsilon_{274} = 1440M^{-1}cm^{-1}$. Concentration calculated from the Lambert-Beer law by UV

3. Preparation of stock solution of IAPP-segments

1mg of IAPP segment was dissolved in a mixture of 72% ACN in water containing 0.004% TFA, aliquoted, lyophilized and stored at -20ºC.

4.   Preparation of fluorescein-labeled (Fluos-labeled) peptides and Dac-Aβ40 using UV spectroscopy

HPLC-purified peptide was dissolved in HFIP and filtered (0.2µm). UV absorbance of the peptide solution was measured between 200 and 600nm and the absorbance at 432nm (for Fluos-labeled peptides) or 445nm (for Dac-Aβ40) was used to determine the exact peptide concentration. At this wavelength, the extinction coefficient in HFIP was determined to be $\varepsilon_{432} = 22770M^{-1}cm^{-1}$, $\varepsilon_{445} = 75940M^{-1}cm^{-1}$ [120]. Concentrations were calculated from the Lambert-Beer law.

5.   Determination of peptide concentration via bicinchoninic acid (BCA) protein assay[121]

The BCA Protein assay combines the reduction of Cu^{+2} to Cu^{+1} by a protein in an alkaline medium with the highly sensitive and selective colorimetric detection of the Cu^{+1} by BCA. The BCA/Cu complex exhibits a strong linear absorbance at 562nm with the increasing protein concentrations. The kit was used to determine the exact amount of Aβ40, which was obtained after HPLC purification.

6.   Determination of peptide concentration via Bio-Rad protein assay[121]

The Bio-Rad protein assay is a simple colorimetric assay for measuring total protein concentration and is based on the Bradford dye-binding method (Bradford 1976). The Bio-Rad protein assay is based on the colour change of Coomassie brilliant blue G-250 dye in response to various concentrations of protein, the dye binds to primarily basic (especially arginine and cysteine) and aromatic amino acid residues (tryptophan and tyrosine).

3.2.4   Thioflavin T (ThT) binding assays

Thioflavin-T binding assay allows the monitoring of fibril formation. It is based on the binding of the dye Thioflavin-T (ThT) to fibrils resulting in fluorescence shift and enhancement of fluorescence emission[122]. ThT binding was measured for Aβ40 (16.5µM), Aβ42 (16.5µM) or IAPP (6µM) incubations alone and with their mixtures with peptides at different concentration ratios, which were made in ThT assay buffer consisted of aqueous 50mM sodium phosphate buffer, pH 7.4, containing 100mM NaCl and 1% HFIP (Aβ40(42) related studies) or 0.5% HFIP (IAPP related studies). Incubations were performed at room temperature and kinetics of fibrillogenesis were followed up to seven days. At the indicated time points, aliquots of the solutions were mixed with the Thioflavin T solution (20µM ThT in 0.05M glycine/NaOH, pH 8.5) and ThT binding was determined immediately by measuring fluorescence emission at 486nm upon excitation at 450nm using a 2030 Multilabel Reader VictorX3 (PerkinElmer Life Sciences)[67, 70, 87].

3.2.5   Assessment of cytotoxicity via the MTT reduction assay

The MTT reduction assay allows quantification of metabolically active cells. These are able to reduce MTT, a tetrazolium salt, to an insoluble formazan product[123], which can be quantified by measuring absorbance at 570nm. In this work the MTT reduction assay is used to detect cytotoxicity of aggregates formed by Aβ40(42) and IAPP and the effects of potential inhibitors. PC-12 cells are pheochromocytoma cancer cells from adrenal medulla granules from rats[124]. PC-12 cells were cultured in RPMI 1640 medium containing 10% heat-inactivated horse serum, 5% fetal calf serum and penicilin/streptomycin (25U/ml). 24h prior to the cell viability assay, PC-12 cells were trypsinized and plated at a density of 1×10^5 cells/ml in polylysine coated 96-well plates. At the indicated time points, aliquots from peptide incubations were diluted with cell culture medium and added to the cells at the indicated final concentrations. PC-12 cells were first incubated with 3-[4,5-dimethylthiazol-2-yl]-2,5-diphenyltetrazolium bromide (MTT) (1mg/ml) for 90min at 37°C. Thereafter, cell lysis buffer (10% SDS in 20mM HCl, pH 4.5) was added to each well. The plate was sealed with parafilm and shaken overnight. The absorbance was measured at 570nm after 24h with a 2030 Multilabel Reader VictorX3. All Aβ40 cell viability studies were performed in combination with the ThT assays. Incubations of

Aβ40 (16.5μM) with inhibitors at different concentration ratios made in ThT assay buffer (50mM sodium phosphate buffer, pH 7.4, containing 100mM NaCl and 1% HFIP). Solutions were added to PC-12 cells (at final concentrations between 1μM and 1nM) at various time points of incubation process as indicated, using peptide solutions incubated for 3d and 7d.

The IAPP cytotoxicity was determined similarly. However, the assay is performed after 24h and 7d (168h) using RINm5F cells[125]. RINm5f cells were cultured in RPMI 1640 medium containing 10% heat-inactivated calf serum, 2mM L-glutamine, 100U/ml penicillin/streptomycin 0.1mM not essential amino-acid (NEAA), 1mg/1ml glucose and 1mM sodium pyruvate. RINm5f cells were trypsinized and plated at a density of 7×10^5 cells/ml 96-well plates. Incubations of IAPP (6μM) with inhibitors in different concentration ratios were made in ThT assay buffer (50mM sodium phosphate buffer, pH 7.4, containing 100mM NaCl and 0.5% HFIP). Incubations were performed at room temperature and added to RINm5F cells (at final concentrations between 500nM and 0.1nM) at various time points. The plate was incubated for 24h at 37°C after pipetting the incubations to the cells. RINm5f cells were then incubated with 3-[4,5-dimethylthiazol-2-yl]-2,5-diphenyltetrazolium bromide (MTT) (1mg/ml) for 2h at 37°C. Thereafter, the entire solution was removed and 100μl of a solution of 0.04M HCl in isopropanol were added. After 10min of shaking, 100μl of ddH$_2$O was added and mixed and the MTT absorbance at 570nm was measured with a 2030 Multilabel Reader VictorX3.

Complete inhibition of metabolic stability (0% cell viability) was defined as the absorbance value obtained in wells containing 0.1% Triton X-100 in H$_2$O. 100% MTT reduction was defined as the absorbance value obtained in wells containing vehicle alone. To analyze the results of the assay, the absorbance values were normalized according to the following formula:

$$\% \text{ MTT reduction} = \frac{\text{Abs(sample)} - \text{Abs(0.1\% Triton)}}{\text{Abs(medium)} - \text{Abs(0.1\% Triton)}} \times 100\%$$

Abs: Absorbance value obtained in wells

To determine IC$_{50}$ values, Aβ40 (500nM) or IAPP (100nM) were titrated with different amounts of peptides under the conditions of the ThT binding assays and cell-damaging effects were determined using 24h-aged solutions (IAPP related effects) or 72h-aged solutions or 7d-aged solutions (Aβ40 related effects) by the MTT assay as described[67, 70, 87].

3.2.6 Insulin oligomerization assay

Insulin isolated from bovine pancreas was dissolved in 80% HPLC-buffer B (1mg/1ml), aliquots were made and then lyophilized. Firstly, 200μM insulin stock solution in H$_2$O/HCl pH 2 has been made and this was then diluted with the same solution to a final concentration of 20μM[71b]. In order to study the inhibitory effects of ISMs on insulin oligomerization, 20μM stock solution of insulin was added to dry peptide (5-fold excess). Solutions were incubated at 60°C for 24h or 48h.

At the indicated time points aliquots were mixed with NuPAGE buffer (13μL) without reducing agent at room temperature and then subjected to NuPAGE electrophoresis at 200V in NuPAGE/XCell without any boiling procedure using 4-12% Bis-Tris gels with MES running buffer according to the manufacturer's recommendations (Invitrogen). Equal amounts of insulin (5μg) were loaded throughout all lanes. Peptides were blotted onto nitrocellulose using a XCell II Blot Module blotting system (Invitrogen). Insulin containing bands (mono-, oligo-, and multimers) were revealed by Western blotting using a monoclonal mouse anti-insulin antibody (Sigma-Aldrich) in combination with peroxidase (POD)-coupled secondary antibody (goat anti-mouse IgG-POD) (Pierce) and the Super Signal Duration ECL staining solution (ThermoFischer Scientific) at LAS 3000 Image Reader (Fujifilm, Düsseldorf). A molecular weight marker ranging from 3-185kDa (Invitrogen) was run in the same gels[71b].

3.2.7 **Peptide stability in human plasma (*in vitro*)**

These assays were performed using a previously established assay system[72]. Accordingly, peptides were dissolved in human blood plasma (obtained from voluntary healthy donors) at a concentration of 200μM and incubated at 37°C for various time intervals. Following quenching (1/1) with aqueous trichloroacetic acid (10%), solutions were incubated on ice for 10 min, subjected to centrifugation to precipitate plasma proteins (20200g; 4min), and the supernatants were mixed (1/2) with a solution consisting of 80% HPLC buffer B and 20% HPLC buffer A. To quantify intact peptide at different time points, solutions containing the supernatants were analyzed by RP-HPLC (detection at 214nm) by using a Nucleosil 100 C18 column (Grace) (length 33mm length, ID 8mm, 7μm particle size) with a flow rate of 2.0 ml/min and eluting buffers A, 0.058% (v/v) TFA in water, and B, 0.05% (v/v) TFA in 90% (v/v) CH_3CN in water[126] The elution gradient was 10-90% B in A over 8min; this step was followed by a 90-10% B in A over 3min step to establish starting conditions. HPLC fractions were collected, lyophilized, and analyzed by MALDI-TOF-MS using a Bruker Daltonik MALDI-TOF MS instrument.

3.2.8 **Spectroscopic methods**

1.   UV/Vis -spectroscopy

The exact concentration of IAPP and other peptides (see paragraph 3.2.3) was determined by UV-spectroscopy with a Jasco V630 spectrophotometer. Peptide concentrations (C) were calculated according to the Beer-Lambert law: $A = \varepsilon \times c \times b$,

A = absorbance, ε = molar extinction coefficient, c = molar concentration, b = path length

2.   Fluorescence spectroscopy

A JASCO FP-6500 fluorescence spectrophotometer was used for the fluorescence spectroscopic titrations, which were performed by using previously described experimental protocols[68, 70, 72, 86b]. Briefly, for titrations of Fluos-IAPP and Fitc-labeled Aβ42, excitation was at 492nm and fluorescence emission spectra were recorded between 500 and 600nm, while for titrations of Dac-Aβ40, excitation was at 430nm and emission spectra were collected between 440 and 550nm. App. K_ds of interactions of IAPP, Aβ40 and Aβ42 with the peptides were determined by titrating freshly made solutions of Fluos-IAPP (5nM), Dac-Aβ40 (10nM) and Fitc-Aβ42 (5nM) with peptides as described[68, 70, 72, 86b]. Of note, this assay system has been previously used for the determination of the affinities (app. K_ds) of interactions of a number of inhibitors of IAPP and Aβ40(42) amyloid self-assembly with these highly amyloidogenic polypeptides and the affinity of the Aβ40(42)-IAPP interactions as well[68, 70, 72, 86b]. Briefly, freshly made stock solutions of peptides and fluorescently labeled analogs in HFIP were used[68, 70, 72, 86b]. Measurements were performed in 10mM sodium phosphate buffer, pH 7.4 (1% HFIP) at room temperature within 2-5min following solution preparation. Under these experimental conditions, freshly made solutions of Fluos-IAPP, Dac-Aβ40 and Fitc-Aβ42 at the applied low nanomolar concentrations contained mostly monomers[68, 70, 72, 86b]. App. K_ds were estimated using 1/1 binding models as previously described[68, 70, 72, 86b]. Of note, due to the inherently high self-assembly potentials of IAPP-derived peptides more complex binding models may also apply[68, 70, 72, 86b]. Determined app. K_ds are means ($\pm$SD) from three binding curves and were estimated using 1/1 binding models. Sigmoidal curve fittings and estimation of affinities of interactions (app. K_d) were performed with Origin software using:

$$F = F_0 + \frac{F_{max} - F_0}{1 + 10^{[(\log K_d - L) \cdot m]}}$$

F: fluorescence intensity
F_0: fluorescence intensity of the Fluos-labeled peptide
F_{max}: maximal fluorescence intensity
$\log K_d$: logarithm of the dissociation constant

L: concentration of the ligand
m: slope of the curve

In case that the calculated K_d is below 100nM, a second formula was applied using the Grafit software to calculate the dissociation constant:

$$F = F_{min} + (F_{max} - F_{min}) \cdot \frac{\frac{[E_0] + [L_0] + [K_D]}{2} - \sqrt{\frac{([E_0] + [L_0] + [K_D])^2}{4} - [E_0] \cdot [L_0]}}{[L_0]} + S \cdot [E_0]$$

F: fluorescence emission
F$_{min/max}$: minimal fluorescence emission /maximal fluorescence emission
L$_0$: concentration of the labeled peptide
E$_0$: concentration of the unlabeled peptide
S: slope
K$_d$: dissociation constant (app. K_d)

3.   <u>CD-spectroscopy</u>

Peptides are optically active substances since firstly any amino acid, except for glycine, has an optically active carbon atom. Furthermore, their overall conformation shows chirality in the form of α-helices and β-sheets. CD spectrum of peptides appear in two spectral regions. In the far UV range (170nm to 250nm), which is characteristic absorption of peptide bonds, and in the near UV range (250nm to 300nm), characteristic CD spectrum for aromatic amino acids. The CD spectrum of an α-helix shows two negative minima at 207 and 222nm and a positive at 192nm. Peptides containing a minimum at 215 to 220nm, and a maximum at 195nm, have β-sheet conformation. The disordered conformation of a peptide provides a negative CD minimum at 195nm. The measurement of the circular dichroism in the absorption range of the aromatic side chains can reveal the tertiary structure of the given protein[127].

Table 11. CD spectra of different secondary structure elements.

Structure element	Properties of the CD spectrum
α-Helix	Minimum at 222 and 208nm; maximum at around 192nm
β-Sheet/β-turn	Minimum at 216nm; Maximum at 195nm
Random coil	Negative CD area below 200nm
Disulfide bond β-Sheet/β-turn	Weak signals around 260nm

Data taken from Kelly et al. ref[127].

CD measurements were performed with a Jasco 715 spectropolarimeter as described. Spectra were measured immediately following solution preparation between 195 and 250nm, at 0.1nm intervals, a response time of 1sec, each spectrum being the average of three spectra and at room temperature. CD measurements were performed using freshly made solutions of peptides in aqueous 10mM sodium phosphate buffer, pH 7.4, containing 1% HFIP (CD assay buffer); peptides were diluted from freshly made stock solutions in HFIP into the aqueous assay buffer. This assay buffer has been used to study conformation of peptides (several other previously developed inhibitors of IAPP or Aβ40(42) aggregation [68, 70, 72, 86b, 87]. The spectrum of the buffer was subtracted from the CD spectra of the peptide solutions prior conversion of the raw data to mean residue ellipticities (MRE) (deg ×cm^2×dmol^{-1}).

$$MRE \left[\frac{deg \cdot cm^2}{dmol} \right] = \frac{100 \cdot \theta}{c \cdot d \cdot n}$$

Thereby, c is the concentration in mol/L, d is the path length in cm, n is the number of amino acids and θ is the ellipticity in deg. The MRE is the plotted versus the wavelength.

4.   <u>Transmission electron microscopy (TEM)</u>

Transmission electron microscopy (TEM) was performed to verify fibril formation and its inhibition. 10μl aliquots of solutions of the ThT binding and MTT assays were applied on carbon-coated grids at indicated time points, washed with distilled water and stained with aqueous 2% (w/v) uranyl acetate as described[68]. Grids were examined using a JEOL JEM 100CX (at 100kV) or a JEOL 1400 Plus electron microscope (at 120kV).

4.   Results

4.1   Studies on cyclic analogues of full length R3-GI

4.1.1   Peptide design and synthesis

In the first part of my PhD thesis, results are presented on the inhibitory effects of three new cyclic analogues of R3-GI (cyclic ISMs, **cISMs**) on Aβ and IAPP aggregation. In previous studies by Andreetto et al.[87], a "hot-segment"-linking approach has been presented to design a series of IAPP cross-amyloid interaction surface mimics (ISMs) as highly potent inhibitors of amyloid self-assembly of Aβ, IAPP or both polypeptides. R3-GI [IAPP(8-18)-R3-(22-28)-GI] has been found to inhibit only Aβ40(42) but not IAPP[87].
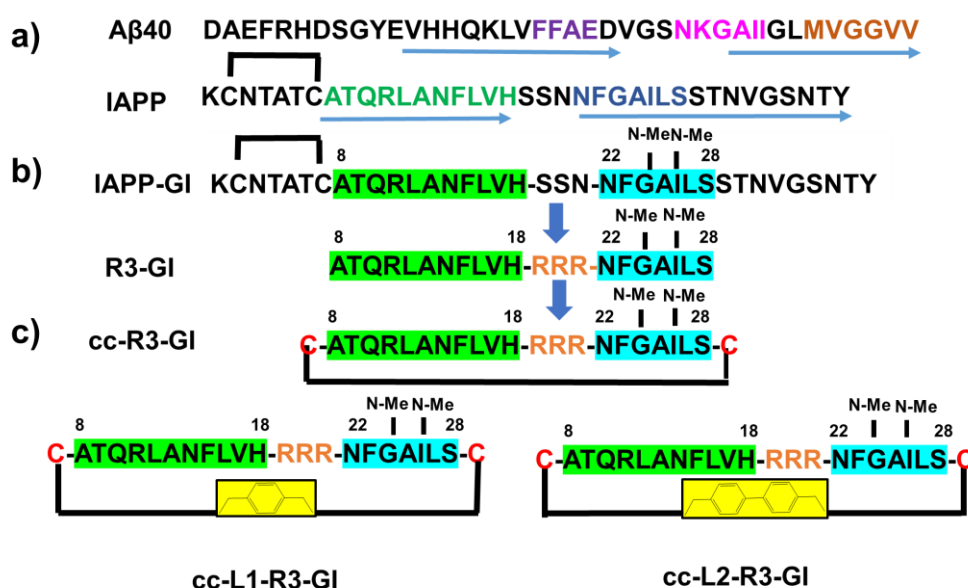
Scheme 2. Design of Cys-bridged R3-GI analogues. (a) Sequences of Aβ40 and IAPP ("hot segments" coloured), (b) ISM design concept (picture modified from Andreetto et al. ref[87], R3-GI is abbreviated based on the name of the residue in the linker tripeptide (Arg) while "-GI" indicates the presence of the N-methyl-residues at G^{24} & I^{26}: "N-Me", (c) rational design of bridging cysteines on R3-GI sequence via cysteine oxidation or crosslinking-based peptide "stapling" strategy, using p-xylene (Linker 1) and 4,4´-Bis(methyl)biphenyl (Linker 2), respectively. Cyclic ISMs (cISMs) were abbreviated based on the abbreviation of R3-GI, while cyclization is indicated by "cc", "red" means reduced form of cysteine containing peptides, L1 and L2, indicates the two different linkers by which the "stapling" is achieved.

The synthesis of the peptides was performed according to the Fmoc-strategy. Crude peptide with cysteines in reduced form (cc-R3-GIred) was purified by RP-HPLC and characterized by MALDI-TOF (Table 12). For disulfide bridge formation, oxidation was performed by stirring cc-R3-GI crude peptide in a mixture of 40% (v/v) DMSO in aqueous NH$_4$HCO$_3$ (0.1mM, pH 8.7) for 3h. cc-R3-GI was purified by RP-HPLC and characterized by MALDI-TOF. Purification could be conducted with a yield of around 30% with respect of crude cc-R3-GI (Table 12).

The purified cc-R3-GIred peptide was then used as basis for the synthesis of the two "stapled" peptides. Accordingly, the side-chains of cysteines were covalently connected using two different cross-linkers: Linker 1 (L1) and Linker 2 (L2). For the synthesis of the first peptide, abbreviated as cc-L1-R3-GI, we used cc-R3-GIred (1eq) and L1 (3eq). Peptide and linker were stirred for 3h in an aqueous solution of NH$_4$HCO$_3$ (1mM, pH 8) and DMF (1:2 (v/v)) (1mg of peptide in 1ml of the previous solution). Reaction was followed by RP-HPLC. The final product (cc-L1-R3-GI) is shown in Scheme 2. After 3h of cyclization, an analytical HPLC run was performed and purification was conducted with a yield of ~5% with regard to cc-R3-GIred (Table 12). The main peak was eluted at 18.7min and detected by MALDI-TOF (Table 12). For the synthesis of the second "stapled" peptide

(cc-L2-R3-GI), cc-R3-GIred peptide (1eq) and L2 (6eq) were mixed in an aqueous solution of NH$_4$HCO$_3$ (10mM, pH 8) and DMF (1:3 (v/v)), containing DTT (1eq) (1mg of peptide in 4ml of the previous solution). Reaction was followed by RP-HPLC and was accomplished after 3h. The final product is shown in Scheme 2. The main peak eluted at 18.8min was found by MALDI-TOF to be the desired product (Table 12). HPLC purification resulted in pure peptide yield of 4% with regard to cc-R3-GIred (Table 12).

Table 12. Characterization of the synthetic "stapled" peptides via HPLC and MALDI-TOF.

Peptide sequence	Peptide abbreviation	HPLC program number	t$_R$ (min)[a]	Yield[b]	[M+H]$^+$ expected[c]	[M+H]$^+$ found[c]
C-ATQRLANFLVHRRRNF(N-Me)GA(N-Me)ILS-C	cc-R3-GIred	1	18.1	40%	2673.39	2673.58
C-ATQRLANFLVHRRRNF(N-Me)GA(N-Me)ILS-C	cc-R3-GI	1	17.8	30%*	2671.39	2671.56
C-ATQRLANFLVHRRRNF(N-Me)GA(N-Me)ILS-C	cc-L1-R3-GI	1	18.7	5%	2775.55	2776.02
C-ATQRLANFLVHRRRNF(N-Me)GA(N-Me)ILS-C	cc-L2-R3-GI	3	18.8	4%	2852.65	2852.30

Peptides were synthesized with free amino-terminal and amidated C-terminal end. [a] t$_R$, HPLC retention time; [b] % yield with regard to cc-R3-GIred or [b*] with regard to crude cc-R3-GI, and [c] monoisotopic molar mass [M+H]$^+$ expected and [M+H]$^+$ found.

4.1.2 **Biophysical characterization**

4.1.2.1 **Conformational studies via CD spectroscopy**

The conformations of the above peptides were determined by CD spectroscopy. Peptides were dissolved in 1×b, pH 7.4 containing 1% HFIP and CD spectra were recorded. CD spectra were measured at different concentrations (5-50μM) to determine aggregation propensies of the peptides.
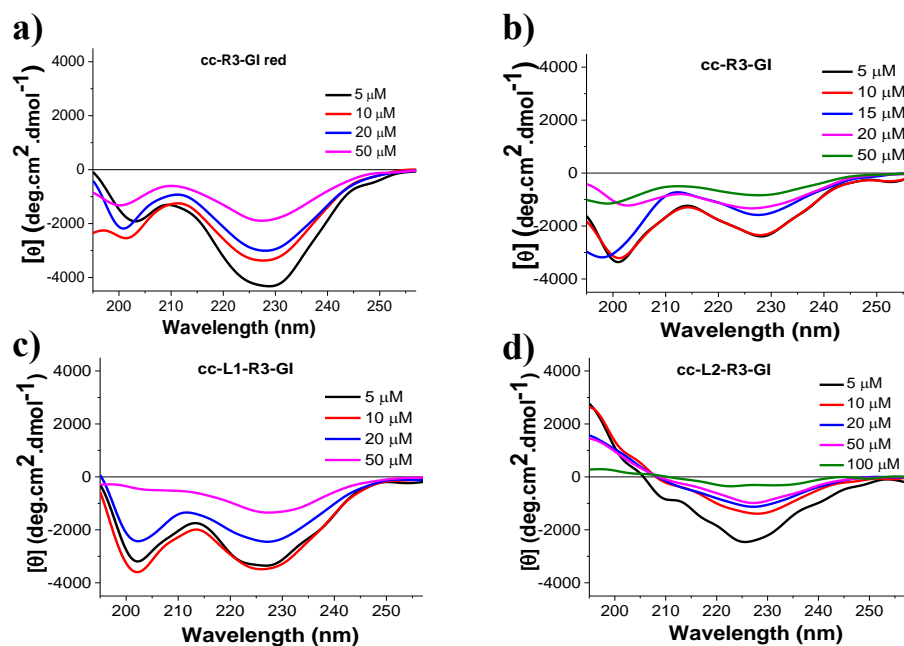
Figure 21. Concentration dependence of CD spectra of linear & cyclic peptides. (a) CD spectra of cc-R3-GIred, (b) cc-R3-GI, (c) cc-L1-R3-GI and (d) cc-L2-R3-GI. Measurements were performed at peptide concentrations between 5-50μM in aq. buffer (1×b), pH 7.4, containing 1% HFIP.

The CD spectra of cc-R3-GIred, cc-R3-GI and cc-L1-R3-GI exhibited two minima: one at 200nm indicative of random coil and a second one at 228nm indicative of β-sheet/β-turn structure (Figure 21a-c). By contrast, the CD spectrum of cc-L2-R3-GI (Figure 21d) exhibited predominantly one strong minimum at 226nm, which indicated mainly β-sheet/β-turn conformation. The c-dependence spectra of cc-R3-GIred, cc-R3-GI, cc-L1-R3-GI analogues indicated that the aggregation started already at 20μM, whereas for cc-L2-R3-GI oligomerization started at lower concentrations $\leq$ 10μM.

4.1.2.2 **Self-association studies via fluorescence spectroscopy**

To quantify the apparent affinity (app. K_d) of the peptides, fluorescence binding assays were performed. App. K_ds of self-assembly of the peptides were determined by titration of freshly made solutions of synthetic N-terminal fluorescein labeled cISM (Fluos-cISM) (5nM) with non-labeled cISM (Figure 22). The measurements were performed in 1×b, pH 7.4 containing 1% HFIP. Binding of 200-fold molar excess of cc-R3-GI and cc-L1-R3-GI to Fluos-cc-R3-GI and to Fluos-cc-L1-R3-GI, respectively caused 35% and 23% fluorescence enhancement (Figures 22a&c). On the other hand, 1000-fold molar excess of cc-L2-R3-GI to Fluos-cc-L2-R3-GI caused 60% enhancement; however, it seems that light scattering effects might be involved (Figure 22e). Sigmoidal binding isotherms were obtained and the app. K_d values were 188.3 ($\pm$76.5) nM for cc-R3-GI and 354 ($\pm$14.4) nM for cc-L1-R3-GI (Figures 22b&d). These data indicated similar self-association propensities for cc-R3-GI and cc-L1-R3-GI. In the case of cc-L2-R3-GI the determined app. K_d value was > 1μM (Figure 22f).

Both cc-R3-GI and cc-L1-R3-GI peptides self-associated in the nanomolar range and their self-association propensities were similar to the self-assembly propensity of both R3-GI and to cc-R3-GI red (Table 13), while cc-L2-R3-GI self-assembled at concentration > 1μM (Table 13).

Table 13. App. K_ds of self-association of linear & cISMs as determined by fluorescence titration studies.

Peptide	app. K_d ($\pm$SD) (nM)[a]
R3-GI	77.1 ($\pm$7.5)
cc-R3-GIred	222 ($\pm$25.6)
cc-R3-GI	188.3 ($\pm$76.5)
cc-L1-R3-GI	354 ($\pm$14.4)
cc-L2-R3-GI	> 1μM

[a] App. K_ds, means ($\pm$SD) from 3 binding curves. Determined by titrations of synthetic N-terminal fluorescein-labeled peptides with non-labeled ones (5nM; aq. buffer 1×b, pH 7.4, containing 1% HFIP).
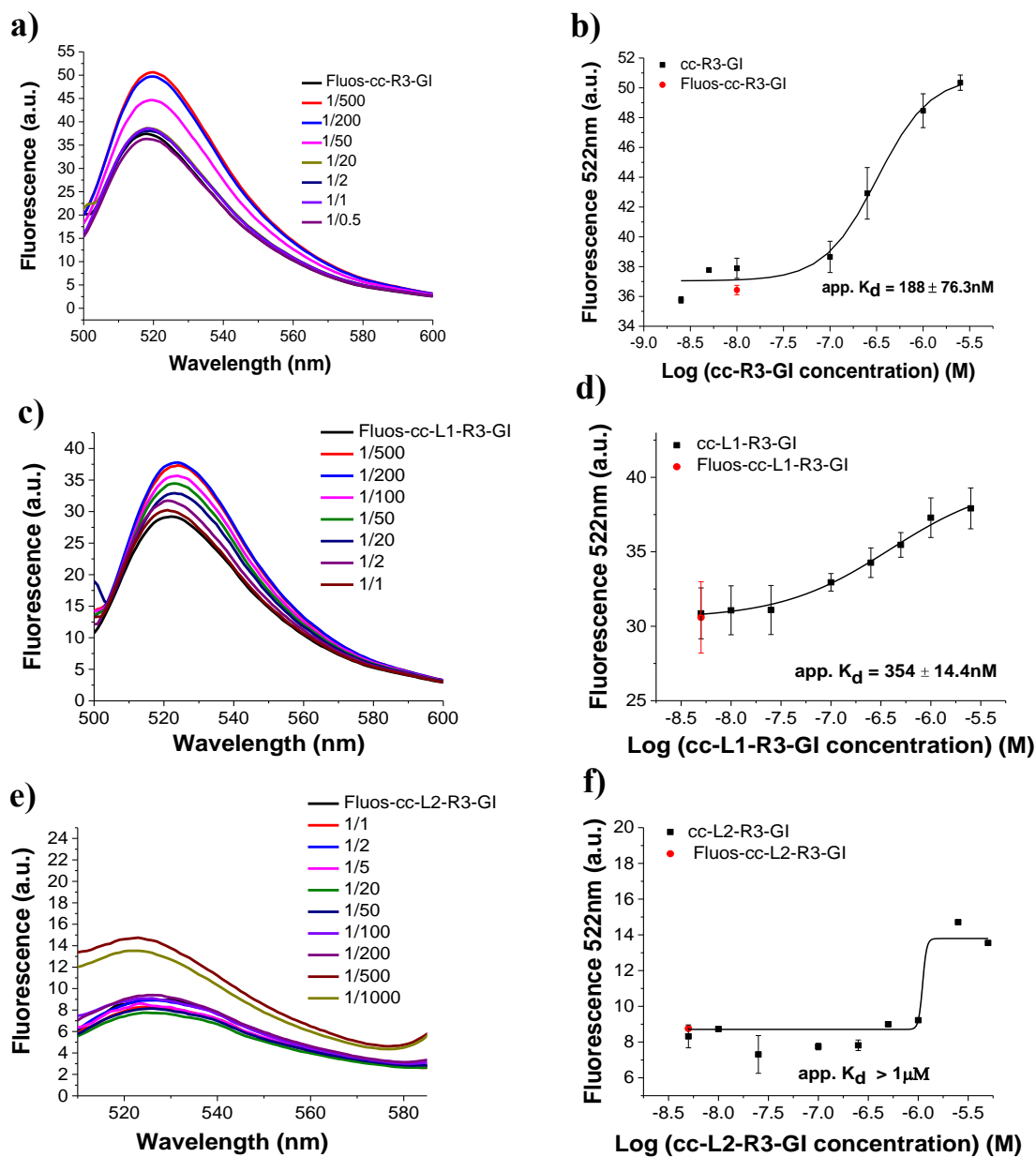
Figure 22. Apparent affinities (app. K$_d$) of self-association of cISMs as determined by fluorescence spectroscopy. Panels a), c), e) show fluorescence spectra of Fluos-cISMs (5nM) alone and its mixtures with various amounts of cc-R3-GI (a), cc-L1-R3-GI (c), cc-L2-R3-GI (e); the molar ratios of Fluos-cISM/cISM are as indicated. Panels b), d), f) show the binding curves of cc-R3-GI (b), cc-L1-R3-GI (d), cc-L2-R3-GI (f); app. K$_d$s are means (±SD) from 3 binding curves (Fluos-cISM 5nM). Measurements were performed in aq. buffer 1×b, pH 7.4, containing 1% HFIP.

4.1.3 **Studies on the inhibitory activities on fibrillogenesis and cytotoxicity of Aβ40 and Aβ42**

Next the question was addressed whether these new cyclic R3-GI analogues could intervene with Aβ40 self-assembly into fibrils and cytotoxic aggregates. Aβ40 alone and 1/1 mixtures of Aβ40 with the peptides were incubated for 7 days and fibrillogenesis and cytotoxicity were followed by the ThT binding and the MTT reduction assay (Figure 23).
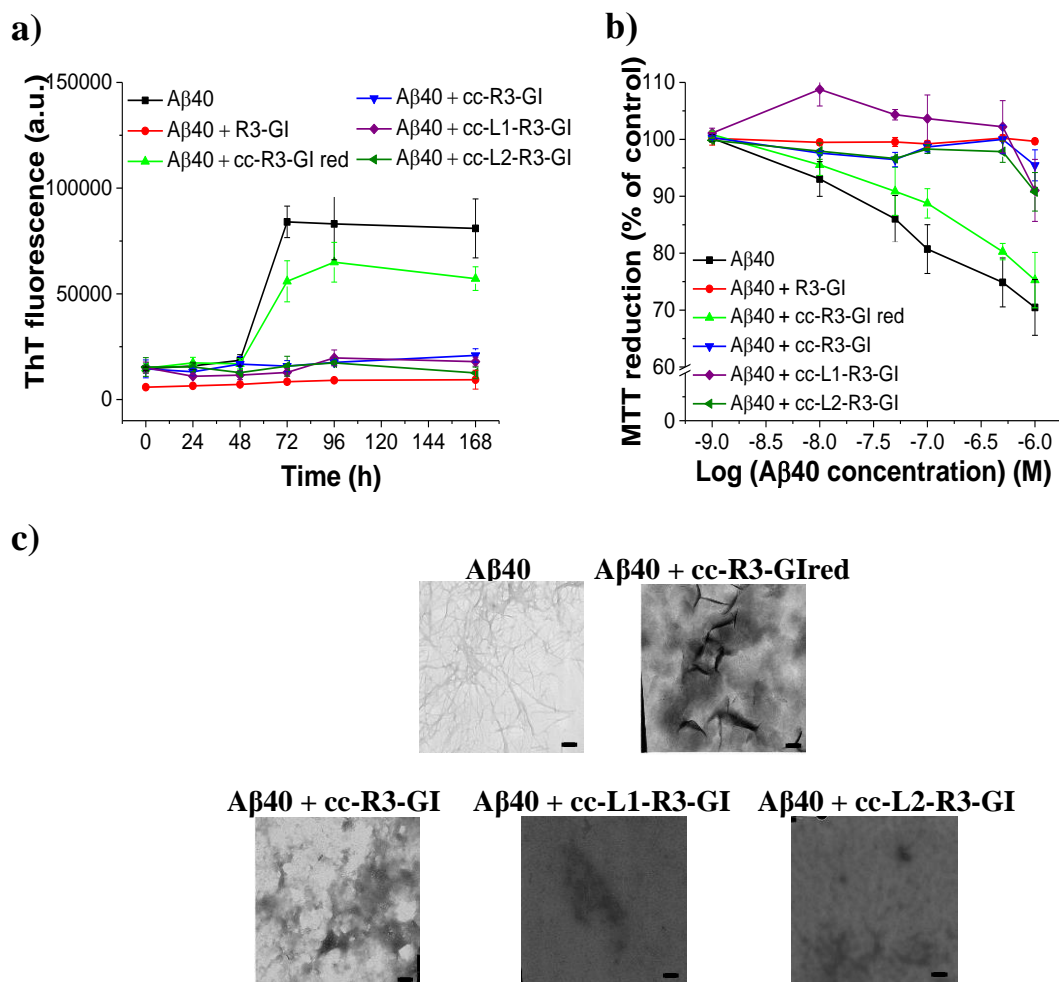
Figure 23. Effects of R3-GI and its cyclic analogues (1/1) on Aβ40 amyloid formation and cytotoxicity. (a) Fibrillogenesis of Aβ40 (16.5μM) or its mixtures (Aβ40/peptide, 1/1) by ThT binding (means (±SD), 3 assays), b) effects on cell viability: solutions from (a) (7 days aged) were added to PC-12 cells; cell damage was determined by MTT reduction (means (±SD), 3 assays (n=3 each)), c) TEM images of Aβ40 and their mixtures with the various analogues (solutions from (a) 7 days aged) (bars, 100nm) (abbrev. cc-R3-GI red: reduced form of cc-R3-GI).

According to the ThT binding assay, Aβ40 fibrillogenesis exhibited a lag time ~ 48h and reached a plateau at 72h (Figure 23a). In the presence of R3-GI, the Aβ40 fibril formation was suppressed, as shown previously[87]. As shown in Figure 23a cc-R3-GIred could not inhibit Aβ40 fibril formation; however, its cyclic analogue cc-R3-GI could decisively do it. Moreover, the two "stapled" peptides (cc-L1-R3-GI, cc-L2-R3-GI) inhibited Aβ40 fibril formation as well (Figure 23a).

To examine whether these cyclic R3-GI analogues may also inhibit formation of cytotoxic Aβ40 aggregates, Aβ40 alone and its mixtures were added to PC-12 cells and cell viability was assessed by the MTT reduction assay. The studies showed that R3-GI inhibited, whereas cc-R3-GIred was unable to suppress Aβ40 cytotoxicity (Figure 23b). However, the respective oxidized peptide cc-R3-GI could inhibit Aβ40 cytotoxicity (Figure 23b). Likewise, the "stapled" analogues cc-L1-R3-GI and

cc-L2-R3-GI inhibited Aβ40 cytotoxicity as well (Figure 23b) as expected from the results of the ThT assay.

The results of the ThT binding assay were confirmed by TEM (Figure23c). In the solutions of Aβ40 and its mixtures with cc-R3-GIred fibrils were found. In contrast, in the solutions of Aβ40 with the cyclic peptides cc-R3-GI, cc-L1-R3-GI and cc-L2-R3-GI mostly amorphous aggregates were found (Figure 23c).

In the following Table 14, the IC_{50}s of the effects of cyclic peptides on Aβ40 toxicity are presented. It was found that the three new cyclic R3-GI analogues had similar IC_{50} values regarding their effects on Aβ40 cytotoxicity and their IC_{50}s were comparable to the IC_{50} of R3-GI (IC_{50} = 116nM) (see Appendix Figure A1).

Table 14. IC_{50} values of inhibitory effects of cISMs on Aβ40 cytotoxicity.

| cISMs	IC_{50} (±SD) (nM)[a]
cc-R3-GI	79.8 (±30.3)
cc-L1-R3-GI	151 (±54.6)
cc-L2-R3-GI	373 (±46)

[a] IC_{50}s, means (±SD) from 3 titration assays (n=3 each); Aβ40 (500nM) was titrated with different amounts of peptides (under ThT experimental conditions) and cell-damaging effects were determined in 72h aged solutions by the MTT reduction assay.

Since cc-R3-GI was a slightly better inhibitor of Aβ40 cytotoxicity, we tested its inhibitory effects when added at pre-or post-nucleation stages of Aβ40 fibrillogenesis as well. Therefore, an Aβ40 incubation was prepared and at indicated time points (0, 24, 48 and 72h) cc-R3-GI was added to it. ThT fluorescence was measured up to 168h of incubation (Figure 24). At 0h and 24h, Aβ40 fibril formation did not start yet; addition of the inhibitor at these time points was able to block fibril formation.
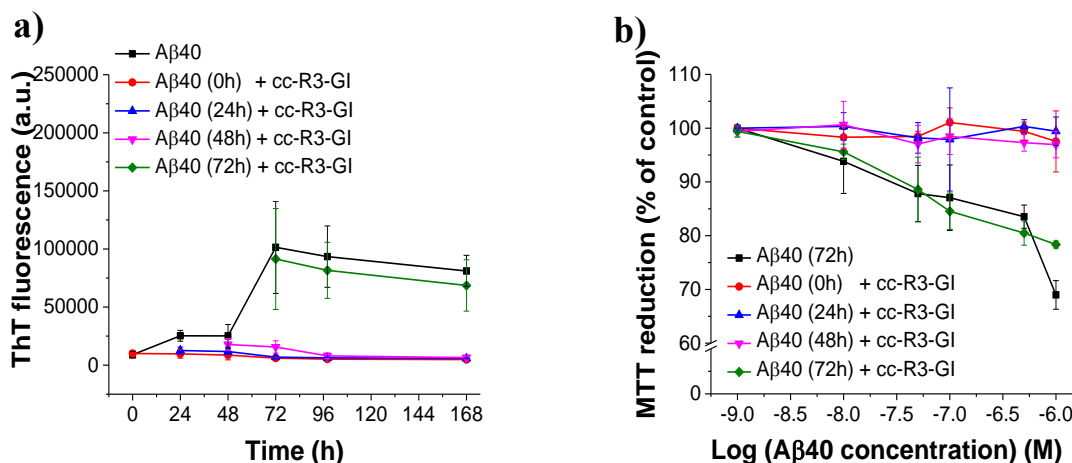
Figure 24. Effects of cc-R3-GI when added at pre- and post-nucleation stages of fibrillogenesis of Aβ40. (a) Effects of cc-R3-GI when added (1/1) before (0h, 24h), at (48h) or after (72h) nucleation on Aβ40 fibrillogenesis (16.5μM) as determined by ThT binding (means (±SD) from 3 assays), (b) effects of cc-R3-GI when added (1/1) before (0h, 24h), at (48h) or after (72h) nucleation on Aβ40 fibrillogenesis (16.5μM) via the MTT reduction assay. Solutions from (a) (3 day-aged) added to PC-12 cells; cell damage determined by MTT reduction (means (±SD), 3 assays (n=3 each)).

After 48h-aging, Aβ40 solution containing fibrils was added to cc-R3-GI and inhibition of Aβ40 fibrillogenesis was also observed. However, when 72h-aged Aβ40 solution containing fibrils was added to the inhibitor, then no inhibition could be observed. Moreover, since no decrease of the ThT fluorescence signal was observed, this indicated that the inhibitor was not able to dissociate already

existing fibrils. It was also investigated, if Aβ40 induced cytotoxicity could be inhibited when cc-R3-GI was added at different time points. Therefore, MTT reduction assays were performed. After the 72h of incubation, inhibition of Aβ40 cytotoxicity was observed only when the inhibitor was added at 0-48h time points (Figure 24b). When the inhibitor was added at later stages of Aβ40 fibrillogenesis, no inhibition of Aβ40 cytotoxicity by cc-R3-GI was found. MTT assays correlated with the results of ThT assay (Figure 24a) and TEM confirmed the findings of the ThT binding assay (see Appendix Figure A2).
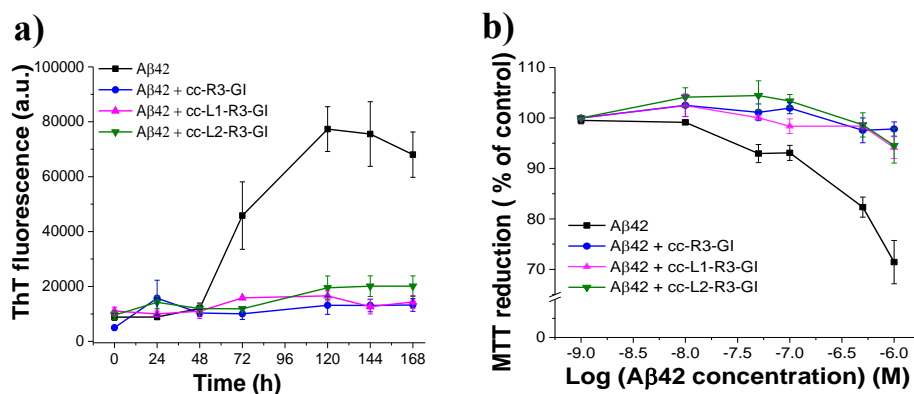
Figure 25. Effects of R3-GI and its cyclic analogues on Aβ42 amyloid formation and cytotoxicity. (a) Fibrillogenesis of Aβ42 (16.5µM) or its mixtures (Aβ42/peptide, 1/1) by ThT binding (means (±SD), n=3), b) effects on cell viability: solutions from (a) (7 days aged) added to PC-12 cells; cell damage determined by MTT reduction (means (±SD), 3 assays (n=3 each)).

Aggregation of Aβ42 has been suggested to play a key role in AD pathogenesis and therefore the above cyclic analogues were tested also with regards to inhibitory effects on Aβ42 fibrillogenesis and cytotoxicity. Aβ42 alone (16.5µM, pH 7.4) and its mixtures with the peptides (16.5µM, pH 7.4) were incubated for 7 days and Aβ42 fibrillogenesis and cytotoxicity were followed by the ThT binding and the MTT reduction assays. All three cyclic Aβ40 inhibitors blocked Aβ42 fibrillogenesis. To evaluate the effects of the cyclic ISMs that inhibited Aβ42 fibrillogenesis on Aβ42-mediated cell damage, 7 days aged solutions (Aβ42 fibrillization plateau; Figure 25a) were added to PC-12 cells and cell viabilities were determined via the MTT reduction assay (Figure 25b). In fact, these cyclic ISMs effectively suppressed formation of Aβ42 cytotoxic assemblies as well.

In conclusion, all three cISMs were found to be potent inhibitors of amyloid formation and cytotoxicity of Aβ40(42).

4.1.4 Determination of binding affinities towards Aβ40(42)

The apparent K_ds of interactions of Aβ40 with cyclic ISMs were determined by titrating synthetic N-terminal fluorescently labeled Aβ40 (7-diethylaminocoumarin-3-carbonyl-Aβ40, abbreviated as Dac-Aβ40) (10nM) with cISMs (Figure 26).

All tested cyclic inhibitors were found to bind with high affinity Dac-Aβ40 and their app. K_ds were in the same range as the one of R3-GI (app. $K_d = 115$nM). These results indicated that there might be a correlation between binding affinities toward Dac-Aβ40 and effects on Aβ40 fibrillogenesis and cytotoxicity (Table 15). On the other hand, all tested cyclic R3-GI analogues (their N-terminal fluos-labeled analogues) showed no binding up to 10µM Aβ40 concentration (data not shown).
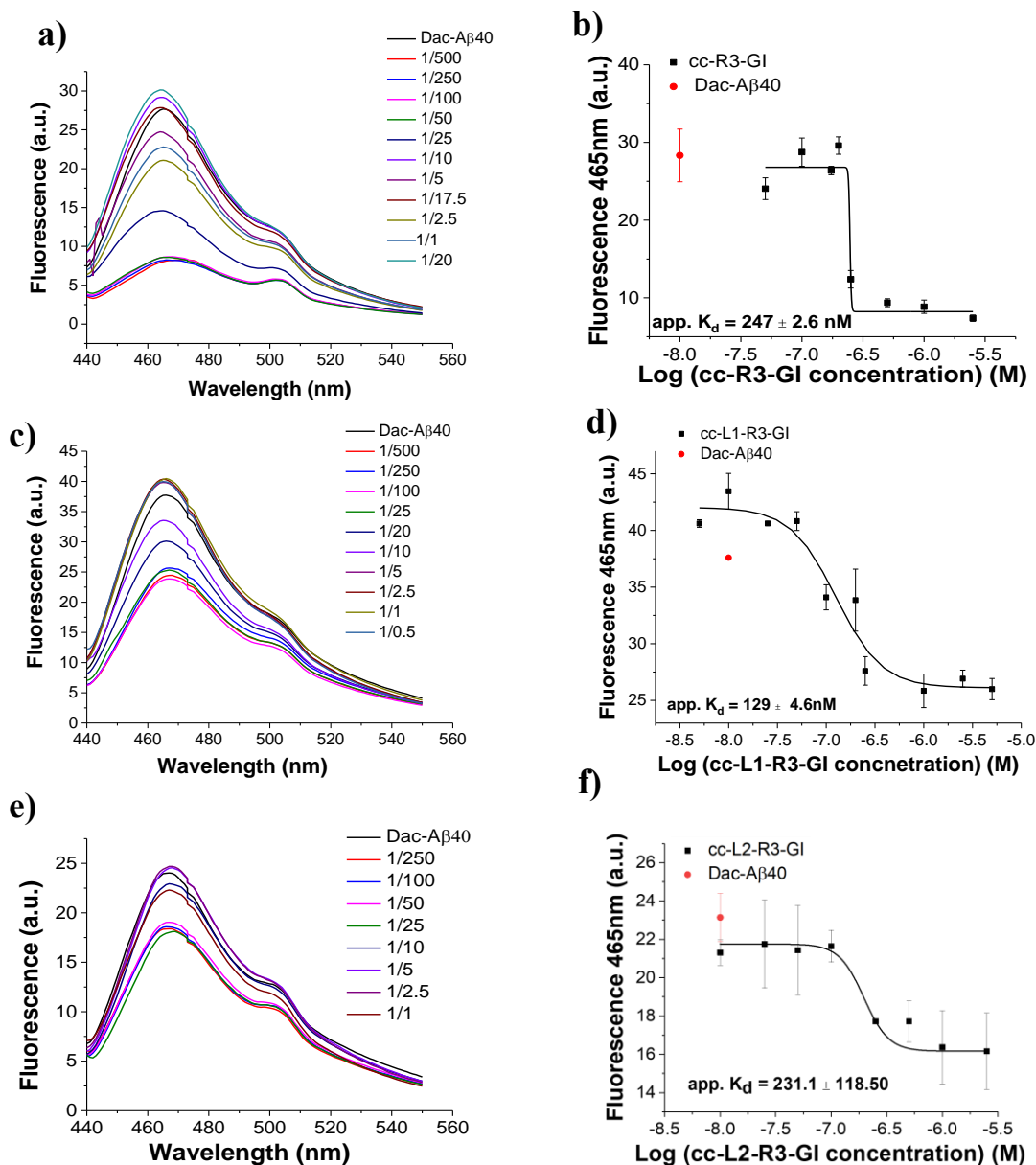
Figure 26. Determination of app. K_ds of interactions of cISMs with Aβ40 by fluorescence spectroscopic titrations. Panels a), c), e) show fluorescence spectra of Dac-Aβ40 (10nM) alone and its mixtures with various amounts of cc-R3-GI (a), cc-L1-R3-GI (c), cc-L2-R3-GI (e); the molar ratios of Dac-Aβ40/cISM are as indicated. Panels b), d), f) show the binding curves of cc-R3-GI (b), cc-L1-R3-GI (d), cc-L2-R3-GI (f); app. K_ds are means (±SD) from 3 binding curves (Dac-Aβ40 10nM). Measurements were performed in aq. buffer 1×b, pH 7.4, containing 1% HFIP.

Next, the interaction of cyclic ISMs with Aβ42 was studied via fluorescence spectroscopy. Fitc-Aβ42 (5nM) was titrated with various amounts of the cyclic R3-GI analogues (Figure 27).
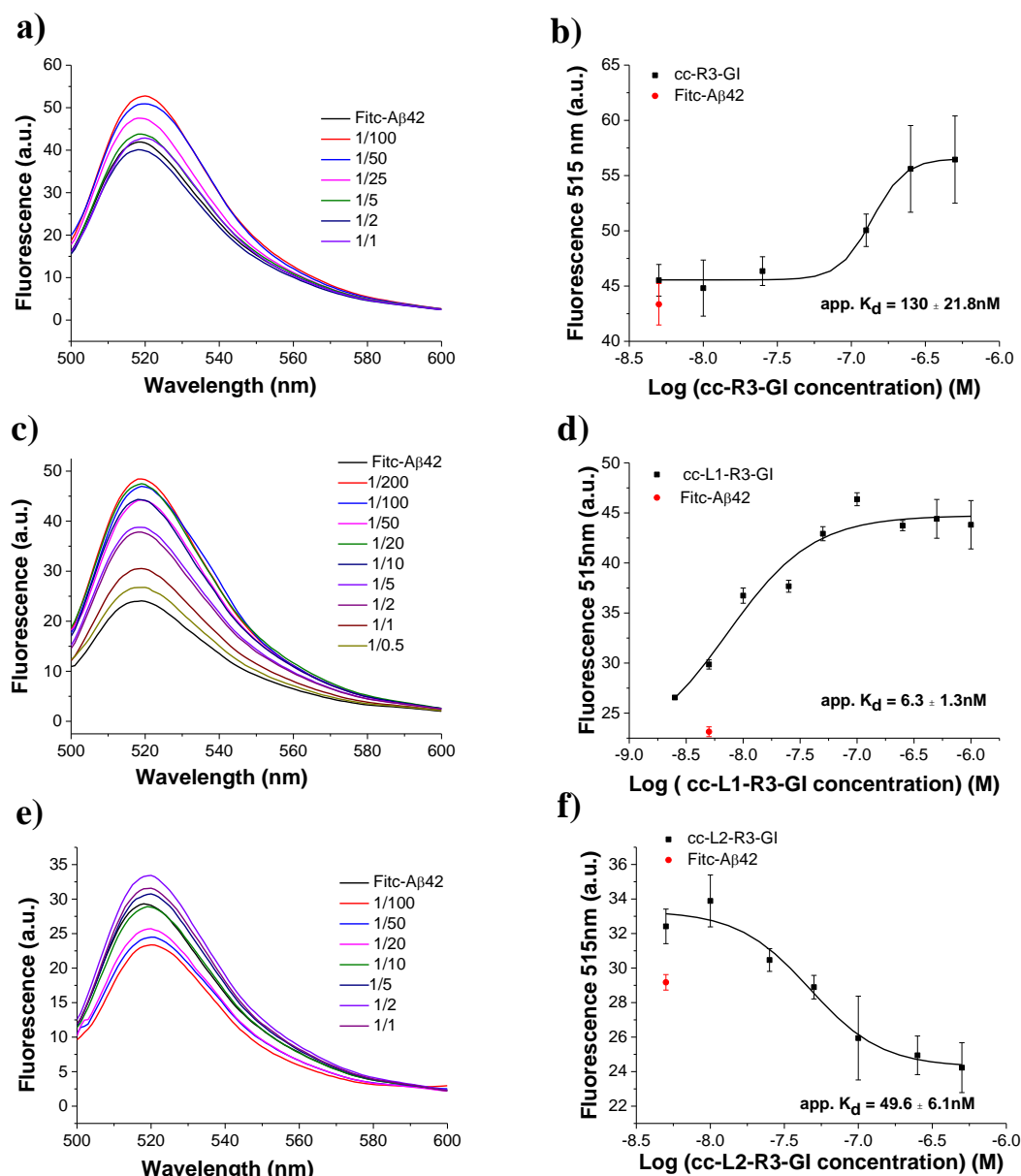
Figure 27. Determination of the K$_d$s of interactions of Aβ42 with cISMS by fluorescence spectroscopy. Panels a), c), e) show fluorescence spectra of Fitc-Aβ42 (5nM) alone and its mixtures with various amounts of cc-R3-GI (a), cc-L1-R3-GI (c), cc-L2-R3-GI (e); the molar ratios of Fitc-Aβ42/cISM are as indicated. Panels b), d), f) show the binding curves of cc-R3-GI (b), cc-L1-R3-GI (d), cc-L2-R3-GI (f); app. K$_d$s are means (±SD) from 3 binding curves (Fitc-Aβ42 5nM). Measurements were performed in aq. buffer 1×b, pH 7.4, containing 1% HFIP.

The three cISMs interacted with Aβ42 with app. K$_d$s in the low nonomolar range (Table 15).

Table 15. Apparent affinities (app. K$_d$s) of interaction of cISMs with Aβ40(42) as determined by fluorescence titration assays.

cISM	app. K$_d$ (±SD) (nM) with Dac-Aβ40[a]	app. K$_d$ (±SD) (nM) with Fitc-Aβ42[a]
cc-R3-GI	247 (±2.6)	130 (±21.8)
cc-L1-R3-GI	129 (±4.6)	6.3 (±1.3)
cc-L2-R3-GI	231.1 (±118.5)	49.6 (±6.1)

[a] App. K$_d$s, means (±SD) from 3 binding curves (Dac-Aβ40, 10nM; Fitc-Aβ42, 5nM; aq. buffer 1×b, pH 7.4, containing 1% HFIP).

4.1.5 **Interactions with Aβ40 by CD spectroscopy**

In order to detect conformational changes in the mixtures of the cyclic peptides with Aβ40, CD spectra were recorded for Aβ40 alone, cISMs alone and for the corresponding mixtures at ratios of 1/1. First R3-GI alone at 5µM showed random coil and in part β-sheet/β-turn (Figure 28a). The spectrum of Aβ40 alone had a strong minimum at around 198nm, which suggested mainly random coil secondary structure. Comparison of the CD spectrum of the mixture with the sum of the CD spectra of Aβ40 and R3-GI showed only a small difference in the random coil area of the spectra. In the case of cc-R3-GI and cc-L1-R3-GI when mixed at 1/1 with Aβ40, clear differences between CD spectra of mixtures and sums of the CD spectra of each of the components of the mixture were observed. This suggested that interactions resulted in conformational changes in Aβ40 and or inhibitor (Figure 28b,c). However, for cc-L2-R3-GI this was not the case, no conformational change was observed. The CD spectra of its mixture with Aβ40 and the sum of the spectra were very similar (Figure 28d).
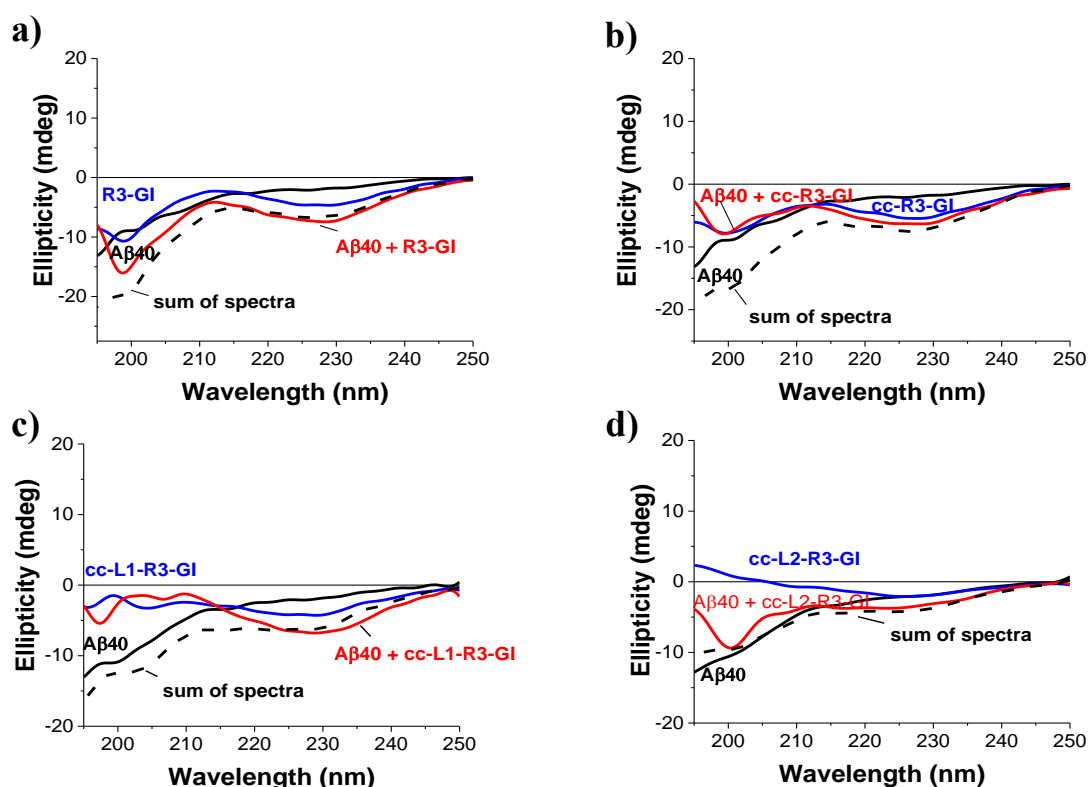
Figure 28. Interactions of Aβ40 with ISMs as studied by far-UV CD spectroscopy. CD spectra of freshly dissolved Aβ40 alone, ISM, cISM alone, a mixture (1/1) of Aβ40 with ISM/cISM and the sum of spectra of Aβ40 with ISM/cISM (5µM, pH 7.4). Panels a)-d) show CD spectra and interactions of (a) R3-GI, (b) cc-R3-GI, (c) cc-L1-R3-GI, (d) cc-L2-R3-GI with Aβ40 as indicated. Measurements were performed in aq. buffer 1×b, pH 7.4, containing 1% HFIP.

4.1.6 **Inhibitory activity on IAPP fibrillogenesis and on cytotoxicity**

Next, we asked whether cyclic R3-GI analogues inhibit IAPP fibrillogenesis and cytotoxicity as well. Investigation of the inhibitory effects of cISMs on IAPP fibril formation and cytotoxicity was performed by the ThT binding assay and the MTT reduction assay. Briefly, IAPP was incubated at a final concentration of 6µM either alone or in mixtures with the cyclic R3-GI analogues at a ratio of 1/2. ThT fluorescence was measured at indicated time points and up to 7 days. Solutions were added to RIN5fm cells after 7 days of incubation and effects on IAPP cytotoxicity were determined by the MTT reduction assay. As recently found, R3-GI was unable to inhibit IAPP fibrillogenesis[87], however cISMs; cc-R3-GI, cc-L1-R3-GI and cc-L2-R3-GI were able to inhibit IAPP fibrillogenesis

and cytotoxicity (Figure 29). These results were confirmed by TEM (Figure 29c): examination of the grids showed for IAPP alone fibrils, needle like fibrils for the IAPP-R3-GI mixture and amorphous aggregates for the IAPP/cISMs mixtures (Figure 29c).
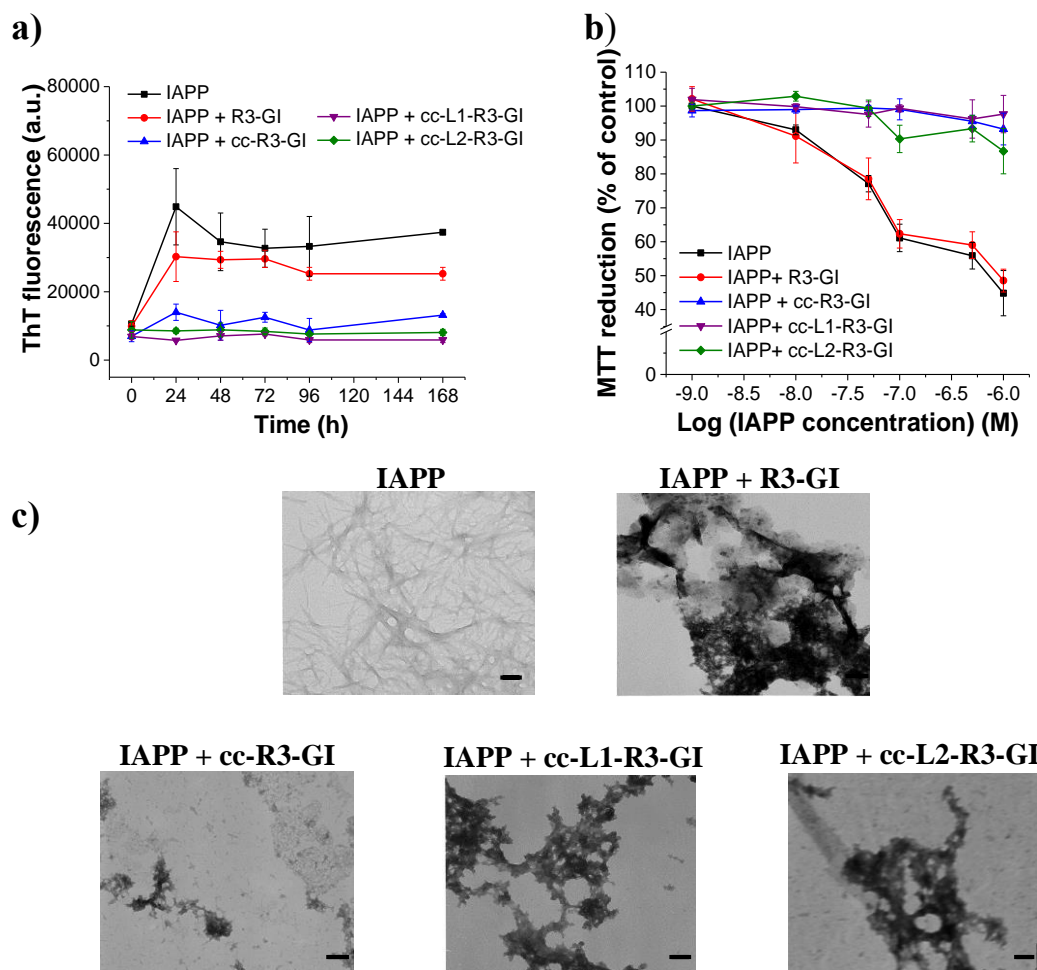
Figure 29. Effects of R3-GI and its cyclic analogues on IAPP amyloid formation and cytotoxicity. (a) Fibrillogenesis of IAPP (6μM) alone and its mixtures (IAPP/peptide, 1/10 (R3-GI) or 1/2 (cISMs)), as determined via the ThT binding assay (means (±SD), 3 assays (n=3)), (b) cell-damaging effects of IAPP and its mixtures (solutions from (a), 7 days aged) on RIN5fm cells via the MTT reduction assay (means (±SD), three assays (n=3)), (c) TEM images of IAPP and its mixtures with the various analogues (solutions from (a), 7 days aged) (bars, 100nm).

Our results showed that cyclization of R3-GI plays a very important role in its effect on IAPP amyloidogenesis and toxicity. IC_{50}s studies on the effects of cISMs on formation of cytotoxic IAPP aggregates showed that all of them are able to inhibit in the nanomolar concentration range (Table 16) (see Appendix Figure A3).

Table 16. IC_{50}s values of inhibitory effects of cISMs on IAPP cytotoxicity.

cISMs	IC_{50} (±SD) (nM)[a]
cc-R3-GI	126 (±40)
cc-L1-R3-GI	71 (±23)
cc-L2-R3-GI	133 (±61)

[a] IC_{50}s, means (±SD) from 3 titration assays (n=3 each); IAPP (100nM) was titrated with different amounts of peptides under ThT conditions; cell-damaging effects were determined in 24h aged solutions by MTT assay.

4.1.7 **Determination of binding affinities towards IAPP**

The interactions of cISMs with IAPP were studied by fluorescence titration assays and CD spectroscopy. Figure 30 shows the results of fluorescence titrations of Fluos-IAPP (5nM) with different concentrations of cISMs. The titration of Fluos-IAPP with cc-R3-GI resulted in an app. K_d of 20.6nM, whereas the titration of Fluos-cc-R3-GI with IAPP showed that app. K_d was higher than 5µM (Figure 31). This data indicated that cc-R3-GI preferably interacted with monomeric IAPP. Furthermore, both cc-L1-R3-GI and cc-L2-R3-GI bound with high affinity not only to Fluos-IAPP (app. K_d = 63.3nM & app. K_d = 59.6nM respectively), but also to IAPP oligomers (app. K_d = 50.6nM & app. K_d = 148nM respectively) (Table 17).
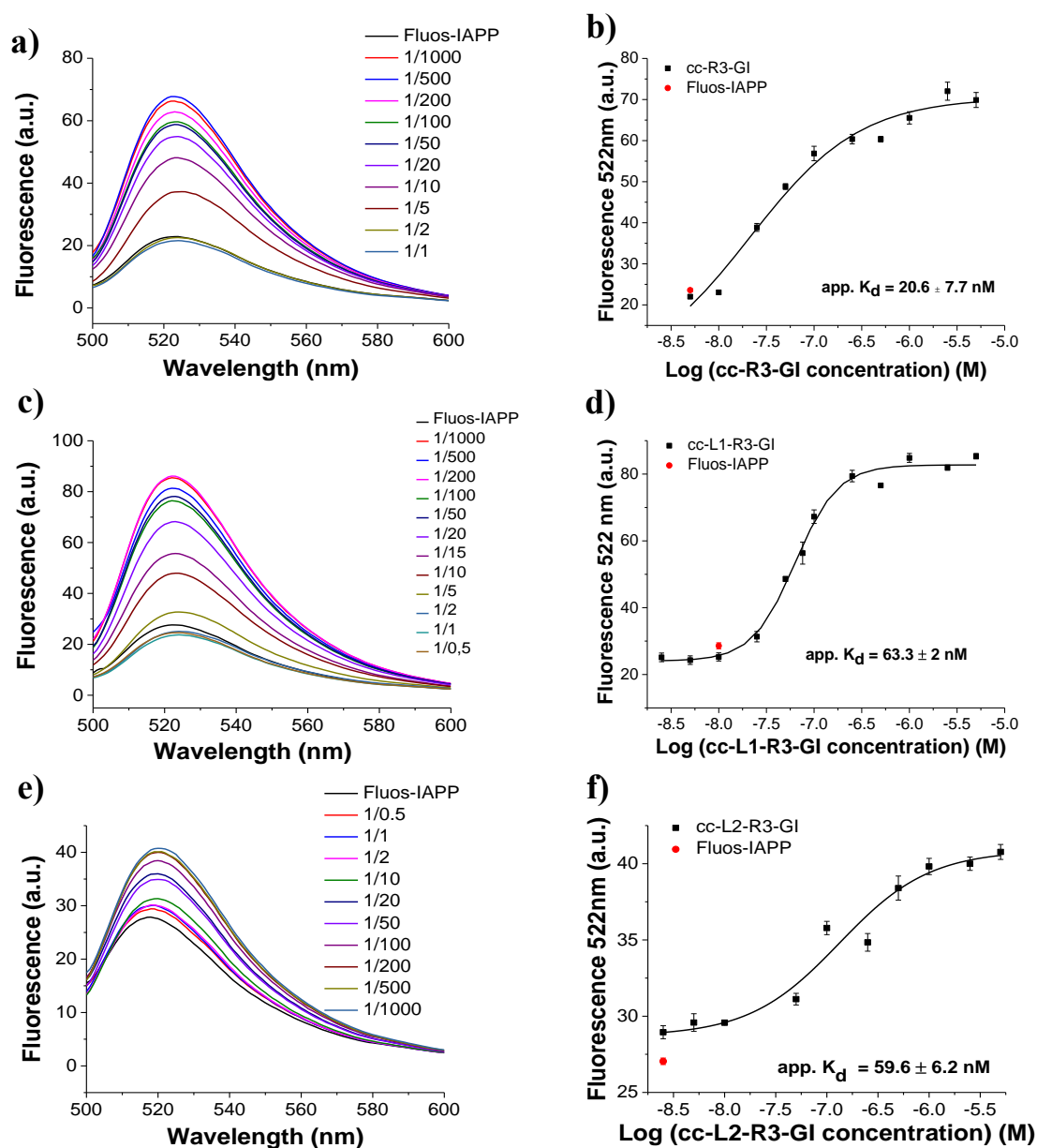
Figure 30. Determination of app. K_ds of interactions of IAPP and cISMs by fluorescence spectroscopic titrations. Panels a), c), e) show fluorescence spectra of Fluos-IAPP (5nM) alone and its mixtures with various amounts of cc-R3-GI (a), cc-L1-R3-GI (c), cc-L2-R3-GI (e); the molar ratios of Fluos-IAPP/cISM are as indicated. Panels b), d), f) show the binding curves of cc-R3-GI (b), cc-L1-R3-GI (d), cc-L2-R3-GI (f); app. K_ds are means (±SD) from 3 binding curves (Fluos-IAPP 5nM). Measurements were performed in aq. buffer 1×b, pH 7.4, containing 1% HFIP.
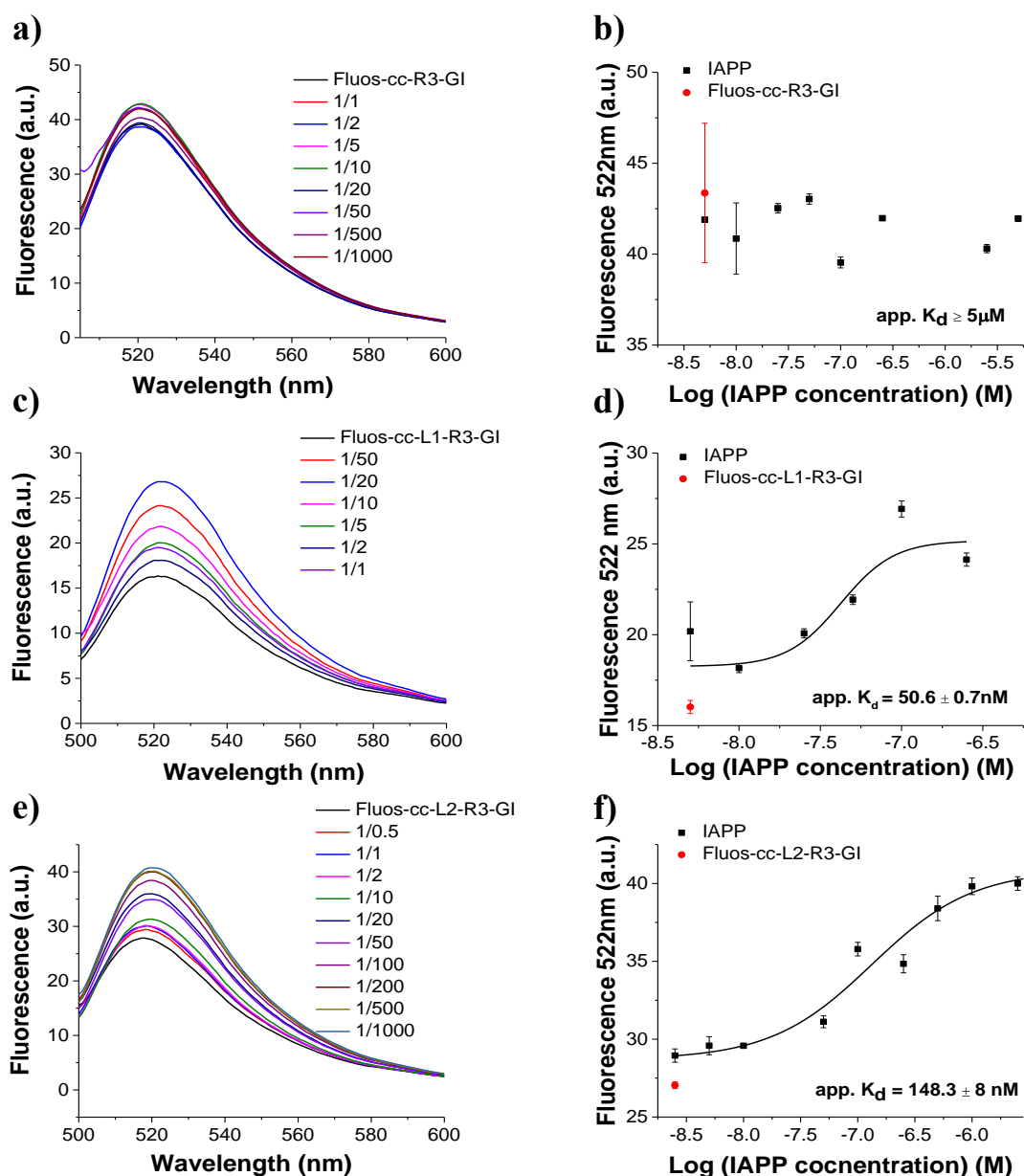
Figure 31. Determination of app. K$_d$s of interactions of IAPP and cISMs by fluorescence spectroscopic titrations. Panels a), c), e) show fluorescence spectra of Fluos-cISM (5nM) alone and its mixtures with various amounts of IAPP; the molar ratios of Fluos-cISM/IAPP are as indicated. Panels b), d), f) show the binding curves of Fluos-cc-R3-GI (b), Fluos-cc-L1-R3-GI (d), Fluos-cc-L2-R3-GI (f); app. K$_d$s are means (±SD) from 3 binding curves (Fluos-cISM 5nM). Measurements were performed in aq. buffer 1×b, pH 7.4, containing 1% HFIP.

Table 17. Apparent affinities (app. K$_{ds}$) of interaction of cISMs with IAPP as determined by fluorescence titration binding assays.

cISM	app. K$_d$ (±SD) (nM) with Fluos-IAPP[a]	app. K$_d$ (±SD) (nM) with IAPP[b]
cc-R3-GI	20.6 (±7)	NB [c]
cc-L1-R3-GI	63.3 (±2)	50.6 (±0.7)
cc-L2-R3-GI	59.6 (±6.2)	148 (±8)

[a] App. K$_d$s, means (±SD) from 3 binding curves Fluos-IAPP (5nM) was titrated with cISMs; [b] app. K$_d$s, means (±SD) from 3 binding curves Fluos-cISMs (5nM) were titrated with IAPP; [c] NB, no binding at IAPP concentrations ≤ 5μM, (aq. buffer 1×b, pH 7.4, containing 1% HFIP).

4.1.8 Interactions with IAPP by CD spectroscopy

To further investigate the interactions between IAPP and cISMs, CD spectroscopy was applied. CD was performed with IAPP/inhibitor ratio of 1/2, which was found to be required for inhibitory effects. The spectra of all three inhibitors at a concentration of 10μM and of IAPP at 5μM as well as of IAPP/inhibitor mixtures were recorded (Figure 32).
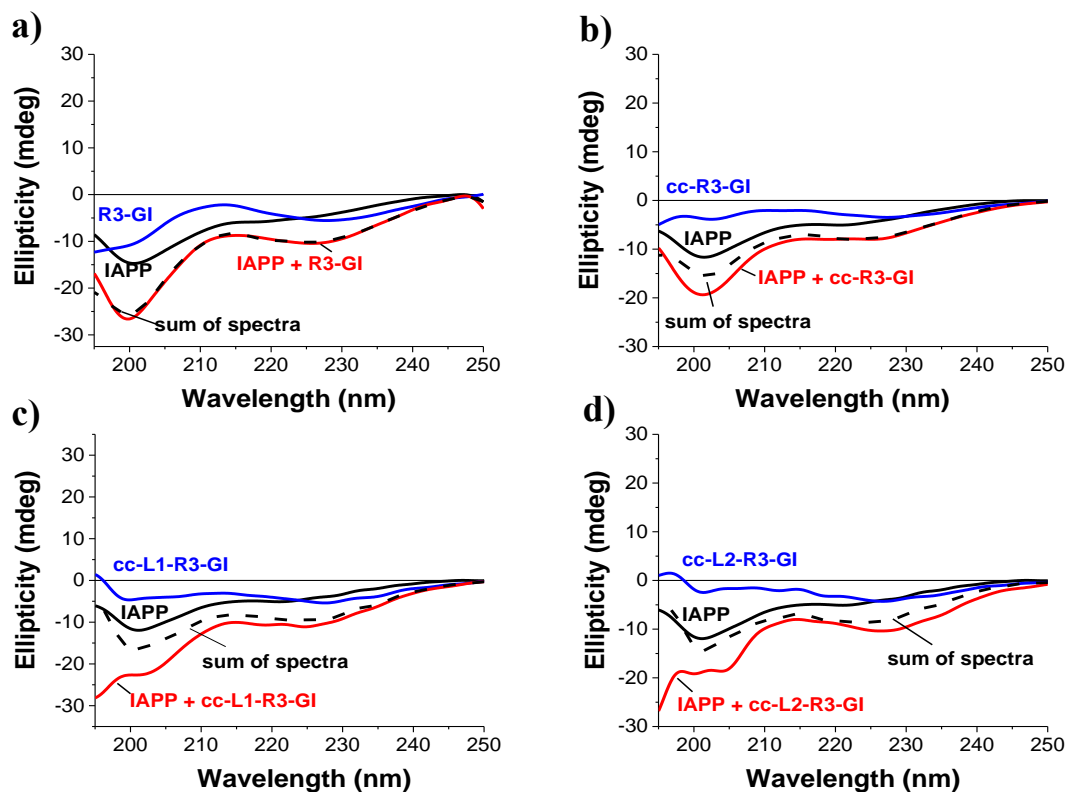
Figure 32. Interaction of IAPP with ISMs studied by far-UV CD spectroscopy. CD spectra of freshly dissolved IAPP alone (5μM), ISM alone, cISM alone (10μM), a mixture (1/2) of IAPP with ISM, cISM and the sum of spectra. Panels a)-d) shows CD spectra and interactions of (a) R3-GI, (b) cc-R3-GI, (c) cc-L1-R3-GI, (d) cc-L2-R3-GI with IAPP as indicated. Measurements were performed in aq. buffer 1×b, pH 7.4, containing 1% HFIP.

The CD spectra of the mixture of IAPP with R3-GI (1/2) did not differ from the sum of the spectra; this indicated that there is no strong change in overall conformation of the two peptides. However, the CD spectra of the mixtures of cISMs with IAPP differed significantly from the sum of the spectra, suggesting the interactions resulted in conformational changes.

4.1.9 Investigation of their proteolytic stabilities

The proteolytic stability of the cISMs in human plasma was measured *in vitro* as a guide for their *in vivo* stability. Peptides were assayed at a concentration of 180μM in human plasma following incubation for 0, 0.5 and 1h, at 37°C. RP-HPLC and MALDI-TOF were used to quantify peptide in plasma. For R3-GI and cc-R3-GI the degradation profile was very similar (Figures 33 & 34); already after 30min degradation occurred. MALDI-TOF identified a degraded product which co-eluted with the same t_R as the non-degraded one (Tables 18 & 19). For this reason, the exact half life time ($t_{1/2}$) of R3-GI could not be estimated based on the height or area oft the HPLC peak. The studies on R3-GI identified many shorter R3-GI segments resulting from its proteolytic degradation (Table 18). In the case of cc-R3-GI, MALDI-TOF identified the shorter sequence of NFLVHRRRNF(N-Me)GA(N-Me)ILSC-amide as main fragment. Notably, this fragment was still present at 1h of incubation.
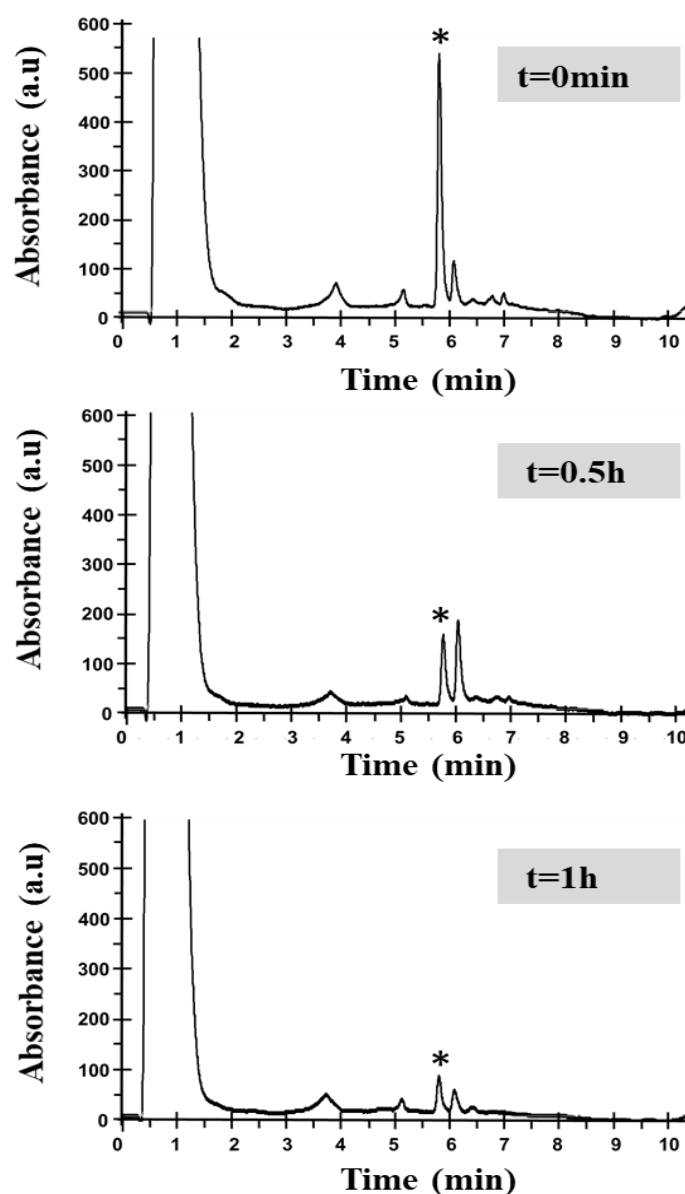
Figure 33. Proteolytic stability of R3-GI in human plasma (*in vitro*). HPLC chromatograms (t_R ~ 5.6 min; HPLC peak marked with a *) corresponding to intact R3-GI following incubation (37°C) with plasma for 0h, 0.5h, or 1h and separation from plasma proteins. Only trace amounts of R3-GI are still present at 0.5h. Peptides were detected in RP-HPLC by their absorbance at 214nm, calculated [M+H]$^+$ for R3-GI is 2467.43; found 2467.62 (0.5h). Representative data from at least 3 assays are shown.

Table 18. Degradation products of R3-GI, with t_R ~5.6 min in human plasma as determined via MALDI-TOF.

Time (h)	Detected peptide sequence	Fragment mass calculated [M+H]$^{+[a]}$	Fragment mass found[a]
0	ATQRLANFLVHRRRNF(N-Me)GA(N-Me)ILS-amide	2467.43	2467.62
0.5	ATQRLANFLVHRRRNF(N-Me)GA(N-Me)ILS-amide	2467.43	2467.62
	RLANFLVHRRRNNF(N-Me)GA(N-Me)ILS-amide	2167.51	2170.11
1	LANFLVHRRRNF(N-Me)GA(N-Me)ILS-amide	2011.33	2031[b]
	VHRRRNF(N-Me)GA(N-Me)ILS-amide	1452.66	1479.82,1496.65[b]
	ATQRLANFLVHR-amide	1424.65	1423

[a] monoisotopic mass [M+H]$^+$; [b] [M+Na]$^+$ or [M+K]$^+$.
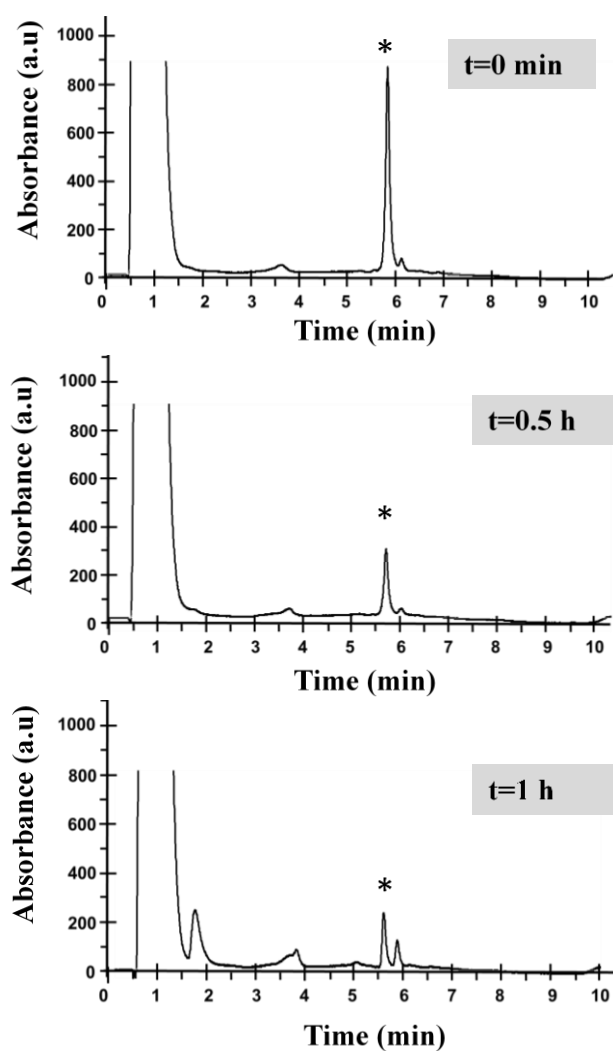
Figure 34. Proteolytic stability of cc-R3-GI in human plasma (*in vitro*). HPLC chromatograms ($t_R \sim 5.6$ min; HPLC peak marked with a *) corresponding to intact cc-R3-GI following incubation (37°C) with plasma for 0h, 0.5h, or 1h and separation from plasma proteins. Only trace amounts of cc-R3-GI are still present at 0.5h. Peptides were detected in RP-HPLC by their absorbance at 214nm, calculated $[M+H]^+$ for cc-R3-GI is 2671.39, found 2671.43 (0.5h). Representative data from at least 3 assays are shown.

Table 19. Degradation products of cc-R3-GI, with $t_R \sim 5.6$ min in human plasma as determined via MALDI-TOF.

Time (h)	Detected peptide sequence	Fragment mass calculated $[M+H]^{+[a]}$	Fragment mass found[a]
0	CATQRLANFLVHRRRNF(N-Me)GA(N-Me)ILSC-amide	2671.39	2671.43
0.5	CATQRLANFLVHRRRNF(N-Me)GA(N-Me)ILSC-amide	2671.39	2671.43
	NFLVHRRRNF(N-Me)GA(N-Me)ILSC-amide	1930.24	1940.33
1	CATQRLANFLVHRRRNF(N-Me)GA(N-Me)ILSC-amide	2671.39	2671.25
	NFLVHRRRNF(N-Me)GA(N-Me)ILSC- amide	1930.24	1939.9

[a] monoisotopic mass $[M+H]^+$.

Figures 35 & 36 showed kinetics of degradation of cc-L1-R3-GI and cc-L2-R3-GI. The stapled analogues presented a more stable profile (113min, 130min), compared to R3-GI or cc-R3-GI. However, as shown in Tables 20 & 21 MALDI-TOF analysis showed that the intact peptide co-eluted with degraded peptide, which does not allow to determine the half life-time ($t_{1/2}$). Finally, MALDI revealed that the degradation of both cc-L1-R3-GI and cc-L2-R3-GI occurred between F[15] and L[16], which resulted in the same stable last product of degradation (LVHRRRNF(N-Me)GA(N-Me)ILS-C-amide).
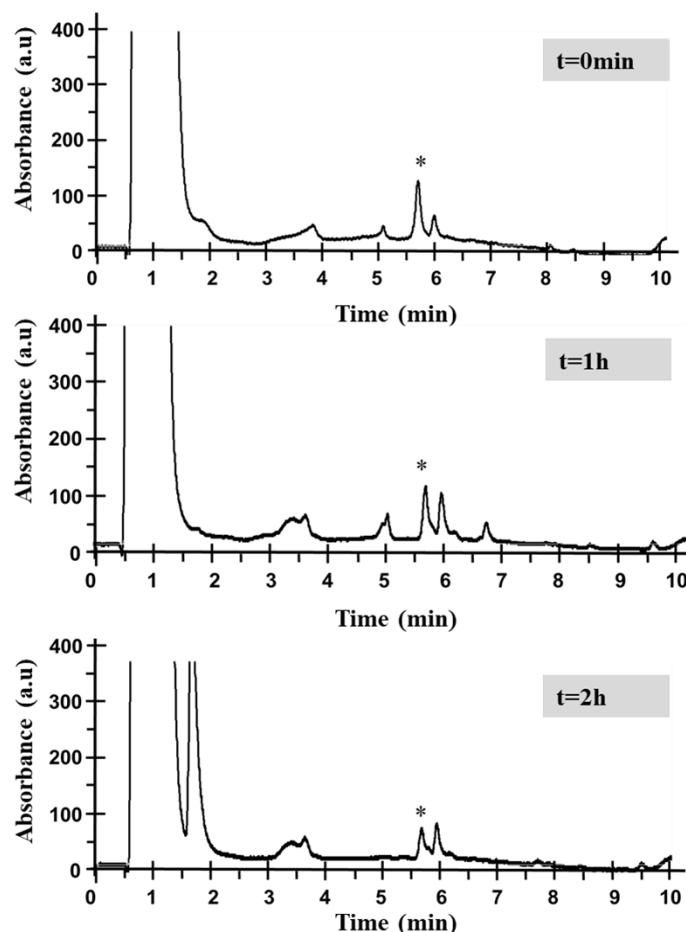
Figure 35. Proteolytic stability of cc-L1-R3-GI in human plasma (*in vitro*). HPLC chromatograms (t_R ~ 5.6 min; HPLC peak marked with a *) corresponding to intact cc-L1-R3-GI following incubation (37 °C) with plasma for 0h, 1h, or 2h and separation from plasma proteins. Only trace amounts of cc-L1-R3-GI are still present at 2h. Peptides were detected in RP-HPLC by their absorbance at 214nm, calculated [M+H]+ for cc-L1-R3-GI is 2755.55, found 2755.33 (1h). Representative data from at least 3 assays are shown.

Table 20. Degradation products of cc-L1-R3-GI, with t_R ~ 5.6 min in human plasma as determined via MALDI-TOF.

Time (h)	Detected peptide sequence	Fragment mass calculated [M+H]+[a]	Fragment mass found[a]
0	CATQRLANFLVHRRRNF(N-Me)GA(N-Me)ILSC-amide	2755.55	2755.53
1	CATQRLANFLVHRRRNF(N-Me)GA(N-Me)ILSC-amide	2755.55	2755.61
	LVHRRRNF(N-Me)GA(N-Me)ILSC-amide	1671.96	1694.96[b]
2	LVHRRRNF(N-Me)GA(N-Me)ILSC-amide	1671.96	1694.96[b]

[a] monoisotopic mass [M+H]+; [b] [M+Na]+.
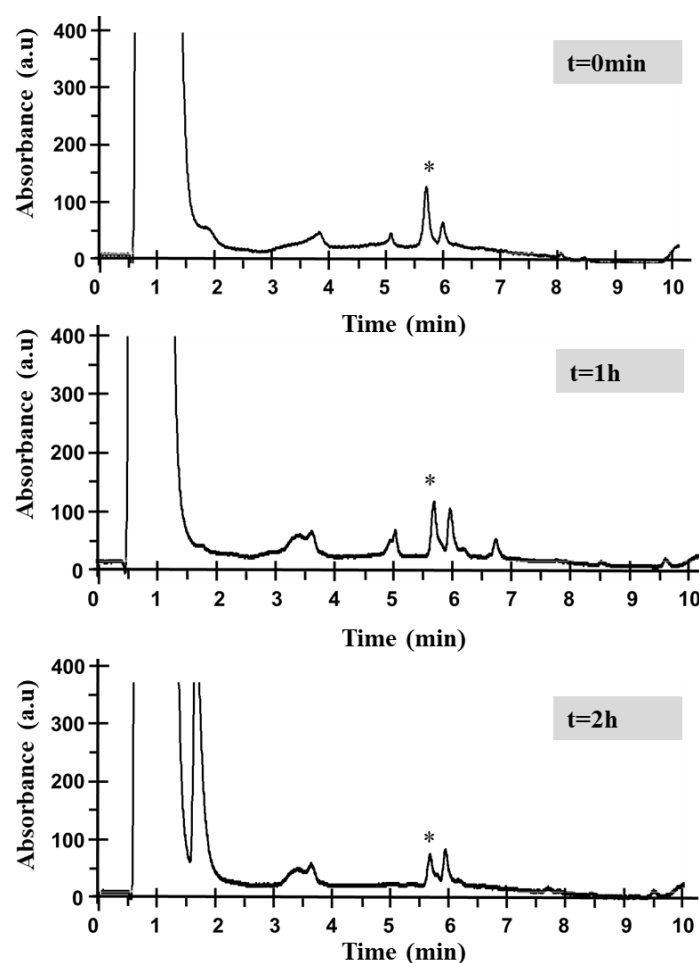
Figure 36. Proteolytic stability of cc-L2-R3-GI in human plasma (*in vitro*). HPLC chromatograms (t_R ~ 5.6 min; HPLC peak marked with a *) corresponding to intact cc-L2-R3-GI following incubation (37°C) with plasma for 0h, 1h, or 2h and separation from plasma proteins. Only trace amounts of cc-L2-R3-GI are still present at 2h. Peptides were detected in RP-HPLC by their absorbance at 214nm, calculated $[M+H]^+$ for cc-L2-R3-GI is 2852.65, found 2852.64 (2h). Representative data from at least 3 assays are shown.

Table 21. Degradation products of cc-L2-R3-GI, with t_R ~ 5.6 min in human plasma as determined via MALDI-TOF.

Time (h)	Peptide sequence post incubation	Fragment mass calculated $[M+H]^{+[a]}$	Fragment mass found[a]
0	L2 CATQRLANFLVHRRRNF(N-Me)GA(N-Me)ILSC-amide	2852.65	2852.64
1	L2 CATQRLANFLVHRRRNF(N-Me)GA(N-Me)ILSC-amide	2852.65	2852.64
	LVHRRRNF(N-Me)GA(N-Me)ILSC-amide	1671.96	1694.96[b]
2	L2 CATQRLANFLVHRRRNF(N-Me)GA(N-Me)ILSC-amide	2852.64	2852.64
	LVHRRRNF(N-Me)GA(N-Me)ILSC-amide	1671.96	1694.96[b]
3	……………LVHRRRNF(N-Me)GA(N-Me)ILSC-amide	1671.96	1694.96[b]

[a] monoisotopic mass $[M+H]^+$; [b] $[M+Na]^+$.

Table 22. $t_{1/2}$ (min) of R3-GI and its cyclic analogues.

Peptides	$t_{1/2}$ (min)
R3-GI	<60
cc-R3-GI	<60
cc-L1-R3-GI	<120
cc-L2-R3-GI	<120

The results from this part showed the importance of cyclization for the inhibitory activity towards both Aβ40(42) and IAPP. Importantly, R3-GI, which was unable to inhibit IAPP became a potent IAPP inhibitor upon cyclization and stapling. Fluorescence and CD spectroscopies confirmed the strong interactions of cISMs with Aβ40(42) and IAPP. However, as far as proteolytic properties are concerned, the exact half time of cISMs could not be estimated. The results of the kinetic analysis of the proteolytic degradation on human plasma showed that proteolytically labile amide bonds were the bonds between Phe^{15}-Leu^{16} and Ala^{13}-Asn^{14}. Relatively stable fragments were identified, the N-terminal NFLVHRRRNF(N-Me)GA(N-Me)ILSC-amide and LVHRRRNF(N-Me)GA(N-Me)ILSC-amide.

4.2 Studies on cyclic analogues of truncated R3-GI

4.2.1 Peptide design and synthesis

The second aim of the thesis focused on the rational design, synthesis and biophysical and biochemical studies of N-terminal truncated cyclic R3-GI analogues as inhibitors of Aβ40(42) and IAPP (abbreviated as **cISMs.sh**). These peptides consisted of IAPP segments, IAPP(14-18) and the N-methylated analogue of IAPP(22-28) IAPP(22-28)-GI, which were covalently connected to each other with different linkers and two flanking cysteines. The applied linker structures between Cys-IAPP(14-18) and IAPP(22-28)-GI-Cys were segments of three natural amino acids, which differed in the hydrophobicity and steric hindrance effects of their side chains[87], this was done in order to examine the effects of the linker on their inhibitory potential.
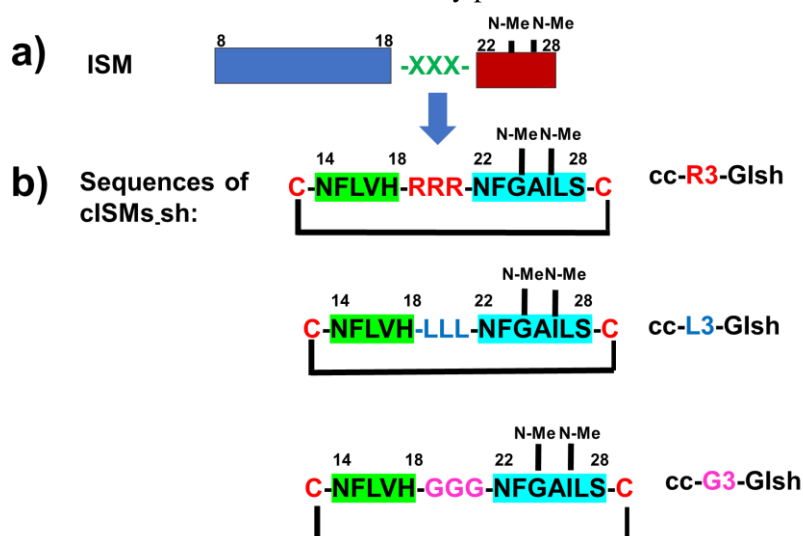
Scheme 3. Rational design of N-terminal truncated cyclic R3-GI analogues containing different linkers. (a) ISM design concept[87], (b) sequences of cISMs.sh; cc-R3-GIsh is abbreviated based on the name of the residue in the linker tripeptide (Arg) while "-GI" indicates the presence of the N-methyl-residues at G^{24} & I^{26}: "N-Me", cc-L3-GIsh is

abbreviated based on the name of the residue in the linker tripeptide Leu, cc-G3-GIsh is abbreviated based on the name of the residue in the linker tripeptide Gly. Cyclization is indicated by "cc" and N-terminal truncation/"shortening" indicated by "sh" (abbrev: cISMs-sh, cyclic short ISMs).

Table 23. Sequences of N-terminal truncated cyclic R3-GI analogues and their abbreviation.

Peptide sequence	Peptide abbreviation
C-NFLVH-**RRR**-NF(N-Me)GA(N-Me)ILS-C-amide	cc-**R3**-GIsh
C-NFLVH-**LLL**-NF(N-Me)GA(N-Me)ILS-C-amide	cc-**L3**-GIsh
C-NFLVH-**GGG**-NF(N-Me)GA(N-Me)ILS-C-amide	cc-**G3**-GIsh

The three novel cyclic peptides (Table 23) were synthesized by SPPS utilizing Fmoc-strategy. Crude peptides with cysteines in reduced form were purified via RP-HPLC and characterized by MALDI-TOF (Table 24). In the case of cc-R3-GIsh and cc-G3-GIsh oxidation was performed by stirring crude peptides in a mixture of 40% (v/v) DMSO in aqueous NH_4HCO_3 (0.1mM) for 3h. cc-R3-GIsh and cc-G3-GIsh were purified by RP-HPLC and characterized by MALDI-TOF; purification could be conducted with a yield of around 40%, 30% of crude, respectively (Table 24). In the case of cc-L3-GIsh another oxidation method was used. 1mg of cc-L3-GIsh crude was dissolved in 300µl DMSO, 500µl ddH₂O, 300µl H₂O₂; no incubation time was needed. cc-L3-GIsh was purified by RP-HPLC, with a yield of pure regarding crude of ~ 14%.

Table 24. Characterization of the synthetic oxidized peptides via HPLC and MALDI-TOF.

Peptide abbreviation[a]	HPLC program	t_R (min)[b]	Yield[7a]	$[M+H]]^+$ expected[d]	$[M+H]^+$ found[d]
cc-R3-GI sh	1	17.4	40%	2031.0	2031.1
cc-L3-GIsh	1	27.1	13.6%	1901.9	1902.2
cc-G3-GIsh	1	19.3	30%	1733.8	1734.0

[a] Peptides were synthesized with free amino terminus and amidated C-terminal end; [b] t_R: HPLC retention time; [c] % yield with regard to respective crude product; [d] monoisotopic molar mass $[M+H]^+$ expected and $[M+H]^+$ found.

4.2.2 Biophysical characterization

4.2.2.1 Conformational studies via CD spectroscopy

Next, conformations of the above peptides were studied by far-UV CD spectroscopy. Peptides were dissolved in 1×b, pH 7.4 containing 1% HFIP and CD spectra were recorded. CD spectra were measured at concentrations between 5-100µM to determine their aggregation propensities. The CD spectrum of cc-R3-GIsh showed two minima: one at 200nm indicative of random coil and a second one at 228nm indicative of β-sheet/β-turn structure (Figure 37a).
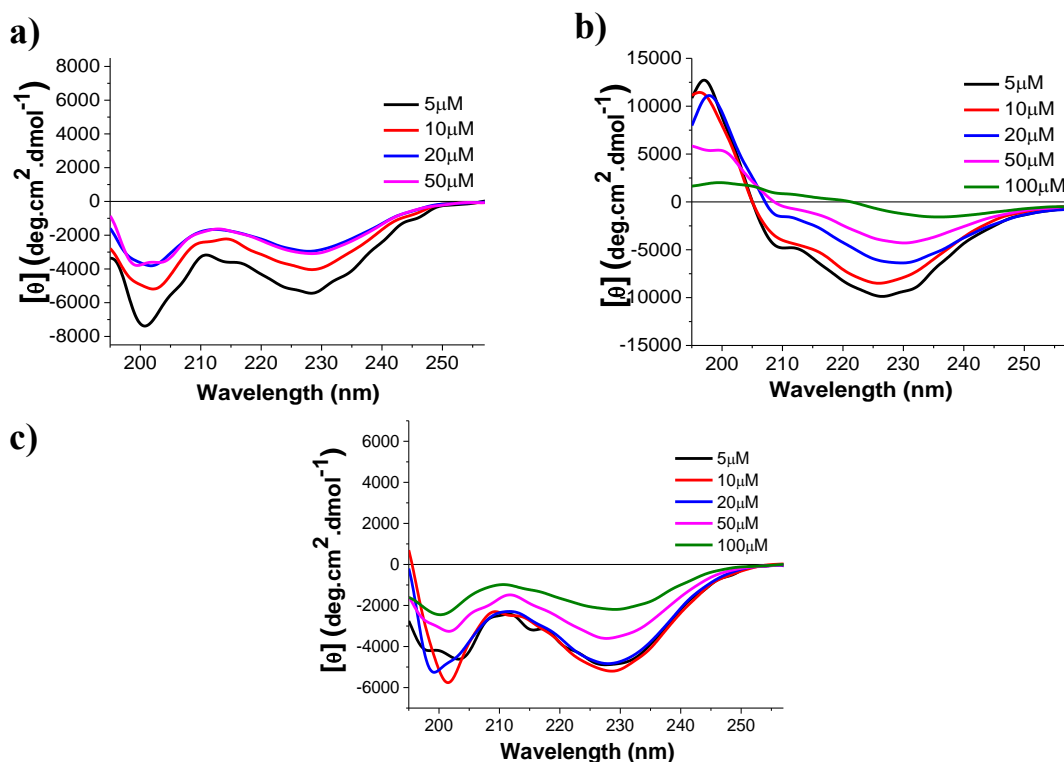
Figure 37. Concentration dependence of the CD spectra of cyclic short ISMs. (a) CD spectra of cc-R3-GIsh, (b) cc-L3-GIsh and (c) cc-G3-GIsh. Measurements were performed at peptide concentrations between 5-50μM in aq. buffer 1×b, pH 7.4, containing 1% HFIP.

The spectrum of cc-L3-GIsh (Figure37b) showed a positive signal at 200nm and a pronounced minimum at 230nm. These features correspond most likely to that of β-sheet/β-turn contents. CD spectra of 5 and 10μM were very similar, which indicated that peptide was present in its monomeric or in the same oligomeric state at these two concentrations. A significant decrease in the MRE signal was observed at concentrations ≥ 20μM. In addition, at 100μM the solution was turbid, consistent with peptide precipitation. Finally, the CD spectra of cc-G3-GIsh (Figure 37c) showed two minima at approximately 200nm and 230nm, which also indicated the presence of random coil and β-turn structural contents. The MRE signals of the CD spectra of the concentrations 5-20μM were almost completely identical, suggesting that the peptide was in monomeric or in the same oligomeric state at these two concentrations. Soluble oligomers formed at peptide concentration > 50μM. No peptide precipitation was observed at 100 μM.

In conclusion, it was observed that by inserting different linkers between the two short IAPP segments IAPP(14-18) and IAPP(22-28)-GI and by confining them into a cyclic conformation, different conformations and aggregation propensities were generated. Three Arg residues as linker resulted in CD spectra characteristic of both random coil and β-sheet/β-turn elements. Three Leu residues in the linker induced β-turn conformation and aggregation occurred already at c > 10μM. Finally, when three Gly residues were introduced in the linker the CD spectra showed both random coil and turn elements and the peptide did not exhibit such a high aggregation propensity as the other two peptides.

4.2.2.2 **Self-association studies via fluorescence spectroscopy**

Next, fluorescence binding assays were performed to quantify the app. K_d of the self-assembly of the peptides. Titrations of freshly made solutions of synthetic N-terminal fluorescein labeled cyclic shortened ISM (Fluos-cISMs-sh) (5nM) with non-labeled truncated cISM-sh were performed (Figure

38). The measurements were performed in 1×b, pH 7.4 containing 1% HFIP. Adding 1000-fold molar excess of cc-R3-GIsh and cc-G3-GIsh to Fluos-cc-R3-GIsh and Fluos-G3-GIsh respectively, caused ∼40% fluorescence enhancement. (Figure 38a,e). Adding 1000-fold molar excess of cc-L3-GIsh to Fluos-cc-L3-GIsh caused 100% fluorescence enhancement (Figure 38b). Sigmoidal binding isotherms were obtained and the determined app. K_ds values were 670 ($\pm$57.7) nM for cc-R3-GIsh, 808 ($\pm$16.8) nM for cc-L3-GIsh and 1503.33 ($\pm$592.4) nM for cc-G3-GIsh (Figure 38b,d,f). These data indicated similar self-association propensies for cc-R3-GIsh and cc-L3-GIsh, whereas in the case of cc-G3-GIsh the determined app. K_d was 2-fold higher than the app. K_d of cc-R3-GIsh (Table 25).
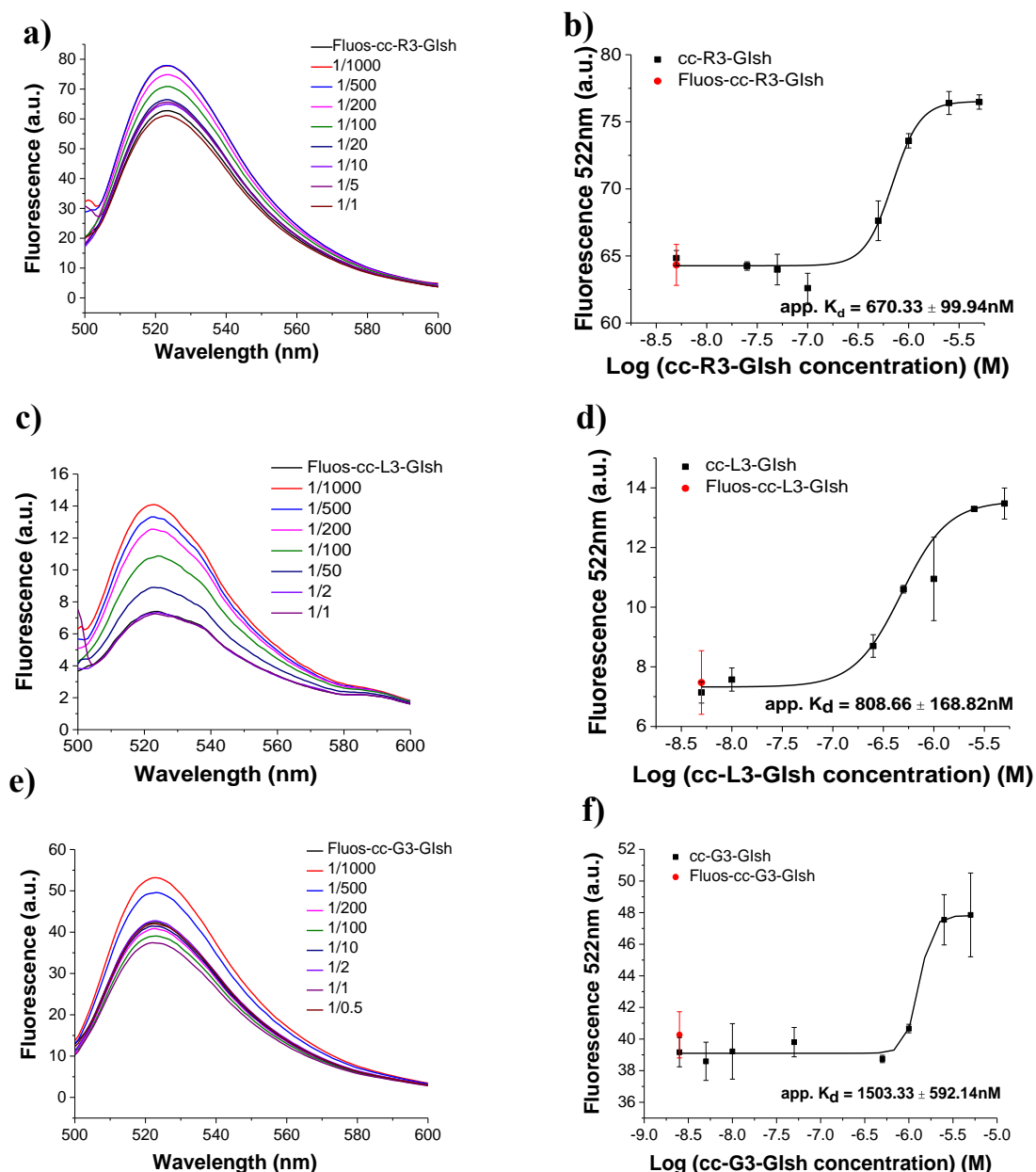
Figure 38. Apparent affinities (app. K_d) of self-association of cISMs-sh as determined by fluorescence spectroscopy. Panels a), c), e) show fluorescence spectra of Fluos-cISMs-sh (5nM) alone and its mixtures with various amounts of f cc-R3-GIsh (a), cc-L3-GIsh (c), cc-G3-GIsh (e); the molar ratios of Fluos-cISM-sh/cISM-sh are as indicated. Panels b), d), f) show the binding curves of cc-R3-GIsh (b), cc-L3-GIsh (d), cc-G3-GIsh (f); app. K_ds are means ($\pm$SD) from 3 binding curves (Fluos-cISM-sh 5nM). Measurements were performed in aq. buffer 1×b, pH 7.4, containing 1% HFIP.

Table 25. App. K_ds of self-assembly of cISMs-sh as determined by fluorescence titration studies.

Peptide	app. K_d ($\pm$SD) (nM)[a]
cc-R3-GIsh	670.33 ($\pm$99.94)
cc-L3-GIsh	808.66 ($\pm$168.82)
cc-G3-GIsh	1503.33 ($\pm$592.14)

[a] App. K_ds are means ($\pm$SD) from 3 binding curves. Determined by titrations of synthetic N-terminal fluorescein-labeled cISMs-sh with non-labeled cISMs-sh, (5nM; aq. buffer 1×b, pH 7.4, containing 1% HFIP).

4.2.3 **Inhibitory activities on Aβ40(42) fibrillogenesis and cytotoxicity**

Next, the question was addressed whether cc-R3-GIsh, cc-L3-GIsh and cc-G3-GIsh could intervene with Aβ40 self-assembly into fibrils and affect formation of cytotoxic Aβ40 aggregates. Aβ40 alone (16.5μM, pH 7.4) and (1/1) mixtures of Aβ40 with the peptides were incubated for 7 days and fibrillogenesis and cytotoxicity were followed by the ThT binding and the MTT reduction assays (Figure 39).
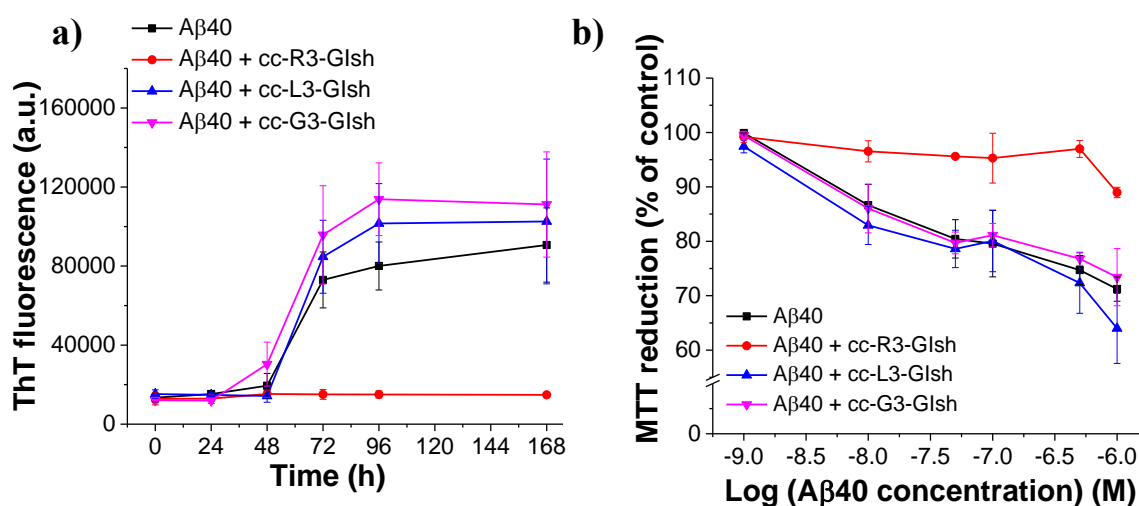
Figure 39. Effects of cISMs-sh on Aβ40 (1/1) amyloid formation and cytotoxicity. (a) Fibrillogenesis of Aβ40 (16.5μM) or its mixtures (Aβ40/peptide, 1/1) by ThT binding (means ($\pm$SD), 3 assays), (b) effects on cell viability: solutions from (a) (7 days aged) were added to PC-12 cells; cell damage was determined by MTT reduction (means ($\pm$SD), 3 assays (n=3 each)).

cc-R3-GIsh inhibited effectively Aβ40 fibril formation whereas cc-L3-GIsh and cc-G3-GIsh could not inhibit Aβ40 fibrillogenesis (Figure 39a). To examine whether these shortened cyclic peptides may also inhibit formation of cytotoxic Aβ40 aggregates, Aβ40 alone and its mixtures were added to PC-12 cells and cell viability was assessed by the MTT reduction assay. The 7 days aged mixture of cc-R3-GIsh with Aβ40 was not cytotoxic, which was in contrast to the mixtures of cc-L3-GIsh or cc-G3-GIsh with Aβ40. Thus, cc-R3-GIsh was able to inhibit Aβ40 at 1/1 ratio whereas cc-L3-GIsh and cc-G3-GIsh were unable to do so (Figure 39b).

The results of the ThT binding assay were confirmed by TEM (see Appendix Figure A4). In the case of Aβ40 and its mixtures with cc-L3-GIsh and cc-G3-GIsh fibrils were found. In the case of Aβ40 mixture with cc-R3-GIsh amorphous aggregates were found.

In Table 26, IC_{50}s of cc-R3-GIsh on Aβ40 toxicity are presented (see Appendix Figure A5a). It was found that cc-R3-GIsh had a 10-fold better IC_{50} regarding the inhibition of Aβ40 cytotoxicity (IC_{50} = 125.1nM) compared to IC_{50} of cc-L3-GIsh (IC_{50} = 1756.66nM). In the case of cc-G3-GIsh an IC_{50} value could not be determined. cc-G3-GIsh was unable to inhibit Aβ40 even at 10-fold excess (see Appendix Figure A6).

Table 26. IC_{50} values of inhibitory effects of cISMs-sh on Aβ40 cytotoxicity.

cIsMs-sh	IC_{50} (±SD) (nM)[a]
cc-R3-GIsh	125.11 (±73.39)
cc-L3-GIsh	1756.66 (±721.75)
cc-G3-GIsh	n.d[b]

[a] IC_{50}s, means (±SD) from 3 titration assays (n=3 each); Aβ40 (500nM) was titrated with different amounts of peptides under ThT conditions and cell-damaging effects were determined after 72h aged solutions by MTT assay; [b] n.d., non-determined (non-inhibitor).

According to the above results there is a kind of "structure-activity relationship"; the inhibitory function depends on the nature of the linker. This is in agreement with previous findings regarding the linear ISMs[87].

Next, the inhibitory effects of cc-R3-GIsh on Aβ42 fibrillogenesis and cytotoxicity were studied. Aβ42 alone (16.5µM, pH 7.4) and its mixture with the peptide (16.5µM, pH 7.4) were incubated up to 7 days and fibrillogenesis and cytotoxicity were followed by the ThT binding and the MTT reduction assays. cc-R3-GIsh, an Aβ40 inhibitor, blocked Aβ42 fibrillogenesis as well. To evaluate the effects of the cc-R3-GIsh on Aβ42-mediated cell damage, 7 days aged solutions (Aβ42 fibrillization plateau; see Appendix Figure A7a were added to PC-12 cells (see Appendix Figure A7b). In fact, cc-R3-GIsh effectively suppressed formation of Aβ42 cytotoxic assemblies as well; TEM analysis confirmed the ThT binding results (see Appendix Figure A7c).

Since cc-R3-GIsh showed the best inhibitory potential on Aβ40 than the other two cISMs-sh, we tested which stages of the Aβ40 self-assembly amyloidogenic pathway cc-R3-GIsh interferes with. cc-R3-GIsh blocked formation of cytotoxic Aβ40 oligomers and fibrils when added (1/1) to Aβ40 species before nucleation of fibrillogenesis (Figure 40). When it was added at 72h (plateau of fibrillogenesis) no effects could be observed. Thus, this peptide could not dissociate already formed Aβ40 fibrils (Figure 40b). These results were confirmed by TEM; similar results were observed with respect to effects on cytotoxic assemblies (see Appendix Figure A8a).
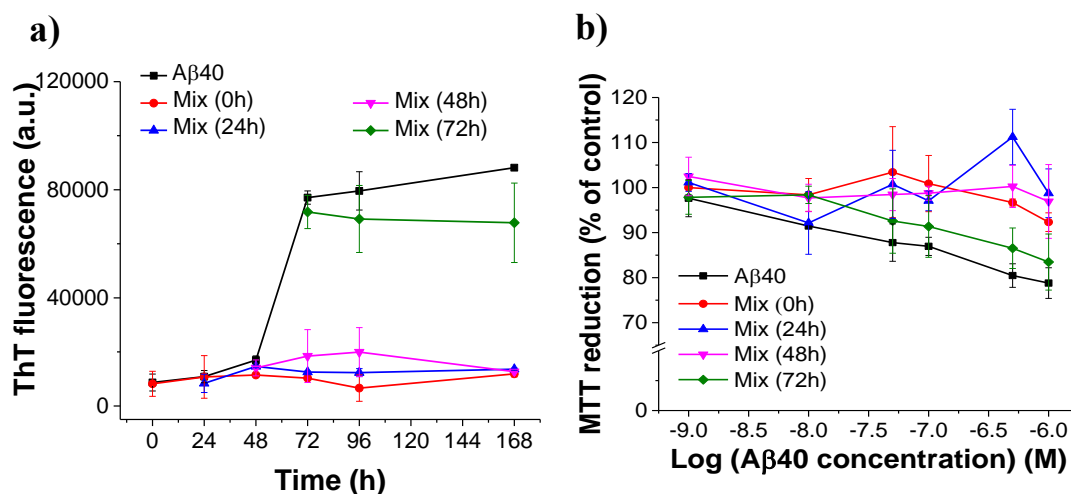
Figure 40. Effects of cc-R3-GIsh when added at pre- or post-nucleation stages of fibrillogenesis of Aβ40. (a) Effects of cc-R3-GIsh when added (1/1) before (0h, 24h), at (48h) or after (72h) nucleation on Aβ40 fibrillogenesis (16.5μM) as determined by ThT binding (means (±SD) from 3 assays), (b) effects of cc-R3-GIsh when added (1/1) before (0h, 24h), at (48h) or after (72h) nucleation on Aβ40 fibrillogenesis (16.5μM) via MTT reduction assay. Solutions from (a) (3 day-aged) added to PC-12 cells; cell damage determined by the MTT reduction (means (±SD), from 3 assays (n=3 each)).

4.2.4 Determination of binding affinities towards Aβ40

The apparent K_ds of interactions of Aβ40 with cISMs-sh were determined by titrating Dac-Aβ40 (10nM) with cISMs-sh (Figure 41). cc-R3-GIsh was found to bind with high affinity Dac-Aβ40 (app. $K_d = 382$nM), whereas cc-L3-GIsh showed an app. K_d of 501nM, however, in the case of cc-G3-GIsh no binding at $c \leq 10$μM could be determined.

In addition, app. K_ds of interactions of monomeric/oligomeric species of Aβ40 towards cISMs-sh were determined by titrating fluorescently labeled cISMs-sh (5nM) with non-labeled Aβ40 (Figure 42). Again, cc-R3-GIsh showed the highest affinity (app. $K_d = 172$nM) in comparison to cc-L3-GIsh and cc-G3-GIsh.
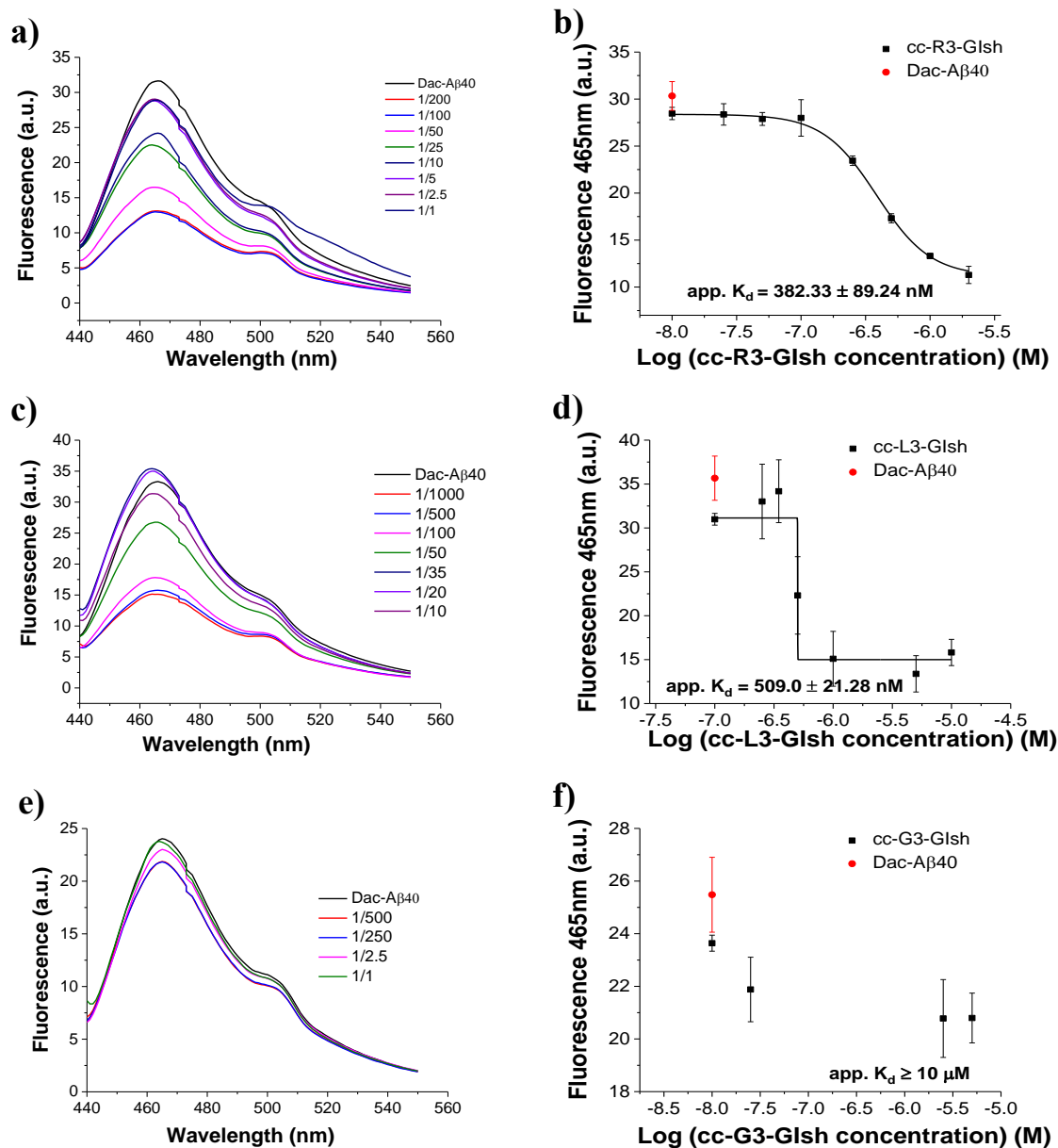
Figure 41. Determination of app. K_ds of interactions of cISMs-sh with Aβ40 by fluorescence titrations. Panels a), c), e) show fluorescence spectra of Dac-Aβ40 (10nM) alone and its mixtures with various amounts of cc-R3-GIsh (a), cc-L3-GIsh (c), cc-G3-GIsh (e); the molar ratios of Dac-Aβ40/cISM-sh are as indicated. Panels b), d), f) show the binding curves of cc-R3-GIsh (b), cc-L3-GIsh (d), cc-G3-GIsh (f); app. K_ds are means (±SD) from 3 binding curves (Dac-Aβ40 10nM). Measurements were performed in aq. buffer 1×b, pH 7.4, containing 1% HFIP.
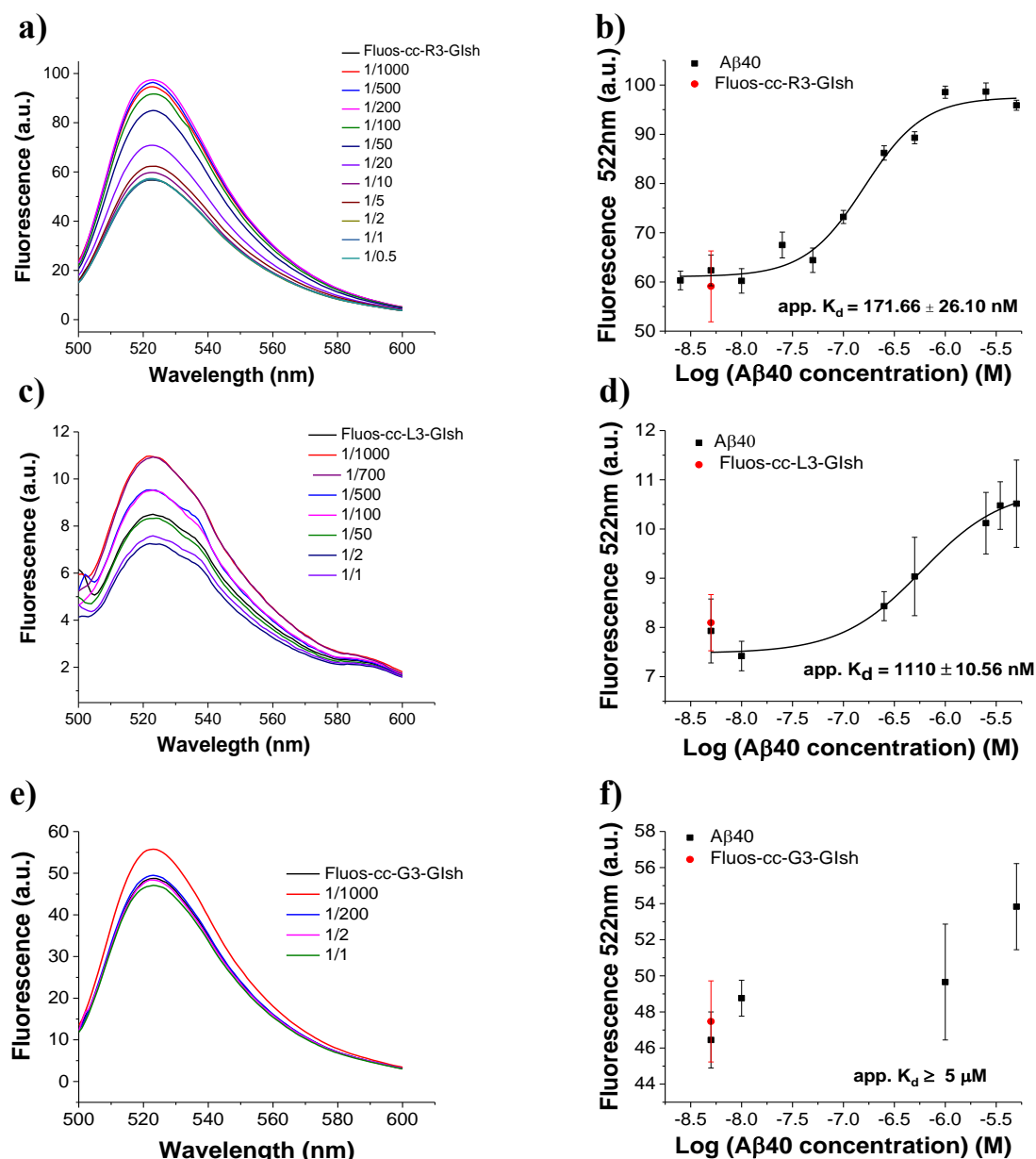
Figure 42. Determination of app. K$_d$s of interactions of cISMs-sh with Aβ40 by fluorescence titrations. Panels a), c), e) show fluorescence spectra of Fluos-cISMs-sh (5nM) alone and its mixtures with various amounts of Aβ40, the molar ratios of Fluos-cISMs-sh/Aβ40 are as indicated. Panels b), d), f) show the binding curves of Fluos-cc-R3-GIsh (b), Fluos-cc-L3-GIsh (d), Fluos-cc-G3-GIsh (f); app. K$_d$s are means (±SD) from 3 binding curves (Fluos-cISM-sh 5nM). Measurements were performed in aq. buffer 1×b, pH 7.4, containing 1% HFIP.

Table 27. Apparent affinities (app. K$_d$s) of interaction of cISMs-sh with Aβ40 as determined by fluorescence titration binding assays.

cISMs-sh	app. K$_d$ (±SD) (nM) with Dac-Aβ40[a]	app. K$_d$ (±SD) (nM) with Aβ40[b]
cc-R3-GIsh	382.33 (±89.24)	171.66 (±26.10)
cc-L3-GIsh	509.0 (±21.28)	1110 (±10.56)
cc-G3-GIsh	NB[c]	NB[d]

[a] App. K$_d$s, means (± SD) from 3 binding curves (Dac-Aβ40, 10nM); [b] app. K$_d$s, means (±SD) from 3 binding curves Fluos-cISMs (5nM) were titrated with Aβ40; [c] NB, no binding at peptide concentration ≤ 10μM; [d] NB, no binding at Aβ40 concentration ≤ 5μM, (aq. buffer 1×b, pH 7.4, containing 1% HFIP).

As expected, cc-R3-GIsh was found to bind with high affinity both to Dac-Aβ40 and to Aβ40 (Table 27). Of note, as shown (see Appendix Figure A10d) cc-R3-GIsh bound also to Aβ42 with an app. K_d of 102nM. In contrast, the app. K_ds of interactions of cc-L3-GIsh to monomeric/oligomeric Aβ40 species was 2-fold and 10-fold weaker (app. K_d = 509nM) (app. K_d = 1110nM), than the app. K_ds of interactions of cc-R3-GIsh with Aβ40 (Table 27). Finally, in the case of cc-G3-GIsh, no binding could be determined. These results indicated a correlation between binding affinities of these peptides and their effects on Aβ40 fibrillogenesis and cytotoxicity. Notably, the IC_{50} of the effect on Aβ40 cytotoxicity of cc-R3-GIsh was 125nM which fitted with its app. K_ds to monomeric/oligomeric Aβ40. On the other hand, in the case of cc-L3-GIsh an IC_{50} of 1740nM and weaker binding affinities to monomeric/oligomeric Aβ40 species were found. Finally, cc-G3-GIsh did not bind to Aβ40 and did not inhibit Aβ40 fibrillogenesis.

4.2.5 Interactions with Aβ40 by CD spectroscopy

To detect conformational changes in the mixtures of the cISMs-sh with Aβ40, CD spectra were recorded for Aβ40, cISMs-sh alone, and for their mixtures at ratios of 1/1. The CD spectrum of cc-R3-GIsh alone at 5μM showed a mixture of both random coil and β-turn contents. Aβ40 alone had a strong minimum at around 198nm which suggested mainly random coil. Comparison of the CD spectra mixture with the sum of the CD spectra of each component indicated that the interaction did not cause strong conformational changes (Figure 43a). In the case of cc-L3-GIsh when mixed at 1/1 with Aβ40, then differences between experimental CD spectra of mixtures and sum CD spectra were observed. The mixture (Figure 43b) presented an intense minimum at 225nm, which was characteristic of more ordered species. Finally, when cc-G3-GIsh was mixed at 1/1 ratio with Aβ40, no conformational change was observed. The CD spectra of its mixture with Aβ40 and the sum of the CD spectra of Aβ40 and cc-G3-GIsh were very similar as expected (Figure 43c).
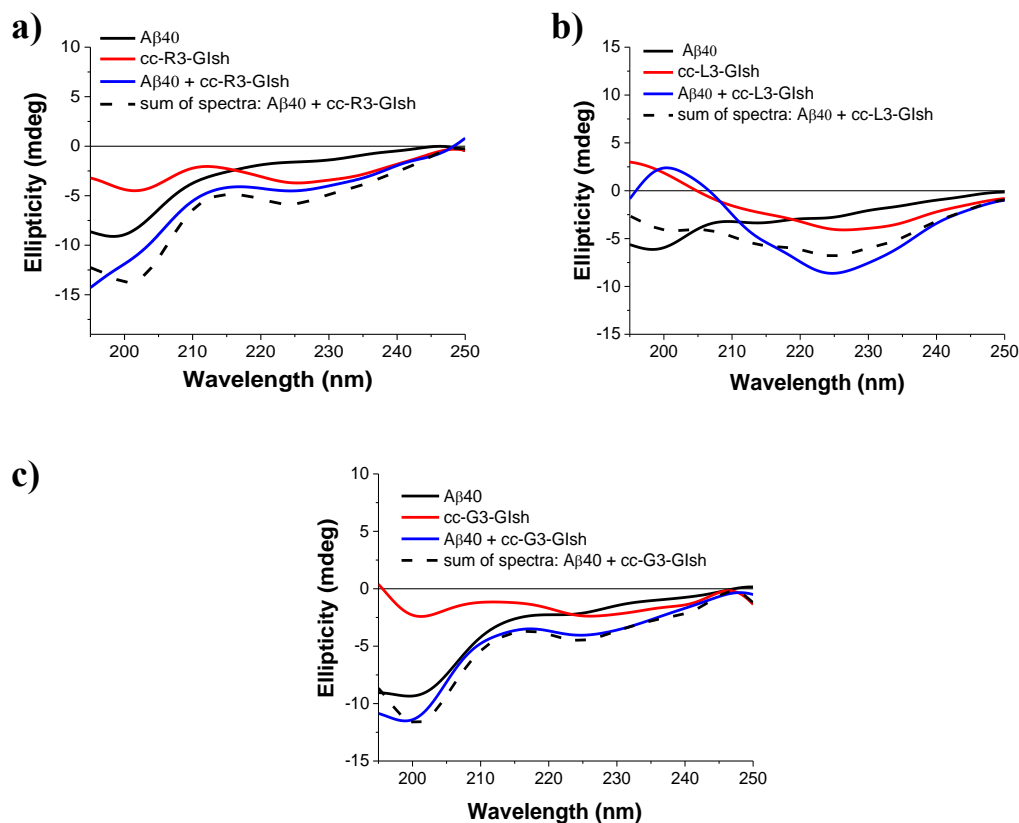
Figure 43. Interactions of Aβ40 and cISMs-sh studied by far-UV CD spectroscopy. CD spectra of freshly dissolved Aβ40 alone, cISM-sh alone, a mixture (1/1) of Aβ40 with cISM-sh and the sum of spectra (5μM, pH 7.4). Panels a)-c)

show CD spectra and interactions of (a) cc-R3-GIsh, (b) cc-L3-GIsh and (c) cc-G3-GIsh with Aβ40 as indicated. Measurements were performed in aq. buffer 1×b, pH 7.4, containing 1% HFIP.

## 4.2.6 **Inhibitory effects on IAPP fibrillogenesis and cytotoxicity**

Next, the effects of cISMs-sh on IAPP fibrillogenesis were studied. The ThT binding assay and the MTT reduction assay were applied. IAPP (6μM) was incubated either alone or in a mixture with cc-R3-GIsh, cc-L3-GIsh at a ratio of 1/2 and with cc-G3-GIsh at a ratio of 1/5. ThT fluorescence was measured at indicated time points and up to 7 days (Figure 44a). Aged solutions (24h and 7d) were added to RIN5fm cells, where the effects on IAPP cytotoxicity were determined by the MTT reduction assay. The results showed that both cc-L3-GIsh and cc-G3-GIsh were not able to inhibit IAPP fibrillogenesis and cytotoxicity (Figure 44a,b). On the contrary, cc-R3-GIsh inhibited IAPP fibrillogenicity and cytotoxicity (Figure 44c). Incubations of 7 days aged solutions were examined by TEM (Figure 44c); in the mixture of IAPP/cc-R3-GIsh amorphous aggregates were found.
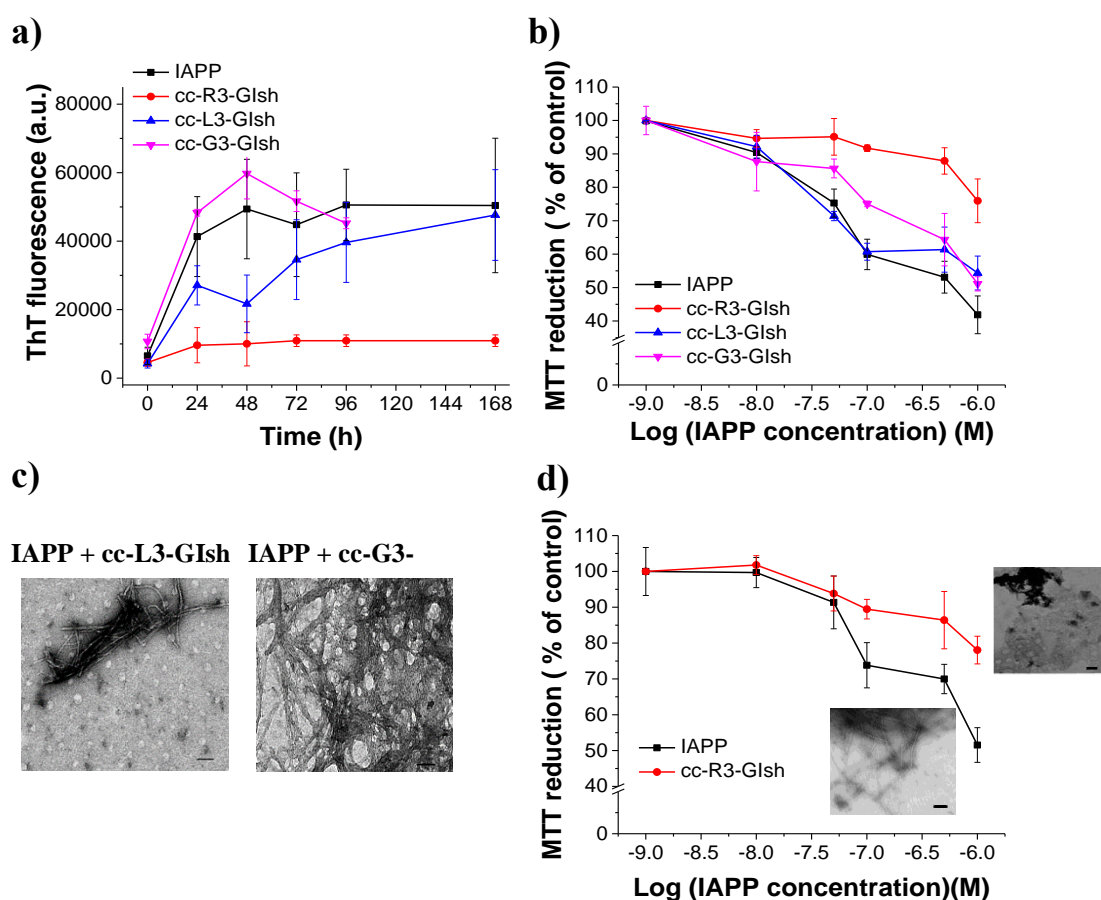
Figure 44. Effects of truncated cISMs on IAPP amyloid formation and cytotoxicity. (a) Fibrillogenesis of IAPP (6μM) alone and its mixtures (IAPP/peptide, 1/2 (cc-R3-GIsh), 1/2 (cc-L3-GIsh) and 1/5 (cc-G3-GIsh)) as determined via ThT binding assay (means (±SD), 3 assays); (b) effects on IAPP cytotoxicity. Solutions from (a) 24h aged were added to RIN5fm cells. Cell damage assessed by MTT reduction assay (means (±SD), 3 assays (n=3)). (c) TEM images of 24h-aged IAPP and its mixtures with cc-L3-GIsh, cc-G3-GIsh (solutions from (a)) (bars, 100nm); (d) cell-damaging effects of IAPP and its mixture (solutions from (a)) (7 day-aged) on RIN5fm cells via MTT reduction (means (±SD), 3 assays (n=3)); insets show TEM images of 7 days aged IAPP and its mixture with cc-R3-GIsh (solutions from (a)) (bars, 100nm).

Here, it is important to be mentioned that the R3-GIsh analogue containing Cys residues at the N- & C- termini (abbreviated as cc-R3-GIshred) was tested towards IAPP fibril formation. In that case as well, no inhibition could be observed (see Appendix Figure A9). From these results it was concluded that the formation of a disulfide bond plays a crucial role on the inhibitory potential of cc-R3-GIsh towards IAPP fibrillogenesis. Indeed, IC_{50} studies showed that cc-R3-GIsh is a potent inhibitor of

IAPP fibril formation with an IC$_{50}$ of 47.6nM (Table 28) (see Appendix Figure A5b). On the other hand, cc-L3-GIsh was a weaker inhibitor of IAPP fibril formation and cytotoxicity. The IC$_{50}$ of cc-L3-GIsh of the effects on formation of cytotoxic species was 314nM (Table 28) and was similar to the IC$_{50}$ of linear truncated L3-GI (abbreviated as L3-GIsh) (IC$_{50}$ = 201nM). Finally, cyclization of linear truncated G3-GI (abbreviated as G3-GIsh) had no effects on IAPP fibrillogenesis.

Table 28. IC$_{50}$s values of inhibitory effects of cISMs-sh on IAPP cytotoxicity.

cISMs-sh	IC$_{50}$ ($\pm$SD) (nM)[a]
cc-R3-GIsh	47.6 ($\pm$4)
cc-L3-GIsh	314 ($\pm$33.4)
cc-G3-GIsh	n.d[b]

[a] IC$_{50}$s, means ($\pm$SD) from 3 titration assays (n=3 each); IAPP (100nM) was titrated with different amounts of peptides under ThT conditions and cell-damaging effects were determined after 24h aged solutions by MTT assay; [b] n.d., non-determined (non-inhibitor).

The effects of cc-R3-GIsh on already nucleated IAPP fibrillogenesis were studied next. 24h-aged IAPP (16.5µM; incubation conditions as described above) containing significant amounts of IAPP fibrils (Figure 45) was added to the inhibitor and ThT binding and MTT reduction assay were determined. cc-R3-GIsh inhibited formation of cytotoxic IAPP oligomers and fibrils when added (1/2) to IAPP species before its nucleation. When the inhibitor was added at 6h where already toxic IAPP species/fibrils were formed, then no inhibition of IAPP cytotoxicity or any dissociation of the IAPP fibrils was found.
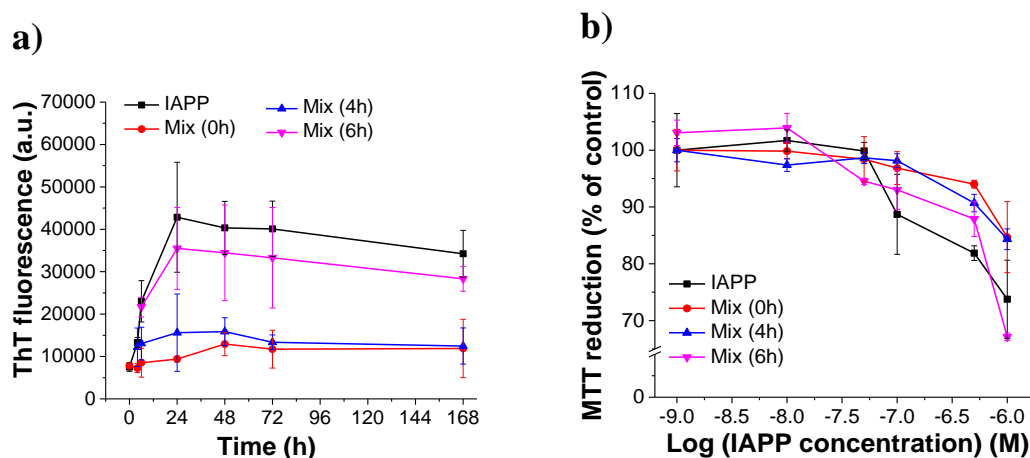
Figure 45. Effects of cc-R3-GIsh when added at pre- or post-nucleation stages of fibrillogenesis of IAPP. (a) Effects of cc-R3-GIsh when added (1/2) before (0h) or after (4h, 6h) nucleation on IAPP fibrillogenesis (16.5µM) as determined by ThT binding (means ($\pm$SD) from 3 assays), (b) effects of cc-R3-GIsh when added (1/2) before (0h) and after (4h ,6h) nucleation on IAPP fibrillogenesis (16.5µM) via the MTT reduction assay. Solutions from (a) (24h aged) added to RIN5fm cells; cell damage determined by MTT reduction (means ($\pm$SD), 3 assays (n=3 each)).

Next, the ability of cc-R3-GIsh to inhibit the cross-seeding interaction between Aβ40 fibrils and IAPP (Figure 46) was studied. For the studies on the effects of cc-R3-GIsh on the cross-seeding effect of fAβ40 seeds (10%) on IAPP (12µM) amyloidogenesis, 7 days aged fibril containing Aβ40 solution (16.5µM) was added to a solution of IAPP (IAPP, 12µM; fibrillization lag-phase of ~6h) or to a mixture of IAPP (12µM) with cc-R3-GIsh (IAPP/peptide, 1/2) to achieve a final fAβ40 seed concentration of 1.2µM. Kinetics of fibrillogenesis of cross-seeded IAPP, the cross-seeded mixture of IAPP with cc-R3-GIsh (1/2), unseeded IAPP, an unseeded mixture of IAPP with cc-R3-GIsh (1/2)

and fAβ40 alone (control) were followed by the ThT binding assay. For the studies on the effects of cc-R3-GIsh on the cross-seeding effect of fAβ40 seeds (10%) on IAPP amyloidogenicity, 24h-aged solutions (as indicated) used for the ThT binding assay were added to RIN5fm cells at the indicated final concentrations following dilution with cell medium. Cell damage was assessed following 20h incubation with the cells by the MTT reduction assay[87]. Of note, incubations of Aβ40 fibrils alone, IAPP alone and IAPP cross-seeded with Aβ40 fibrils were included in each assay to exclude that observed differences in lag-times or seeding effects in the presence of cc-R3-GIsh might be due to differences in IAPP lag-time or the cross-seeding ability of the applied seed preparation. As shown (Figure 46), cc-R3-GIsh was able to suppress Aβ40-mediated cross-seeding of IAPP fibrillogenesis and cytotoxicity. These results were confirmed by TEM analysis (see Appendix Figure A10).
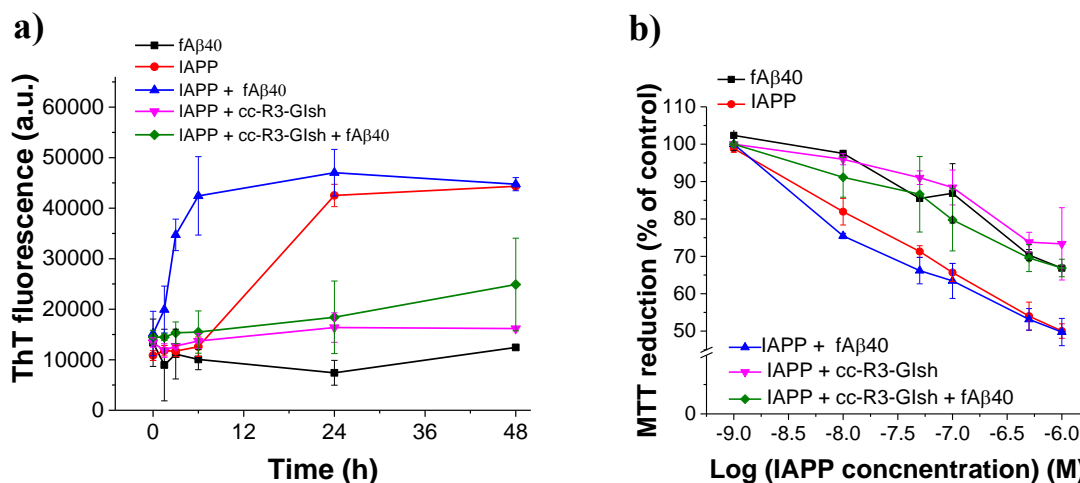
Figure 46. Suppression of Aβ40-mediated cross-seeding of IAPP fibrillogenesis and cytotoxicity by cc-R3-GIsh. (a) Suppression of Aβ40-mediated (fAβ40) (10%) cross-seeding of IAPP (12μM) fibrillogenesis in the presence of cc-R3-GIsh (2-fold) as assessed by ThT binding (means ($\pm$SD), 3 assays) and (b) effects of cross-seeding inhibition of cc-R3-GIsh via the MTT reduction assay following addition of 24h-aged solutions of (a) to RIN5fm cells (means ($\pm$SD), 3 assays (n=3 each)).

In conclusion: 1st) the hypothesis that the nature of the linker determines ISM structure and inhibitory function was confirmed including both potency and target selectivity also for the short segments of IAPP(14-18) and IAPP(22-28)-GI. 2nd) The data also showed that cyclization was very important in the case of cc-R3-GIsh and made a non-IAPP inhibitor to a potent inhibitor. Moreover, cc-R3-GIsh interacted with Aβ040(42) and inhibited both Aβ40 and Aβ42. Finally, it could also inhibit the cross-seeding of IAPP fibrillization mediated by Aβ fibrils. However, cyclization of L3-GIsh resulted in a weak Aβ40 inhibitor and to non-IAPP inhibitor. Finally, cyclization of G3-GIsh resulted in a peptide which could inhibit neither Aβ40 nor IAPP fibrillogenesis.

4.2.7 Determination of binding affinities towards IAPP

The interaction of truncated cISMs with IAPP was studied by fluorescence titration assays and CD spectroscopy. The app. K_ds of interactions of IAPP with cISMs-sh were determined by titrations of freshly made solutions of synthetic N-terminal fluorescein labelled IAPP (Fluos-IAPP) (5nM) with cISMs-sh (Figure 47). The titration of Fluos-IAPP with cc-R3-GIsh resulted in an app. K_d of 13.2nM, whereas the app. K_d that obtained from titration of Fluos-IAPP with cc-L3-GIsh was 60-fold weaker (app. K_d=817nM). The app. K_d of cc-G3-GIsh could not be determined (app. $K_d \geq$ 5μM).

The app. K_ds of interactions of mixtures of IAPP monomers/oligomers with cISMs-sh were then determined by titrating fluorescently labeled cyclic short peptides (5nM) with non-labeled IAPP (Figure 48). As found above, app. K_d of cc-R3-GIsh was 14-fold stronger (app. K_d = 172nM) than

the app. K_d that obtained from titration of Fluos-cc-L3-GIsh with IAPP (app. K_d. = 304nM). In the case of cc-G3-GIsh an app. K_d could not be determined (app. $K_d \geq 5\mu M$).
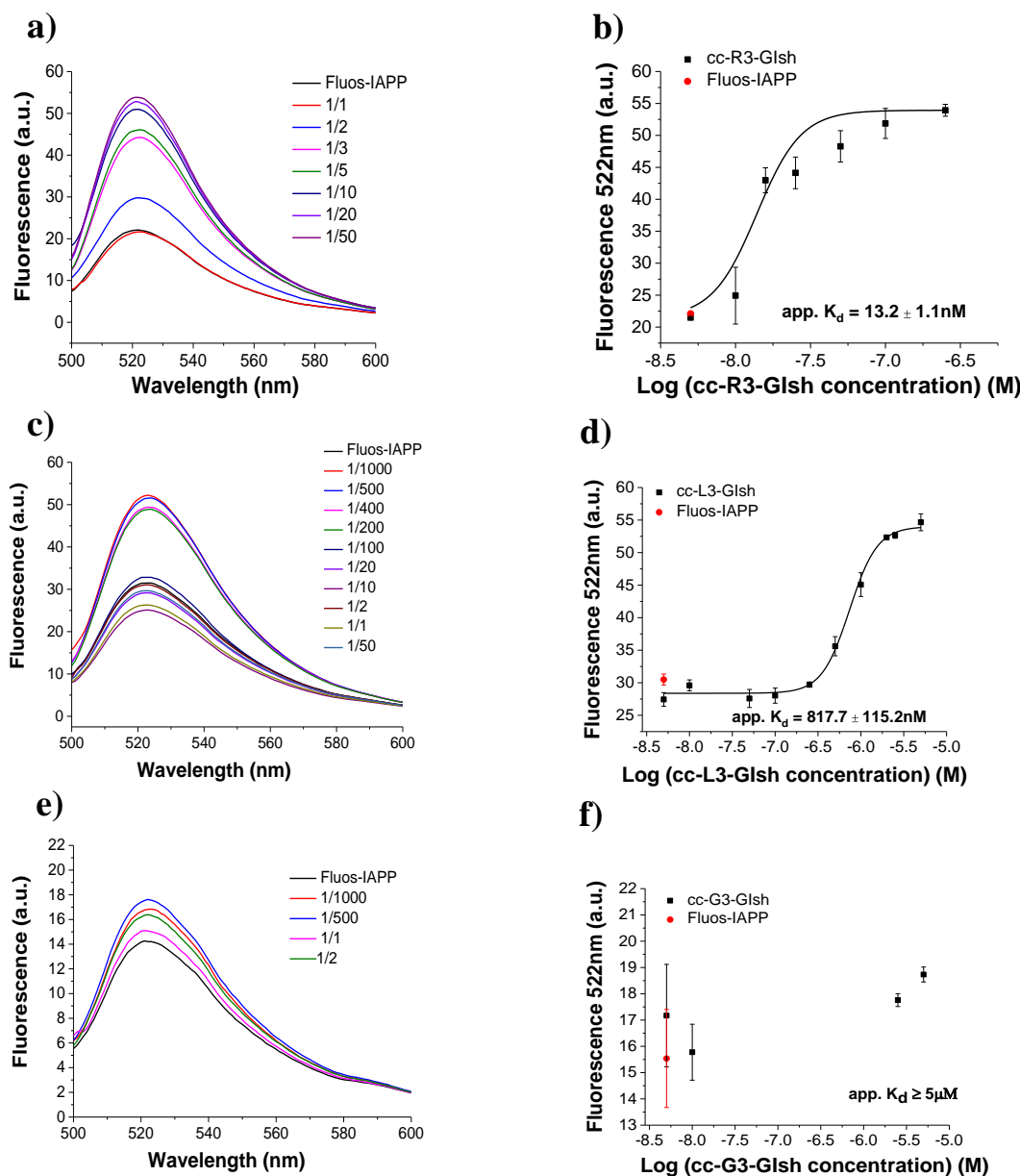
Figure 47. Determination of app. K_ds of interactions of IAPP and cISMs.sh by fluorescence spectroscopic titrations.
Panels a), c), e) show fluorescence spectra of Fluos-IAPP (5nM) alone and its mixtures with various amounts of f cc-R3-GIsh (a), cc-L3-GIsh (c), cc-G3-GIsh (e); the molar ratios of Fluos-IAPP/cISMs.sh are as indicated. Panels b), d), f) show the binding curves of cc-R3-GIsh (b), cc-L3-GIsh (d), cc-G3-GIsh (f); app. K_ds are means (±SD) from 3 binding curves (Fluos-IAPP 5nM). Measurements were performed in aq. buffer 1×b, pH 7.4, containing 1% HFIP.
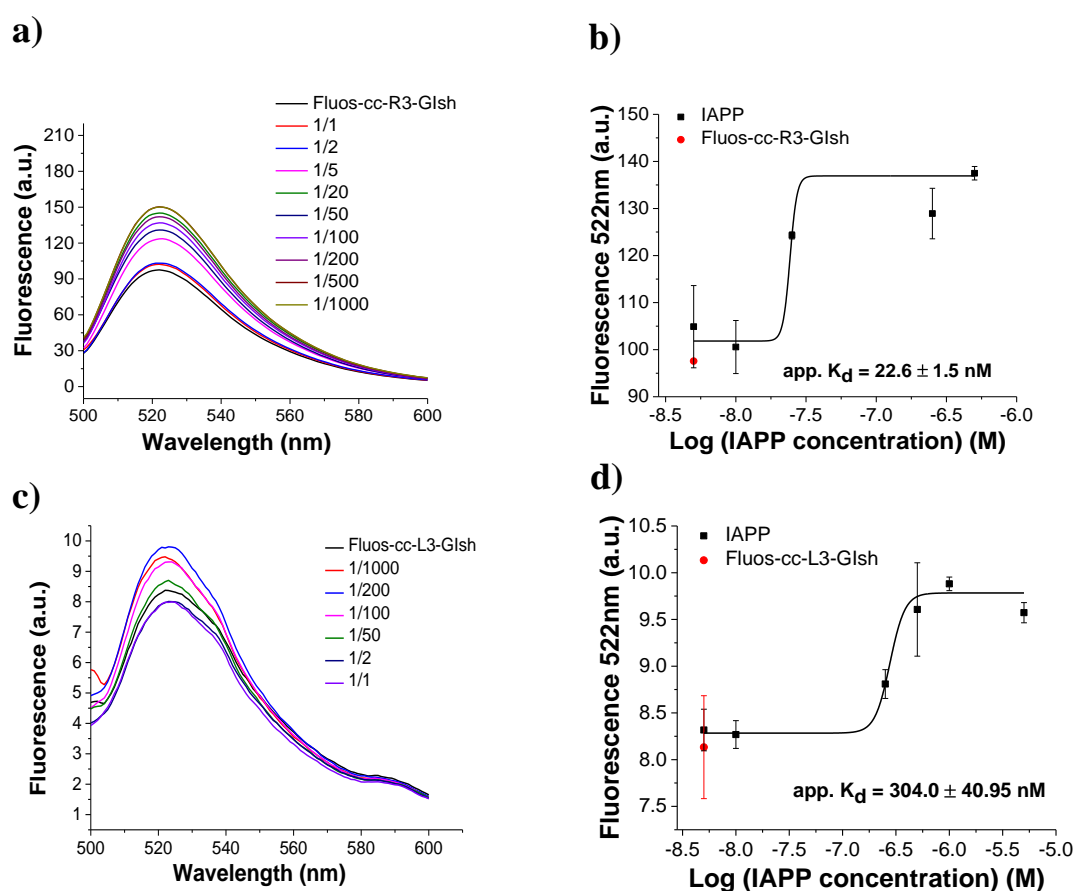
Figure 48. Determination of app. K_ds of interactions of IAPP and cISMs-sh by fluorescence spectroscopic titrations. Panels a), c) show fluorescence spectra of Fluos-cISMs-sh (5nM) alone and its mixtures with various amounts of IAPP; the molar ratios of Fluos-cISMs-sh/IAPP are as indicated. Panels b), d) show the binding curves of Fluos-cc-R3-GIsh (b), Fluos-cc-L3-GIsh (d); app. K_ds are means ($\pm$SD) from 3 binding curves (Fluos-cISM-sh 5nMeasurements were performed in aq. buffer 1×b, pH 7.4, containing 1% HFIP.

Apparent K_ds of interaction of cyclic shortened ISMs with IAPP are shown in Table 29. cc-R3-GIsh was found to interact with both monomeric and oligomeric species in low nanomolar range affinities. These results correlated very nice with the IC_{50} value found upon IAPP inhibition ($IC_{50} = 47$nM). Next, the app. K_d of cc-L3-GIsh with IAPP showed that it interacts with both species of IAPP in a similar manner, although weaker binding than in case of cc-R3-GIsh was observed. These results also correlated with the results of the studies on the inhibitory effects on IAPP fibrillogenesis and cytotoxicity ($IC_{50} = 314$nM). Finally, in the case of cc-G3-GIsh no binding affinity with IAPP (app. $K_d \geq 5\mu$M), which explained its inability to inhibit.

Table 29. Apparent affinities (app. K_ds) of interaction of cISMs-sh with IAPP as determined by fluorescence titration binding assays.

cISMs-sh	app. K_d ($\pm$SD) (nM) with Fluos-IAPP[a]	app. K_d ($\pm$SD) (nM) with IAPP[b]
cc-R3-GIsh	13.2 ($\pm$1.1)	22.6 ($\pm$1.5)
cc-L3-GIsh	817.66 ($\pm$115.24)	304 ($\pm$26)
cc-G3-GIsh	NB[c]	n.d[d]

[a] App. K_ds, means($\pm$SD) from 3 binding curves Fluos-IAPP (5nM) titrated with cISMS-sh; [b] app. K_ds, ($\pm$SD) from 3 binding curves Fluos-cISMs (5nM) titrated with IAPP; [c] NB, no binding at peptide concentration $\leq 5\mu$M; [d] n.d not determined, (aq. buffer 1×b, pH 7.4, containing 1% HFIP).

4.2.8 **Interactions with IAPP by CD spectroscopy**

To further investigate the interaction between IAPP and the two cyclic short inhibitors, CD spectroscopy was applied. CD was performed with IAPP/inhibitors at the ratio of 1/2 and 1/3 which was found to be required for inhibitory effects. The spectra of the two inhibitors at a concentration of 10μM, 15μM and of IAPP at 5μM as well as of IAPP/inhibitors mixture were recorded (Figure 48). The CD spectrum of the mixture of IAPP with cc-R3-GIsh (1/2) was differed from the sum of the spectra; this indicated that there is a change in overall conformation of the two peptides (Figure 48a). In the case of CD spectra of the mixture of IAPP with cc-L3-GIsh (1/3) only a small difference was observed between the CD spectra of sum IAPP and cc-L3-GIsh with the CD spectra of the mixture of cc-L3-GIsh with IAPP (Figure 48b); this indicated a small conformational change upon interaction of inhibitor with IAPP.
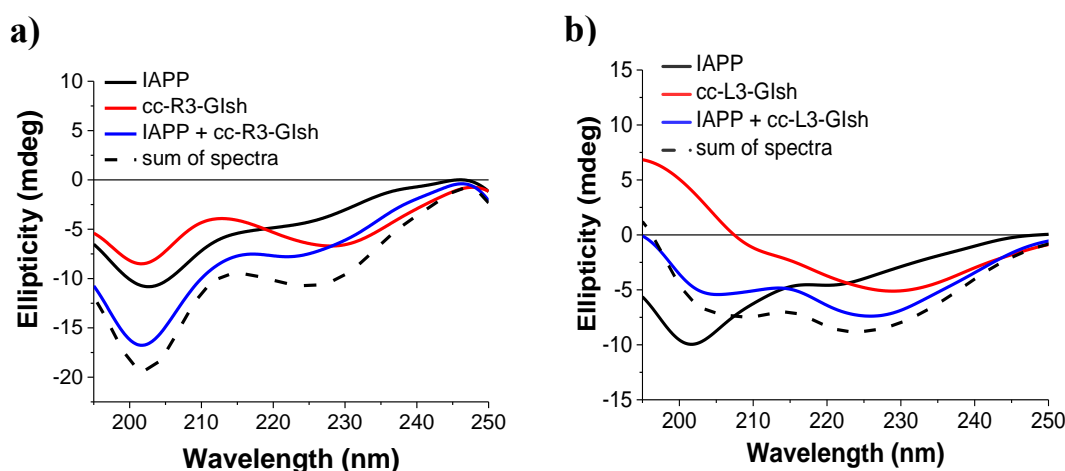
Figure 49. Interactions of IAPP with cISMs-sh as studied by far-UV CD spectroscopy. CD spectra of freshly dissolved IAPP alone (5μM), cISM-sh alone (10μM) or (15μM), a mixture (1/2) or (1/3) of IAPP with cISM-sh and the sum of spectra. Panels a), b) show CD spectra and interactions of (a) cc-R3-GIsh, (b) cc-L3-GIsh, with IAPP as indicated. Measurements were performed in aq. buffer 1×b, pH 7.4, containing 1% HFIP.

The studies in this chapter showed that truncation and cyclization of IAPP segments connected with RRR tripeptide resulted not only in a nanomolar inhibitor of Aβ40 but in nanomolar inhibitor of as well. In addition, high binding affinities of cc-R3-GIsh to both polypeptides were found. Moreover, it was found that cyclization of peptide with the LLL linker didn't improve significantly neither the Aβ nor the IAPP amyloid inhibition properties. Finally, truncation and cyclization of IAPP segments which are connected with GGG linker did not affect the effects towards Aβ and IAPP inhibition. We concluded: 1st) arginines are very important in the linker and 2nd) cyclization of R3-GIsh, might be reasons for its inhibitory properties on interaction and inhibition Aβ and IAPP.

4.3 **Studies on glycine containing cyclic analogues of truncated R3-GI**

4.3.1 **Peptide design and synthesis**

According to Bakou et al.[88], F15, L16, F23 and I26 play key roles in the self-assembly of IAPP and in its hetero-assembly with Aβ. Ttherefore, we asked whether these 4 amino acids may be important for inhibitory effects on amyloidogenesis of IAPP and Aβ. To investigate this hypothesis, all the amino acids were substituted with glycine except for the aromatic/hydrophobic residues F15, L16, F23 and I26 (analogues abbreviated as **cALLG.sh**) in peptides containing the 4 different linkers RRR, LLL, GGG and Aoc-Peg (which is as combination of a hydrophobic-flexible linker 8-

aminooctanoic acid (Aoc) and 8-Amino-3,6-dioxaoctanoic acid (PEG)) as a flexible and hydrophilic linker (Scheme 4). I then tested these analogues regarding their inhibitory potential towards Aβ40(42) and IAPP fibrillogenesis and cytotoxicity.
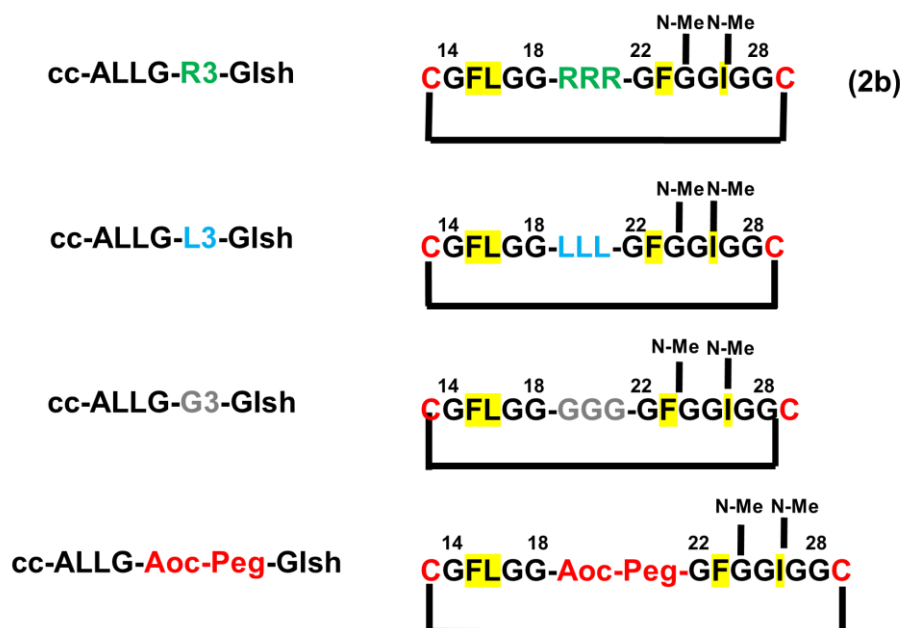
Scheme 4. Rational design of cyclic glycine containing analogues with different linkers (cALLG-sh). Sequences of cALLG-sh analogues; cc-ALLG-R3-GIsh, cc-ALLG-L3-GIsh, cc-ALLG-G3-GIsh and cc-ALLG-Aoc-Peg-GIsh. Analogues abbreviation is based on the name of the residue on the linker. Cyclization is indicated by "cc" and short indicated by "sh"; glycine substituents are indicated by "ALLG", „-GI„ indicated the presence of the N-methyl-residues at G^{24} & I^{26}: "N-Me" and the 4 important AA for self-assembly of IAPP and in its hetero-assembly with the Aβ are highlighted with yellow; numbering is based on IAPP sequence[88].

Table 30. Sequences of N-terminal truncated cyclic ALLG-analogues and their abbreviations (cALLG-sh).

Peptide sequence	Peptide abbreviation
C-G**FL**GG-**RRR**-GF(N-Me)GG(N-Me)**I**GG-C-amide	cc-ALLG-**R3**-GI sh
C-G**FL**GG-**LLL**-GF(N-Me)GG(N-Me)**I**GG-C-amide	cc-ALLG-**L3**-GIsh
C-G**FL**GG-**GGG**-GF(N-Me)GG(N-Me)**I**GG-C-amide	cc-ALLG-**G3**-GIsh
C-G**FL**GG-**Aoc-Peg**-GF(N-Me)GG(N-Me)**I**GG-C-amide	cc-ALLG-**Aoc-Peg**-GIsh

Cyclic peptides (Table 30) were synthesized by solid phase peptide synthesis (SPPS) utilizing Fmoc-strategy. Crude peptide with cysteines in reduced form were purified via RP-HPLC and characterized by MALDI-TOF (Table 31). In the case of cc-ALLG-R3-GIsh and cc-ALLG-G3-GIsh oxidation was performed by stirring crude peptides in a mixture of 40% (v/v) DMSO in aqueous NH_4HCO_3 (0.1mM, pH 8.7) for 3h. cc-ALLG-R3-GIsh, cc-ALLG-G3-GIsh and cc-ALLG-Aoc-Peg-GIsh were purified by RP-HPLC and characterized by MALDI-TOF. Purifications were conducted with a yield of around 5%, 5.5% and 4.8% of crude respectively (Table 31). In the case of cc-ALLG-L3-GIsh another oxidation method was used. 1mg of cc-ALLG-L3-GIsh crude was dissolved in 300μl DMSO, 500μl ddH2O and 300μl H_2O_2; no incubation time was needed. cc-ALLG-L3-GIsh was purified by RP-HPLC, with a yield of pure (regarding crude) ∼10.6%.

Table 31. Characterization of the synthetic oxidized peptides via HPLC and MALDI-TOF.

cALLG-sh peptides[a]	HPLC program	t_R (min)[b]	Yield[c]	[M+H]+ expected[d]	[M+H]+ found[d]
cc-ALLG-R3-GIsh	1	17.1	5%	1695.95	1695.30
cc-ALLG-L3-GIsh	1	22.0	10.6%	1566.87	1588.87[d]
cc-ALLG-G3-GIsh	1	27.5	5.5%	1398.0	1421.04
cc-ALLG-Aoc-Peg-GIsh	1	24.38	4.8%	1420.70	1420.714

[a] Peptides were synthesized with free amino terminus and amidated C-terminal end; [b] t_R: HPLC retention time; [c] % yield with regard to respective crude product; [d] monoisotopic molar mass [M+H]+ expected and [M+H]+ found.

4.3.2 Biophysical characterization

4.3.2.1 Conformational studies via CD spectroscopy

Next, the conformations of the above peptides were determined by far-UV CD spectroscopy. For these measurements, peptides were dissolved in 10mM sodium phosphate buffer, pH 7.4 containing 1% HFIP and CD spectra were recorded. First, CD spectra of the peptides were measured at different concentrations between 5-50μM to determine their aggregation propensities. All of them exhibited similar oligomerization profiles (Figure 50). Two common features were observed in the C-dependence spectra of the cyclic-ALLG analogues: 1st) the substitution of N14, V17, H18, N22, A25 and S27 with Gly in the cc-ALLG-R3-GIsh, cc-ALLG-L3-GIsh, cc-ALLG-G3-GIsh induced β-sheet/β-turn conformation with the characteristic minima at 225-230nm. The 2nd) common characteristic was the weak CD signal of the cALLG-sh analogues which was probably related to their fast aggregation propensity (Figure 50).
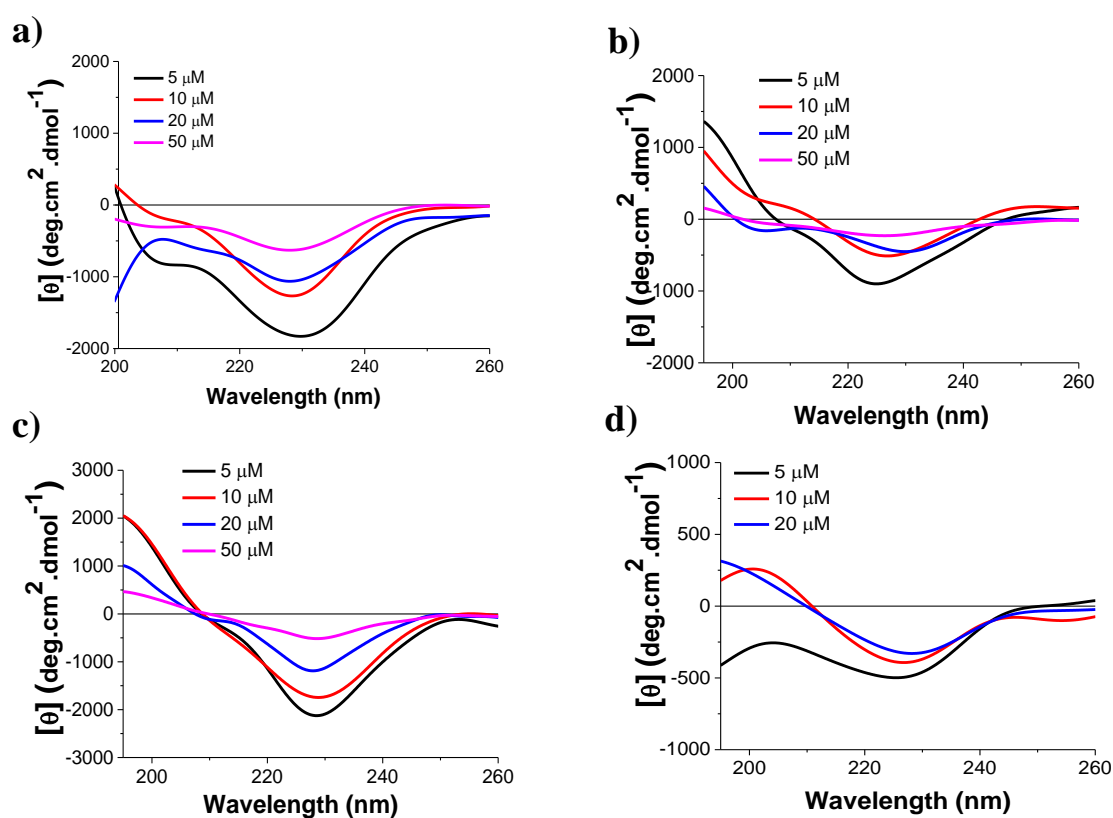
Figure 50. Concentration dependence of the CD spectra of cALLG-sh peptides. (a) CD spectra of cc-ALLG-R3-GIsh, (b) cc-ALLG-L3-GIsh, (c) cc-ALLG-G3-GIsh and (d) cc-ALLG-Aoc-Peg-GIsh. Measurements were performed at peptide concentrations between 5-50μM in aq. buffer 1×b, pH 7.4, containing 1% HFIP.

4.3.2.2 **Self-association studies via fluorescence spectroscopy**

Next, the self-association propensities of cc-ALLG.sh peptides were studied in more detailed and fluorescence binding assays were performed to quantify the apparent affinity (app. K_d) of their interactions with themselves. App. K_ds of self-association of cyclic-ALLG-analogues (cALLG.sh) were determined by titration of freshly made solutions of synthetic N-terminal fluorescein labeled cALLG.sh analogues (Fluos-cALLG-analogue) (5nM) with non-labeled cyclic-ALLG-analogue (cALLG.sh) (Figure 51). Binding of 250-fold molar excess of cc-ALLG-R3-GIsh to Fluos-cc-ALLG-R3-GIsh caused 30% fluorescence enhancement. 500-fold molar excess of cc-ALLG-L3-GIsh and cc-ALLG-G3-GIsh to Fluos-cc-ALLG-L3-GIsh and Fluos-ALLG-G3-GIsh respectively, caused ~40% fluorescence enhancement (Figure 51a-f). However, no interaction was found for cc-ALLG-Aoc-Peg-GIsh even at 1000-fold higher concentration. Sigmoidal binding isotherms were obtained and the determined apparent affinities of the interactions (app. K_d values) were 43.3 (±3.5) nM for cc-ALLG-R3-GIsh, which was 14-fold stronger than cc-ALLG-L3-GIsh (app. K_d = 608nM) and 25-fold better than in the case of cc-ALLG-G3-GIsh (app. K_d = 1054.33nM). In the case of cc-ALLG-Aoc-Peg-GIsh apparent affinity was higher than 5μM (app. $K_d \geq$ 5μM). Table 32 shows the app. K_ds of self-assembly of all tested cALLG.sh analogues.

Table 32. App. K_ds of self assembly of cALLG.sh peptides as determined by fluorescence titration studies.

cALLG.sh peptides	app. K_d (±SD) nM[a]
cc-ALLG-R3-GIsh	43 (±3)
cc-ALLG-L3-GIsh	608 (±68)
cc-ALLG-G3-GIsh	1054 (±145)
cc-ALLG-Aoc-Peg-GIsh	NB[b

[a] App. K_ds are means (±SD) from 3 binding curves Determined by titrations of synthetic N-terminal fluorescein-labeled cALLG.sh (5nM) with non-labeled cALLG.sh; [b] NB, no binding at peptide concentration $\leq$ 5μM, (aq. buffer 1×b, pH 7.4, containing 1% HFIP).
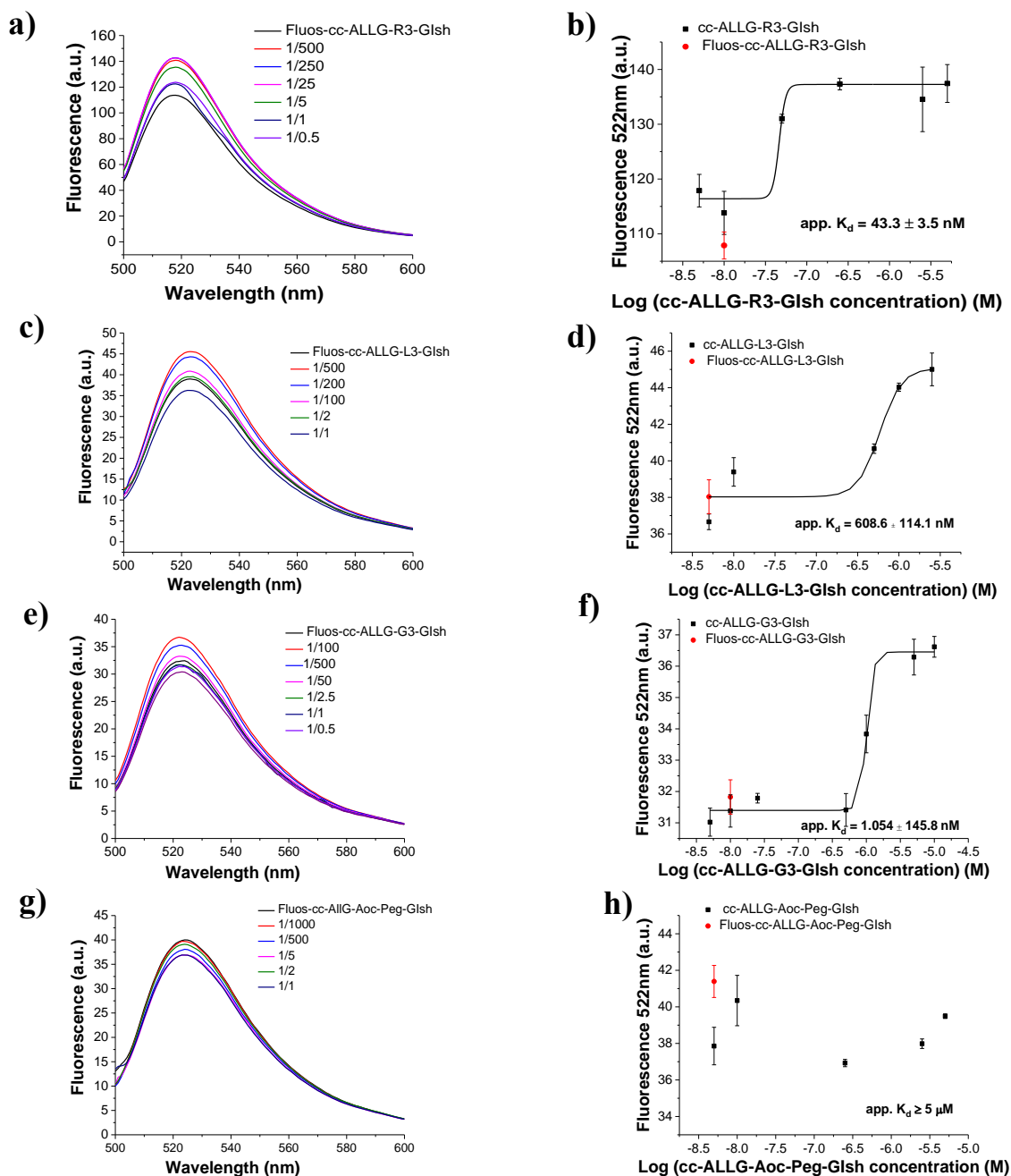
Figure 51. Apparent affinities (app. K$_d$) of self- association of cALLG-sh analogues as determined by fluorecence spectroscopy. Panels a), c), e), g) show fluorescence spectra of Fluos-cALLG-sh (5nM) alone and its mixtures with various amounts of cc-ALLG-R3-GIsh (a), cc-ALLG-L3-GIsh (c), cc-ALLG-G3-GIsh (e), cc-ALLG-Aoc-Peg-GIsh (g); the molar ratios of Fluos-cALLG-sh/cALLG-sh are as indicated. Panels b), d), f), h) show the binding curves of cc-ALLG-R3-GIsh (b), cc-ALLG-L3-GIsh (d), cc-ALLG-G3-GIsh (f), cc-ALLG-Aoc-Peg-GIsh (h); app. K$_d$s are means (±SD) from 3 binding curves (Fluos-cALLG-sh 5nM). Measurements were performed in aq. buffer 1×b, pH 7.4, containing 1% HFIP.

4.3.3 Effects on fibrillogenesis and cytotoxicity of Aβ40(42)

Next, the question was addressed whether the short cyclic peptides (cALLG-sh) could intervene with Aβ40 self-assembly into fibrils and affect formation of cytotoxic Aβ40 aggregates. As all peptides did not inhibit Aβ40 fibrillogenesis and cytotoxicity at 1/1 ratio (data not shown), I tested them at 5- and 10 -fold molar excess to Aβ40. Aβ40 alone (16.5μM, pH 7.4) and the (1/5 or 1/10) mixtures of Aβ40 with the peptides were incubated for 3 or 7 days and fibrillogenesis and cytotoxicity were quantified by the ThT binding and the MTT reduction assay (Figure 52).
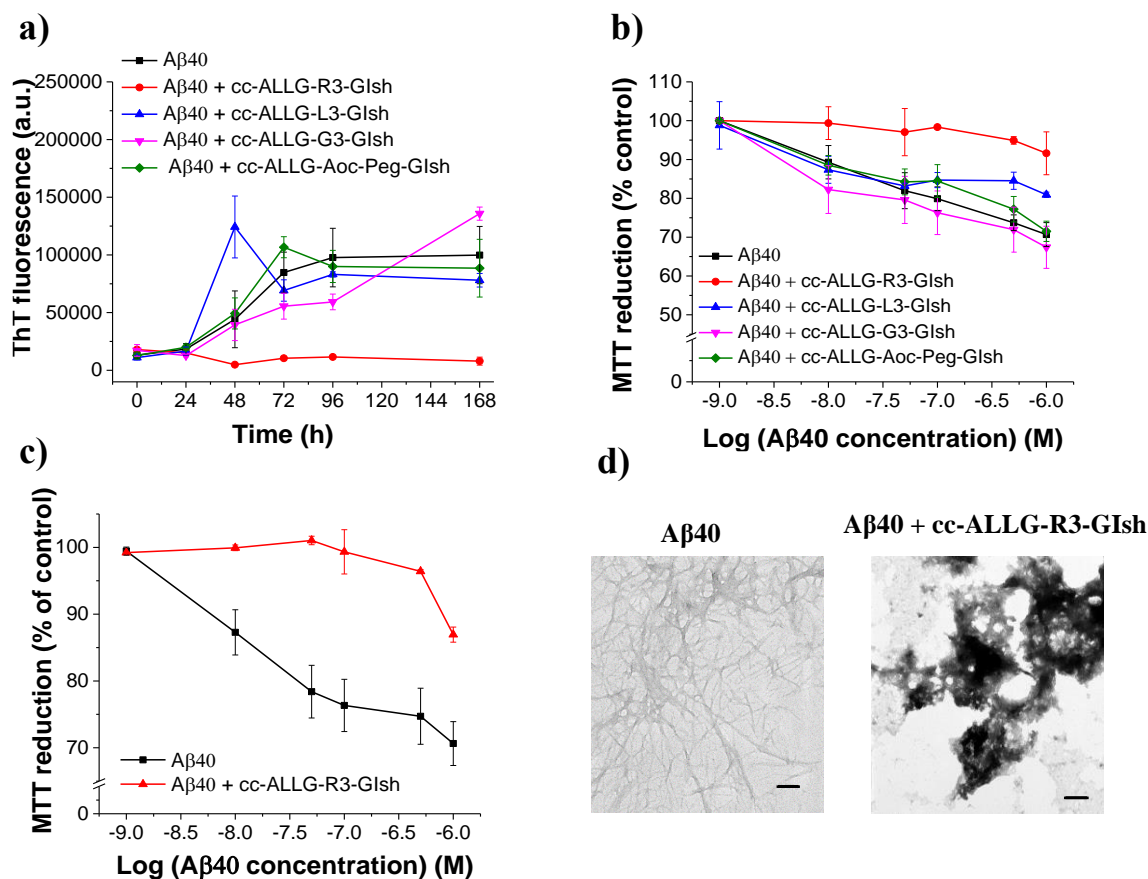
Figure 52. Effects of cALLG-sh peptides on Aβ40 amyloid formation and cytotoxicity. (a) Fibrillogenesis of Aβ40 (16.5μM) or its mixtures with cc-ALLG-R3-GIsh, cc-ALLG-L3-GIsh (1/5) or cc-ALLG-G3-GIsh, cc-ALLG-Aoc-Peg-GIsh (1/10) by the ThT binding assay (means (±SD), 3 assays), (b) effects on cell viabillity: solutions from (a) (3 day-aged) added to PC-12 cells, (c) effects of cc-ALLG-R3-GIsh on cell viability: solutions from (a) (7 days aged) added to PC-12 cells; cell damage determined by the MTT reduction assay (means (±SD), 3 assays,(n=3 each)), (d) TEM images of 7 days aged Aβ40 and its mixture with cc-ALLG-R3-GIsh (solutions from (a)) (bars, 100nm).

As shown (Figure 52) cc-ALLG-R3-GIsh was the only peptide that at 5-fold excess could inhibit up to 7 days Aβ40 fibrillogenesis and cytotoxicity (Figure 52b,c); by TEM analysis only amorphous aggregates were found in mixture with Aβ40, whereas the TEM picture of Aβ40 showed only fibrils (Figure 52d).

As next, the effects of cc-ALLG-R3-GIsh on Aβ42 fibrillogenesis and cytotoxicity were studied. Aβ42 alone (16.5μM, pH 7.4) and its mixture with the peptide (1/5) was incubated up to 7 days and fibrillogenesis and cytotoxicity were followed by the ThT binding and the MTT reduction assays. In fact, cc-ALLG-R3-GIsh, an Aβ40 inhibitor, blocked Aβ42 fibrillogenesis as well (see Appendix Figure A11). To evaluate the effects of the cc-ALLG-R3-GIsh that inhibited Aβ42 fibrillogenesis on Aβ42-mediated cell damage, 7 days aged solutions (Aβ42 fibrillization plateau; see Appendix Figure A11a) were added to PC-12 cells and cell viabilities were determined via the MTT reduction assay (see Appendix Figure A11b). In fact, cc-ALLG-R3-GIsh Aβ40 inhibitor effectively suppressed formation of Aβ42 cytotoxic assemblies as well and TEM analysis confirmed the above results (see Appendix Figure A11b; insets).

Finally, since cc-ALLG-R3-GIsh showed the best inhibitory effect on Aβ40 amyloid self-assembly (IC$_{50}$ = 654.3nM), (see Figure Appendix A12a), we tested at which stages of the Aβ40 self-assembly pathway cc-ALG-R3-GIsh interfers with. cc-ALLG-R3-GIsh blocked and inhibited formation of cytotoxic Aβ40 oligomers and fibrils (when added at 5-fold excess to Aβ40) before (0h, 24h) nucleation of Aβ40 fibrillogenesis (Figure 53). However, when cc-ALLG-R3-GIsh was added after

(72h) nucleation of Aβ40 fibrillogenesis then any inhibitory effects could be observed. Moreover, no dissociation of fibrils or cytotoxic aggregates was observed (Figure 53b).
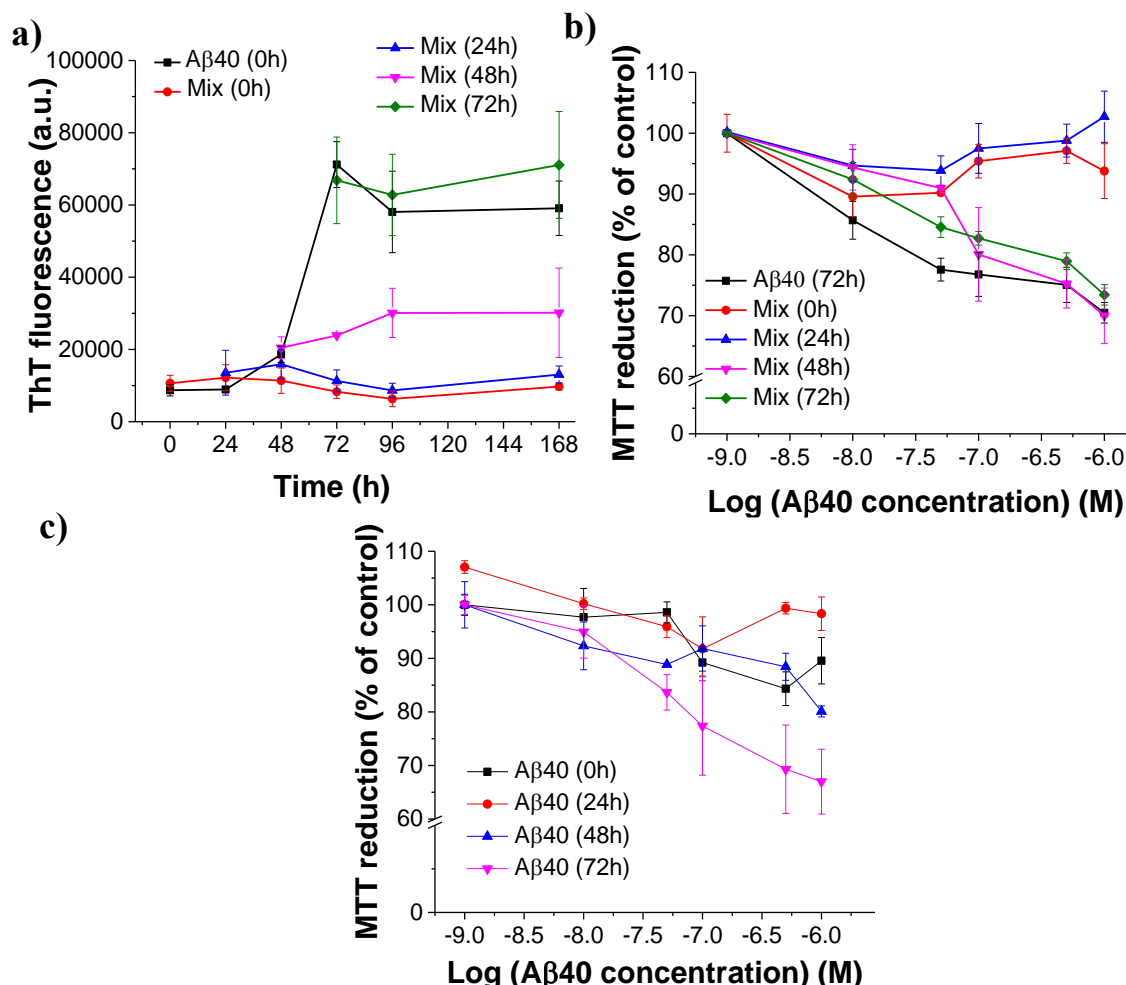
Figure 53. Inhibitory effects of cc-ALLG-R3-GIsh when added at pre- or postnucleation stages of fibrillogenesis of Aβ40. (a) Effects of cc-ALLG-R3-GIsh when added (1/5) before (0h, 24h), at (48h) or after (72h) nucleation on Aβ40 fibrillogenesis (16.5μM) as determined by ThT binding (means ($\pm$SD) from 3 assays), (b) effects of cc-ALLG-R3-GIsh when added (1/5) before (0h, 24h), at (48h) or after (72h) nucleation on Aβ40 fibrillogenesis (16.5μM) via MTT reduction assay. Solutions from (a) (8 days aged) were added to PC-12 cells; cell damage was determined by the MTT reduction (means ($\pm$SD) from 3 assays (n=3 each)), c) formation of cytotoxic assemblies within the Aβ40 fibrillogenesis process. Aged Aβ40 solutions from (a) were added at the indicated time points to PC12 cells and cell damage was assessed by the MTT reduction assay (means ($\pm$SD), from 3 assays (n=3 each)).

The results suggested that the 4 aromatic/hydrophobic IAPP residues F15, L16, F23, I26 in cc-ALLG-R3-GIsh are enough for its amyloid activity. However, the presence of only the four amino acids and the "wrong" linker resulted in no inhibitory activity.

4.3.4 **Determination of binding affinities towards Aβ40**

Next, fluorescence studies with cc-ALLG-peptides followed to find out whether the peptides interact with Aβ40. The apparent K_ds of interactions of Aβ40 with cyclic ALLG-peptides were determined by titrating synthetic Dac-Aβ40 (10nM) with cALLG-sh peptides (Figure 54). All app. K_ds of cALLG-sh peptides are presented in Table 33. cc-ALLG-R3-GIsh showed the best binding affinities compared to the other three cALLG-sh peptides. cc-ALLG-R3-GIsh was found to bind to both monomeric and oligomeric species of Aβ40 with low nanomolar affinities (app. K_d = 187nM and app. K_d = 130nM respectively). cc-ALLG-L3-GIsh bound only to Dac-Aβ40 with an app. K_d =

673nM; no binding to Fluos-Aβ0 could be observed at c ≤ 5μM. In the case of cc-ALLG-G3-GIsh app. K_ds to Dac-Aβ40 was around 3μM while binding to Fluos-Aβ40 could not be determined (at c ≤ 5μM). cc-ALLG-Aoc-Peg-GIsh was found to bind to Aβ40 mono/and or oligomers with app. K_ds 742.46nM and 297nM, respectively. The results showed that two of the three new short cyclic ALLG-peptides were able to bind both monomeric/oligomeric species of Aβ40. These results correlated with the inhibitory properties of cc-ALLG-R3-GIsh. Of note, the app. K_d of cc-ALLG-R3-GIsh with Fitc-Aβ42 was determined and found to be in low nanomolar range (app. K_d = 199 ± 25.5nM) (see Appendix Figure A11c,d).
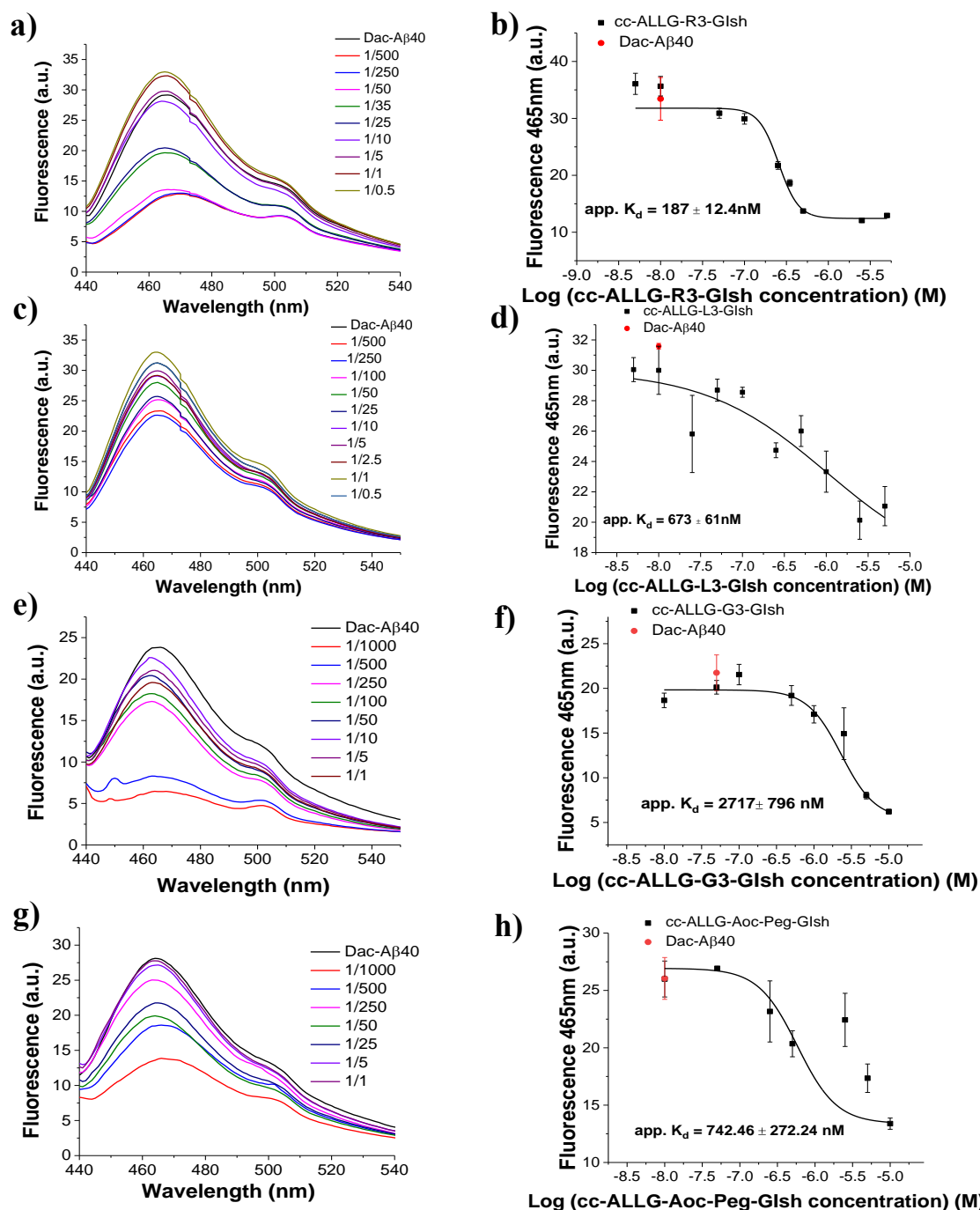
Figure 54. Determination of app. K_ds of interactions of cALLG-sh peptides with Aβ40 by fluorescence titrations. Panels a), c), e), g) show fluorescence spectra of Dac-Aβ (10nM) alone and its mixtures with various amounts of cc-ALLG-R3-GIsh (a), cc-ALLG-L3-GIsh (c), cc-ALLG-G3-GIsh (e), cc-ALLG-Aoc-Peg-GIsh (g); the molar ratios of Fluos-cALLG-sh/cALLG-sh are as indicated. Panels b), d), f), h) show the binding curves of cc-ALLG-R3-GIsh (b), cc-ALLG-

L3-GIsh (d), cc-ALLG-G3-GIsh (f), cc-ALLG-Aoc-Peg-GIsh (h); app. K_ds are means (±SD) from 3 binding curves (Dac-Aβ 10nM). Measurements were performed in aq. buffer 1×b, pH 7.4, containing 1% HFIP.

Figure 55. Determination of app. K_ds of interactions of oligomeric Aβ40 species with cALLG-sh by fluorescence spectroscopy. Panels a), c), e), g) show fluorescence spectra of Fluos-cALLG-sh (5nM) alone and its mixtures with various amounts of Aβ40 the molar ratios of Fluos-cALLG-sh/Aβ40 are as indicated. Panels b), d), f), h) show the binding curves of Fluos-cc-ALLG-R3-GIsh (b), Fluos-cc-ALLG-L3-GIsh (d), Fluos-cc-ALLG-G3-GIsh (f), Fluos-cc-ALLG-Aoc-Peg-GIsh (h) with Aβ40; app. K_ds are means (±SD) from 3 binding curves (Fluos-cALLG-sh 5nM). Measurements were performed in aq. buffer 1×b, pH 7.4, containing 1% HFIP.

Table 33. Apparent affinities (app. K_ds) of interaction of cALLG-sh peptides with Aβ40 as determined by fluorescence titration binding assays.

cALLG-sh peptides	app. K_d (±SD) (nM) with Dac-Aβ40[a]	app. K_d (±SD) (nM) with Aβ40[b]
cc-ALLG-R3-GIsh	187 (±12)	130 (±36)
cc-ALLG-L3-GIsh	673 (±61)	NB[c]
cc-ALLG-G3-GIsh	2717 (±796)	NB[c]
cc-ALLG-Aoc-Peg-GIsh	742.46 (±272.24)	297 (±122)

[a] App. K_ds, means (±SD) from 3 binding curves Dac-Aβ40 (10nM) titrated with cALLG-sh peptides; [b] app. K_ds, means (±SD) from 3 binding curves Fluos-cALLG-sh peptides (5nM) were titrated with Aβ40; [c] NB, no binding at Aβ40 concentration ≤ 5µM, (aq. buffer 1×b, pH 7.4, containing 1% HFIP).

4.3.5 Interactions with Aβ40 by CD spectroscopy

To investigate conformationally changes occurringin the interactions of the cALLG-sh peptides with Aβ40, CD spectroscopy was applied. CD spectra were recorded for Aβ40, the cyclic ALLG-peptides alone and their mixtures with Aβ40 at ratio of 1/1. Firstly, the CD spectra of cc-ALLG-R3-GIsh were recorded, where at 5µM only ordered species were observed. Aβ40 alone had a strong minimum at around 198nm which suggested mainly random coil. By comparing the CD of the mixture with the sum of CD spectra, a difference was observed which indicated an interaction and the presence of both unordered and ordered species (Figure 56a). On the other hand, this was not the case for the rest of cALLG-sh peptides when mixed at 1/1 with Aβ40; no conformational change was observed (Figure 56b-d).
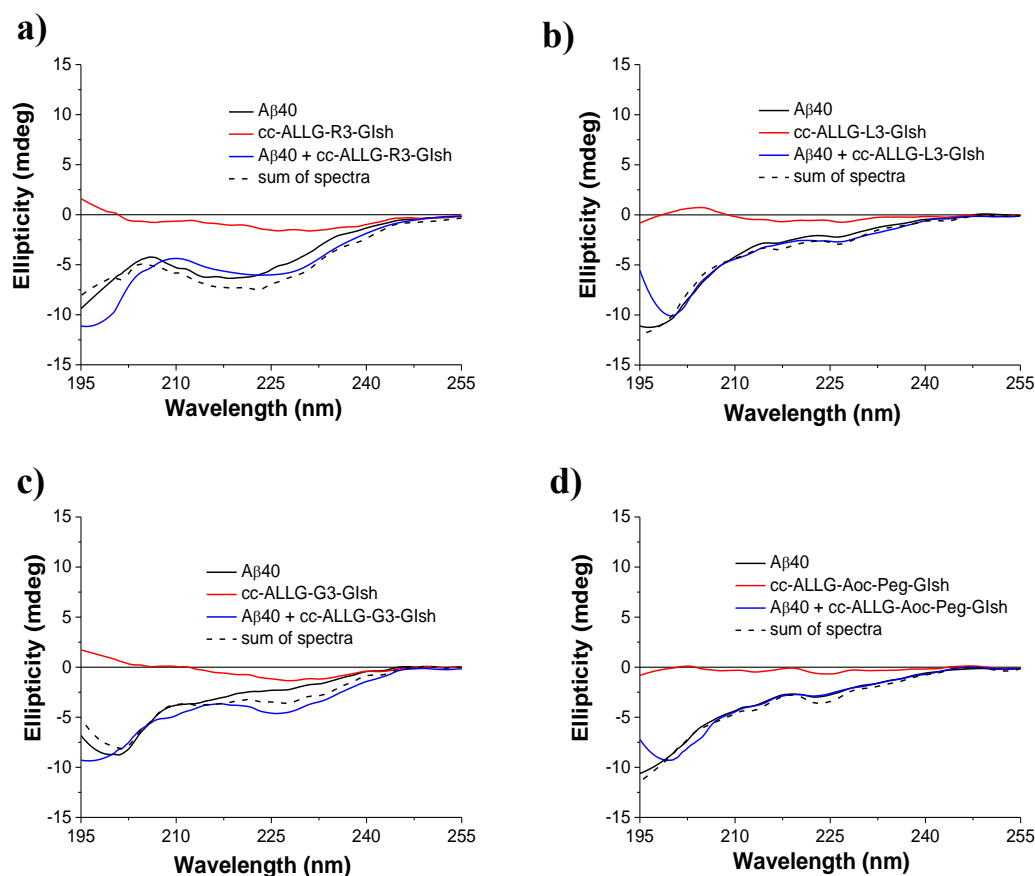
Figure 56. Interaction of Aβ40 and cALLG-sh studied by far-UV CD spectroscopy. CD spectra of freshly dissolved Aβ40 alone, cALLG-sh peptides, a mixture (1/1) of Aβ40 with cALLG-sh peptide and the sum of spectra (5µM, pH.7.4). Panels a)-d) show CD spectra and interactions of (a) cc-ALLG-R3-GIsh, (b) cc-ALLG-L3-GIsh, (c) cc-ALLG-G3-GIsh and (d) cc-ALLG-Aoc-Peg-GIsh, as indicated. Measurements were performed in aq. buffer 1×b, pH 7.4, containing 1% HFIP.

As shown previously, cc-ALLG-R3-GIsh could inhibit Aβ40 at 5-fold excess. Therefore, the interactions of cc-ALLG-R3-GIsh with Aβ40 was also investigated using a 5-fold excess of cc-ALLG-R3-GIsh by CD spectroscopy. Comparison of the CD spectra of the mixture with the sum of the CD spectra of each component indicated that the interaction caused conformational changes in Aβ40, inhibitor or both (see Appendix Figure A13).

4.3.6 **Effects on fibrillogenesis and cytotoxicity of IAPP**

Unfortunately, none of the above presented cALLG-sh peptides were able to inhibit IAPP fibrillogenesis and cytotoxicity at 1/5 (IAPP/peptide) molar ratio (see Appendix Figure A14). Therefore, I tested the inhibitory properties of cc-ALLG-R3-GIsh at 10-fold excess to IAPP (Figure 57). As shown, cc-ALLG-R3-GIsh could inhibit IAPP amyloidogenesis and TEM analysis confirmed the results of ThT binding assay (Figure 57d). Morover, the IC_{50} value was calculated against IAPP fibrillogenesis and cytotoxicity and found 425nM (see Appendix Figure A12b) and as found above for cc-R3-GIsh IC_{50} was 47.6nM.
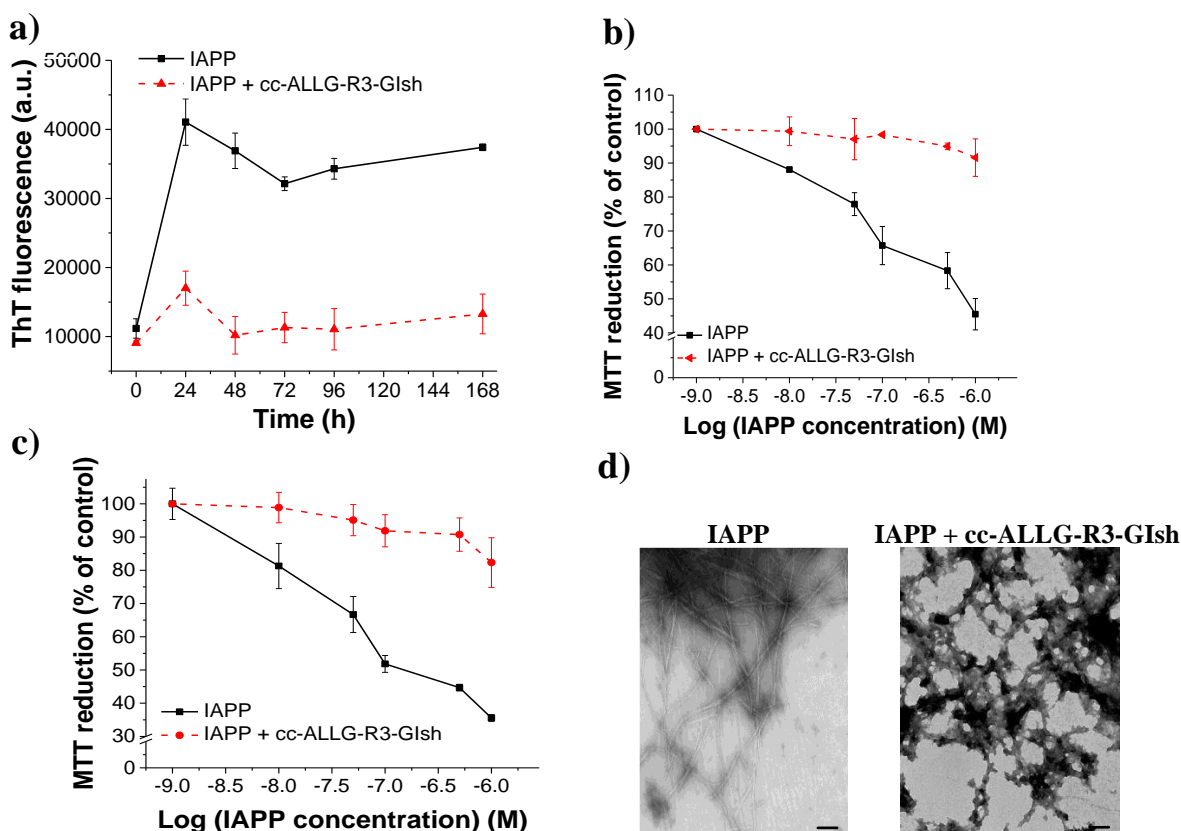
Figure 57. Effects of cc-ALLG-R3-GI on IAPP amyloid formation and cytotoxicity. (a) Fibrillogenesis of IAPP (6μM) alone or with cc-ALLG-R3-GIsh (10-fold excess) as determined via the ThT binding assay (means (±SD), 3 assays), (b) effects on IAPP cytotoxicity. Solutions from (a) aged for 24h were added to RINcells, (c) effects on IAPP cytotoxicity. Solutions from (a) aged for 7d were added to RINcells. Cell damage was assessed by the MTT reduction assay (means (±SD), 3 assays (n=3 each)), (d) TEM images of 7 days aged IAPP and its mixture with cc-ALLG-R3-GIsh (solutions from (a)) (bars, 100nm).

Furthermore, I investigated the effects of cc-ALLG-R3-GIsh on already nucleated IAPP fibrillogenesis. Inhibitor was added to 24h aged IAPP (16.5μM), containing significant amounts of IAPP fibrils and ThT binding and MTT reduction assay were performed. cc-ALLG-R3-GIsh inhibited formation of cytotoxic IAPP oligomers when added 10-fold molar excess to IAPP species before (0h) nucleation. When the inhibitor was added after (4h, 6h) nucleation of IAPP

fibrillogenesis, the formation of fibrils was blocked (Figure 58a). However, no effects on IAPP cytotoxicity were observed, since IAPP was already highly cytotoxic already at 6h of incubation (Figure 58b).
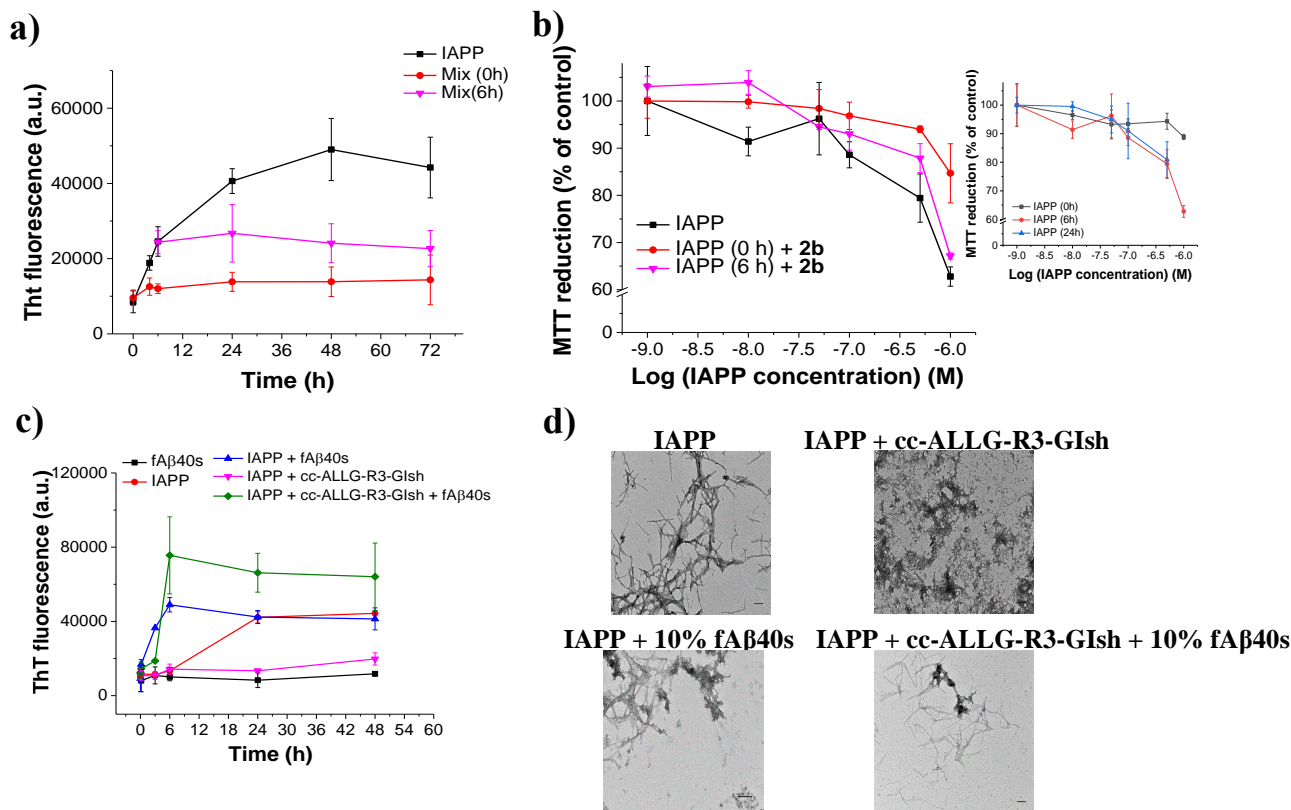
Figure 58. Effects of cc-ALLG-R3-GIsh when added at pre- or postnucleation stages of fibrillogenesis of IAPP (a,b) and effects on Aβ40-mediated cross-seeding of IAPP fibrillogenesis and cytotoxicity (c,d). (a) Effects of cc-ALLG-R3-GIsh when added (1/10) before (0h) and after (4h, 6h) nucleation on IAPP fibrillogenesis (16.5μM) as determined by ThT binding (means (±SD) from 3 assays), (b) effects of cc-ALLG-R3-GIsh when added (1/10) before (0h) and after (4h, 6h) nucleation on IAPP fibrillogenesis (16.5μM) via the MTT reduction assay. Solution from (a) (24h-aged) added to RINcells; cell damage determined by the MTT reduction assay (means (±SD) from 3 assays (n=3 each); inset show kinetics of cell-damaging effects of IAPP alone (16.5μM). Solutions from (a) were added at the indicated time points to RIN5fm cells and cell damge was assed by the MTT reduction assay (means (±SD), 3 assays (n=3 each)), (c) suppression of Aβ40-mediated (fAβ40) (10%) cross-seeding of IAPP (12μM) fibrillogenesis by cc-ALLG-R3-GIsh fibrillogenesis (10-fold) as assessed by ThT binding (means (±SD), 3 assays), (d) TEM images of 24h-aged IAPP and its mixtures at 24h (solutions from (c)) (bars, 100nm).

Next, the effects of cc-ALLG-R3-GIsh on the cross-seeding effect of fAβ40 seeds (fAβ40s) (10%) on IAPP(12μM) amyloidogenesis were studied. As shown in Figure 58c, cc-ALLG-R3-GIsh was unable to suppress fibrillar Aβ40-mediated cross-seeding of IAPP fibrillogenesis, even though it could inhibit amyloidogenesis of each polypeptide (Aβ and IAPP) alone. The results were confirmed by TEM (Figure 58d).

In conclusion, the IAPP related inhibition assays showed that cc-ALLG-R3-GIsh was able to completely inhibit IAPP (at a 10-fold molar excess to IAPP) and also could potently block IAPP nucleation stages. On the other hand, cc-ALLG-R3-GIsh could not suppress fibrillar Aβ40 mediated IAPP fibrillization.

Taken together the above results revealed the importance of the linker and of a potential pharmacophore motif consisting of 4 IAPP residues F15, L16, F23 and I26 for inhibitory function of short IAPP-derived analogues.

4.3.7 **Determination of binding affinities towards IAPP**

The interactions of cALLG-sh peptides with IAPP were studied by fluorescence titration assays. The app. K_ds of these interactions were determined by titrations of freshly made solutions of synthetic N-terminal fluorescein labeled IAPP (Fluos-IAPP) (5nM) with cALLG-sh peptides (Figure 59). The titration of Fluos-IAPP with cc-ALLG-R3-GIsh resulted in an app. K_d of 217nM, whereas the app. K_d of the interaction of Fluos-IAPP with cc-ALLG-L3-GIsh was 5-fold weaker. The app. K_ds of cc-ALLG-G3-GIsh and cc-ALLG-Aoc-Peg-GIsh could not be determined (app. $K_d \geq 5\mu M$).
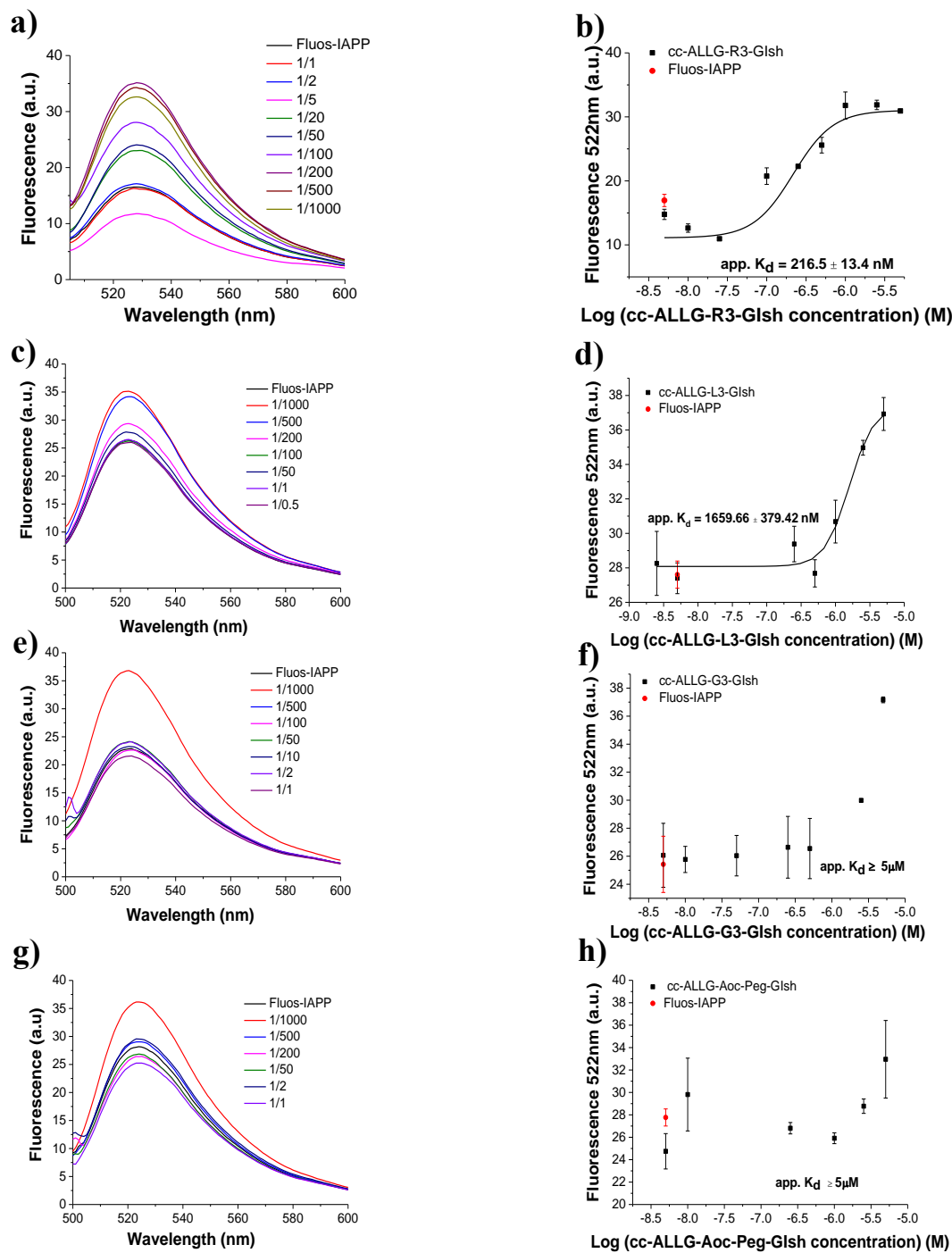
Figure 59. Determination of app. K_ds of interactions of IAPP and cALLG-sh by fluorescence spectroscopic titrations. **Panels a), c), e), g) show fluorescence spectra of Fluos-IAPP** (5nM) alone and its mixtures with various amounts of f cc-ALLG-R3-GIsh (a), cc-ALLG-L3-GIsh (c), cc-ALLG-G3-GIsh (e), cc-ALLG-Aoc-Peg-GIsh (g); the molar ratios of Fluos-IAPP/cALLG-sh are as indicated. Panels b), d), f), h) show the binding curves of cc-ALLG-R3-GIsh (b), cc-ALLG-L3-GIsh (d), cc-ALLG-G3-GIsh (f), cc-ALLG-Aoc-Peg-GIsh (h); app. K_ds are means ($\pm$SD) from 3 binding curves (Fluos-IAPP 5nM). Measurements were performed in aq. buffer 1×b, pH 7.4, containing 1% HFIP.

non-labeled IAPP (Figure 60), resulting in an app. K_d of 10nM. The app. K_ds of the other cALLG-sh peptides could not be determined (app. $K_d \geq 5\mu M$).
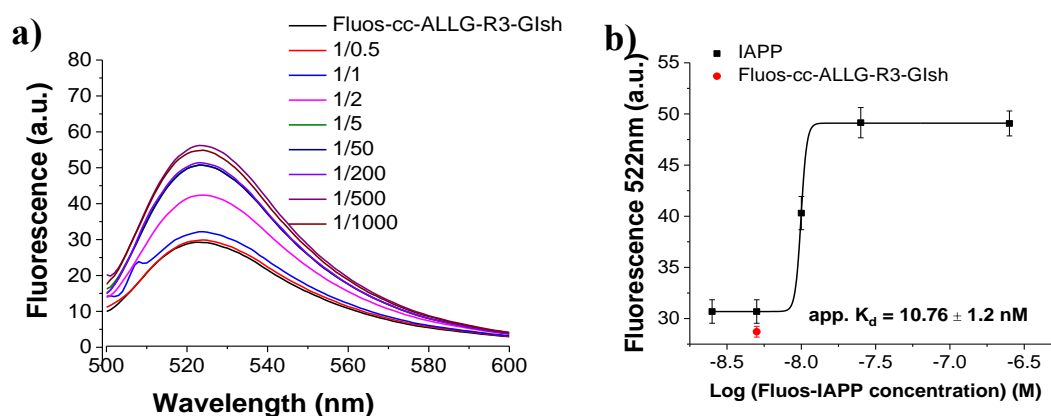
Figure 60. Determination of app. K_d of interactions of IAPP and cc-ALLR-R3-GIsh by fluorescence spectroscopic titrations. (a) Fluorescence emission spectra of Fluos-cc-ALLG-R3-GIsh (5nM) and following titration with various amounts of IAPP (Fluos-cc-ALLG-R3-GIsh/IAPP molar ratios as indicated), (b) binding curve of Fluos-cc-ALLG-R3-GIsh obtained upon titration with IAPP. Data in (b) are app. K_ds, means (±SD) from 3 binding curves (Fluos-cc-ALLG-R3-GIsh 5nM). Measurements were performed in aq. buffer 1×b, pH 7.4, containing 1% HFIP.

Table 34. Apparent affinities (app. K_ds) of interaction of cALLG-sh peptides with IAPP as determined by fluorescence titration binding assays.

cALLG-sh peptides	app. K_d (±SD) (nM) with Fluos-IAPP[a]	app. K_d (±SD) (nM) with IAPP[b]
cc-ALLG-R3-GIsh	217 (±13)	10.76 (±1.2)
cc-ALLG-L3-GIsh	1650 (±0.2)	n.d[d]
cc-ALLG-G3-GIsh	NB[c]	n.d[d]
cc-ALLG-Aoc-Peg-GIsh	NB[c]	n.d[d]

[a] App. K_ds, means (±SD) from 3 binding curves Fluos-IAPP (5nM) was titrated with cALLG-sh peptides;
[b] app. K_ds, means (±SD) from 3 binding curves Fluos-cALLG-sh peptides (5nM) were titrated with IAPP;
[c] NB, no binding at peptide concentration ≤ 5μM; [d] n.d., not determined, (aq. buffer 1×b, pH 7.4, containing 1% HFIP).

Finally, the interactions of cc-ALLG-R3-GIsh with IAPP were investigated using CD spectroscopy. CD was performed in a mixture (1/10 IAPP/cc-ALLG-R3-GIsh); found to be required for inhibitory effects. The spectra of the inhibitor at a concentration of 20μM and of IAPP at 2μM as well as of the mixture of IAPP with cc-ALLG-R3-GIsh were recorded (Figure 61). The CD spectra of the mixture of IAPP with cc-ALLG-R3-GIsh (1/10) differed from the CD spectra of sum IAPP/cc-ALLG-R3-GIsh. This indicated interaction, which caused conformational changes in IAPP, peptide, or both.
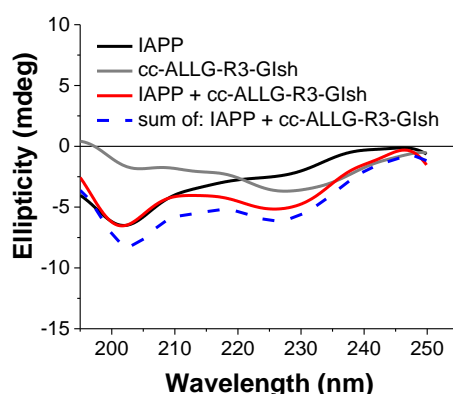
Figure 61. Interaction studies of IAPP and cc-ALLG-R3-GIsh studied by far-UV CD spectroscopy. CD spectra of freshly dissolved IAPP alone (2μM), cc-ALLG-R3-GIsh alone (20μM) and a mixture (1/10) of IAPP with cc-ALLG-R3-GIsh and the sum of spectra. Measurements were performed in aq. buffer 1×b, pH 7.4, containing 1% HFIP.

4.4 Studies on analogues of cc-ALLG-R3-GIsh (2b)

4.4.1 Peptides synthesis

The above results suggested a cyclic-pharmacophore motif which contained the 4 amino acids (F15, L16, F23, I26) and three arginines in the linker (**cc-ALLG-R3-GIsh (2b)**). To investigate the importance of the position of the Arg residues in the linker, each of Arg residues was substituted with Gly. A new series of cyclic peptides was designed, synthesized (abbreviated as **2b analogues)** (Table 35). I then tested these analogues regarding their properties as inhibitors of Aβ and IAPP amyloid self-assembly.

Table 35. 2b and its designed (2b) analogues.

Peptide sequence	Peptide abbreviation
C-^{14}G**FL**GG-**RRR**-**G****F**(N-Me)GG(N-Me)**I**G^{28}G-C-amide	2b
C-^{14}G**FL**GG-**RGG**-**G****F**(N-Me)GG(N-Me)**I**G^{28}G-C-amide	2b-RGG
C-^{14}G**FL**GG-**GRG**-**G****F**(N-Me)GG(N-Me)**I**G^{28}G-C-amide	2b-GRG
C-^{14}G**FL**GG-**RRG**-**G****F**(N-Me) GG(N-Me)**I**G^{28}G-C-amide	2b-RRG
C-^{14}G**FL**GG-**GRR**-**G****F**(N-Me) GG(N-Me)**I**G^{28}G-C-amide	2b-GRR
C-^{14}G**FL**GG-**GGR**-**G****F**(N-Me)GG(N-Me)**I**G^{28}G-C-amide	2b-GGR
C-^{14}G**FL**GG-**RGR**-**G****F**(N-Me)GG(N-Me)**I**G^{28}G-C-amide	2b-RGR

Analogues of 2b (Table 35) were synthesized by solid phase peptide synthesis (SPPS) utilizing Fmoc-strategy. Crude peptides with cysteines in reduced form were purified via RP-HPLC and characterized by MALDI-TOF (Table 36). Oxidations were performed by stirring crude peptides in a mixture of 40% (v/v) DMSO in aqueous NH$_4$HCO$_3$ (0.1mM, pH 8.7) for 3h. Analogues were purified by RP-HPLC and characterized by MALDI-TOF. Purification could be conducted with a yield between 7-23% (Table 36).

Table 36. Characterization of the synthetic oxidized peptides via HPLC and MALDI-TOF.

2b analogues[a]	HPLC program	t$_R$ (min)[b]	Yield[c]	[M+H]$^+$ expected[d]	[M+H]$^+$ found[d]
2b-RGG	1	19.36	7%	1493.65	1493.80
2b-GRG	1	21.56	20%	1493.65	1493.77
2b-RRG	1	19.60	20%	1592.73	1592.77
2b-GRR	1	21.23	20%	1592.73	1592.73
2b-GGR	1	20.11	12%	1493.65	1493.87
2b-RGR	1	17.9	23%	1594.73	1592.97

[a] Peptides were synthesized with free amino-terminal and amidated C-terminal end; [b] t$_R$, HPLC retention time; [c] % yield with regard to respective crude product; [d] monoisotopic molar mass [M+H]$^+$ expected; [d] [M+H]$^+$ found.

4.4.2 **Biophysical characterization**

4.4.2.1 **Conformational studies via CD spectroscopy**

Next, the conformations of the above peptides were determined by far-UV CD spectroscopy. For these measurements, peptides were dissolved in 10mM sodium phosphate buffer, pH 7.4 containing 1% HFIP and CD spectra were recorded. CD spectra of the peptides were measured at different concentrations (5-50μM) to determine their aggregation propensities. All of them showed a minimum at 230 nm, which indicated mostly β-sheet/β-turn contents and similar aggregation propensities (Figure 62).
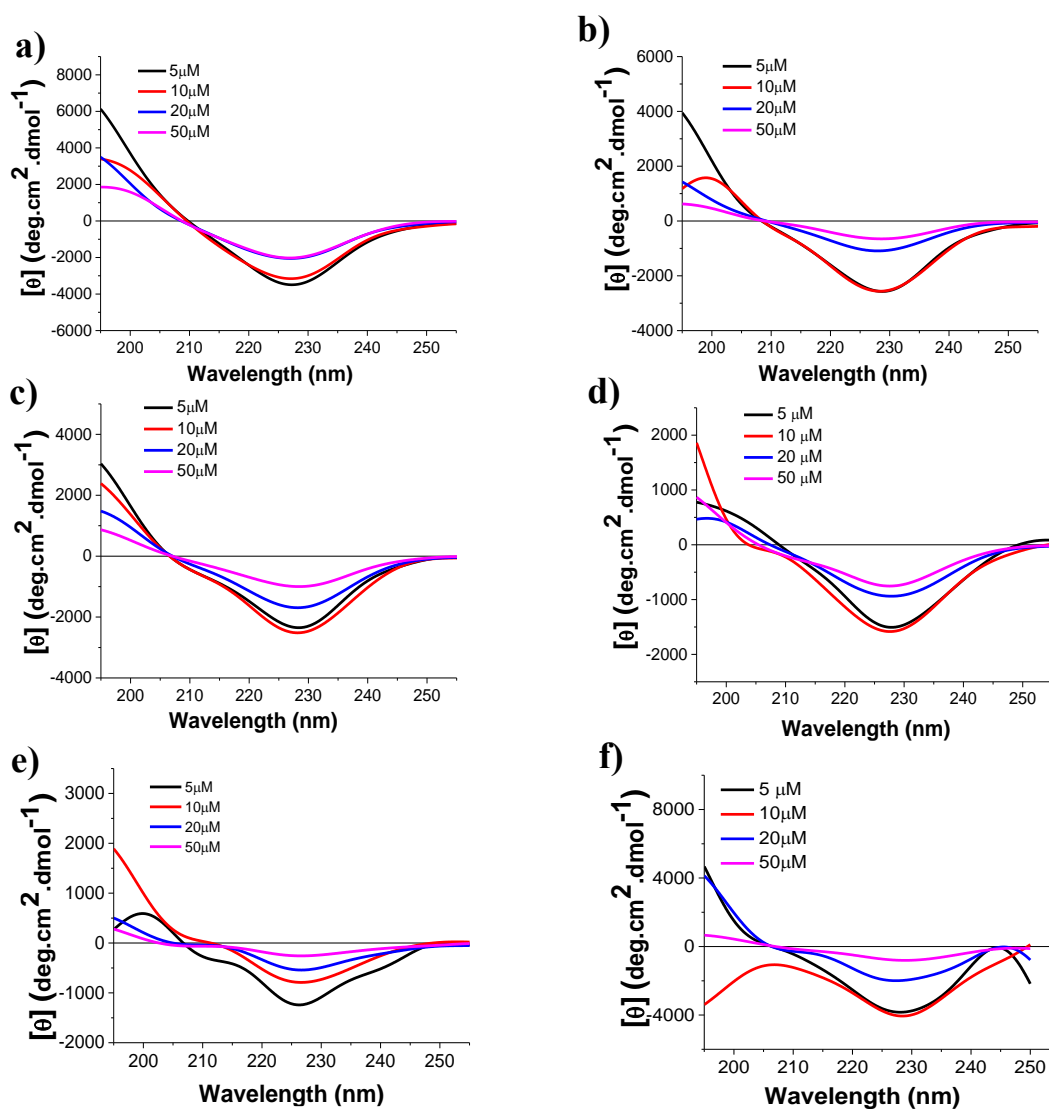
Figure 62. Concentration dependence of CD spectra of the 2b analogues. CD spectra of (a) 2b-RGG, (b) 2b-GRG and (c) 2b-RRG, (d) 2b-GRR, (e) 2b-GGR, (f) 2b-RGR. Measurements were performed at peptide concentrations between 5-50μM in aq. buffer 1×b, pH 7.4, containing 1% HFIP.

4.4.2.2 **Self-association studies via fluorescence spectroscopy**

Next, fluorescence binding assays were performed to quantify the apparent affinity (app. K_d) of the interactions of 2b-analogues with themselves. App. K_ds of self-association were determined by titration of freshly made solutions of N-terminal fluorescein labeled peptides (Fluos-2b analogues) (5nM) with non-labeled peptides (Figure 63). Measurements were performed in 1×b, pH 7.4 containing 1% HFIP.
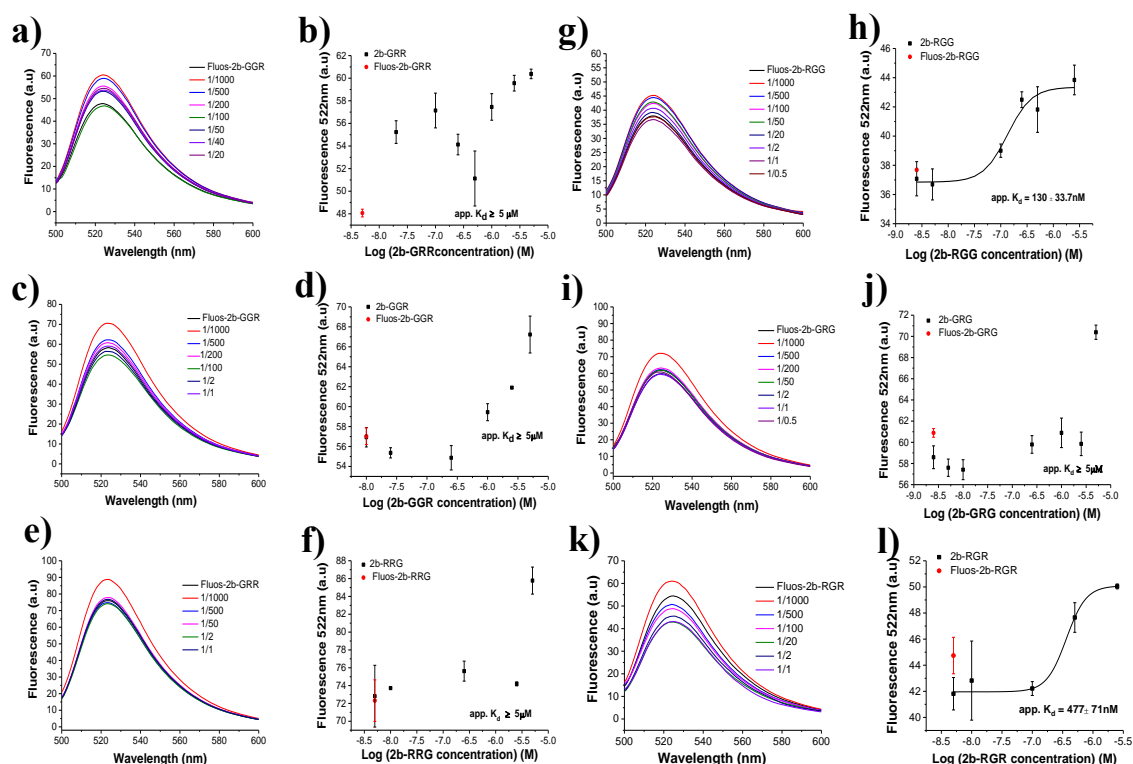
Figure 63. Apparent affinities (app. K$_d$) of self-association of 2b analogues as determined by fluorecence spectroscopy. Panels a), c), e), g), i), k) show fluorescence spectra of Fluos**-**2b analogue (5nM) alone and its mixtures with various amounts of f 2b-GRR (a), 2b-RGG (c), 2b-GGR (e), 2b-GRG (g), 2b-RRG (i), 2b-RGR (k); the molar ratios of Fluos-2b analogues/2b analogues are as indicated. Panels b), d), f), h), j), l) show the binding curves of 2b-GRR (b), 2b-RGG (d), 2b-GGR (f), 2b-GRG (h), 2b-RRG (j), 2b-RGR (l); app. K$_d$s are means (±SD) from 3 binding curves (Fluos-2b peptide 5nM). Measurements were performed in aq. buffer 1×b, pH 7.4, containing 1% HFIP.

Table 37 shows app. K$_d$s of self-assembly of 2b analogues. All peptides showed weak binding affinities, which varied in the micromolar range. It seemed that substitution of the Arg with Gly in 2b analogues strongly affected their self-association. Comparison of the app. K$_d$s of the 2b analogues to the app. K$_d$ of cc-ALLG-R3-GIsh (**2b**) (43nM) and the app. K$_d$ of cc-ALLG-G3-GI (**2b-G3**) (1μM) suggested that all three Arg residues play an important role in the self-assembly of these peptides.

Table 37. App. K$_d$s of self assembly of 2b analogues as dertermined by fluorescence titration studies.

2b analogues	app. K$_d$ (±SD) nM[a]
2b	43 (±3)
2b-GRR	NB[b]
2b-GGR	NB[b]
2b-RRG	NB[b]
2b-RGG	130 (±33.7)
2b-GRG	NB[b]
2b-RGR	477 (±71)
2b-G3	1054 (±145)

[a] App. K$_d$s are means (±SD) from 3 binding curves. Determined by titrations of synthetic N-terminal fluorescein-labeled 2b analogues (5nM) with non-labeled 2b analogues; [b] NB, no binding at peptide concentration ≤ 5μM, (aq. buffer 1×b, pH 7.4, containing 1% HFIP).

4.4.3 **Effects of 2b analogues on fibrillogenesis and cytotoxicity of Aβ40**

As next, it was studied whether the cyclic 2b analogues could intervene with Aβ40 self-assembly into fibrils and affect formation of cytotoxic aggregates. Aβ40 (16.5μM, pH 7.4) and mixtures of Aβ40 with the 2b analogues (5-fold molar excess) were incubated up to 7 days and fibrillogenesis was followed by the ThT binding assay and cytotoxicity was followed by the MTT reduction assay. All of them showed no strong inhibitory activity at 1/5 ratio. Only the template peptide cc-ALLG-R3-GIsh (2b) was able to inhbit IAPP amyloidogenesis (Figure 64). Also, 2b-GRR with Arg in positions 20, 21 showed some inhibitory potential in the ThT assay, which indicated the importance of the Arg in positions 20, 21. All other cyclic 2b showed no activity. Interesting, 2b-GGR, accelerated Aβ40 amyloidogenesis. Thus, the position of Arg in all three positions (19-21) strongly affects inhibitory function of 2b towards Aβ40 amyloidogenesis.
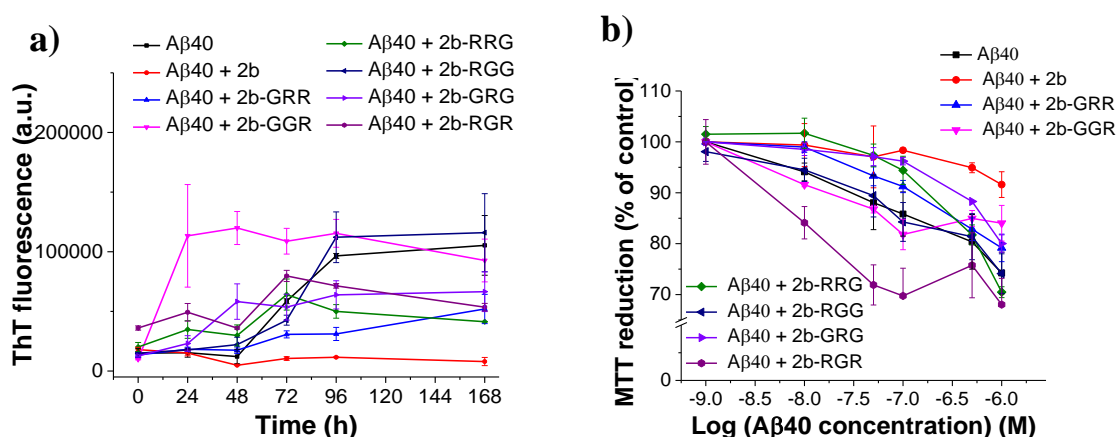
Figure 64. Effects of 2b analogues on Aβ40 amyloid formation and cytotoxicity. (a) Fibrillogenesis of Aβ40 (16.5μM) or its mixtures with 2b, 2b-GRR, 2b-GGR, 2b-RRG, 2b-RGG, 2b-GRG, 2b-RGR (1/5) by the ThT binding assay (means (±SD), 3 assays), (b) effects on cell viabillity: solutions from (a) (3 day-aged) added to PC-12 cells, cell damage determined by the MTT reduction assay (means (±SD), 3 assays, (n=3 each)).

Since these analogues could not inhibit Aβ40, we didn't examine their effects on IAPP fibrillogenesis or cytotoxicity. Together these studies confirmed the importance of the three Arg in the linker of 2b. Substitution of each of the Arg residues in 2b with Gly resulted in analogues, which could not inhibit Aβ40 amyloidogenesis.

4.4.4 **Determination of binding affinities towards Aβ40**

In Table 38 the app. K_ds of interactions of Aβ40 with 2b analogues are presented. Dac-Aβ40 (10nM) was titrated with 2b analogues (Figure 65). Most of the new cyclic analogues, except from 2b-RGR showed very similar weak binding affinities to Dac-Aβ40 (app. K_ds in the micromolar range). Moreover, for most of 2b-analogues no binding to Fluos-Aβ0 could be observed at c ≤ 5μM, except from 2b-RGR which showed an app. K_d = 47nM (see Appendix Figure A15). Thus, substitution of even one Arg affected the biding affinity to Aβ40. Thus, the three Arg residues of the linker (possibly their positive charge) might be important for the interactions between the 2b and Aβ40.
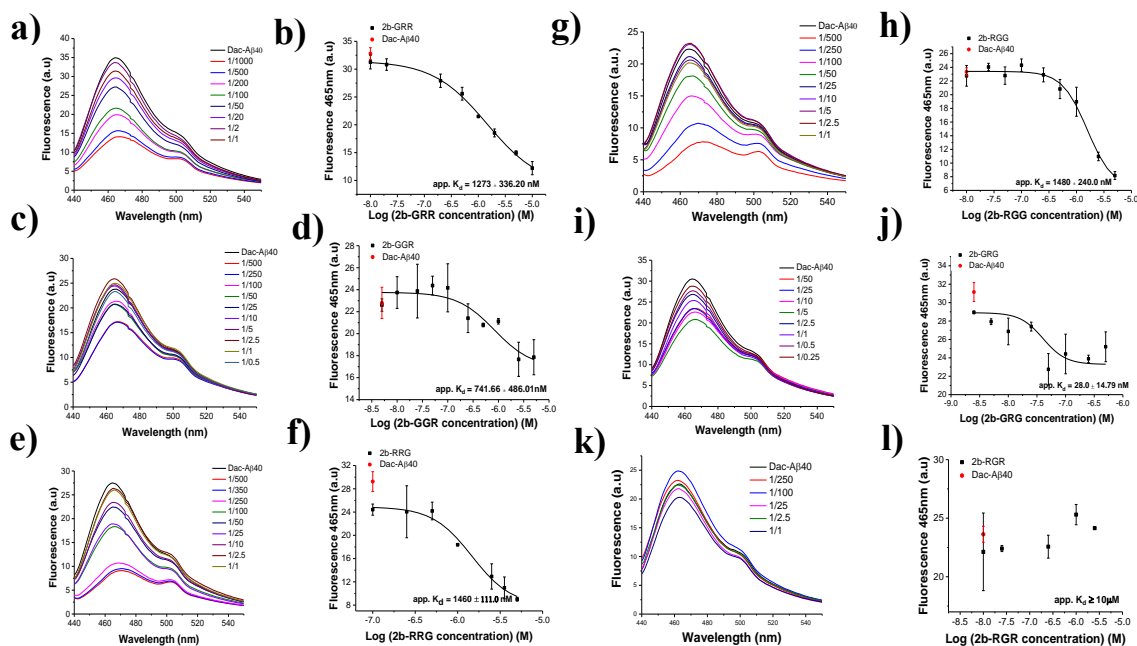
Figure 65. Determination of app. K$_d$s of interactions of 2b analogues with Aβ40 as determined by fluorescence titrations. Panels a), c), e), g), i), k) show fluorescence spectra of Dac-Aβ40 (10nM) alone and its mixtures with various amounts of f 2b-GRR (a), 2b-RGG (c), 2b-GGR (e), 2b-GRG (g), 2b-RRG (i), 2b-RGR (k); the molar ratios of Dac-Aβ40/2b analogues are as indicated. Panels b), d), f), h), j), l) show the binding curves of 2b-GRR (b), 2b-RGG (d), 2b-GGR (f), 2b-GRG (h), 2b-RRG (j), 2b-RGR (l); app. K$_d$s are means (±SD) from 3 binding curves (Dac-Aβ40 10nM). Measurements were performed in aq. buffer 1×b, pH 7.4, containing 1% HFIP.

Table 38. Apparent affinities (app. K$_d$s) of interaction of 2b analogues with Aβ40 as determined by fluorescence titration binding assays.

2b analogues	app. K$_d$ (±SD) (nM) with Dac-Aβ40[a]	app. K$_d$ (±SD) (nM) with Aβ40[b]
2b	187 (±12)	130 (±36)
2b-GRR	1273 (336.20)	NB[d]
2b-GGR	741.66 (±486.01)	NB[d]
2b-RRG	1460 (±111.0)	NB[d]
2b-RGG	1480 (±240.0)	NB[d]
2b-GRG	28.0 (±14.79)	NB[d]
2b-RGR	NB[c]	44 (±25)
2b-G3	NB [c]	NB[d]

[a] App. K$_d$s, means (±SD) from 3 binding curves Dac-Aβ40, (10nM) was titrated with 2b analogues; [b] Fluos-2b analogues (5nM);were titrated with Aβ40; [c] NB, no binding at peptide concentrations ≤ 10μM; [d] No binding at Aβ40 concnentrations ≤ 5μM; (aq. buffer 1×b, pH 7.4, containing 1% HFIP).

4.5 Studies on D-amino acids containing 2b analogues

4.5.1 Peptide synthesis

In order to improve the stability of cc-ALLG-R3-GIsh (2b) towards proteolytic degradation by human plasma proteases three new 2b analogues containing D-amino acids instead L-ones were designed and synthesized (analogues abbreviated as **2b** containing D-amino acids). Firstly, (L)-Arg7, (L)-Arg8, and (L)-Arg9 of the cc-ALLG-R3-GIsh (2b) were substituted with the corresponding D-amino acids to yield cc-AllG-r3-GIsh (**2c**). Secondly, (L)-Phe3, (L)-Leu4 and (L)-Phe11 were substituted with the D-amino acids as well yield to cc-ALLG-(f3, l4, f11)-r3-GIsh (**2d**). And additionally, substitution of two L-Cys with D-Cys yield to cc-ALLG-ALLD-r3-GI sh (**2e**) (Scheme 5). Of note, synthesis of 2d and 2e and some of the studies presented here were performed by L. Heidrich as indicated in text/figure legends (L. Heidrich, Msc Thesis, TUM (2016))[169].
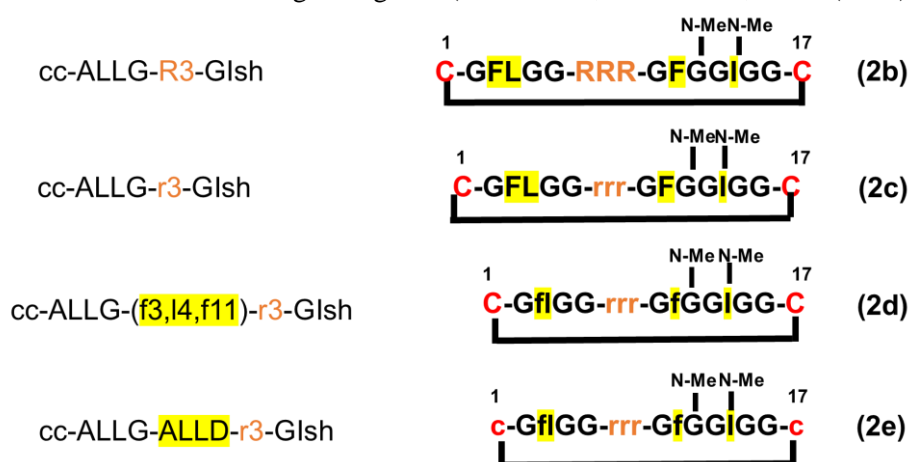
Scheme 5. Rational designed of 2b analogues containing D-amino acids. Sequences of 2b amd its analogues containing D-amino acids; cc-ALLG-R3-GIsh (2b), cc-ALLG-r3-GI (2c), cc-ALLG-(f3,l4,f11)-r3-GIsh (2d), cc-ALLD-ALLG-r3-GIsh (2e); D-residues: lower-case (highlighted yellow).

Cyclic peptides (Scheme 5) were synthesized by solid phase peptide synthesis (SPPS) utilizing Fmoc-strategy. Peptides cleaved from the resin with Reagent K, without EDT. Crude peptides with cysteines in reduced form were oxidized, purified via RP-HPLC and characterized by MALDI-TOF (Table 39). Oxidation was performed by stirring crude peptides in a mixture of 40% (v/v) DMSO in aqueous NH_4HCO_3 (0.1mM, pH 8.7) for 1.5h. Purification was conducted with a yield of around 20-25% of crude (Table 39).

Table 39. Characterization of 2b analogues containing D-amino acids via HPLC and MALDI-TOF.

2b analogues containing D-amino acids[a]	HPLC program	t_R (min) [b]	Yield[c]	[M+H]+ expected[e]	[M+H]+ found[e]
2c	1	17.9	7%	1694.88	1694.82
2d[d]	1	17.7	20%	1694.88	1694.99
2e[d]	1	17.9	20%	1694.88	1595.11

[a] Peptides were synthesized with free amino-terminal and amidated C-terminal end; [b] t_R, HPLC retention time; [c] % yield with regard to respective crude product; [d] Peptides were synthesized and studied by Luzia Heidrich[169]; [e] monoisotopic molar mass [M+H]+ expected and [M+H]+ found.

The goal of the last part was to investigate whether these modifications could increase the proteolytic stability but maintain the inhibitory function towards fibril formation and cytotoxicity of Aβ40(42) and/or IAPP.

4.5.2 **Biophysical characterization**

4.5.2.1 **Conformational studies via CD spectroscopy**

Next, the conformations of the above peptides were studied by far-UV CD spectroscopy.
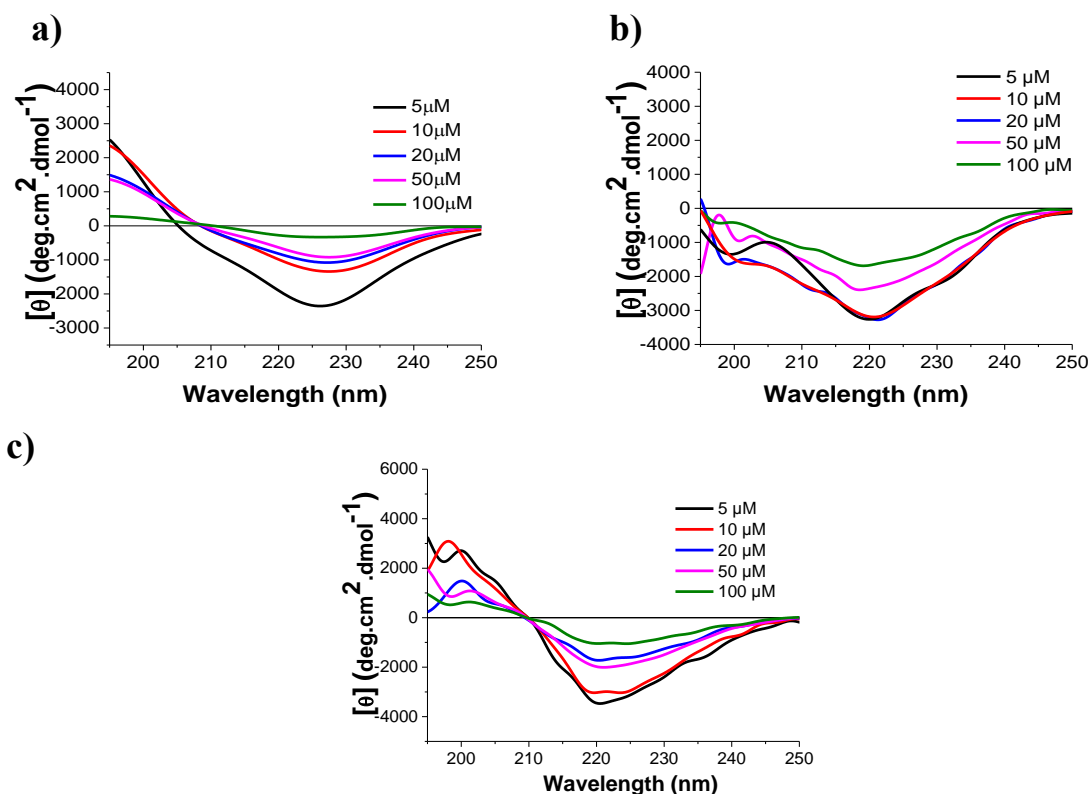
Figure 66. Concentration depedance of the CD spectra of 2b analogues containing D-amino acids. CD spectra of (a) 2c, (b) 2d and (c) 2e, as assessed by far-UV spectroscopy. Measurements were performed at peptide concentrations between 5-50µM in aq. buffer 1×b, pH 7.4, containing 1% HFIP. Data shown in b, c) are from MSc-Thesis of Luzia Heidrich[169].

The CD spectra of all new cyclic peptides had minima at 220-230nm which indicated a β-sheet/β-turn secondary structure (Figure 66). In case the of 2c, oligomerization started already at 10µM (Figure 66a). Substitution of F3, L4 and F11 with D-amino acids of 2b and additionally substitution of C^1, C17 with D-residues resulted in peptides with similar oligomerization propensities (Figure 66b,c).

4.5.2.2 **Self-association studies via fluorescence spectroscopy**

Next, K_ds of self-association of 2b analogues containing D-amino acids were determined by titration of freshly made solutions of N-terminal fluorescein labeled 2b analogues (5nM) with non-labeled 2b analogues (Figure 67), (Table 40). The measurements were performed in 1×b, pH 7.4, containing 1% HFIP. Binding of 100-fold molar excess of 2c to Fluos-2c caused ~42% fluorescence enhancement. Binding of 500-fold molar excess of 2d to Fluos-2d caused 100% fluorescence enhancement, whereas binding of 50-fold molar excess of 2e to Fluos-2e caused 100% enhancement (Figure 67). Sigmoidal binding isotherms were obtained and the determined apparent affinities of the interactions (app. K_d values) were 65 (±12.5) nM for 2c, which was 3 times worse than 2d (app. K_d = 17.4nM) and 2e (app. K_d = 11.6nM).

It seems that consecutive substitution of L-AA to D-amino acids enhanced the self-association properties of the peptides. Substitution of Arg7,8,9 of 2b with the corresponding D-residues had no significant effect on the self-assembly (app. K_d of 2c, 69nM). Moreover, substitution of two more L-to D-amino acids (F3, F11) showed 3-fold stronger app. K_d than 2b (app. K_d of 2d, 17.4nM). Finally,

2e had 4-fold stronger app. K_d than 2b (app. K_d of 2e, 11.6nM). It seemed that substitution of L with D residues of 2b triggered self-assembly.
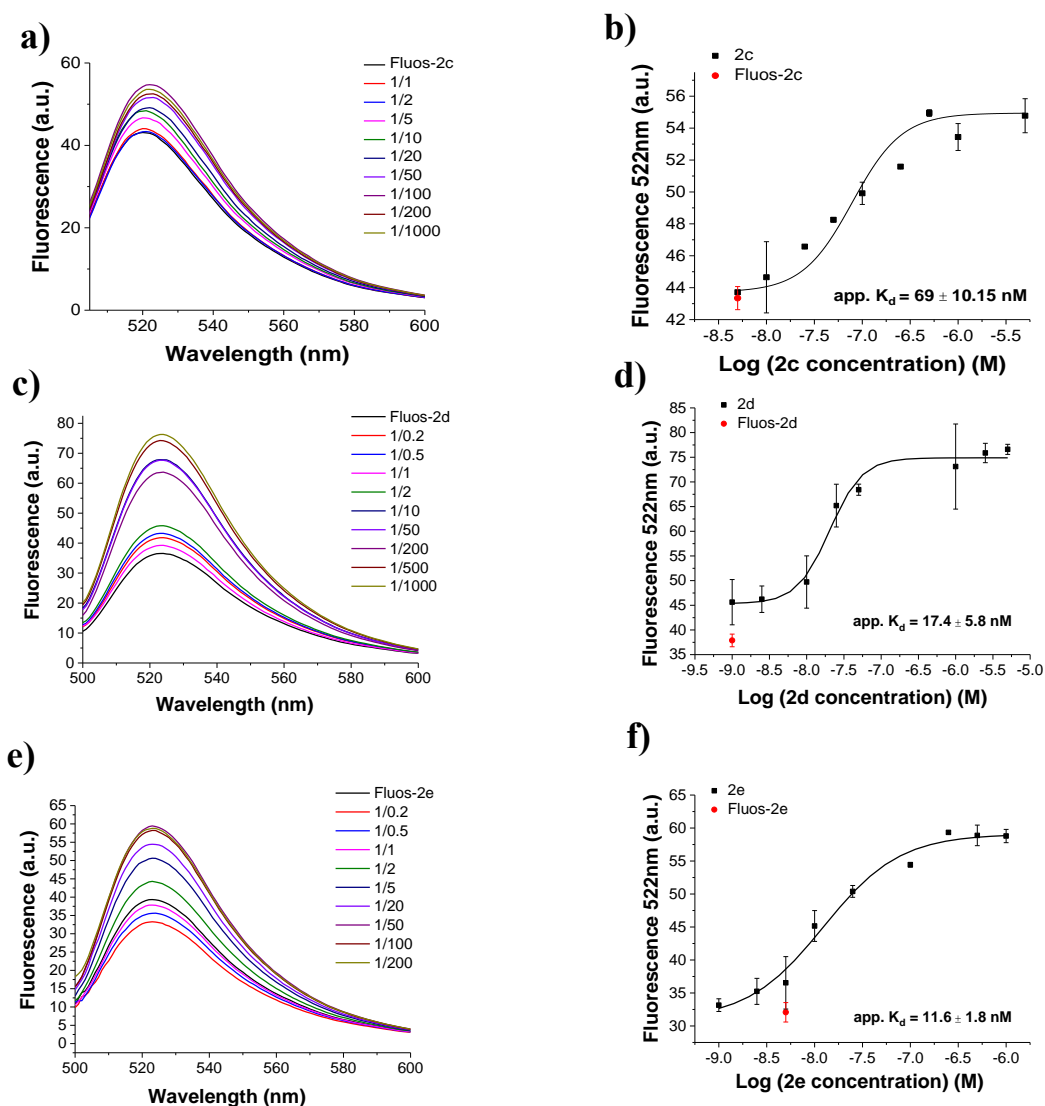
Figure 67. Apparent affinities (app. K_d) of self-association of 2b analogues containing D-amino acids as determined by fluorescence spectroscopy. Panels a), c), e) show fluorescence spectra of Fluos-2b analogue containing D-amino acids (5nM) alone and its mixtures with various amounts of 2c (a), 2d (c) and 2e (e); the molar ratios of Fluos-2b containing D-amino acids analogues/2b analogues containing D-amino acids are as indicated. Panels b), d), f) show the binding curves of 2c (b), 2d (d), 2e (f); app. K_ds are means (±SD) from 3 binding curves (Fluos-D-2b analogue 5nM). Measurements were performed in aq. buffer 1×b, pH 7.4, containing 1% HFIP. Data shown in c-f) are from MSc-thesis of Luzia Heidrich[169].

Table 40. App. K_ds of self-assembly of 2b analogues containing D-amino acids as dertermined by fluorescence titration studies.

2b analogues containing D-amino acids	app. K_d (±SD) nM[a]
2b	43 (±3)
2c	65 (±12.5)
2d	17.4 (±5.8)
2e	11.6 (±1.8)

[a] App. K_ds are means (±SD) from 3 binding curves. Determined by titrations of synthetic N-terminal fluorescein-labeled peptides (Fluos-peptides 5nM) with non-labeled peptides, (aq. buffer 1×b, pH 7.4, containing 1% HFIP).

4.5.3   **Inhibitory activity on Aβ40(42) fibrillogenesis and cytotoxicity**

Next the question was addressed whether 2c, 2d and 2e could intervene with Aβ40 self-assembly into fibrils and affect formation of cytotoxic Aβ40 aggregates. Aβ40 alone (16.5μM, pH 7.4) and the (1/5) mixtures of Aβ40 with the peptides were incubated for 7 days and fibrillogenesis and cytotoxicity were followed by the ThT binding and the MTT reduction assay (Figure 68).
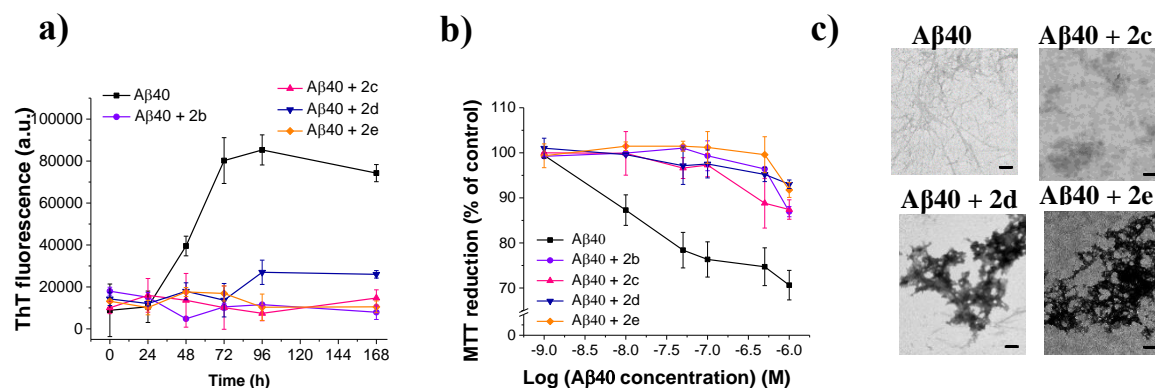
Figure 68. Effects of 2b analogues containing D-amino acids on amyloid formation and cytotoxicity of Aβ40. (a) Fibrillogenesis of Aβ40 (16.5μM) and its mixtures with 2b, 2c, 2d and 2e (1/5) by the ThT binding assay (means (±SD), 3 assays), (b) effects on cell viabillity: solutions from (a) (7 days aged) were added to PC-12 cells, cell damage determined by the MTT reduction assay (means (±SD), 3 assays (n=3 each)), (c) TEM images of 7 days aged Aβ40 and its mixtures with the various analogues (solutions from (a)) (bars, 100nm). Data of 2d & 2e shown in Figure 68a-c are from MSc-thesis of Luzia Heidrich[169].

As shown in Figure 68, all of them could inhibit Aβ40 (Aβ40/peptide 1/5) fibril formation, similar to 2b. To examine whether these peptides may also inhibit formation of cytotoxic Aβ40 aggregates, Aβ40 alone and its mixtures were added to PC-12 cells and cell viability was assessed by the MTT reduction assay. All of them were found to suppress Aβ40 cytotoxicity (Figure 68b). The results of the ThT binding assay were confirmed using TEM (Figure 68c), which showed amorphous aggregates in all incubations except from Aβ40 alone.

In the following Table 41, IC_{50}s of the effects of 2b analogues containing D-residues on Aβ40 toxicity are presented. Importantly, all three peptides were nanomolar inhibitors of Aβ40 amyloid self-assembly; their IC_{50} values were very similar to the IC_{50} of 2b (see Figure Appendix A16).

Table 41. IC_{50} values of inhibitory effects of 2b analogues containing D-amino acids on Aβ40 cytotoxicity.

Peptides	IC_{50} (±SD) (nM)[a]
2c	204 (±83.6)
2d	702 (±339.3)
2e	542.5 (±240.7)

[a] IC_{50}s, means (±SD) from three titration assays (n=3 each); Aβ40, 500nM). Data of 2e are from the MSc-thesis of Luzia Heidrich[169].

a)

b)

c)

Aβ42 **Aβ42 + 2b**

Aβ42 + 2c **Aβ42 + 2d** **Aβ42 + 2e**
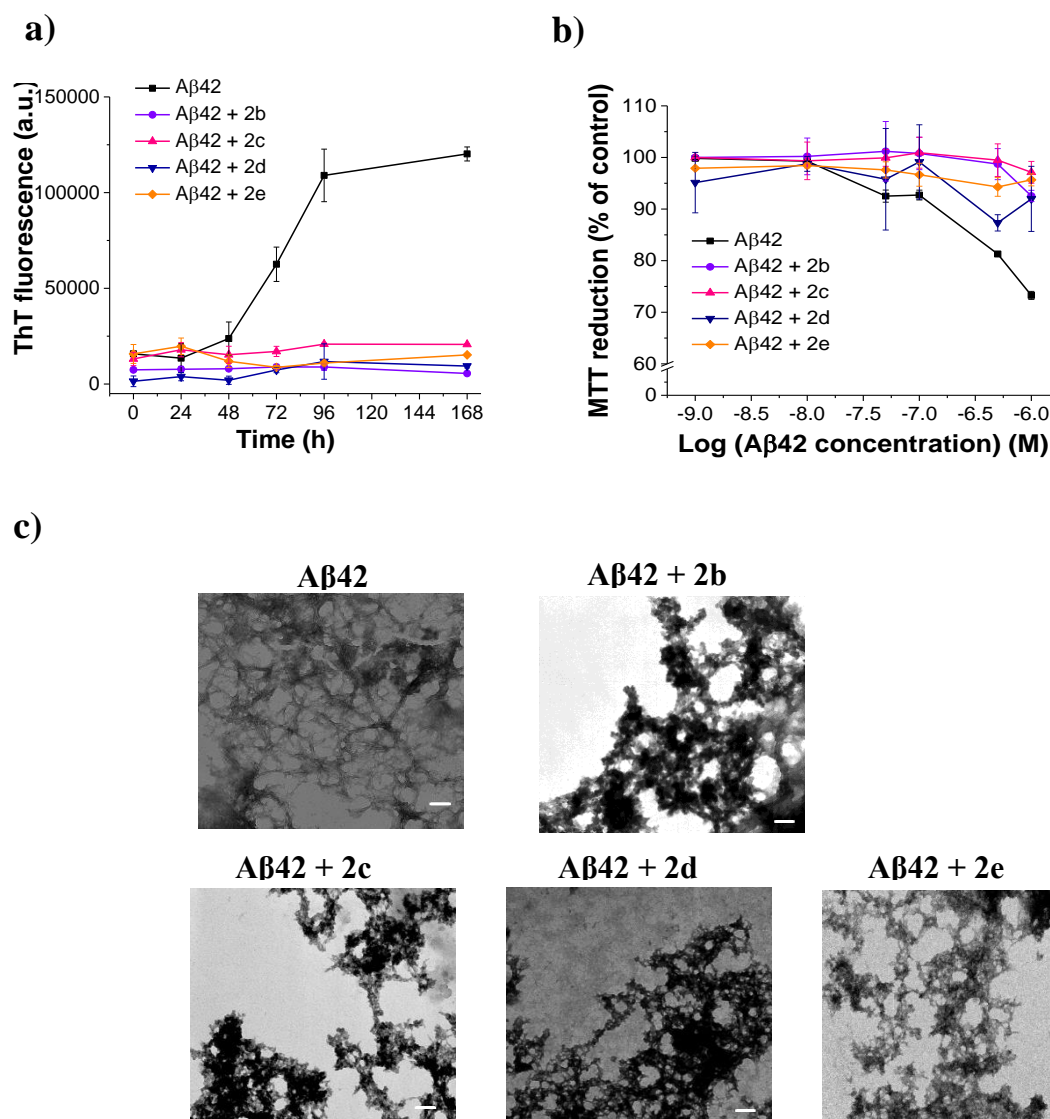
Figure 69. Effects of 2b analogues containing D-amino acids on amyloid formation and cytotoxicity of Aβ42. (a) Fibrillogenesis of Aβ42 (16.5μM) and its mixtures with 2b, 2c, 2d and 2e (1/5) by the ThT binding assay (means (±SD), 3 assays), (b) effects on cell viability: solutions from (a) (7 days aged) added to PC-12 cells, cell damage determined by the MTT reduction assay (means (±SD), 3 assays, (n=3 each)), (c) TEM images of 7 days aged Aβ40 and its mixtures with the various analogues (solutions from (a)) (bars, 100nm). Data of 2d & 2e shown in Figure 69a-c are from the MSc-thesis of Luzia Heidrich[169].

The above cyclic analogues were tested also regarding inhibitory effects on Aβ42 fibrillogenesis and cytotoxicity. Aβ42 alone (16.5μM, pH 7.4) and its mixtures with the peptides (16.5μM, pH 7.4) were incubated for 7 days and fibrillogenesis and cytotoxicity were followed by the ThT binding and the MTT reduction assays (Figure 69 a & b). After 7 days of incubation the solutions from ThT binding assay examined with TEM (Figure 69c) and results confirmed the ThT findings.

4.5.4 Determination of binding affinities towards Aβ40(42)

The apparent K_ds of interactions of 2b analogues containing D-amino acids with Aβ40 were determined by titrating (Dac-Aβ40) (10nM) with 2b analogues containing D-amino acids (Figure 70). All tested cyclic inhibitors were found to bind with high affinity Dac-Aβ40 and their app. K_ds were in the same range as the L-analogue (2b) (app. K_d = 187.6nM).
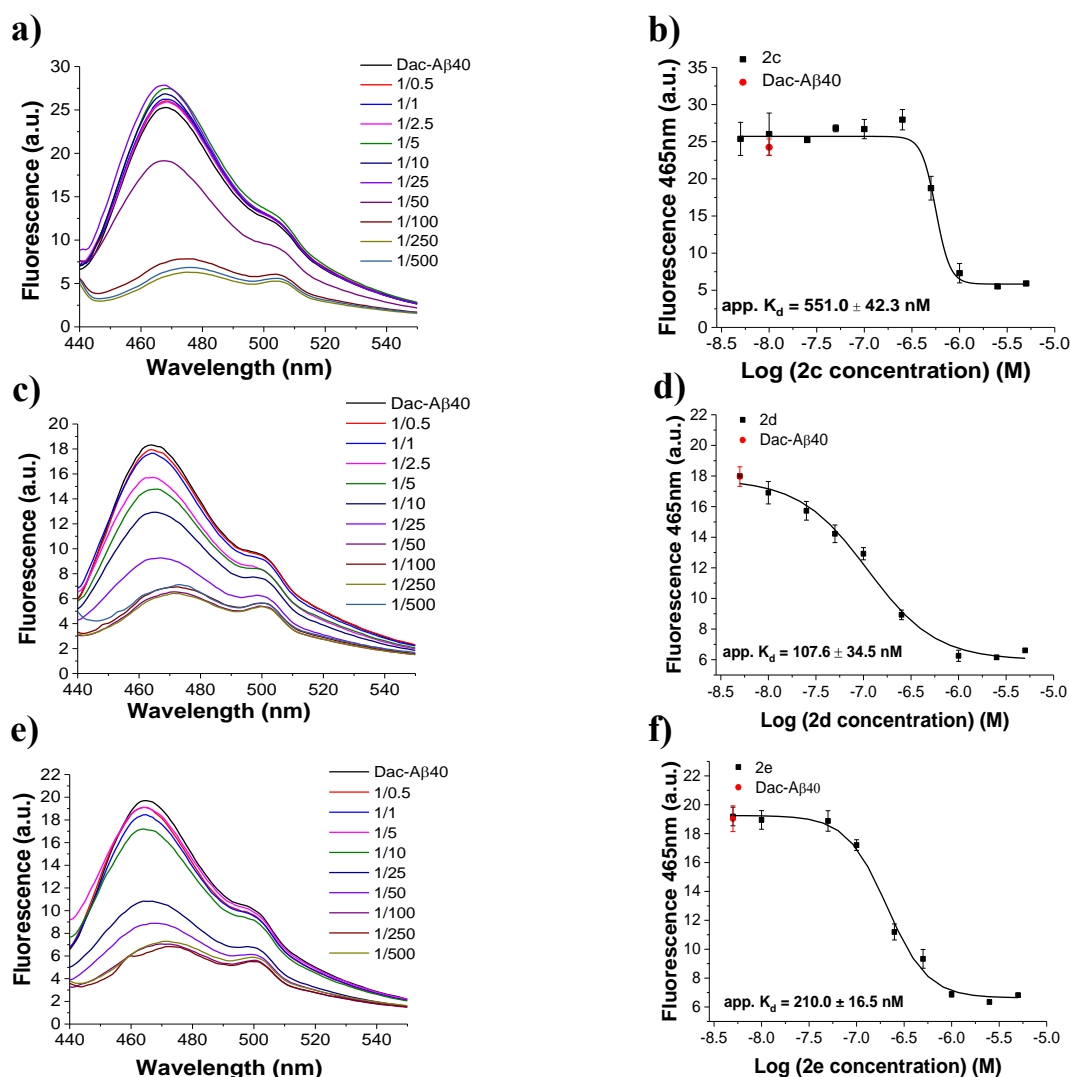
Figure 70. Apparent affinities (app. K$_d$s) of interactions of 2b analogues containing D-amino acids with Aβ40 as determined by fluorescence titrations. Panels a), c), e) show fluorescence spectra of Dac-Aβ40 (10nM) alone and its mixtures with various amounts of 2c (a), 2d (c), 2e (e); the molar ratios of Dac-Aβ40/2b analogues containing D-amino acids are as indicated. Panels b), d), f) show the binding curves of 2c (b), 2d (d), 2e (f); app. K$_d$s are means (±SD) from 3 binding curves (Dac-Aβ40 10nM). Measurements were performed in aq. buffer 1×b, pH 7.4, containing 1% HFIP. Data shown in c-f) are from the MSc-thesis of Luzia Heidrich[169].

The app. K$_d$s of the interactions of 2c, 2d and 2e with Aβ40 were studied next. It was found that the new peptides bound to oligomeric species of Aβ40 as well in low nanomolar app. K$_d$s (Figure 71). Finally, the interactions of Fitc-Aβ42 with the analogues were investigated. As shown in Figure 72 and Table 42 all of them showed nanomolar app. K$_d$s. In conclusion, 2d & 2e bind much stronger Aβ42 than 2b (app. K$_d$ = 5.7nM and app. K$_d$ = 25.6nM respectively).
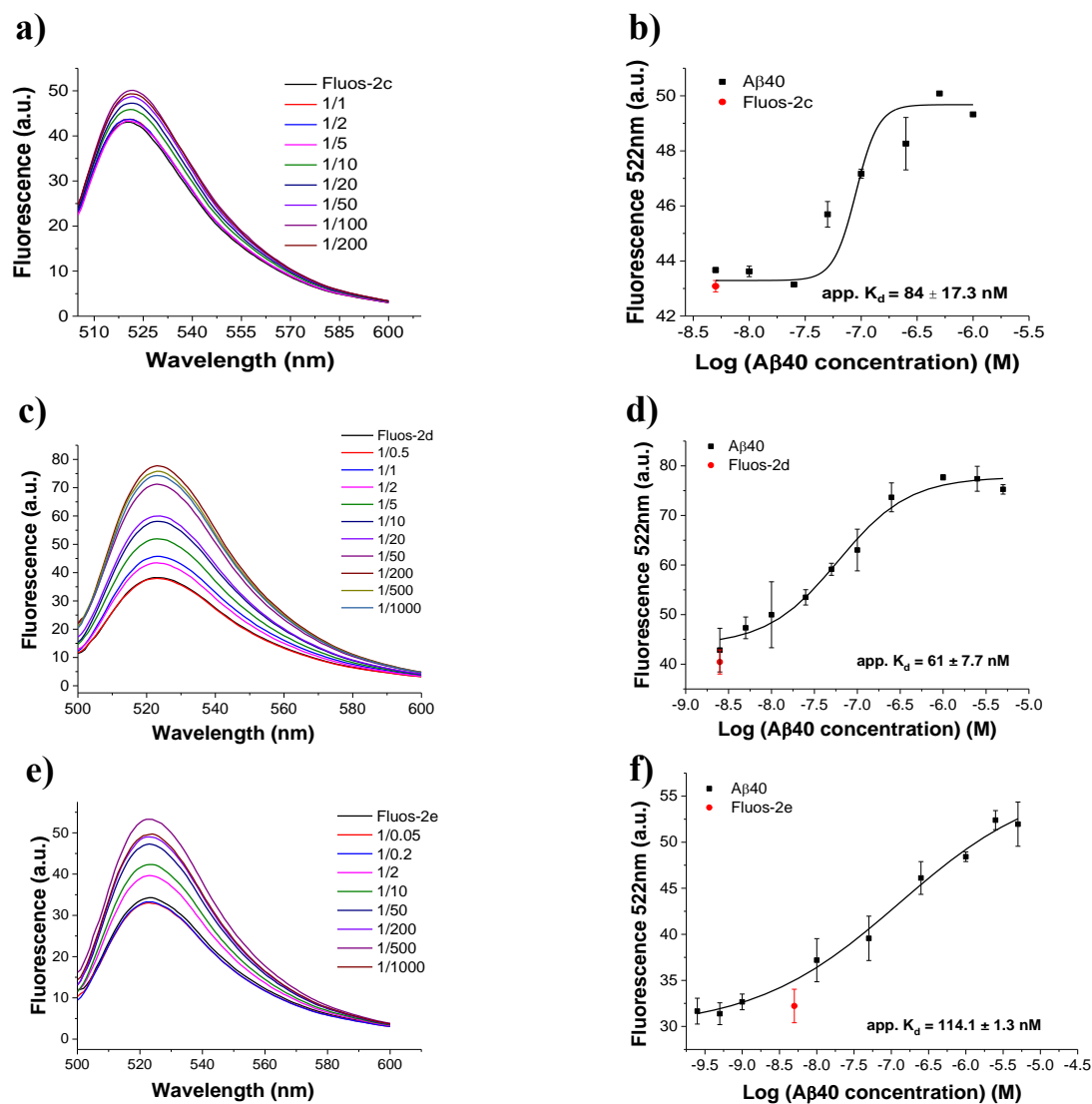
Figure 71. Determination of app. K_ds of interactions of 2b analogues containing D-amino acids with oligomeric Aβ40 species with by fluorescence spectroscopy. Panels a), c), e) show fluorescence spectra of Fluos-2b analogue containing D-amino acids (5nM) alone and its mixtures with various amounts of Aβ40; the molar ratios of Fluos-peptide/Aβ40 are as indicated. Panels b), d), f) show the binding curves of Aβ40 with Fluos-2c (b), Fluos-2d (d) and Fluos-2e (f); app. K_ds are means (±SD) from 3 binding curves (Fluos-peptide 5nM). Measurements were performed in aq. buffer 1×b, pH 7.4, containing 1% HFIP. Data shown in c-f) are from the MSc-thesis of Luzia Heidrich[169].
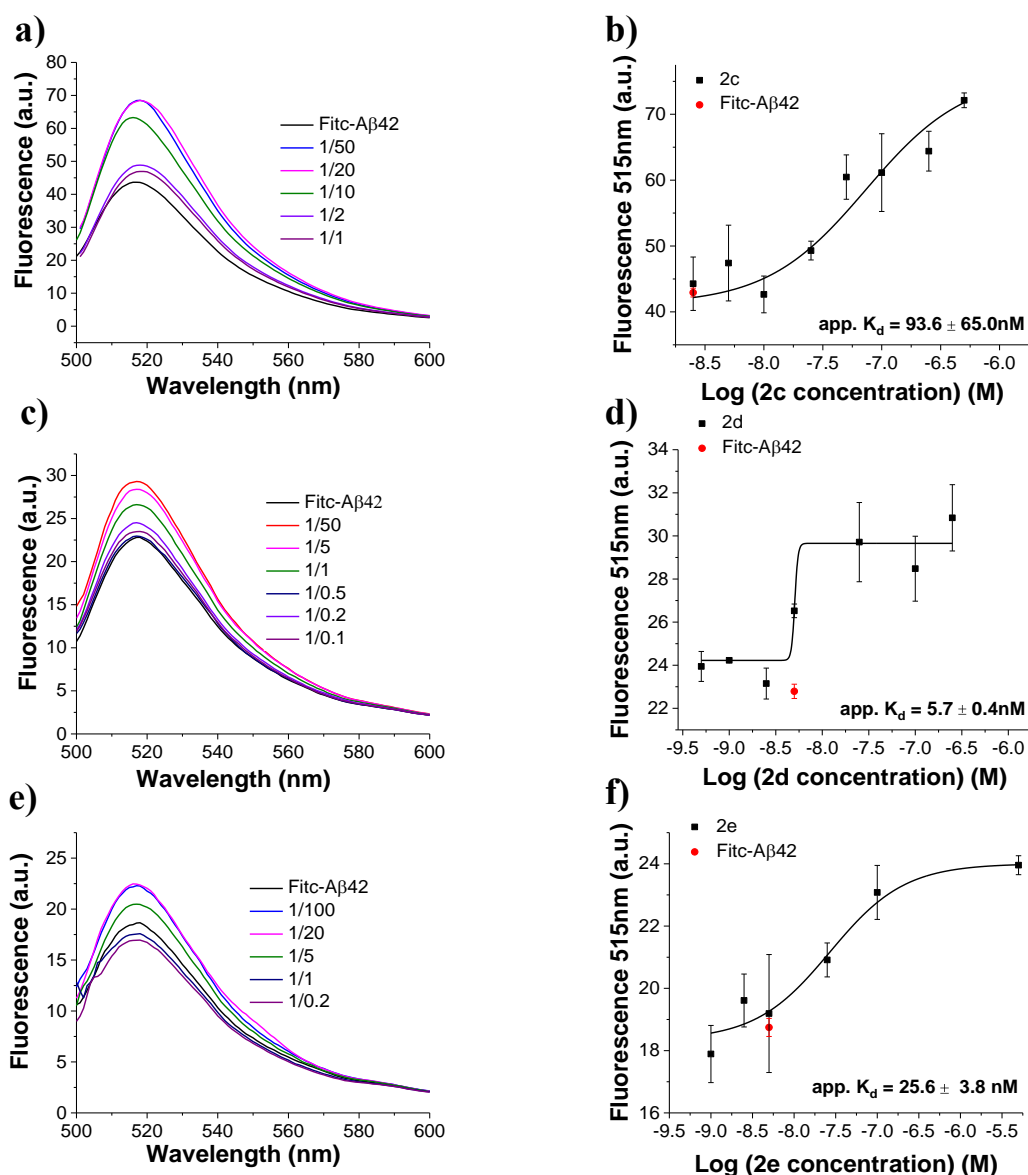
Figure 72. Determination of app. K$_d$s of interactions of Fitc-Aβ42 with 2b analogues containing D-amino acids by fluorescence spectroscopy. Panels a), c), e) show fluorescence spectra of Fitc-Aβ42 (5nM) alone and its mixtures with various amounts of 2c (a), 2d (c), 2e (e); the molar ratios of Fitc-Aβ42/2b analogues containing D-amino acids are as indicated. Panels b), d), f) show the binding curves of 2c (b), 2d (d), 2e (f); app. K$_d$s are means (±SD) from 3 binding curves (Fitc-Aβ42 5nM). Measurements were performed in aq. buffer 1×b, pH 7.4, containing 1% HFIP. Data shown in c-f) are from the MSc-thesis of Luzia Heidrich[169].

Table 42. Apparent affinities (app. K$_d$s) of interaction of peptides with Aβ40(42) as determined by fluorescence titration assays.

Peptide	app. K$_d$ (±SD) (nM) with Dac-Aβ40[a]	app. K$_d$ (±SD) (nM) with Aβ40[b]	app. K$_d$ (±SD) (nM) with Aβ42[a]
2b	187 (±12)	130 (±36)	199 (±25.5)
2c	551.0 (±42.3)	84 (±7.3)	93.6 (±65.0)
2d	107.6 (±34.3)	61 (±7.7)	5.7 (±0.4)
2e	210.0 (±16.5)	114.1(±1.3)	25.6 (±3.8)

[a] App. K$_d$s, means (±SD) from 3 binding curves Dac-Aβ40 (10nM) and Fitc-Aβ42 (5nM) were titrated with peptides; [b] app. K$_d$s, means (±SD) from 3 binding curves Fluos-peptides (5nM) were titrated with Aβ40, (aq. buffer 1×b, pH 7.4, containing 1% HFIP).

4.5.5 Interactions with Aβ40 by CD spectroscopy

To investigate the interactions of the 2b analogues containing D-amino acids with Aβ40, CD spectroscopy was applied. CD was performed with Aβ/peptides at the ratio of 1/5 corresponding to the ratio required for inhibition of Aβ40 amyloidogenensis by the peptides. Aβ40 alone had a strong minimum at around 198nm which suggested mainly random coil. By comparing the CD spectra of the mixture with the sum of CD spectra, a small difference was observed which indicated an interaction and the presence of both unordered and ordered species (Figure 73a). On the other hand, this was not the case for the 2d when was mixed at 1/5 with Aβ40, no conformational change was observed (Figure 73b). Finally, by comparing the CD spectra of the Aβ/2e at the ratio of 1/5 with the sum of the CD spectra, a difference was observed, which indicated a conformational change upon interaction of 2e with Aβ40 (Figure 73c).
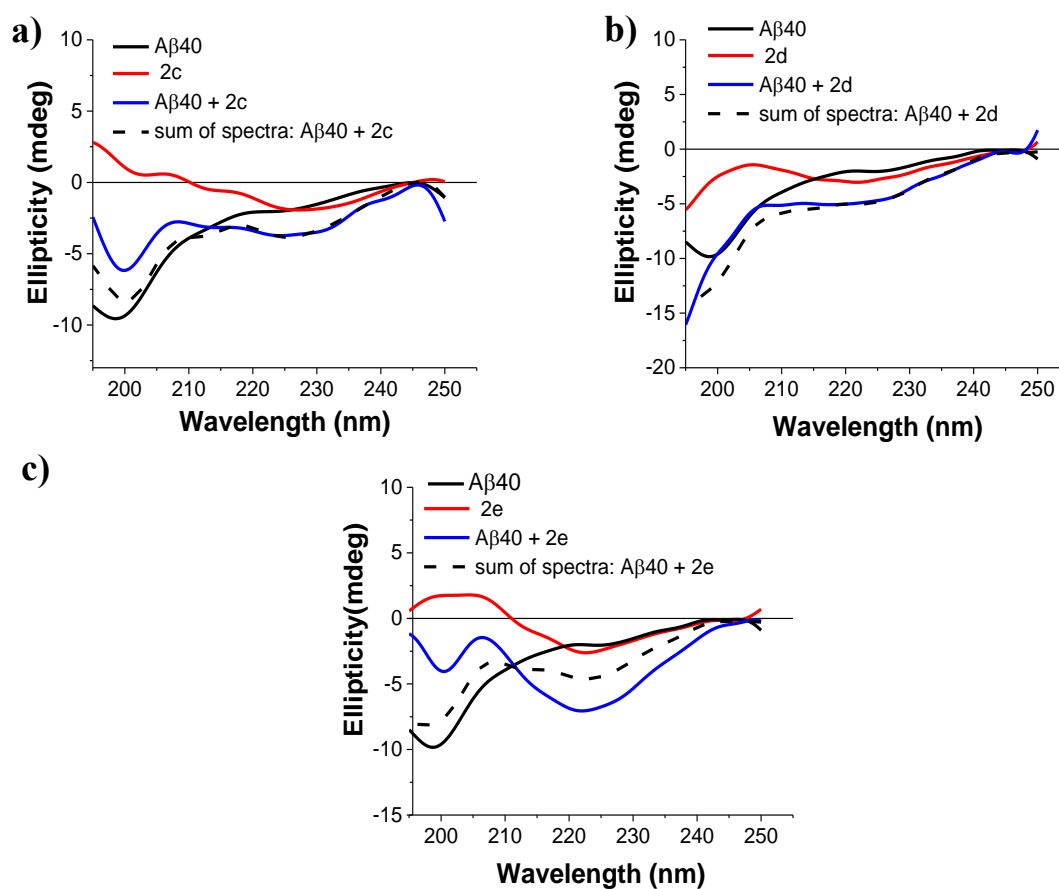
Figure 73. Interaction of Aβ40 and 2b analogues containing D-amino acids as studied by far-UV CD spectroscopy
CD spectra of freshly dissolved Aβ40 alone, peptides, a mixture (1/5) of Aβ40 with peptides and the sum of spectra (5μM). Panels a)-c) show CD spectra and interactions of (a) 2c, (b) 2d and (c) 2e, as indicated. Measurements were performed in aq. buffer 1×b, pH 7.4, containing 1% HFIP. Data shown in b&c are from the MSc-thesis of Luzia Heidrich[169].

4.5.6 Effects on fibrillogenesis and cytotoxicity of IAPP

Next it was investigated whether 2c, 2d and 2e could inhibit IAPP fibrillogenesis. Fibrillogenesis of IAPP (6μM) alone and in mixture with 2c, 2d and 2e analogues at a ratio of 1/10 was studied. ThT fluorescence was measured at the indicated time points and up to 7 days (Figure 74a). Moreover, solutions were added to RIN5fm cells after 24 h of incubation and effects on IAPP cytotoxicity were determined by the MTT reduction assay (Figure 74b). Importantly, none of them was able to inhibit IAPP fibrillogenesis and cytotoxicity and the results were confirmed by TEM (Figure 74c).

a)

b)

c)
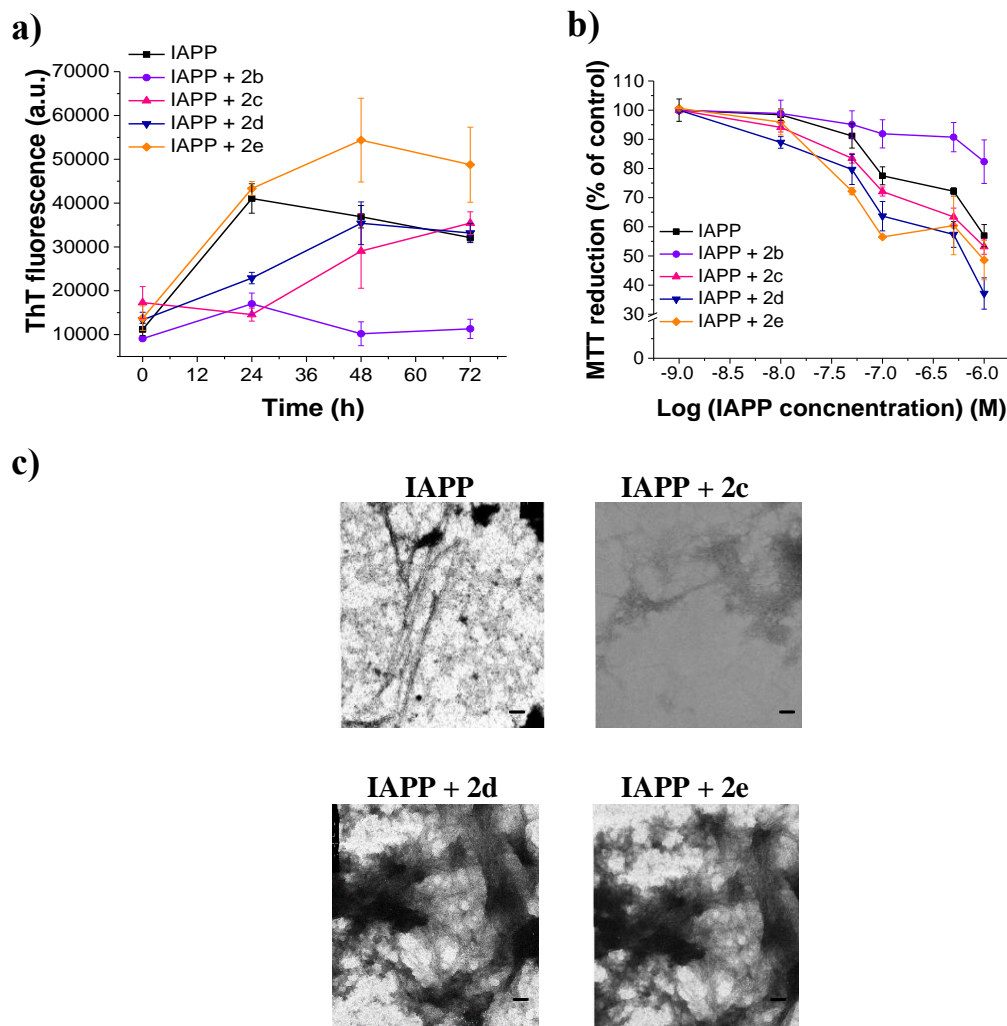
Figure 74. Effects of 2b analogues containing D-amino acids on IAPP amyloid formation and cytotoxicity. (a) Fibrillogenesis of IAPP (6μM) alone and with 2b, 2c, 2d and 2e at 10-fold excess were determined via the ThT binding assay (means (±SD), 3 assays), (b) effects on IAPP cytotoxicity; solutions from (a) aged 24h were added to RINcells. Cell damage assessed by the MTT reduction assay (means (±SD), 3 assays, n=3 each). (c) TEM images of aged IAPP and IAPP mixtures with non/inhibitory peptides. Aliquots from 7 days aged solutions from (a) were used (bars: 100nm). Data of 2d & 2e are from the MSc-thesis of Luzia Heidrich[169].

The above results suggested that the incorporation of D-residues in 2b affected its IAPP inhibition ability. Although higher concentrations were used (50-fold excess), 2e was not able to inhibit IAPP fibrillization (see Figure Appendix A17). In combination with inhibition studies on Aβ40(42) amyloid self-assembly, where all peptides were able to inhibit at five fold excess, these findings suggest that 2e is a selective inhibitor of Aβ40(42).

4.5.7 Determination of binding affinities towards IAPP

The app. K_ds of interactions of IAPP with 2c, 2d and 2e were determined by titrations of Fluos-IAPP (5nM) with various amounts of analogues (Figure 75). The titration of Fluos-IAPP with 2c resulted in an app. K_d of 250nM. In the same nanomolar range apparent affinities were determined for the other two peptides; app. K_d of 2d was 313.4nM and app. K_d of 2e was 245nM (Table 43). It seems that switching chiralities did not affect the binding properties of the peptides to IAPP. Moreover, the app. K_ds of interaction of fluorescently labeled 2c, 2d and 2e with IAPP were determined (Figure 76). Titration of Fluos-2c with IAPP resulted in an app. K_d of 1μM indicated that the L-configuration of the three arginines in the linker are important for binding of 2b with IAPP mono-/oligomers. On

the contrary, the app. K_ds of Fluos- 2d and Fluos-2e with IAPP were determined in low nanomolar range (app. K_d = 3.8nM and app. K_d = 41.6nM respectively). It seems that continuous substitution of L- with D-residues reverse the effects of the D-configuration of the three arginines as the 2d and 2e had high binding affinities to IAPP (Table 43).
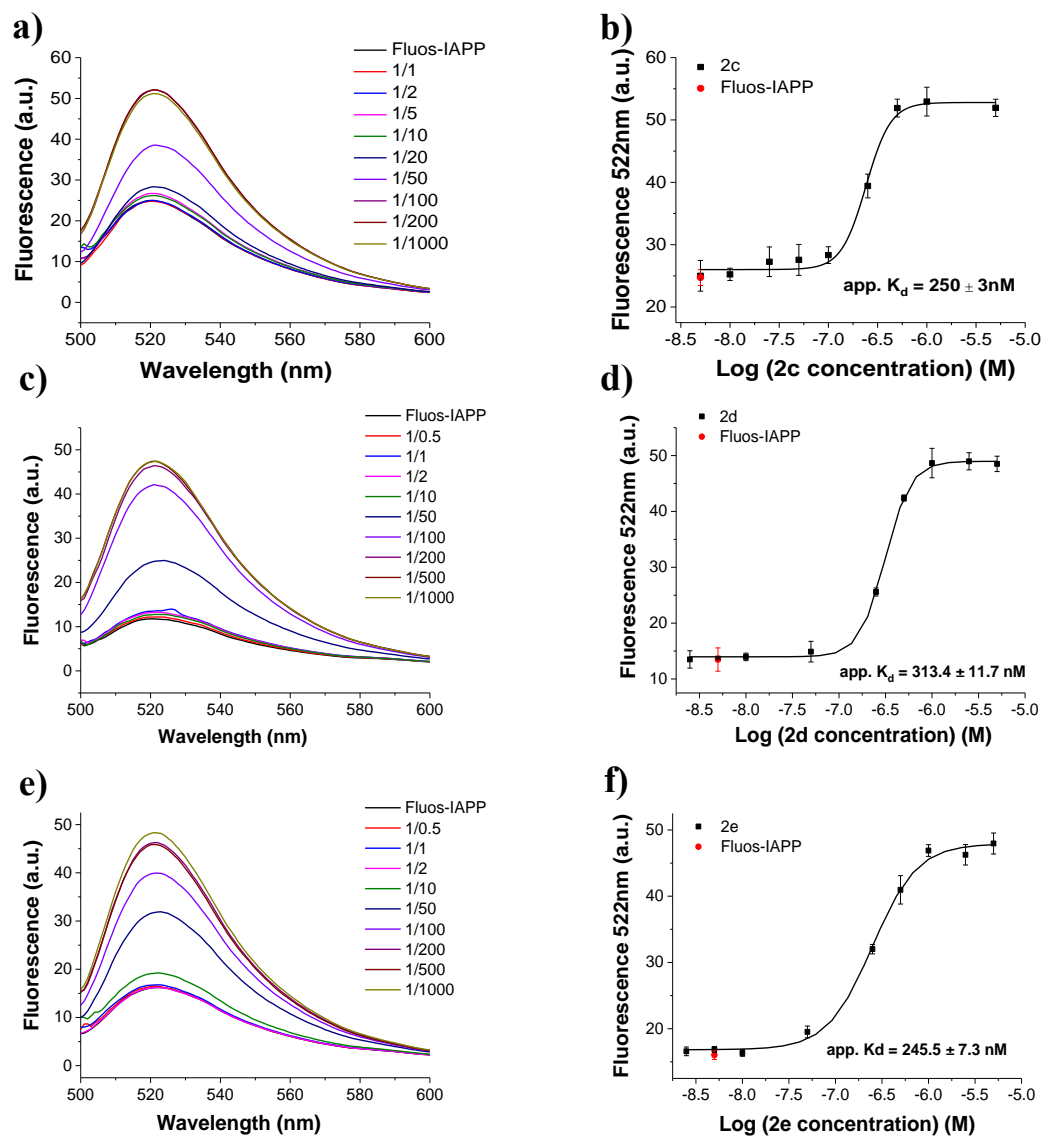
Figure 75. Determination of app. K_ds of the interactions of Fluos-IAPP with 2b analogues containing D-amino acids by fluorescence spectroscopic titrations. Panels a), c), e) show fluorescence spectra of Fluos-IAPP (5nM) alone and its mixtures with various amounts of 2c (a), 2d (c) and 2e (e); the molar ratios of Fluos-IAPP/peptides are as indicated. Panels b), d), f) show the binding curves of 2c (b), 2d (d) and 2e (f); app. K_ds are means (±SD) from 3 binding curves (Fluos-IAPP 5nM). Measurements were performed in aq. buffer 1×b, pH 7.4, containing 1% HFIP. Data shown in c-f) are from the MSc-thesis of Luzia Heidrich[169].
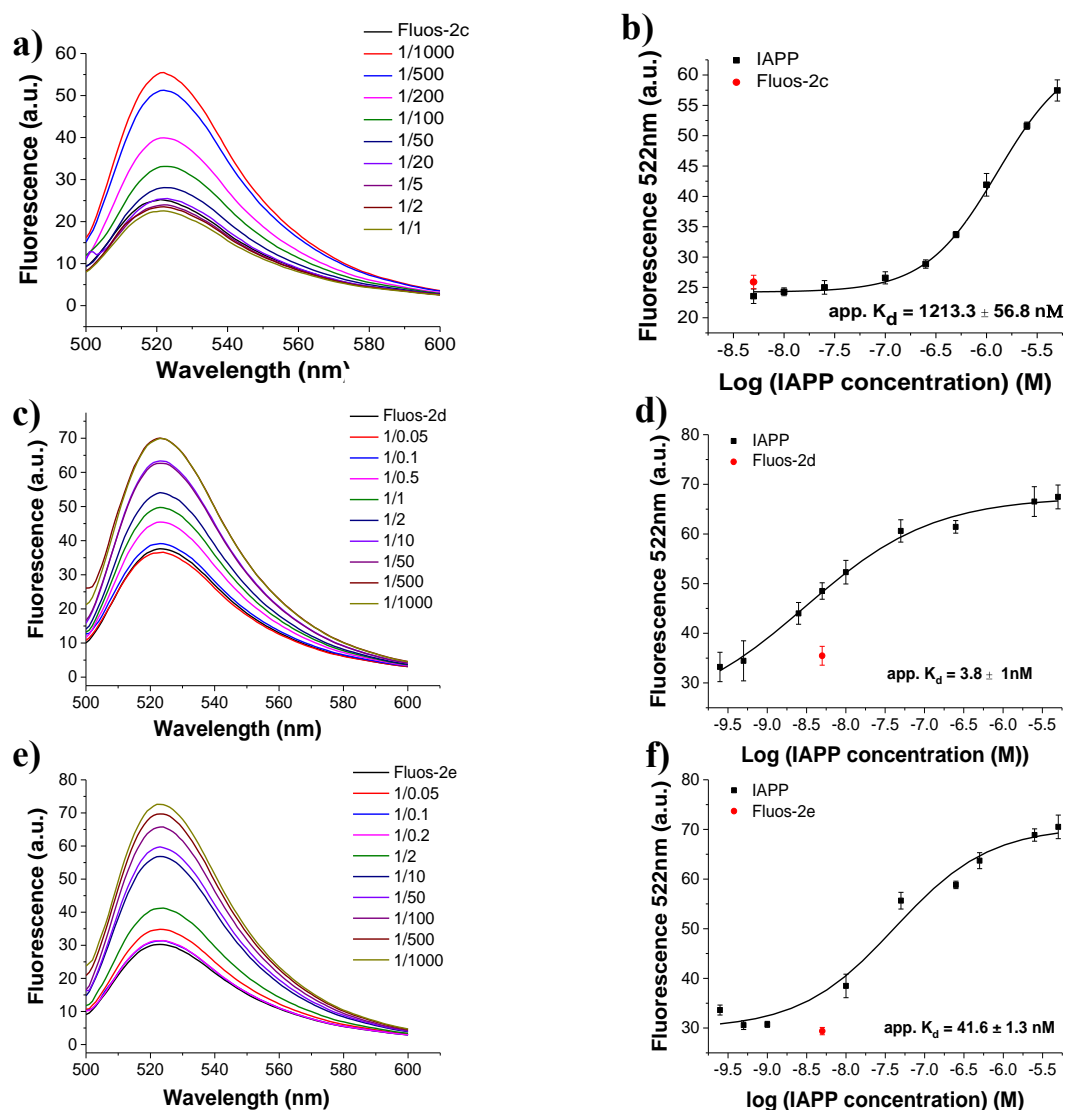
Figure 76. Determination of app. K_ds of interactions of IAPP and 2b analogues containing D-amino acids by fluorescence spectroscopic titrations. Panels a), c), e) show fluorescence spectra of Fluos-peptides (5nM) alone and its mixtures with various amounts of IAPP; the molar ratios of Fluos-peptide/IAPP are as indicated. Panels b), d), f) show the binding curves of IAPP with Fluos-2c (b), Fluos-2d (d) and Fluos-2e (f); app. K_ds are means (±SD) from 3 binding curves (Fluos-peptide 5nM). Measurements were performed in aq. buffer 1×b, pH 7.4, containing 1% HFIP. Data shown in c-f) are from the MSc-thesis of Luzia Heidrich[169].

Table 43. Apparent affinities (app. K_ds) of interaction of peptides with IAPP as determined by fluorescence titration binding assays.

Peptide	app. K_d (±SD) (nM) withFluos-IAPP[a]	app. K_d (±SD) (nM) with IAPP[b]
2b	216.5 (±13.4)	10.76 (±1.2)
2c	250.3 (±3.5)	1213.3 (±56.8)
2d	313.4 (±11.7)	3.8 (±1.7)
2e	245.5 (±7.3)	41.6 (±1.3)

[a] App. K_ds, means (±SD) from three binding curves Fluos-IAPP (5nM) was titrated with peptides; [b] Fluos-peptides (5nM) were titrated with IAPP, (aq. buffer 1×b, pH 7.4, containing 1% HFIP).

4.5.8 Interactions with IAPP by CD spectroscopy

To further investigate the interaction between IAPP and the cyclic analogues containing D-amino acids, CD spectroscopy was applied. CD was performed with IAPP/peptides at the ratio of 1/10

corresponding to the ratio required for inhibition of IAPP amyloidogenensis by 2b (Figure 77). The CD spectra of the mixture of IAPP with 2c, 2d and 2e (1/10) did not differ from the CD spectra of sum IAPP/peptides. This indicated no interaction, which did not cause any conformational changes in IAPP, peptides, or both.
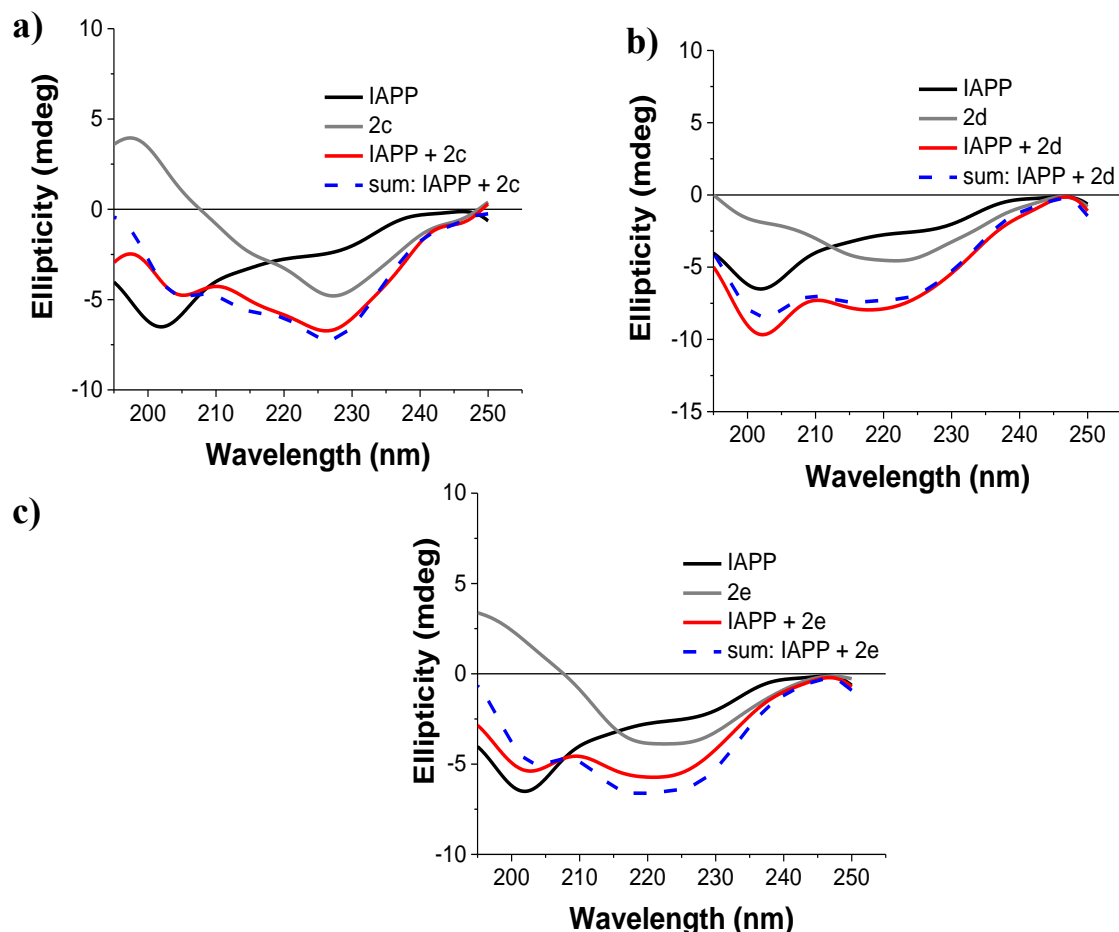
Figure 77. Interaction studies of IAPP and 2b analogues containing D-amino acids studied by far-UV CD spectroscopy. CD spectra of freshly dissolved IAPP alone (2μM), 2c, 2d and 2e (20μM), a mixture (1/10) of IAPP with 2c, 2d and 2e and the sum of spectra. Panels a)-c) show CD spectra and interactions of (a) 2c, (b) 2d and (c) 2e with IAPP as indicated. Measurements were performed in aq. buffer 1×b, pH 7.4, containing 1% HFIP.

4.5.9 **Proteolytic stabilities**

Peptides have emerged as a commercially relevant class of drugs that offer the advantage of grater specificity and potency and lower toxicity profiles over traditional small molecule pharmaceuticals[128]. On the other hand, peptides have several known drawbacks that have prevented them from becoming a mainstream source of drug candidates, including short circulation time half time, poor proteolytic stability and low oral bioavailability[128]. We applied several strategies in the design as shown in scheme 7 to get proteolytic stable peptide. We started from a "long" Aβ inhibitor R3-GI (1), which as shown in chapter 4.15 was very fast degraded in human plasma ($t_{1/2} \sim 20$min) (Table 49). Then by cyclization we maintained the Aβ inhibitory activity and in addition we gained inhibitory function against IAPP amyloidogenicity; however, the proteolytic stability for cc-R3-GI (1a) was also low ($t_{1/2} \sim 30$min) (Table 49). The proteolytic studies of cc-R3-GI (1a) showed a proteolytically stable NFLVHRRRNF(N-Me)GA(N-Me)ILSC-amide. The next modifications that applied were: 1st) truncation of the sequence and 2nd) cyclization where the first lead compound cc-R3-GIsh (2a) was born. Apart from that, cc-R3-GIsh (2a) had a high binding affinity to both Aβ and

IAPP, cc-R3-GIsh (2a) was also a great inhibitor for both amyloid polypeptides. Figure 78 describes the degradation kinetics of the shorter analogue as determined in human plasma using RP-HPLC and MALDI-TOF (Table 44). cc-R3-GIsh (2a) exhibited as well low proteolytic stability ($t_{1/2} \sim$ 20min) (Table 50) with the segment of IAPP(14-17) to be rapidly cleaved. Moreover, aiming at minimizing IAPP–derived elements, we showed that F15, L16, F23, I26 and the RRR linker are sufficient for amyloid inhibitory function and cc-AllG-R3-GIsh (2b) was synthesized and studied with 7 out of 11 non-Gly residues of 2a substituted with Gly (except for Cys); only the side chains of the above 4 residues were maintained (Scheme 7). Its degradation kinetics were determined in human plasma the half-life time was estimated by RP-HPLC at 45min (Figure 79) (Table 45). As next 2b analogues containing D-amino acids regarding their proteolytic degradation in human plasma. Figure 80 shows the degradation kinetics of 2c. The half-life time was estimated ~70 min (Table 49), which indicated that the replacement of L-Arg residues in the linker with D-ones affected the proteolytic stability of 2b. Table 46 shows that after 2h the segment GGFLGGrrrGF(N-Me)GG appeared. Figure 81 presented the degradation kinetics of 2d the exact half-life estimated to be more than an hour ($t_{1/2}$ ~78min) (Table 49). Here was detected after 2 h the same cleaved peptide as in the case of 2c GGflGGrrrf(N-Me)GG (Table 47). However, the $t_{1/2}$ is slightly improved by the replacement of Phe and Leu to D-ones (see Figure Appendix A18). Finally, Figure 82 presented the degradation kinetics of the 2e analogue[163]. The results indicated that 2e was stable for at least 11 h, which was clearly longer than the $t_{1/2}$ of 2b or the $t_{1/2}$ of 2a. These results were confirmed by MALD-TOF mass spectrometry where only the desired peptide peak was found and no degradation products (Table 48 & Figure 82).
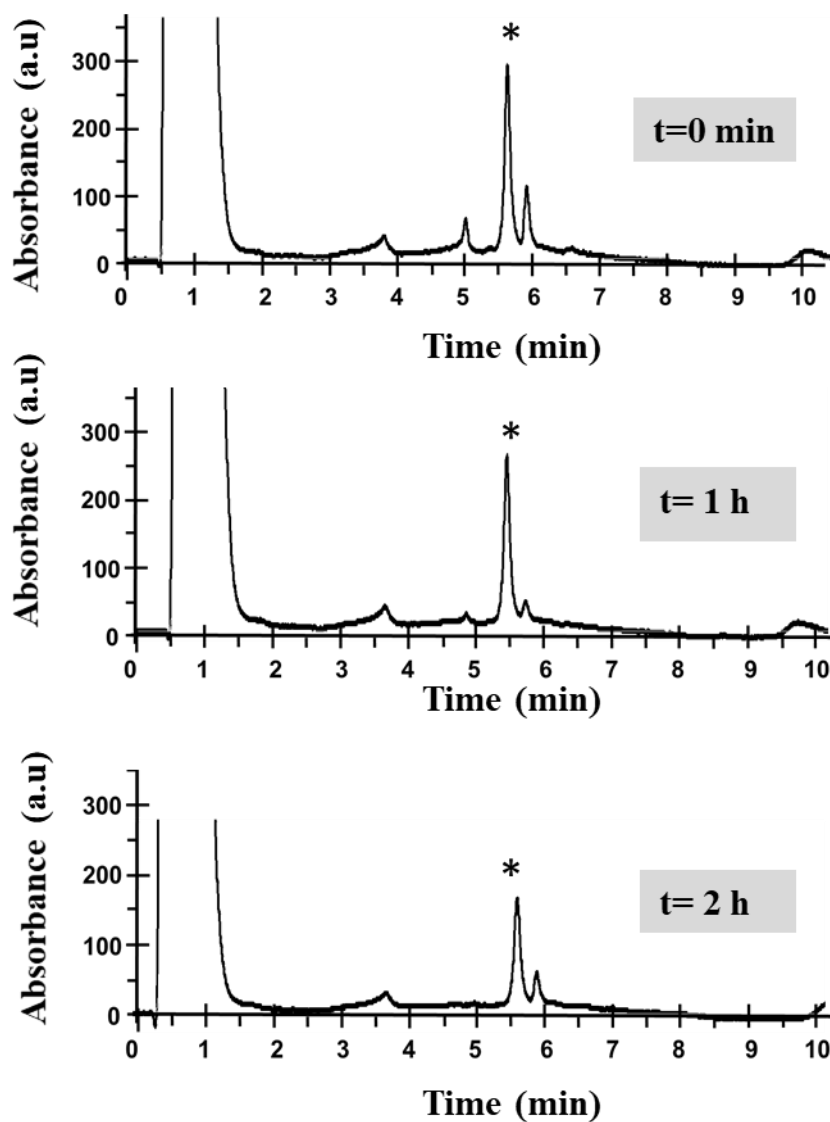
Figure 78. Proteolytic stability of 2a in human plasma (*in vitro*). HPLC chromatograms (HPLC peak with $t_R \sim 5.6$ min marked with a *) corresponding to intact 2a following incubation (37°C) with plasma for 0h, 1h, or 2h and separation from plasma proteins. Only trace amounts of 2a are still present at 1h. Peptides were detected in RP-HPLC by their absorbance at 214nm; calculated $[M+H]^+$ for 2a is 2031.107 and found 2031.107 (1h). Representative data from at least 3 assays are shown.

Table 44. Possible degradation products of 2a in human plasma (HPLC peak with t_R ~5.6 min) as determined via MALDI-TOF.

Time (h)	Detected peptide sequence	Fragment mass calculated [M+H][+][a]	Fragment mass found [M+H][+][a]
0	CNFLVHRRRNF(N-Me)GA(N-Me)ILSC-amide	2031.04	2031.107
1	CNFLVHRRRNF(N-Me)GA(N-Me)ILSC-amide	2031.04	2031.107
	CNFLVHRRRNFG-amide	1518.77	1495.72[b]
2	CNFLVHRRRNFG-amide	1518.77	1495.72[b]

[a] monoisotopic mass; [b] [M+Na][+].
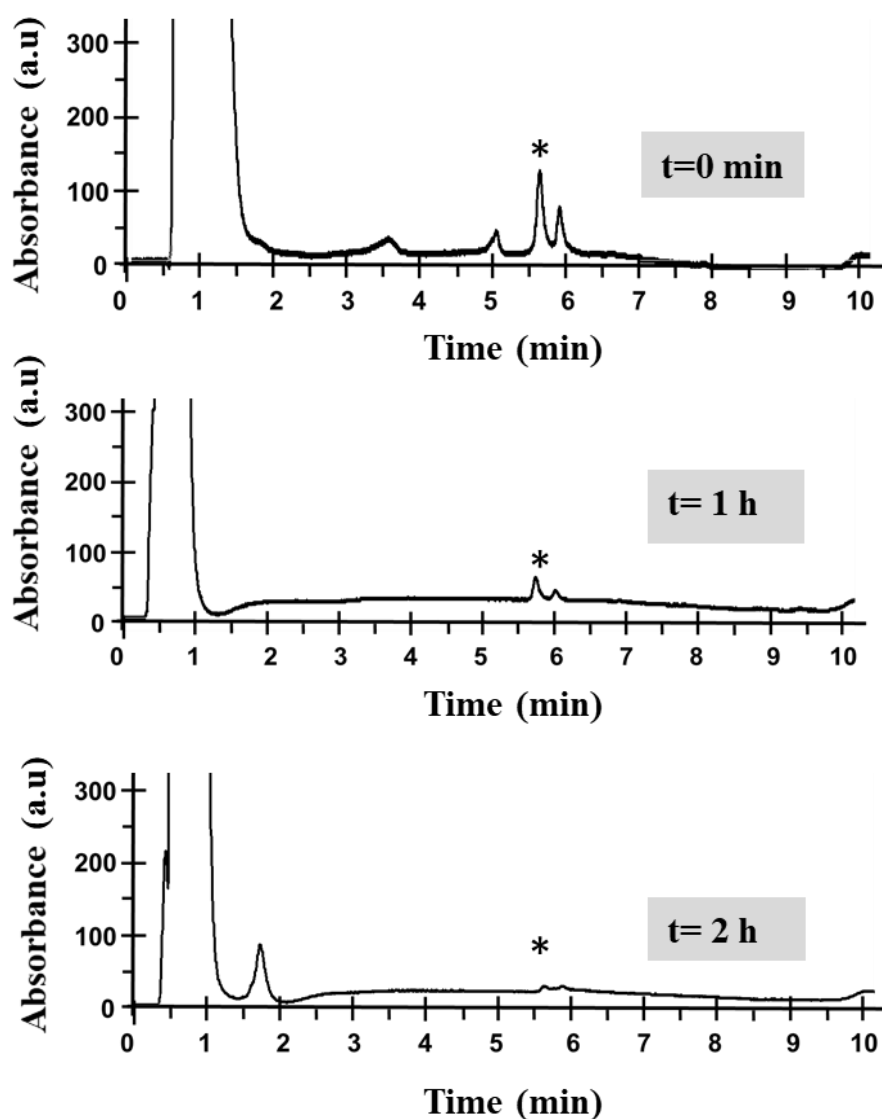
Figure 79. Proteolytic stability of 2b in human plasma (*in vitro*). HPLC chromatograms (HPLC peak with t_R ~ 5.6 min marked with a *) corresponding to intact 2b following incubation (37°C) with plasma for 0h, 1h, or 2h and separation from plasma proteins. Only trace amounts of 2b are still present at 1h. Peptides were detected in RP-HPLC by their absorbance at 214nm; calculated [M+H][+] for 2b is 1694.88 and found 1694.86 (1h). Representative data from at least 3 assays are shown.

Table 45. Possible degradation products of 2b in human plasma (HPLC peak with t_R ~5.6 min) as determined via MALDI-TOF.

Time (h)	Detected peptide sequence	Fragment mass calculated [M+H]+[a]	Fragment mass found [M+H]+[a]
0	CGFLGGRRRGF(N-Me)GG(N-Me)IGGC-amide	1694.88	1694.86
1	CGFLGGRRRGF(N-Me)GG(N-Me)IGGC-amide	1694.88	1694.86
	CGFLGGRRRGF-amide	1224.44	1245.59[b]

[a] monoisotopic mass; [b] [M+Na]+; [c] n.d not determined.
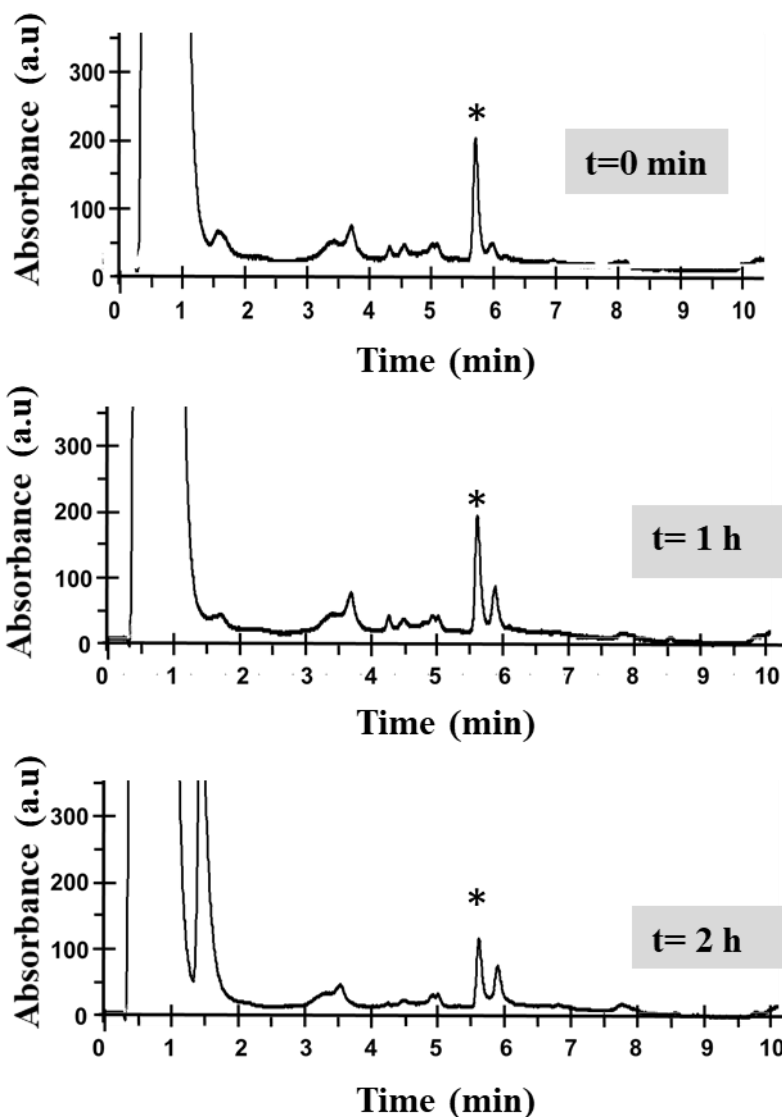
Figure 80. Proteolytic stability of 2c in human plasma (*in vitro*). HPLC chromatograms (HPLC peak with t_R ~ 5.6 min marked with a *) corresponding to intact 2c following incubation (37°C) with plasma for 0h, 1h, or 2h and separation from plasma proteins. Only trace amounts of 2c are still present at 2h. Peptides were detected in RP-HPLC by their absorbance at 214nm; calculated [M+H]+ for 2c is 1694.88 and found 1695.15 (2h). Representative data from at least 3 assays are shown.

Table 46. Possible degradation products of 2c (HPLC peak with t$_R$ ~5.6 min) in human plasma as determined via MALDI-TOF.

Time (h)	Detected peptide sequence	Fragment mass calculated [M+H]$^{+[a]}$	Fragment mass found [M+H]$^{+[a]}$
0	CGFLGGrrrGF(N-Me)GG(N-Me)IGGC-amide	1694.88	1694.96
1	CGFLGGrrrGF(N-Me)GG(N-Me)IGGC-amide	1694.88	1694.96
2	CGFLGGrrrGF(N-Me)GG(N-Me)IGGC-amide	1694.88	1695.15
	CGFLGGrrrGF(N-Me)GG	1353.53	1379.74[b]

[a] monoisotopic mass; [b] [M+Na]$^+$.

Figure 81. Proteolytic stability of 2d in human plasma (*in vitro*). HPLC chromatograms (HPLC peak with t$_R$ ~ 5.6 min; marked with a *) corresponding to intact 2d following incubation (37ºC) with plasma for 0h, 1h, or 2h and separation from plasma proteins. Only trace amounts of 2d are still present at 2h. Peptides were detected in RP-HPLC by their absorbance at 214nm; calculated [M+H]$^+$ for 2d is 1694.88 and found 1695.15 (2h). Representative data from at least 3 assays are shown.

Table 47. Possible degradation products of 2d (HPLC peak with t_R ~5.6 min) in human plasma as determined via MALDI-TOF.

Time (h)	Detected peptide sequence	Fragment mass calculated [M+H]+[a]	Fragment mass found [M+H]+[a]
0	CGflGGrrrGf(N-Me)GG(N-Me)IGGC-amide	1694.88	1694.96
1	CGflGGrrrGf(N-Me)GG(N-Me)IGGC-amide	1694.88	1694.96
2	CGflGGrrrGf(N-Me)GG(N-Me)IGGC-amide	1694.88	1695.15
	CGflGGrrrGf(N-Me)GG	1353.53	1379.74[b]

[a] monoisotopic mass; [b] [M+Na]+.

Figure 82. Proteolytic stability of 2e in human plasma (*in vitro*). HPLC chromatograms (left) and MALDI spectra (right) of the collected HPLC fraction (HPLC peak with t_R ~ 5.6 min marked with a *) corresponding to intact **2e** in plasma following its incubation with human plasma (37°C) for 0h (a), 1h (b), or 11h (c) and separation from plasma proteins. Nearly the complete amount of **2e** is present after 11 h of incubation. Peptides were detected in RP-HPLC by their absorbance at 214nm; calculated [M+H]+ for **2e** was 1694.88 and found 1695.26 (11h). Representative data from at least 3 assays are shown.

Table 48. Possible degradation products of 2e (HPLC peak with t_R ~5.6 min) in human plasma as determined via MALDI-TOF.

Time (h)	Detected peptide sequence	Fragment mass calculated [M+H]+[a]	Fragment mass found [M+H]+[a]
0	cGflGGrrrGf(N-Me)GG(N-Me)IGGc-amide	1694.88	1695.11
1	cGflGGrrrGf(N-Me)GG(N-Me)IGGc-amide	1694.88	1695.11
11	cGflGGrrrGf(N-Me)GG(N-Me)IGGc-amide	1694.88	1695.15

[a] monoisotopic mass.

Table 49. Proteolytic stability of cyclic-R3-GI analogues in human plasma as determined by % peak height by RP-HPLC analysis.

R3-GI analogues	$t_{1/2}$ (min)[a, b]
cc-R3-GI (**1a**)	30.0 (±17.0)
cc-R3-GIsh (**2a**)	26.0 (±7.4)
cc-ALLG-R3-GIsh (**2b**)	46.0 (±5.0)
cc-ALLG-r3-GIsh (**2c**)	71 (±18.0)
cc-ALLG-(f15,I16,f23)-r3-GIsh (**2d**)	78 (±16.0)
cc-ALLG-ALLD-r3-GIsh (**2e**)	>660

[a] $t_{1/2}$ (±SD) from at least 3 plasma degradation assays); [b] peak height: correlated with integrated peak (data not shown).

4.6   Studies on "interaction surface mimics" (ISMs)

4.6.1   Effects of ISMs on insulin fibrillogenesis and cytotoxicity

In vitro studies have shown that insulin binds to IAPP and can inhibit IAPP fibrillogenesis and vice versa[109e],[109a, 109c, 109d, 129]. Some years ago, it has been found that IAPP-GI is a nano-molar affinity inhibitor of insulin aggregation and it does so without affecting insulin function[71b]. It has been suggested that IAPP-GI (an IAPP mimic) could become a lead peptide for development of new drugs and therapeutic concepts for targeting both AD and T2D[71b] (Scheme 6a). In this part of my PhD thesis, I investigated, whether the ISMs could interact with insulin and could inhibit insulin aggregation.

a)

insulin

GIVEQCCTSICSLYQLENYCN
1   6 7   11   20

NH2-FVNQHLCGSHLVEALYLVCGERGFFYTPKT
1   19

IAPP

KCNTATCATQRLANFLVHSSNNFGAILSSTNVGSNTY

b)

IAPP-GI

N-Me N-Me
| | 28
8
KCNTATCATQRLANFLVHSSNNFGAILSSTNVGSNTY

ISMs

N-Me N-Me
| | 28
8
ATQRLANFLVH-XXX-NFGAILS

-XXX-
8-Aoc (8Aoc-GI); 8-Adooc (8Adooc-GI), Gly-Gly-Gly (G3-GI), Ala-Ala-Ala (A3-GI),
Val-Val-Val (V3-GI), Leu-Leu-Leu (L3-GI), Ile-Ile-Ile (I3-GI), Nle-Nle-Nle (Nle3-GI),
(2-Aoc)-(2-Aoc)-(2-Aoc) (2Aoc3-GI), Phe-Phe-Phe (F3-GI), Cha-Cha-Cha (Cha3-GI),
Lys-Lys-Lys (33-GI), Dap-Dap-Dap (Dap3-GI), Arg-Arg-Arg (R3-GI),
Lys(Ac)-Lys(Ac)-Lys(Ac) (KAc3-GI), Ser-(D-Pro)-Gly (SpG-GI)

Scheme 6. Concept underlying the studies on inhibitory effects of ISMs on insulin aggregation. Primary structures of insulin, IAPP, (b) IAPP-GI and ISM inhibitor design concept[87]. Residues in common to all sequences are in blue and similar residues are in green[71b].

According to the ISM design concept the "hot segments" of IAPP IAPP(8-18) and IAPP(22-28) were linked with tripeptide segments, consisting of identical amino acids. It has been demonstrated that depending on the nature of the linker (hydrophobic, hydrophilic, polar) ISMs exhibited different structures and thus different effects on IAPP or Aβ amyloid self-assembly[87]. I addressed the question whether ISMs could also inhibit insulin amyloid formation and toxicity. Insulin alone or with ISMs (1/5) was incubated at pH 2, (60°C) and fibrillogenesis was followed by ThT binding. Insulin fibrillogenesis had a lag time of roughly five days (Figure 83a); however, in the presence of L3-GI and V3-GI fibrillization was strongly suppressed. Importantly, G3-GI and A3-GI were unable to inhibit (Figure 83a). Because of the non-native self-assembly of insulin, leads to cytotoxic oligomers, I then investigated whether ISMs might also intervene with this process as well. Of note, IAPP-GI has been shown to inhibit insulin cytotoxicity[71b]. Insulin or insulin/ISMs mixtures (1/5) were incubated (4 days, pH 2, 60°C) and added to RIN5fm cells; cell viabilities were determined by the MTT reduction assay (Figure 83b). It was found that L3-GI and V3-GI completely blocked formation of cytotoxic species, whereas G3-GI, A3-GI were unable to do so (Figure 83b).
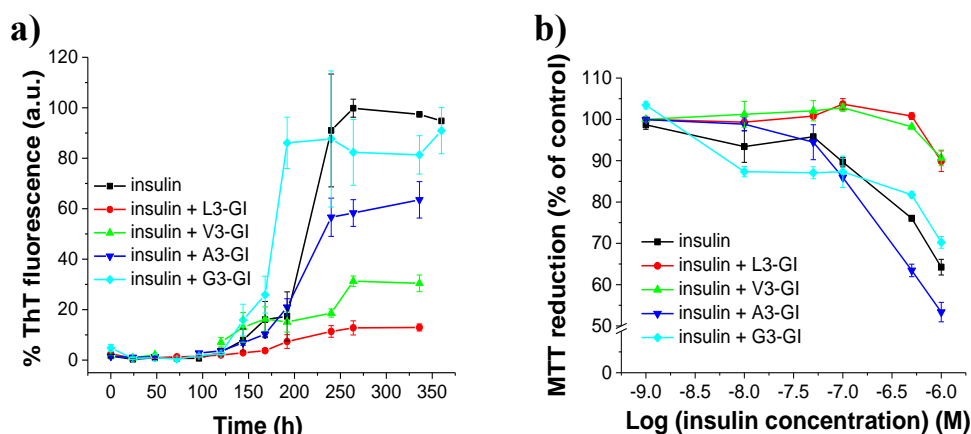
Figure 83. Effects of ISMs on insulin fibrillogenesis and cytotoxicity. (a) Fibrillogenesis of insulin (10µM) alone or in mixture with ISMs (insulin/ISM (1/5)) were determined by the ThT binding assay (means (±SD) from 3 assays). (b) Effects

of 4 days aged insulin (20μM) alone or in mixture with ISMs (insulin/ISM (1/5)) on RIN5fm cell viabillity; cell damage determined by the MTT reduction assay (means (±SD), 3 assays, (n=3 each).

Next, the effects of the five hydrophobic linker-containing I3-GI, Nle3-GI, 2Aoc3-GI, F3-GI, and Cha3-GI and the four polar-linker-containing K3-GI, Dap3-GI, R3-GI, and KAc3-GI were studied (Figure 84 & Figure 85). Four of them (I3-GI, Nle3-GI and F3-GI) blocked both insulin fibrillogenesis and cytotoxicity (Figure 84). However, in the case of of Aoc3-GI, only insulin fibril foprmation but not cytotoxicity was blocked (Figure 84). Importantly, two polar linker containing ISMs (SpG-GI and K3-GI) inhibited insulin self-assembly and cytotoxicity (Figure 85), but the other three (R3-GI, Dap3-GI snd KAc3-GI) did not inhibit insulin fibril formation and cytotoxicity (Figure 85).
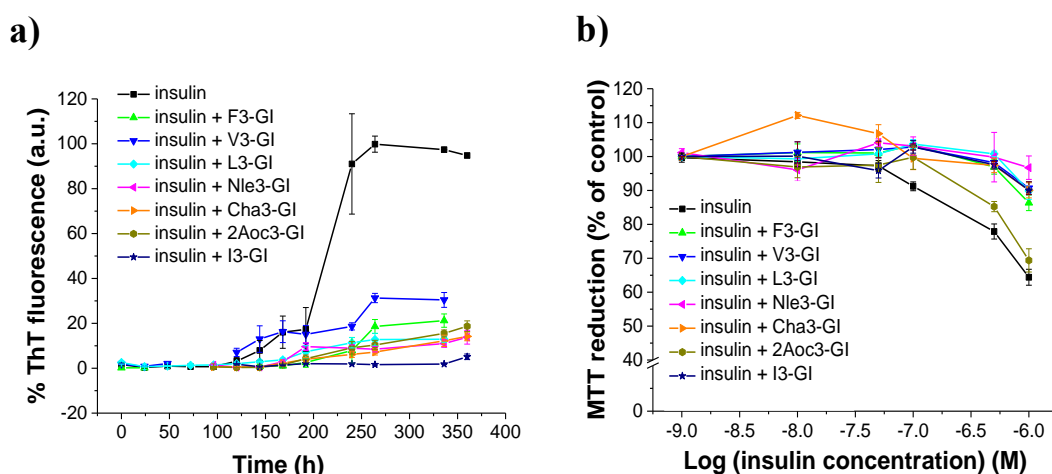
Figure 84. Effects of hydrophobic linker containing ISMs on insulin fibrillogenesis and cytotoxicity. (a) Fibrillogenesis of insulin (10μM) alone or in mixture with ISMs (insulin/ISM (1/5)) were determined by the ThT binding assay (means (±SD) from 3 assays). (b) Effects of 4 days aged insulin (20μM) alone or in mixture with ISMs (insulin/ISM (1/5)) on RIN5fm cell viabillity; cell damage determined by the MTT reduction assay (means (±SD), 3 assays, (n=3 each).
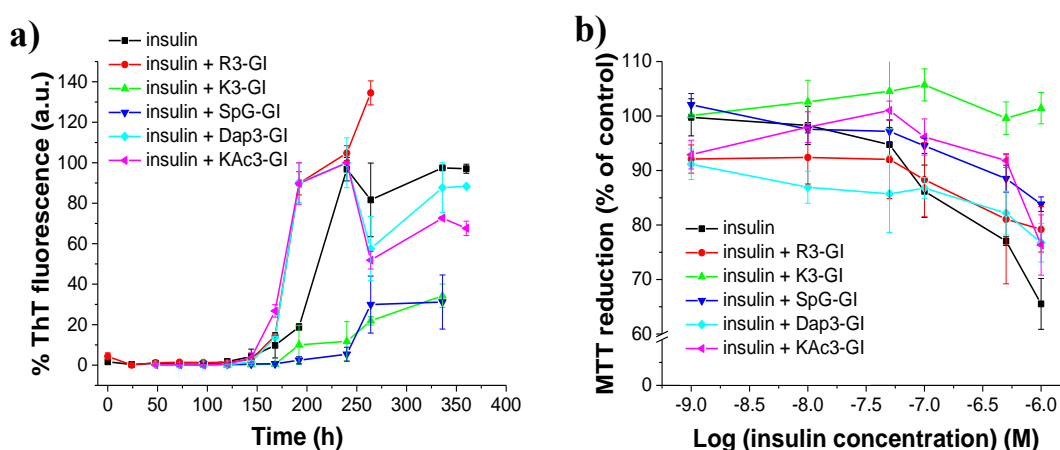
Figure 85. Effects of polar linker containing ISMs on insulin fibrillogenesis and cytotoxicity. (a) Fibrillogenesis of insulin (10μM) alone or in mixture with ISMs (insulin/ISM (1/5)) were determined by the ThT binding assay (means (±SD) from 3 assays). (b) Effects of 4 days aged insulin (20μM) alone or in mixture with ISMs (insulin/ISM (1/5)) on RIN5fm cell viabillity; cell damage getermined by the MTT reduction assay (means (±SD), 3 assays, (n=3 each).

4.6.2 Interactions with insulin as studied by CD spectroscopy

To characterize the insulin/ISM interactions, far-UV CD was applied. The CD spectrum of insulin (20μM) at a pH of 2 (25°C) was characterized by significant amounts of α-helical components (see minima at 207 and 222nm) (Figure 86). The spectrum of L3-GI (100μM) alone had a minimum at a

wavelength of ∼198nm, which indicated disordered conformation and a minimum at ∼228nm, which indicated β-turn conformation. The spectrum of the mixture of insulin with L3-GI (insulin/L3-GI (1/5)) indicated the formation of ordered heterocomplexes, which had larger helical content than insulin. Additionally, the mathematical sum of the spectra of the single components clearly differed from the CD spectrum of the insulin/L3-GI mixture, consistent with conformational changes upon interaction of the 2 peptides (Figure 86a). By contrast, no significant differences were observed in the spectra of the mixtures of V3-GI, G3-GI with insulin (1/5) (Figure 86b & c). Finally, in the case of A3-GI a small but clear difference was observed in the spectra of its mixture with insulin (1/5), indicating conformational changes upon interaction of the 2 peptides (Figure 86d).
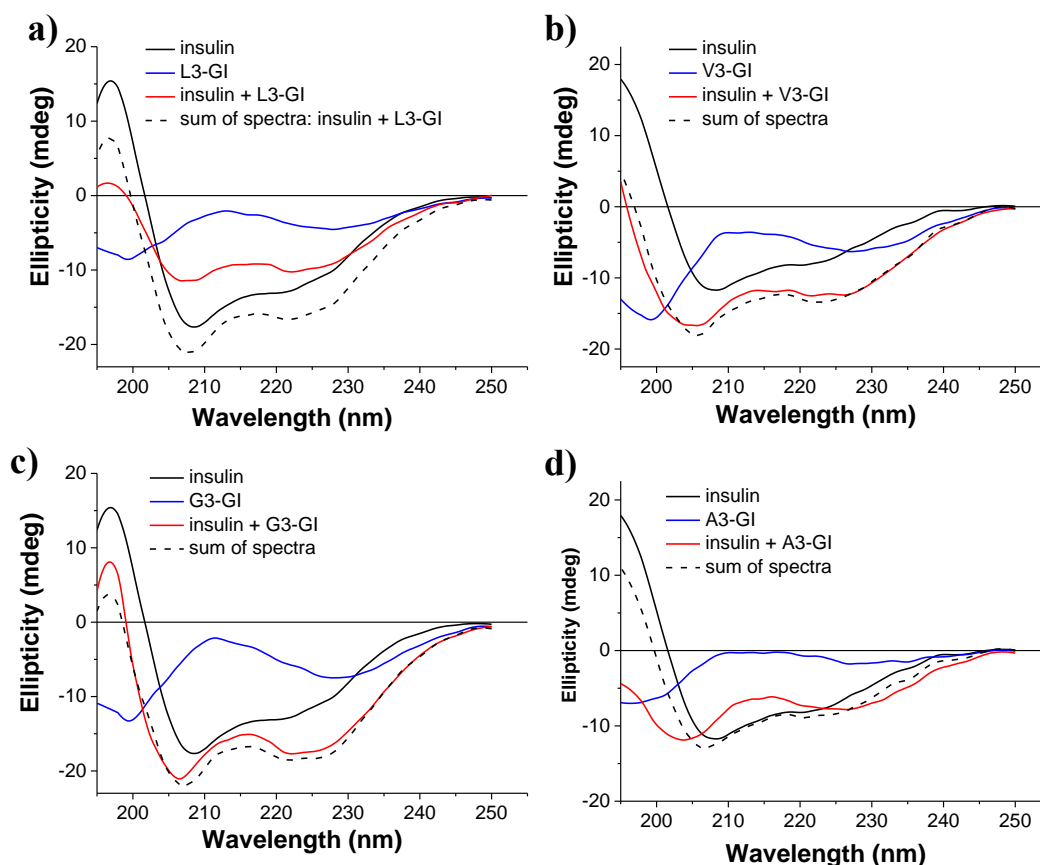
Figure 86. Interaction of insulin with ISMs studied by far-UV CD spectroscopy. CD spectra of freshly prepared insulin alone (20μM), ISM alone (100μM), a mixture (1/5) of insulin with ISM and the sum of spectra are shown. Panels a-d) show CD spectra and interactions of (a) L3-GI, (b) V3-GI, (c) G3-GI and (d) A3-GI with insulin as indicated. Measurements were performed in H_2O/HCl, pH 2.

Next the interactions of insulin with the five hydrophobic linker containing ISMs (I3-GI, Nle3-GI, 2Aoc3-GI, F3-GI, Cha3-GI) were investigated (Figure 87). The mathematical sum of the spectra of the hydrophobic linker containing ISMs clearly differed from the CD spectra of the insulin/ISMs mixtures, consistent with conformational changes upon interaction. In particular, the CD spectrum of I3-GI (100μM) alone was measured at pH 2 and two minima were observed, one at 198nm and one at 225nm, which indicated both unordered and β-turn contents (Figure 87). The CD spectra of mixture insulin/Ie3-GI showed more helical content compared to the spectra of mathematical addition (Figure 87a). The CD spectra of Nle3-GI (100μM) at pH 2 showed as well both amounts ordered and ordered in 1/1 ratio but interestingly in the mixture (1/5) insulin/Nle3-GI the conformation changed to more ordered one with a minimum ∼225nm. The difference between CD spectra of the mixture insulin/Nle3-GI and the CD spectra of the sum indicated conformational

changes upon interaction of the 2 peptides (Figure 87b). Next the interaction of insulin with 2Aoc3-GI peptide was studied. The CD spectra of 2Aoc-3GI alone in pH 2 showed only a minimum at ~222nm, which indicated large amount of β-sheet contents. The CD spectra of the mixture of insulin/2Aoc3-GI also exhibited a minimum at ~220nm, which was indicative of high amounts of β-sheet conformational as well (Figure 87c).
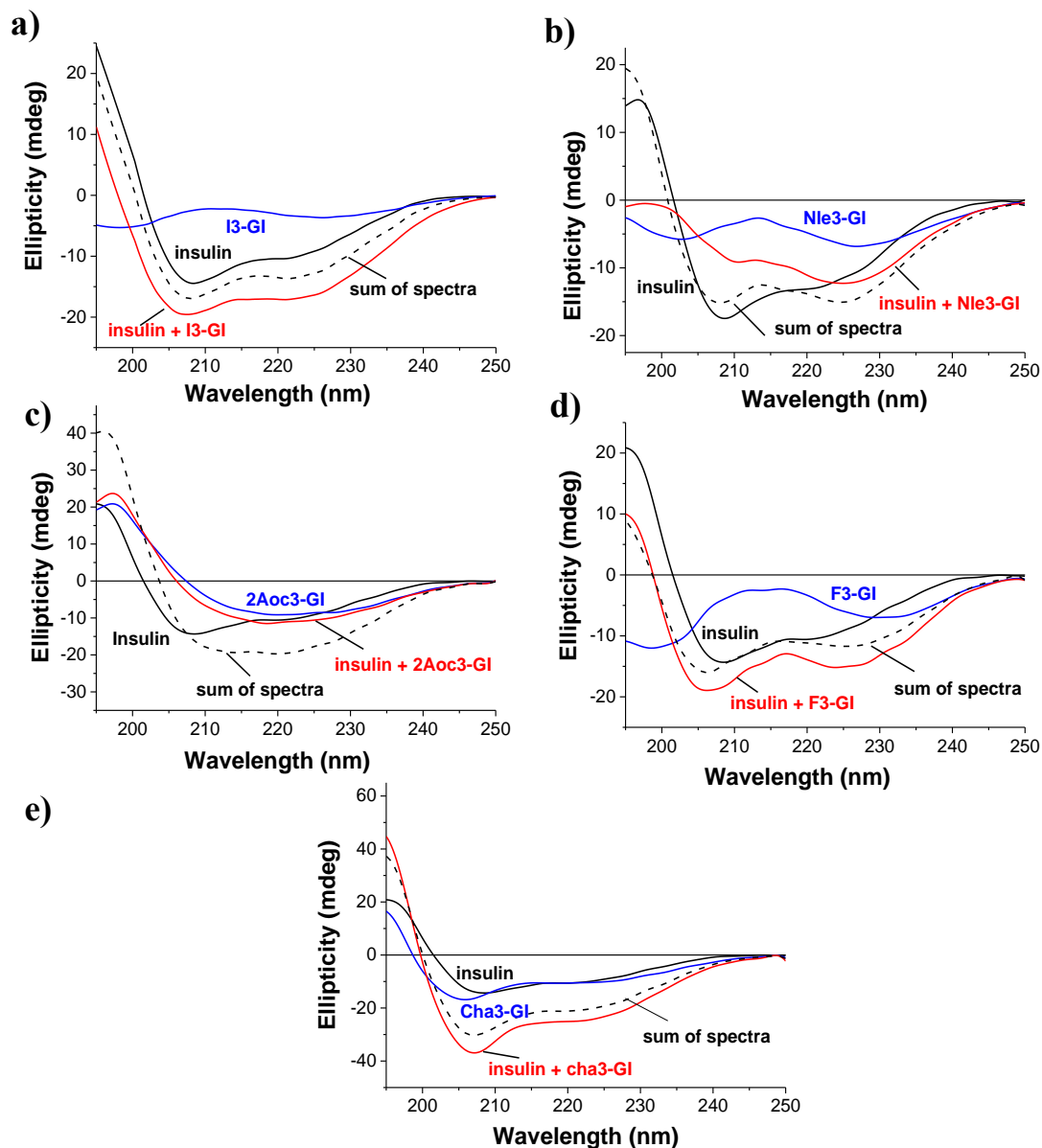
Figure 87. Interaction of insulin and hydrophobic linker containing ISMs studied by far-UV CD spectroscopy. CD spectra of freshly prepared insulin alone (20μM), ISM alone (100μM), a mixture (1/5) of insulin with ISM and the sum of spectra. Panels a-e) show CD spectra and interactions of (a) Ie3-GI, (b) Nle3-GI, (c) 2Aoc3-GI , (d) F3-GI and e) Cha3-GI with insulin as indicated. Measurements were performed in H_2O/HCl, pH 2.

Next, the interaction between insulin and F3-GI was investigated. The CD spectrum of F3-GI (100μM) was measured at pH 2 and two minimum were observed, one at 198nm and one at 225nm; this indicated both unordered and β-turn contents. Finally, the CD spectra of the mixtures of insulin with F3-GI and Cha3-GI and the CD spectra of the sums showed no strong difference (Figure 87d,e), resulted in weaker interaction of the peptides.

Furthermore, in Figure 88 the CD spectra of the polar linker containing mixtures of insulin with different ISMs i.e. K3-GI, Dap3-GI, R3-GI, KAc3-GI and SpG-GI are shown. In the case of CD spectra of the mixtures of K3-GI and KAc3-GI with insulin did not differ form the CD spectra of the sums, indicated no confomaational changes upon interaction of the peptides with insulin. Significant differences between the CD spectra of the mixtures versus the CD spectra of the sums were found only in the case of Dap3-GI, R3-GI and SpG-GI. These findings suggested that interaction of Dap3-GI, R3-GI and SpG-GI with insulin resulted in significant conformational changes.
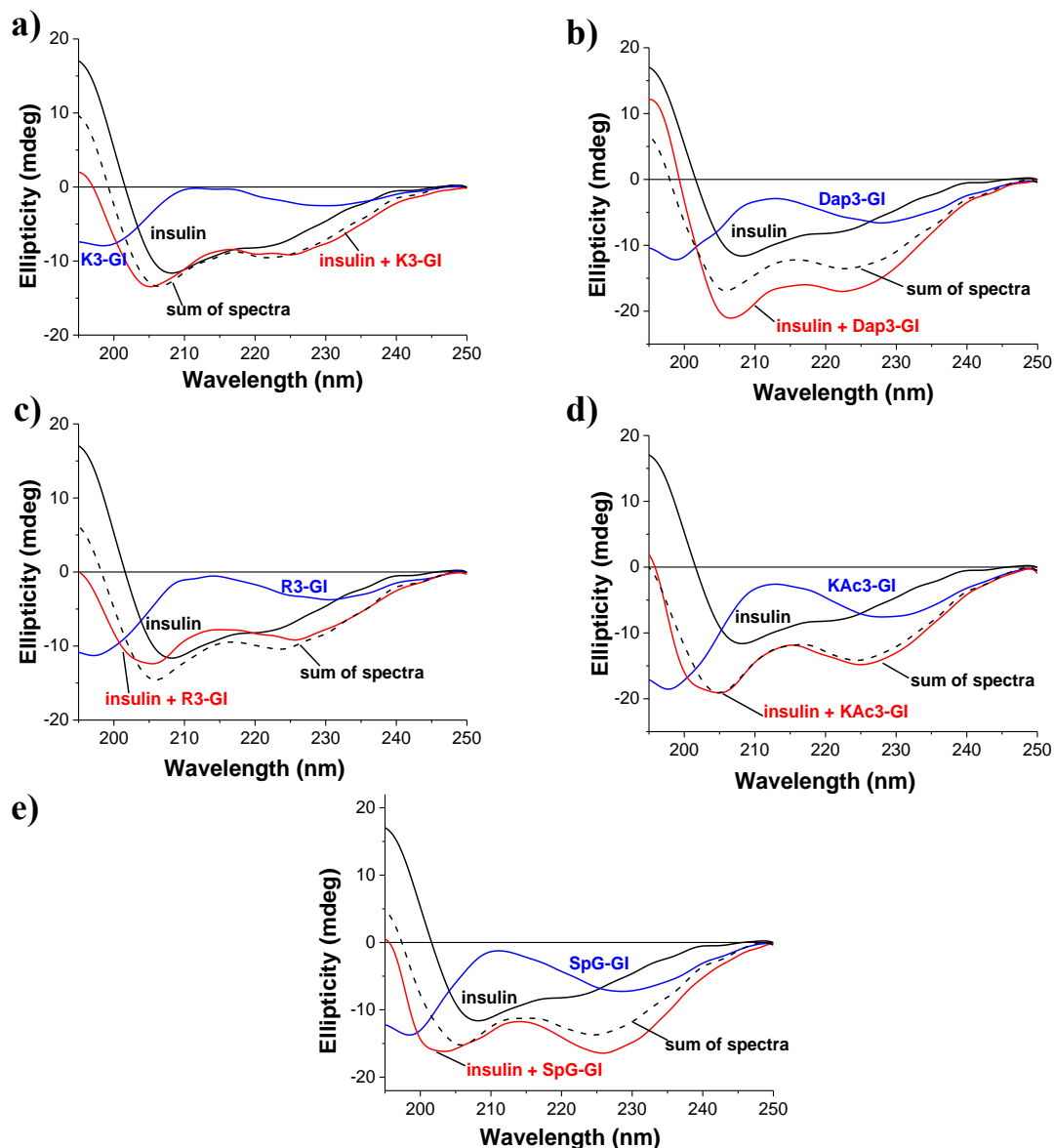
Figure 88. Interaction of insulin with polar linker containing ISMs as studied by far-UV CD spectroscopy. CD spectra of freshly prepared insulin alone (20µM), ISM alone (100µM), a mixture (1/5) of insulin with ISM and the sum of spectra. Panels a-e) show CD spectra and interactions of (a) K3-GI, (b) Dap3-GI, (c) R3-GI, (d) KAc3-GI and e) SpG-GI with insulin as indicated. Measurements were performed in H_2O/HCl, pH 2.

4.6.3 Effects on insulin oligomerization

Insulin aggregation occurs through its dissociation and partial unfolding steps[130]. At pH 2 and 25°C, mainly mono- and dimers of insulin are present[130]. At higher temperatures, however, the dimer dissociates and by partial unfolding misfolded monomers form which then aggregate into oligomers

and fibrils[130]. Since it has been shown that IAPP-GI inhibits the formation of both insulin fibrils and toxic oligomers[71b], I wanted to investigate if this was the case for the above mentioned ISMs as well. The kinetic course of insulin oligomerization was followed using non-reducing NuPAGE electrophoresis in combination with Western Blot (WB). The insulin solution (20 μM) and 1/5 mixtures with ISMs (freshly dissolved, non-fibrillar) were incubated (pH 2, 60°C) up to 48h. Figure 89 shows kinetics of insulin oligomerization and the effects of L3-GI, V3-GI, A3-GI and G3-GI. Freshly dissolved insulin (t=0h) consisted mainly of mono- and dimers, whereas after 24 and 48h significant amounts of oligo- and multimers appeared. The insulin/L3-GI mixture consisted, however, only from monomers and dimers, indicating a significant inhibitory effect of L3-GI on the formation of insulin oligomers. In the presence of V3-GI the formation of insulin oligomers and multimers was also inhibited. The insulin/V3-GI mixture contained additionally small amounts insulin trimers. On the other hand, in the presence of A3-GI and G3-GI the formation of insulin oligomers was not inhibited either at 24h (data not shown) or at 48 h, confirming the linker specificity of inhibition effects.
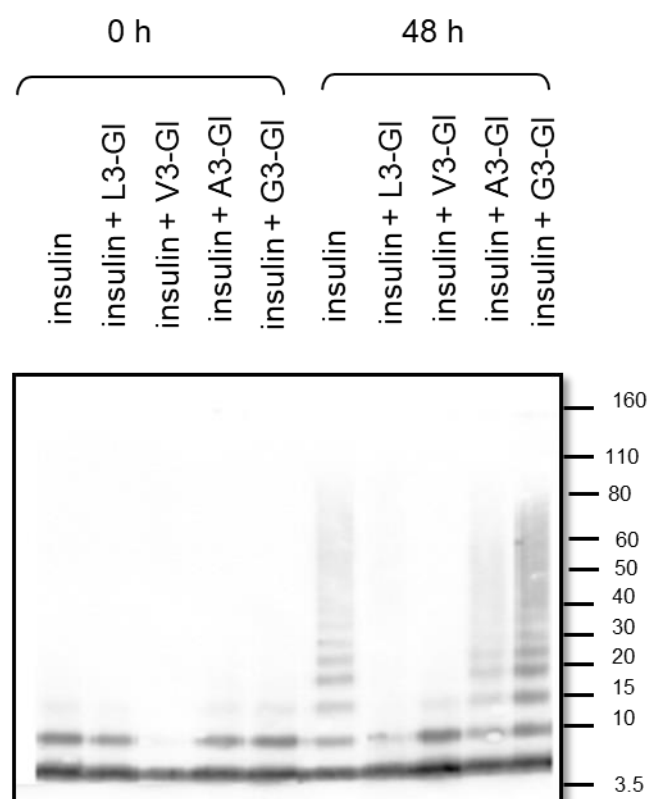
Figure 89. Kinetics of insulin oligomerization effects of L3-GI, V3-GI, A3-GI and G3-GI as assessed by native-like non-reducing NuPAGE followed by WB with anti-insulin antibody. Solutions of insulin alone (20μM) or its mixtures with L3-GI (100μM), V3-GI (100μM), A3-GI (100μM) and G3-GI (100μM) in water/HCl, pH 2, were incubated at 60°C for 48h. After 48h the incubations were mixed with NuPAGE buffer without reducing agent at room temperature and subjected to NuPAGE (without boiling).

Next, we tested whether the hydrophobic linker-containing ISMs; Nle3-GI, 2Aoc3-GI, F3-GI and Cha3-GI could inhibit insulin oligomerization. The insulin solution (20μM) and 1/5 mixtures with the hydrophobic linker ISMs were incubated (pH 2, 60 °C) for 24h. Figure 90 shows the kinetics of insulin and the effects of Nle3-GI, 2Aoc3-GI, F3-GI towards insulin oligomerization. Freshly dissolved insulin (t=0h) consisted mainly of mono- and dimers, whereas after 24h oligo- and multimers appeared. In the presence of Nle3-GI, 2Aoc3-GI, F3-GI and Cha3-GI insulin oligomerization was strongly suppressed. On the contrary, in the case of R3-GI and Dap3-GI after

24h of incubation with insulin oligo and multimers appeared (Figure 90) which confirmed their non-inhibitory properties.
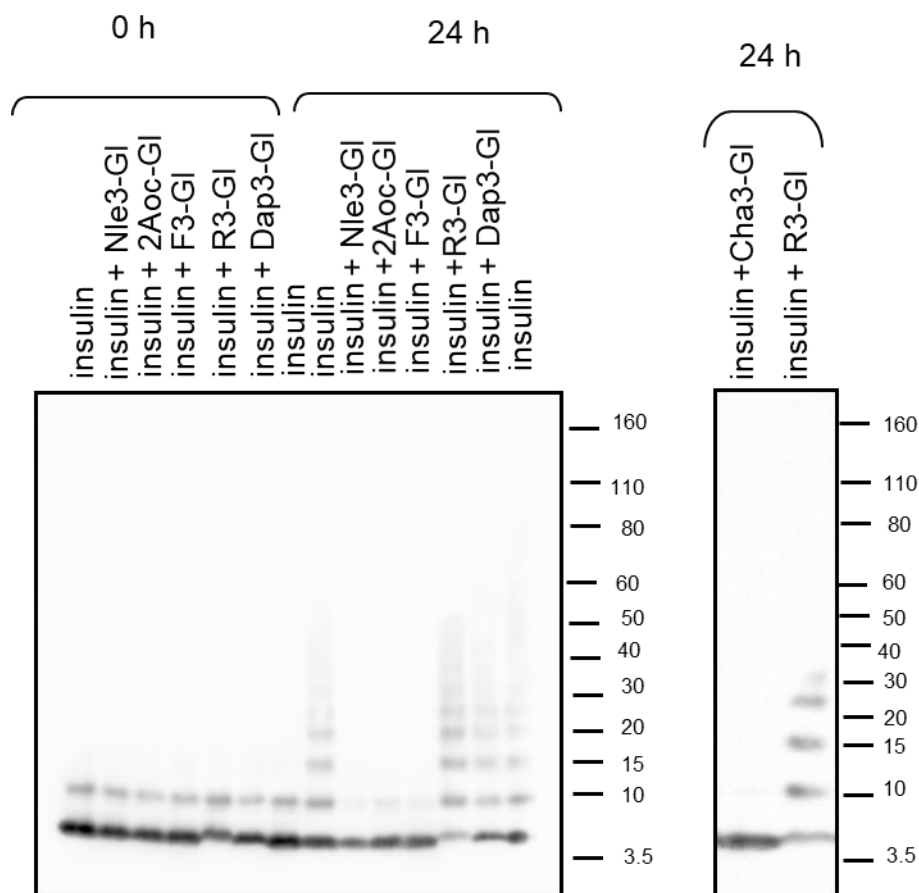
Figure 90. Kinetics of insulin oligomerization effects of Nle3-GI, 2Aoc3-GI, F3-GI, R3-GI, Dap3-GI and Cha3-GI as assessed by native-like non-reducing NuPAGE followed by WB with anti-insulin antibody. Solutions of insulin alone (20μM) or its mixtures with Nle3-GI (100μM), 2Aoc3-GI (100μM), F3-GI (100μM), R3-GI (100μM), Dap3-GI (100μM) and Cha3-GI (100μM) in water/HCl, pH 2, were incubated at 60ºC for 24h. After 24h the incubations were mixed with NuPAGE buffer without reducing agent at room temperature and then subjected to NuPAGE (without any boiling).

Finally, the last group of peptides that were tested against insulin oligomerization was I3-GI, K3-GI, KAc3-GI and the SpG-GI. The insulin solution (20μM) and 1/5 mixtures with ISMs were incubated (pH 2, 60°C) for 24h. Figure 91 shows the kinetics of insulin and the effects of the above mentioned peptides. As negative control G3-GI was used (as non-inhibitor) and as positive control I3-GI (inhibitor). Freshly dissolved insulin (t=0h) consisted mainly of mono- and dimers, whereas after 24h oligo- and multimers appeared. As shown in previous studies, KAc3-GI and G3-GI could not inhibit insulin fibril formation or cytotoxicity and we expected a negative result. Indeed, in the presence of these 2 ISMs no inhibition of insulin oligomers was found. However, in the presence of K3-GI, SpG-GI and I3-GI after 24h all mixtures consisted only of monomers and dimers, indicating an inhibitory activity of these peptides on insulin oligomerization.
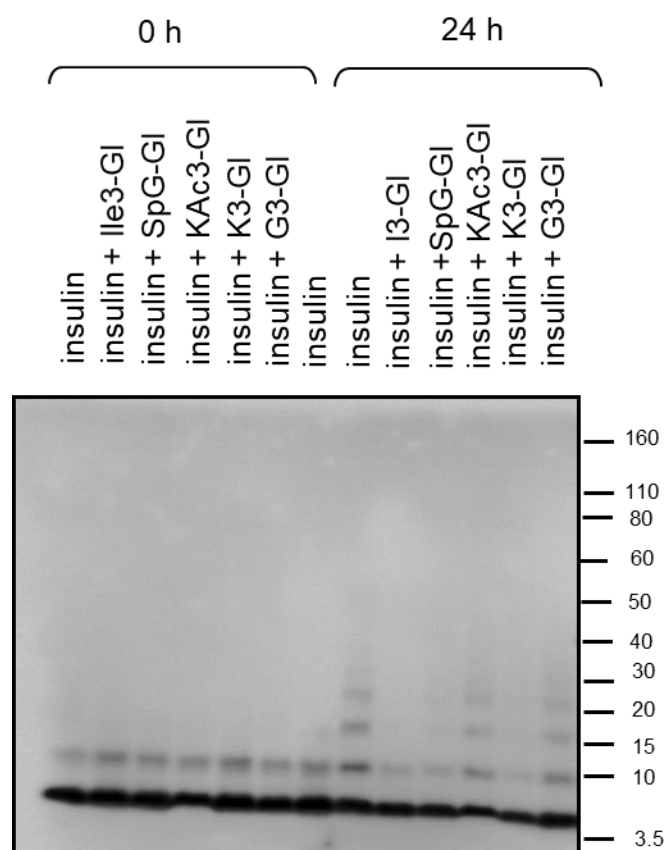
Figure 91. Kinetics of insulin oligomerization effects of I3-GI, SpG-GI, KAc3-GI, K3-GI and G3-GI as assessed by native-like non-reducing NuPAGE followed by WB with anti-insulin antibody. Solutions of insulin alone (20μM) or its mixtures with I3-GI (100μM), SpG-GI-GI (100μM), KA3-GI-GI (100μM), K3-GI (100μM) and G3-GI (100μM) in water/HCl, pH 2, were incubated at 60ºC for 24h. After 24h the incubations were mixed with NuPAGE buffer without reducing agent at room temperature and then subjected to NuPAGE (without any boiling).

Table 50. Effects of ISMs on insulin fibrillization and cytotoxicity.

Peptides	Fibril formation inhibition effect	Cytotoxicity inhibition effect	Conformational change by CD spectroscopy	Inhibition of oligomerization
G3-GI	-	-	-	-
A3-GI	-	-	+	-
V3-GI	+	+	-	+
L3-GI	+	+	+	+
I3-GI	+	+	+	+
Nle3-GI	+	+	+	+
2-Aoc3-GI	+	-	+	+
F3-GI	+	+	+	+
Cha3-GI	+	+	+	+
K3-GI	+	+	-	+
Dap3-GI	-	-	+	-
R3-GI	-	-	+	-
KAc3-GI	-	-	-	-
SpG-GI	+	+	+	+

"+"indicates inhibition, "-"indicates no inhibition.

In conclusion, it was found that ISMs containing hydrophobic linkers (L3-GI, V3-GI, I3-GI, Nle3-GI, F3-GI and Cha3-GI) interacted with insulin and inhibited insulin aggregation. These ISMs with exception of F3-GI inhibited Aβ and IAPP aggregation; the last could inhibit only IAPP. On the other hand, ISMs containing polar amino acids in the linker (except from R3-GI) were not able to interact and inhibit insulin aggregation. Interstingly, most of the ISMs with polar linkers did not inhibit Aβ or IAPP as well. Thus, my studies here indicated that K3-GI and SpG-GI are selective inhibitors of insulin amyloid formation and toxicity. In addition, my studies indicated that L3-GI and Cha3-GI can inhibit all 3 polypeptides. It was found that some of the linkers containing hydrophobic β-sheet-structure propagating residues yielded in inhibitory ISMs against insulin, while linkers containing small or polar residues, rather resulted in non-inhibitory ISMs insulin (Table 50).

5.   Discussion

Peptide based drugs usually offer an alternative and synthetically appealing strategy in the field of rational drug design [131]. Linear peptides are not very promising therapeutics agents owing to the low proteolytic stability and usually no BBB permeability. Nevertheless, a large number of natural occurring peptides exhibit a limited applicability due to their poor stability in physiological conditions, which have inspired the scientists to develop the so called peptidomimetics (non peptide mimetics or cyclic peptides). Cyclic peptides have been broadly exploited over the past 20 years in medicine as active ingredients of natural extracts (bacteria, fungi, plants, animal venoms), some representative examples in the current pharmaceutical market include the well-known cyclosporine A, gramicidin-S, vasopressin, oxytocin, vancomycin, and insulin[132]. Moreover, the continuous advances of solid phase and solution phase synthesis and purification strategies have enabled the pharmacological progress and competitiveness of cyclic peptides as therapeutically relevant targets[119b]. Diverse chemical modifications protocols have evolved to diminish the above mentioned drawbacks include cyclization (increased stability)[133], N-methylation (increased membrane permeability and stability)[134], incorporation of unnatural amino acids (increased specificity and stability)[135], PeGylation (reduced clearance)[133a], assorted structural constraints (e.g., disulfide bonds) and "stapled peptides" (improved potency and specificity)[136]. Confining a peptide into a cyclic structure reduces conformational freedom of its parent structure and might enhance its metabolic stability, bioavailability and specificity, providing promising classes of molecules with "drug –like properties"[137].

5.1   Cyclic R3-GI analogues as potent inhibitors of Aβ40(42) and IAPP amyloid formation

Many cell degenerative diseases, like Alzheimer's or diabetes type II, are linked to amyloid protein fibril formation. The two diseases are characterized by the aggregation of two related amyloidogenic polypeptides: the amyloid-β peptide (Aβ40(42)) in AD and islet amyloid polypeptide (IAPP) in T2D. It has been shown that these two peptides are able to cross-interact and that the formation of hetero assemblies of Aβ40(42)-IAPP suppresses Aβ40(42) and IAPP amyloid self-assembly[70, 86b]. These findings suggest that the Aβ-IAPP interaction could be a molecular link between AD and T2D[70]. An interaction of Aβ and IAPP is possible in vivo since both peptides are presence in similar concentrations in serum and cerebrospinal fluid[138]. Molecules blocking the amyloidogenesis of these two polypeptides could thus become promising therapeutic candidates[5, 139]. However, the rational design of amyloid inhibitors is a difficult task[5]. A large number of peptide-based inhibitors of Aβ40(42) or IAPP amyloidogenesis has been derived from their target polypeptides[67, 70, 140]. However, more recently various IAPP analogues have been shown to inhibit amyloid self-assembly of Aβ40(42) as well[70, 75]. The molecular basis of this cross-amyloid inhibitory function is the IAPP-Aβ40(42) interaction. Thereby, IAPP uses the same binding sites "hot-segments" IAPP(8-18) and IAPP(22-28) for both self-and hetero-assembly indicating similarities between the involved interaction surfaces[86b, 88].

In agreement with these findings, a "hot-segment"-linking approach has been recently presented to design a series of IAPP cross-amyloid interaction surface mimics (ISMs) as highly potent inhibitors of amyloid self-assembly of Aβ, IAPP or both polypeptides. ISMs have shown to bind with high affinity and inhibit Aβ40(42) and/or IAPP[87] (Scheme 7).
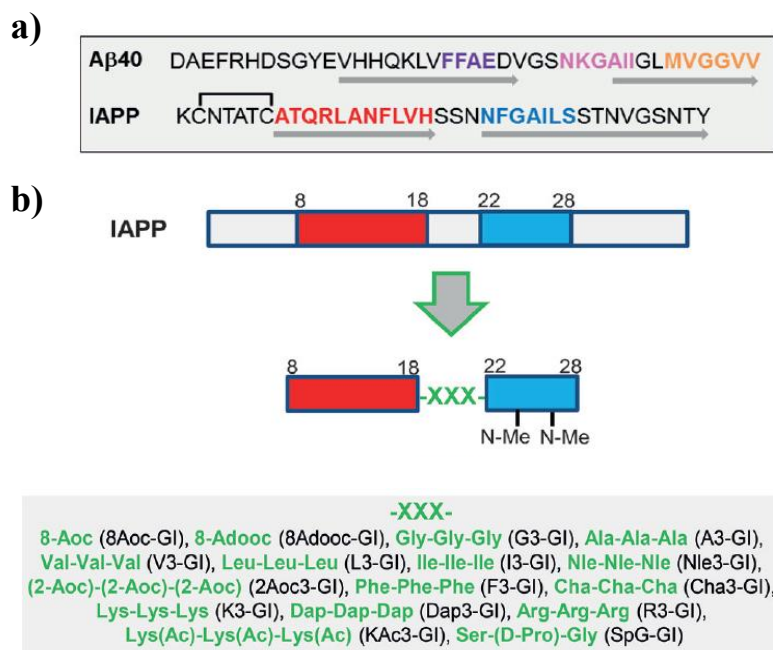
Scheme 7. Design concept, linkers and ISMs. a) Sequences of Aβ40and IAPP; hot segments of the Aβ40/IAPP interaction interface are colored[86b]. Gray arrows: segments involved in amyloid b-sheet formation[27, 129b]. b) Design concept and linkers (green) (abbreviations: 2- or 8- Aoc: 2-or 8-aminooctanoic acid; 8-Adooc: 8-amino-3,6-dioxaoctanoic acid; Cha: cyclohexylalanine; Dap: 2,3 diaminopropionic acid; Lys(Ac): lysine with acetylated Ne-amino group). Short names of ISMs (C-terminal amides) are in parentheses (picture taken from Andreetto et al. ref.[87]).

In the first part of my PhD thesis I presented studies on three novel cyclic analogues of R3-GI, an ISM which has been previously shown to be a potent inhibitor of amyloid self-assembly of Aβ but was unable to inhibit IAPP[87]. These cyclic ISMs (**cISMs**) were generated via a cysteine crosslinking-based peptide "stapling strategy"[111] (Scheme 8).
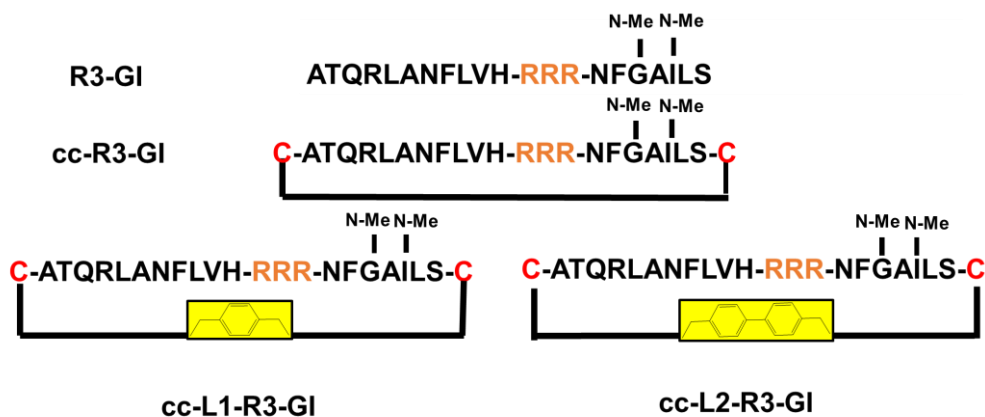
Scheme 8. Design concept of Cys-bridged R3-GI analogues. Design of cyclic ISMs (cISMs) by introducing a Cys-Cys-bridge in R3-GI via cysteine oxidation and cysteine-based "stapling" using p-xylene (for Linker 1) and 4,4´-bis(methyl)biphenyl (for Linker 2), respectively. Cyclization is indicated by "cc", L1 and L2 indicates the two linkers.

First, we examined the conformations of the cISMs by far-UV CD spectroscopy in comparison to R3-GI (Figure 92).
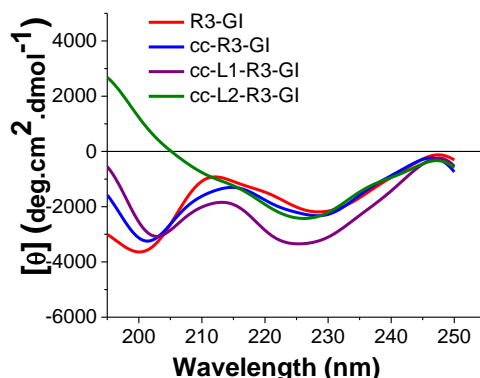
Figure 92. Conformations of cISMs as determined by far-UV CD spectroscopy. CD spectra shown were measured at a peptide concentration of 5μM (aq. buffer (1×b), pH 7.4, containing 1% HFIP).

The two cISMs cc-R3-GI and cc-L1-R3-GI exhibited pronounced β-sheet/β-turn signal and random coil structures similar to R3-GI, whereas cc-L2-R3-GI exhibited only β-sheet/β-turn structure. This suggested that the insertion of a larger, aromatic molecule as bridge between the side chains of the two cysteines may stabilize better the conformation of the peptide. In fact, thiol-reactive reagents (including bis-substituted benzyl, alkyl, maleimide and biphenyl groups) have been used for synthesizing constrained cyclic peptides[141]. Moreover, recently it has been shown that the two β-strands corresponding to the two amyloidogenic IAPP segments, IAPP(12-18) and IAPP(22-28) are connected by a turn established around Ser-20 and so the β-hairpin can serve as a molecular recognition motif enabling control of IAPP aggregation[73]. Our cISMs consisted of theese IAPP segments (or parts) and thereof we envisioned a stabilization of a β-hairpin-like fold through stapling (or cys oxidation). According to Calentano et al. β-hairpin peptides were conformationally stabilized through triazole bridge. This method was successfully applied to stabilize helix, β-turn and it was also used as a disulfide bond mimetic in bioactive peptides[142]. In addition, studies showed that a single disulfide bridge could stabilize an antiparallel β-hairpin and enhance peptide stability and potency[143].

Next, we asked whether cyclization of R3-GI would affect its inhibitory function against Aβ40(42) and IAPP amyloidogenesis. All three cyclic-ISMs were found to be potent Aβ40(42) inhibitors and their IC$_{50}$s were very similar to the IC$_{50}$ of R3-GI (116nM)[87] (Table 51). Most importantly, and in contrast to R3-GI[87], all three cyclic analogues were inhibitors of IAPP as well (Table 51). cc-R3-GI was also able to suppress fibrillar Aβ40-mediated cross-seeding of IAPP fibrillogenesis and cytotoxicity (Figure 93). The effects of cc-L1-R3-GI and cc-L2-R3-GI on Aβ40-mediated cross-seeding of IAPP fibrillogenesis and cytotoxicity have not been tested.
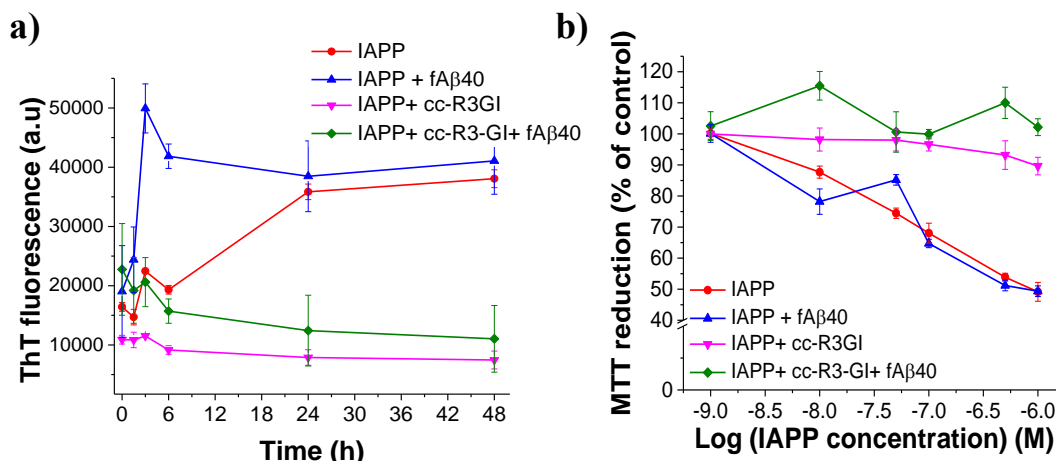
Figure 93. Effects of cc-R3-GI on Aβ40-mediated cross-seeding of IAPP fibrillogenesis and cytotoxicity (a,b). (a) suppression of Aβ40-mediated (fAβ40) (10%) cross-seeding of IAPP (12μM) fibrillogenesis by cc-R3-GI fibrillogenesis (2-fold) as assessed by the ThT binding assay (means (±SD), 3 assays), (b) effects of suppression of Aβ40-mediated (fAβ40) (10%) cross-seeding of IAPP (12μM) cytotoxicity by cc-R3-GI (2-fold) via the MTT reduction assay. Solutions from (a) (24h-aged) added to RINcells; cell damge determined by the MTT reduction assay (means (±SD), 3 assays (n=3 each)).

Next, the interactions between the new cyclic ISMs and Aβ40(42) and IAPP were studied using fluorescence spectroscopy (Table 52). All tested cyclic inhibitors were able to interact and bind to Dac-Aβ40 with mid-nanomolar app. K_ds as found for R3-GI as well (Table 52). However, weak affinities were found for their interaction with Aβ40 (c≥5μM). Moreover, cISMs were able to bind Aβ42 with low nanomolar app. K_ds as found for R3-GI as well (Table 52). Finally, all three new cyclic inhibitors were able to bind IAPP with nanomolar app. K_ds as found for R3-GI as well (app. K_d of cc-R3-GI 20nM, app. K_d of cc-L1-R3-GI 63nM and app. K_d of cc-L2-R3-GI 59nM) (Table 52).

Table 51. IC_{50} values of inhibitory effects of cISMs on cell-damaging of Aβ40 or IAPP.

ISMs	Inhibition Aβ40(42)	IC_{50} (±SD) (nM)[a]	Inhibition IAPP	IC_{50} (±SD) (nM)[a]
R3-GI	+	116 (±11)	-	n.d[b]
cc-R3-GI	+	79.8 (±30.3)	+	126 (±40)
cc-L1-R3-GI	+	151 (±54.6)	+	71 (±23)
cc-L2-R3-GI	+	373 (±46)	+	133 (±61)

[a] IC_{50}s, means (±SD) from 3 titration assays (n=3 each) (Aβ40, 500nM; IAPP, 100nM). [b] n.d non-determined (non-inhibitory ISM). "+" indicates inhibition and "-" indicates no inhibition.

Table 52. App.K_ds values of self-assembly potential and app. K_ds of interactions of peptides with Aβ40(42) and IAPP as determined by fluorescence titration binding assays.

Peptide	app. K_d (±SD) (nM) (self-assembly[a])	app. K_d (±SD) (nM) (with Dac-Aβ40[b])	app. K_d (±SD) (nM) (with Aβ40[a])	app. K_d (±SD) (nM) (with Aβ42[b])	app. K_d (±SD) (nM) (with Fluos-IAPP[b])	app. K_d (±SD) (nM) (with IAPP[a])
R3-GI	77.1 (±7.5)	115 (±21.5)	80	12.8±0.8	5.7±0.4	63
cc-R3-GI	188.3 (±25.6)	247 (±2.6)	NB	130 (±21.8)	20.6 (±7)	NB[c]
cc-L1-R3-GI	354 (±14.4)	129 (±4.6)	NB[c]	6.3 (±1.3)	63.3 (±2)	233 (±8.5)
cc-L2-R3-GI	NB[c]	231.1 (±118.5)	NB[c]	49.6 (±6.1)	59.6 (±6.2)	148 (±8)

[a] App. K_ds, means (±SD) from 3 binding curves. Determined via titrations of fluorescein-labeled peptides (Fluos-peptides, 5nM) with non-labeled peptides, Aβ40 and IAPP; [b] app. K_ds, means (±SD) from 3 binding curves; Dac-Aβ40 (10nM), Fitc-Aβ42 (5nM) and Fluos-IAPP (5nM) were titrated with peptides; [c] NB, no binding at peptide concentrations ≤ 5μM, (aq. buffer 1×b, pH 7.4, containing 1% HFIP).

CD studies were performed to determine the interaction of new cISMs with Aβ40 and IAPP. The CD spectra of the mixtures of cISMs with Aβ40 were very similar to the CD spectrum of the mixture of R3-GI with Aβ40, which indicated not strong differences between the structures of the complexes between Aβ40 and the various peptides (excpect in the case oft he mixture of cc-L2-R3-GI with Aβ40) (Figure 94a). The

interactions between IAPP and cISMs were investigated by CD spectroscopy as well. The CD spectra of the mixtures of cISMs with IAPP were similar to the CD spectrum of the mixture of IAPP with R3-GI which indicated no strong differences between the structures of the hetero complexes between IAPP and the different peptides (Figure 94b).
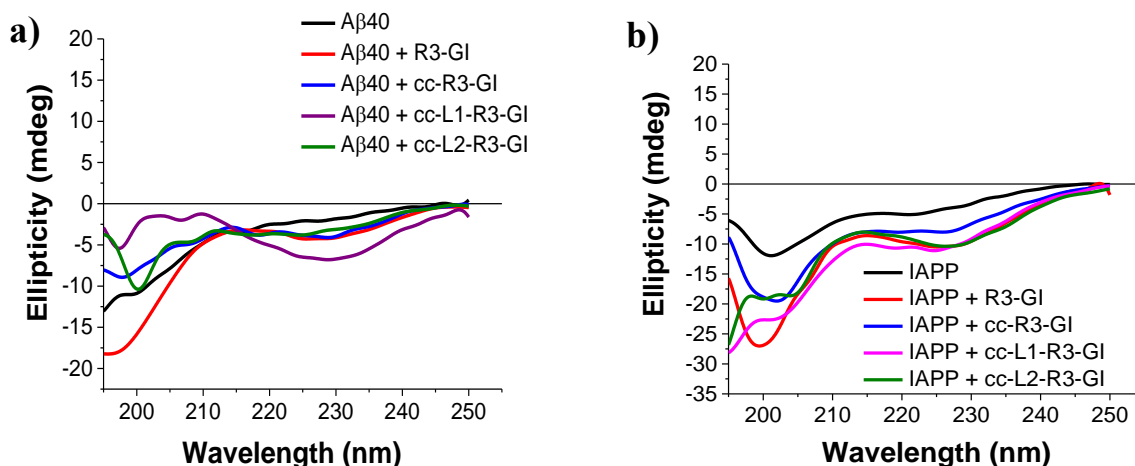
Figure 94. Characterization of interactions of ISMs with Aβ40/IAPP. (a) CD spectra are shown of Aβ40 (5μM) and its mixtures (1/1) with R3-GI, cc-R3-GI, cc-L1-R3-GI and cc-L2-R3-GI peptides. (b) CD spectra of IAPP (5μM) and its mixtures (1/2) with R3-GI, cc-R3-GI, cc-L1-R3-GI and cc-L2-R3-GI peptides (aq. buffer 1×b, pH 7.4, containing 1% HFIP).

Constraining peptide conformation using disulfide bonds or using cysteine crosslinking-based "stapling" have expanded the chances of generating bioactive peptide analogues[111]. However, the inherent vulnerability to enzymatic cleavage and poor stability is one challenge that potentially limits the pharmaceutical use of peptides[143]. The developed cyclic peptides were tested towards their proteolytic degradation properties. Their stabilities were described in Table 22. The linear R3-GI and the cyclic cc-R3-GI exhibited similar stabilities: within 30 min more than 50% of both peptides were degraded[144]. On the contrary, the two stapled peptides appeared to have around 3 to 4 times better stability than the linear R3-GI. However, by MALDI-TOF the HPLC peak of the stapled peptides was found to contain their degradation products. Previously, it has been demonstrated that stapling with rigid hydrophobic groups may enhanc stability to proteolysis[145]. For example the Lin group, used the rigid and hydrophobic cross linker 4,4,'-bisbromomethyl-biphenyl (Bph) to staple cysteines of the Noxa BH3 peptide and thus to enhance its proteolytic resistance and cellular uptake[146]. Other studies have shown that constraining peptides with a single staple was not sufficient to inhibit respiratory virus, whereas insertion of double staples lead to exceptionally robust peptides towards proteolytic degradation[136]. Although, the here synthesized cc-L1-R3-GI and cc-L2-R3-GI did not present high stabilities in human plasma. Finally, the MALDI-TOF results for cc-R3-GI and R3-GI showed that [14]NFLVH-RRR-NF(N-Me)GA(N-Me)ILS-[29]Cys was a stable product throughout the degradation process.

5.2 Cyclic analogues of truncated ISMs (cISMs‑sh) as potent inhibitors of Aβ40 and IAPP amyloid self-assembly

The second aim of my PhD thesis focused on the rational design, synthesis and biophysical and biochemical studies of **cISMs‑sh** as inhibitors of Aβ and/or IAPP. Inhibitors consisted of the IAPP segments, IAPP(14-18) and IAPP(22-28)-GI, which have been suggested to form the core of the β-hairpin of IAPP[73] to mediate key interactions for both IAPP self- and hetero-assembly[88]. These two IAPP segments were connected to each other with different linkers and intramolecular cyclization was performed via cysteines placed at the N-/C- terminus (Scheme 9). The linkers between Cys-IAPP(14-18) and IAPP(22-28)-GI-Cys were segments of 3 natural amino acids which differed in the hydrophobicity and steric hindrance effect of their side chains[87].

In this part of the thesis, I mainly addressed the question whether truncation and conformational restriction via cyclization of already known ISMs might affect their biophysical and biochemical properties and thus their inhibitory effects towards Aβ and/or IAPP amyloid self-assembly[87]. The CD spectra of the three shortened cyclic analogues with the different linkers are shown (Figure 95). cc-R3-GIsh and cc-G3-GIsh showed amounts of both unordered and ordered species; however, cc-R3-GIsh was more disordered. Intrestingly, the indroduction of a hydrophobic linker resulted in stabilization of β-sheet/β-turn structure in cc-L3-GIsh.
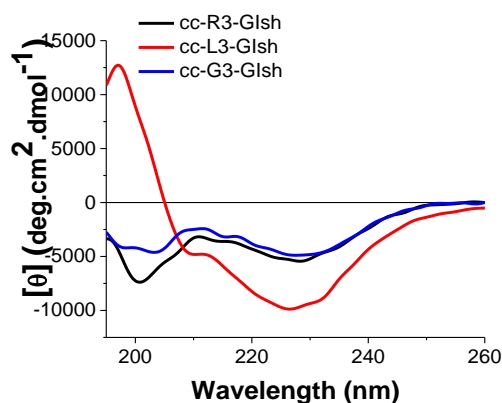
Figure 95. Conformations of cISMs‑sh as determined by far-UV CD spectroscopy. CD spectra shown were measured at a peptide concentration of 5µM, (aq. buffer 1×b, pH 7.4, containing 1% HFIP).

Detailed studies on the **cISMS.sh** were done; the results were compared with the results of the studies with the linear peptide[5] (Scheme 9).
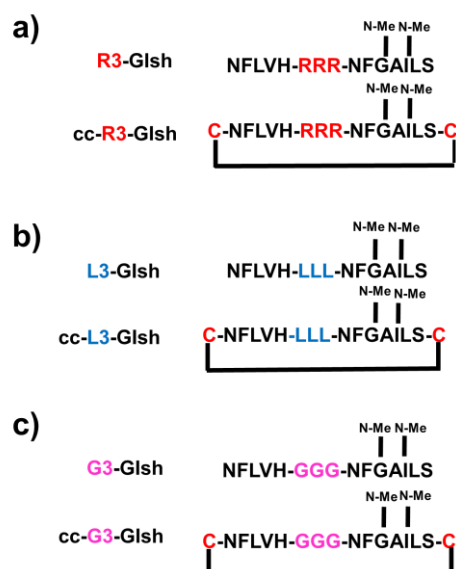
Scheme 9. Sequences of designed truncated linear ISMs (ISMs‑sh) and cyclic ISMs (cISMs‑sh) containing different linkers. Sequences of (a) R3-GIsh and cc-R3-GIsh, (b) L3-GIsh and cc-L3-GIsh and (c) G3-GIsh and cc-G3-GIsh.**"**-GI indicates the presence of the N-methyl-residues at G^{24} & I^{26}: "N-Me"; cyclization is indicated by "cc" and shortened indicated by "sh" (abbreviations are based on the name of the residue in the linker tripeptide Arg, Leu ang Gly; ISMs‑sh, short ISMs; cISMs‑sh, cyclic short ISMs); ISMs‑sh synthesized from Malideli et al. ref.[170].

Firstly, I compared the CD spectra of R3-GIsh and cc-R3-GIsh where both peptides showed similar conformation with amounts of random coil but also β-sheet/β-turn (Figure 96).
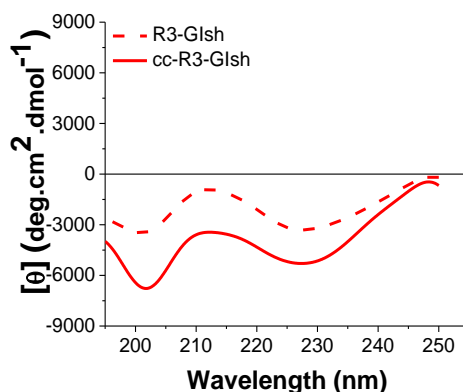
Figure 96. Conformations of R3-GIsh/cc-R3-GIsh as determined by far-UV CD spectroscopy. CD spectra shown were measured at a peptide concentration of 5μM, (aq. buffer 1×b, pH 7.4, containing 1% HFIP). CD spectra of ISMs-sh taken from Malideli et al. ref.[170].

cc-R3-GIsh showed an app. K_d of 670nM of self-assembly which was 3-fold better than the app. K_d of R3-GIsh (app. K_d = 1.9μM) (Table 54). To investigate the interactions between Aβ with R3-GIsh and cc-R3-GIsh, CD spectroscopy was applied. The CD spectra of the mixture of R3-GIsh versus the CD spectra of the mixture of cc-R3-GIsh with Aβ (Figure 43a) were very similar (random coil and β- sheet/β turn) and any conformational change was found (Figure 97).
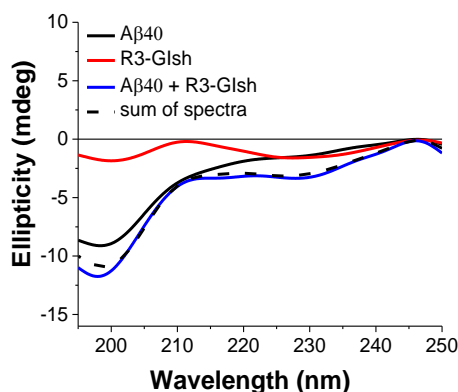
Figure 97. Interactions of Aβ40 and R3-GIsh studied by far-UV CD spectroscopy. CD spectra of freshly dissolved Aβ40 alone, R3-GIsh alone, a mixture (1/1) of Aβ40 with R3-GIsh and the sum of spectra (5μM, pH 7.4). Measurements were performed in aq. buffer 1×b, pH 7.4, containing 1% HFIP.

However, binding studies of Dac-Aβ40 with cc-R3-GIsh showed 10-fold higher binding affinity (app. K_d = 382nM) than in the case of R3-GIsh (app. K_d = 3μM). Both peptides showed similar binding affinities Aβ40 (app. K_d of R3-GIsh 382nM, app. K_d of cc-R3-GIsh 168nM) (Table 54). Figure 98 shows the effects of linear versus cc-R3-GIsh on Aβ40 amyloid formation: cc-R3-GIsh was found to inhibit Aβ40 at 1/1 up to 7days, while the linear counterpart was unable to inhibit it.

a)

b)
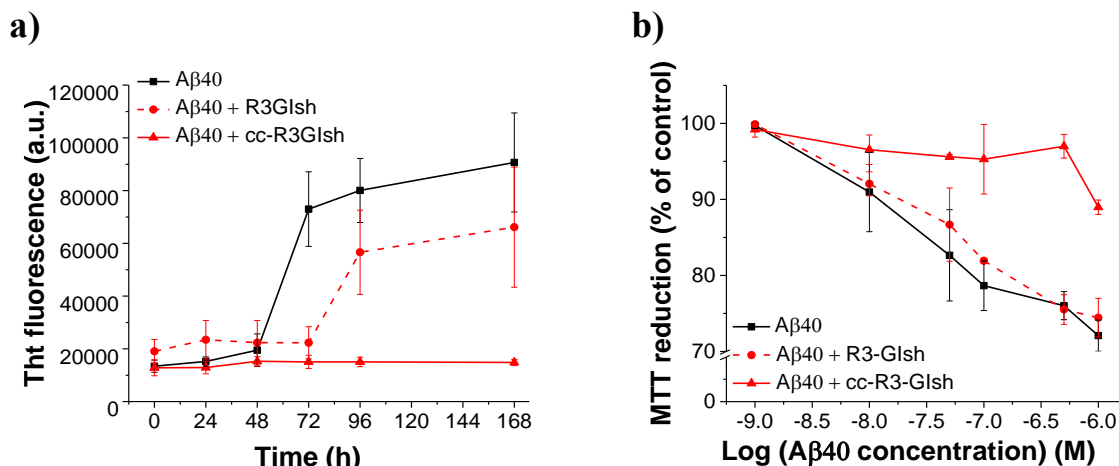
Figure 98. Effects of R3-GIsh versus cc-R3-GIsh on Aβ40 amyloid formation. (a) Fibrillogenesis of Aβ40 (16.5μM) or its mixtures (Aβ40/peptide, 1/1) by the ThT binding assay (means (±SD), 3 assays)**, (b)** effects on cell viability: solutions from (a) (3 day-aged) added to PC-12 cells; cell damage determined by the MTT reduction assay (means (±SD), 3 assays (n=3 each)).

Next, I examined the effects of cyclization of R3-GIsh on IAPP amyloid formation. IAPP (6μM) was incubated either alone or in a mixture with R3-GIsh at a molar ratio of 1/10 and with cc-R3-GIsh at a molar ratio of 1/2. ThT fluorescence was measured at indicated time points and up to 7 days (Figure 99). It was found that R3-GIsh even at 10 times molar excess could not inhibit IAPP fibrillogenesis and cytotoxicity.
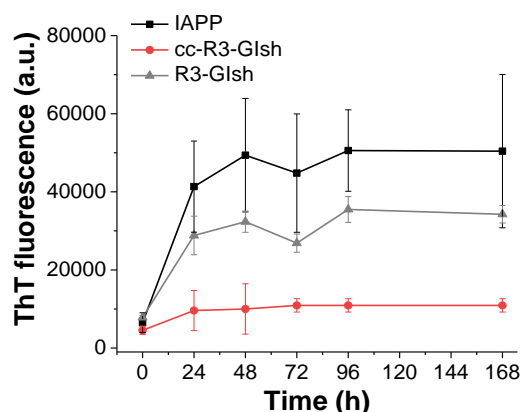
Figure 99. Effects of R3-GIsh versus cc-R3-GIsh on IAPP amyloid formation. Fibrillogenesis of IAPP (6μM) alone and its mixtures (IAPP/peptide, 1/2 (cc-R3-GIsh), 1/10 (R3-GIsh)) as determined via the ThT binding assay (means (±SD), 3 assays)**.**

Apparently, cyclization and conformational restriction played a crucial role on the inhibitory potential of cc-R3-GIsh towards IAPP fibrillogenesis. IC_{50} studies showed that cc-R3-GIsh is a potent inhibitor of IAPP fibril formation with an IC_{50} of 47.6nM. Next, the interaction of R3-GIsh and cc-R3-GIsh with IAPP were investigated via CD spectroscopy and fluorescence spectroscopy. CD was performed with IAPP/inhibitors at the ratio of 1/2 which was found to be required for inhibitory effects. It was found that both analogues interacted with IAPP, but any conformational change was observed (Figure 49a & Figure 100).
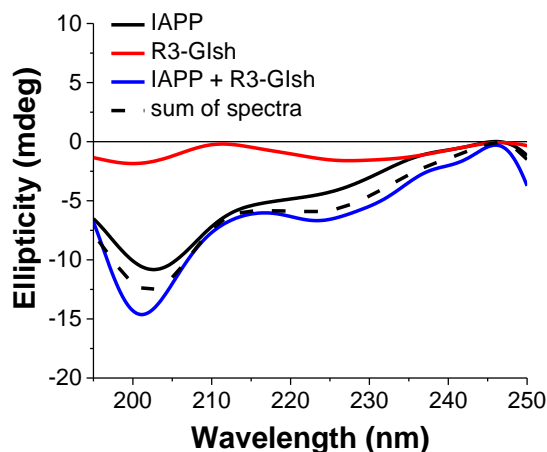
Figure 100. Interactions of IAPP with cISMs-sh as studied by far-UV CD spectroscopy. CD spectra of freshly dissolved IAPP alone (5μM), R3-GIsh alone (10μM), a mixture (1/2) of IAPP with R3-GIsh and the sum of spectra. Measurements were performed in aq. buffer 1×b, pH 7.4, containing 1% HFIP.

Next, I studied the interactions of the peptides with IAPP using fluorescene spectrosctropy (Table 54). The results showed a stronger binding affinity of cc-R3-GIsh (app. K_d = 13nM) than for R3-GIsh (app. K_d = 1.2μM). On the other hand, both peptides appeared to have similar binding affinities towards monomeric/oligomeric IAPP (app. K_d = 10nM, app. K_d = 22.6nM, respectively). From above results it was concluded that cyclizing the R3-GIsh altered its properties. cc-R3-GIsh binds with high affinity both Aβ and IAPP and suppresses effectively the amyloid self-assembly of both polypeptides.

Then, I examined whether truncation and cyclization of L3-GI might affect its biophysical and biochemical properties and thus its inhibitory effects on Aβ and/or IAPP amyloid self-assembly. It has been previously shown that L3-GI could complete inhibit Aβ40 and IAPP fibrillogenesis and cytotoxicity in 1/1 and 1/2 ratio[87]. Here, I first examined whether cyclization of L3-GIsh affected its conformation by CD spectroscopy (Figure 101). The CD spectra of the two peptides exhibited a pronounced minimm at ~227nm and a maximum at ~197nm consistent with large amounts of β-sheet/β-turn structures, as previously found for L3-GI as well[87].
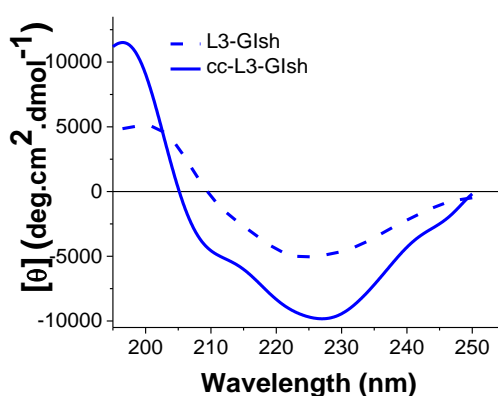
Figure 101. Conformations of L3-GIsh/cc-L3-GIsh as determined by far-UV CD spectroscopy. CD spectra shown were measured at a peptide concentration of 5μM (aq. buffer 1×b, pH 7.4, containing 1% HFIP). CD spectra of ISMs-sh taken from Malideli et al. ref.[170].

Since L3-GI could suppress Aβ40 fibrillogenesis and cytotoxicity both short analogues (L3-GIsh and cc-L3-GIsh) were examined in parallel regarding their effects on Aβ40 fibrillogenesis and cytotoxicity. As shown (Figure 102) neither L3-GIsh nor cc-L3-GIsh could intervene with Aβ40 self-assembly into fibrils and cytotoxic aggregates at the 1/1 molar ratio.

a)

b)
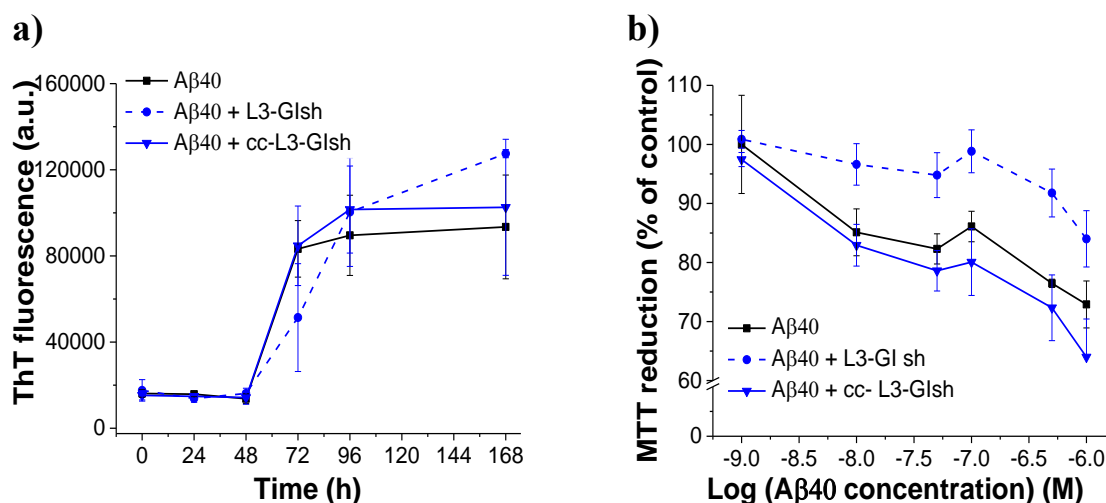
Figure 102. Effects of L3-GIsh versus cc-L3-GIsh on Aβ40 amyloid formation and cytotoxicity. (a) Fibrillogenesis of Aβ40 (16.5μM) or its mixtures (Aβ40/peptide, 1/1) by the ThT binding assay (means (±SD), 3 assays), (b) effects on cell viability: solutions from (a) (3 day-aged) were added to PC-12 cells; cell damage was determined by the MTT reduction assay (means (±SD), 3 assays (n=3 each)).

Indeed, IC_{50}s of the inhibition effects on Aβ40 cytotoxicity were estimated and found to be 5-fold weaker for L3-GIsh (IC_{50} = 458nM) and 10-fold weaker for cc-L3-GIsh (IC_{50} = 1.7μM) than for L3-GI (81nM). It seemed that truncation and cyclization of L3-GI were unfavorable regarding its inhibitory potential towards Aβ40 amyloid self-assembly. The interactions of the two peptides with Aβ40 were investigated by CD and fluorescence spectroscopy. In the case of cc-L3-GIsh when mixed at 1/1 with Aβ40, then differences between the CD spectrum of mixtures and the sums were observed (Figure 43b), which indicated an interaction between the two peptides. However, as shown in Figure 103 the CD spectra of the mixture of Aβ40 with L3-GI did not differ from the CD spectra of the sum, which showed no conformational change upon interaction between the two peptides. Next, the apparent K_ds of interactions of Aβ40 with L3-GIsh were determined and compared with the apparent K_ds of interactions of cc-L3-GIsh with Aβ0. The results form fluorescence binding assays showed weak binding affinities either with Dac-Aβ40 or with Aβ40 for both peptides (Table 54).
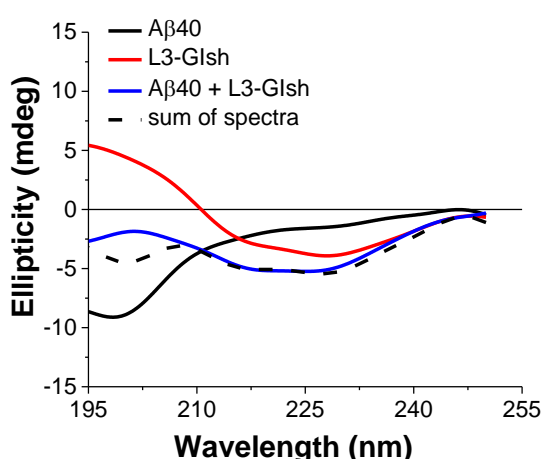
Figure 103. Interactions of Aβ40 and L3-GIsh studied by far-UV CD spectroscopy. CD spectra of freshly dissolved Aβ40 alone, L3-GIsh alone, a mixture (1/1) of Aβ40 with L3-GIsh and the sum of spectra (5μM, pH 7.4). Measurements were performed in aq. buffer 1×b, pH 7.4, containing 1% HFIP.

Next, I studied the effects of truncation and cyclization of L3-GI towards IAPP amyloid formation. IC_{50}s were estimated for L3-GIsh and cc-L3-GIsh and were found to be very similar (IC_{50} for L3-GIsh was 201nM

and IC_{50} for cc-L3-GIsh was 314nM); however their inhibition activities found to be 4-fold weaker than the inhibition properties of L3-GI (IC_{50} =55nM)[87] (Table 53).

a)

b)
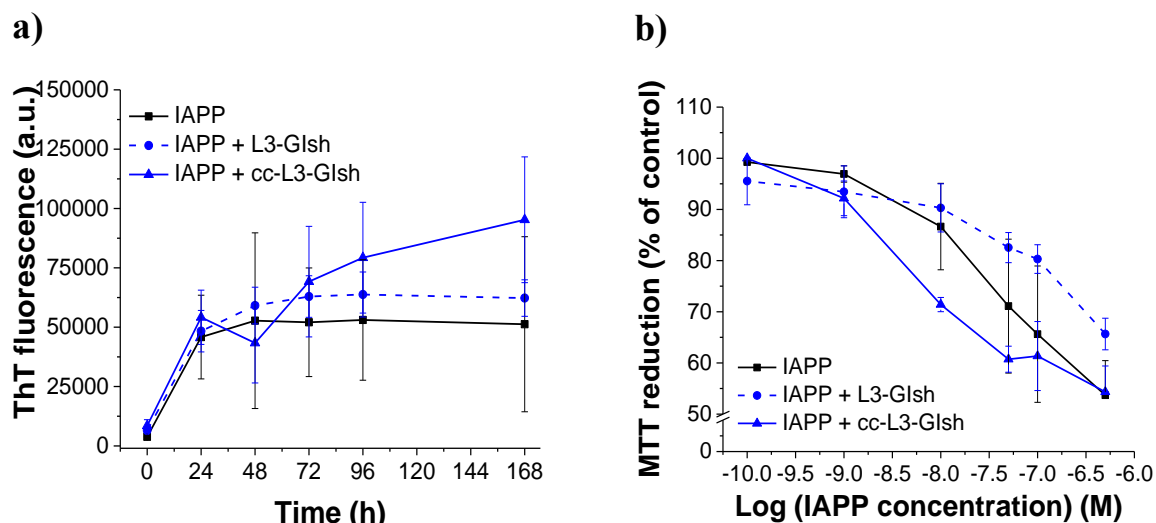
Figure 104. Effects of L3-GIsh versus cc-L3-GIsh on IAPP amyloid formation and cytotoxicity. (a) Fibrillogenesis of IAPP (16.5µM) alone and its mixtures (IAPP/peptide, 1/2 (L3-GIsh), 1/2 (cc-L3-GIsh)) as determined via the ThT binding assay (means (±SD), 3 assays), (b) effects on cell viability: solutions from (a) (24h-aged) were added to RIN5fm cells; cell damage was determined by the MTT reduction assay (means (±SD), 3 assays (n=3 each)).

Next, the interactions of L3-GIsh and cc-L3-GIsh with IAPP were studied via CD spectroscopy and fluorescence spectroscopy. CD was performed with IAPP/inhibitors at the ratio of 1/3 which was found to be required for inhibitory effects in the casse of cc-L3-GIsh. The CD spectra of the mixture of IAPP with L3-GIsh showed only one minimum at 225nm as observed for L3-GIsh as well. On the contrary, the CD spectra of the mixture of cc-L3-GIsh with IAPP revealed two minimum, a small one at 195nm (r.c) and one more intense at 225nm (β-sheet/β-turn) (Figure 105).
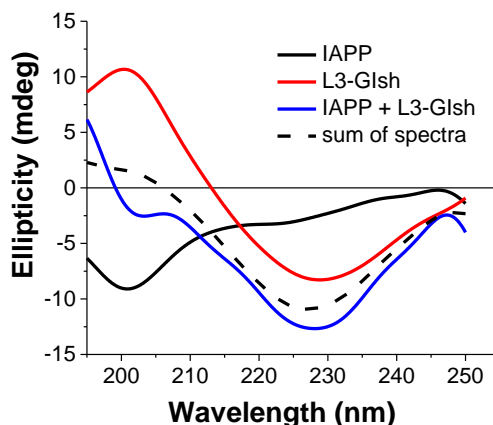
Figure 105. Interactions of IAPP with cISMs-sh as studied by far-UV CD spectroscopy. CD spectra of freshly dissolved IAPP alone (5µM), L3-GIsh alone (15µM), a mixture (1/3) of IAPP with L3-GIsh and the sum of spectra. Measurements were performed in aq. buffer 1×b, pH 7.4, containing 1% HFIP.

In addition, fluorescence studies were performed. The results showed similar app. K_ds of interactions of L3-GIsh and cc-L3-GIsh with Fluos-IAPP. However, their apparent affinities were weaker than the app. Kd of L3-GI with Fluos-IAPP (app. K_d = 43nM) (Table 54). These findings suggested that truncation and cyclization of L3-GI altered dramatically its inhibition properties toward both Aβ and IAPP amyloid self-assembly.

As next, I tested the effects of shortening and cyclization of a non-inhibitor (G3-GI) on Aβ and IAPP fibrillogenesis[87]. To investigate whether the truncated and cyclized G3-GI analogue G3-GIsh influenced G3-GIsh conformation, CD spectroscopy was applied. The CD spectra of both peptides shared both amounts of random coil and β-turn (Figure 106).
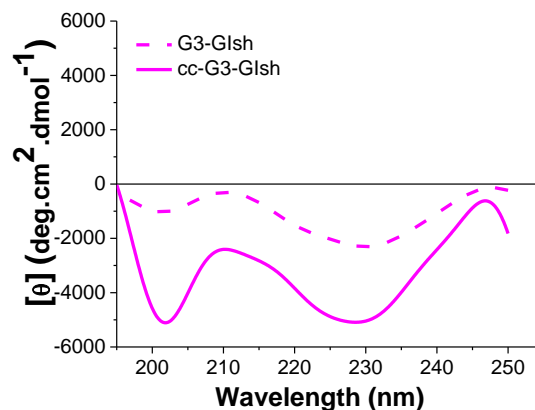
Figure 106. Conformations of L3-GIsh/cc-L3-GIsh as determined by far-UV CD spectroscopy. CD spectra shown were measured at a peptide concentration of 5μM (aq. buffer 1×b, pH 7.4, containing 1% HFIP). CD spectra of ISMs-sh taken from Malideli et al. ref.[170].

To determine whether truncation and cyclization of G3-GI effected its inhibitory effects on Aβ40, both peptides (G3-GIsh, cc-G3-GIsh) were tested regarding their ability to inhibit Aβ40 self-assembly via the ThT binding assay and the MTTT reduction assay (Figure 107), (Table 53).
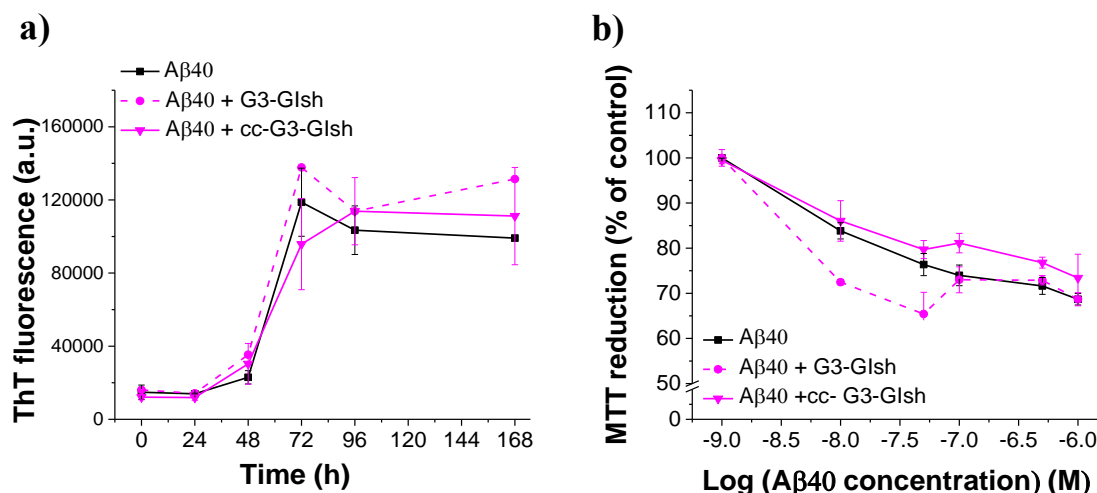
Figure 107. Effects of L3-GIsh versus cc-L3-GIsh on Aβ40 amyloid formation. (a) Fibrillogenesis of Aβ40 (16.5μM) and its mixtures (Aβ40/peptide, 1/1) as determined via the ThT binding assay (means (±SD), 3 assays), (b) effects on cell viability: solutions from (a) (3 day-aged) were added to PC-12 cells; cell damage was determined via the MTT reduction assay (means (±SD), 3 assays (n=3 each)).

Neither G3-GIsh nor cc-G3-GIsh could inhibit Aβ40 and no interaction was found either via CD spectroscopy (data not shown) nor by fluorescence titration assays (Table 54).
Furthermore, both G3-GIsh and cc-G3-GIsh were tested with regard their ability to inhibit IAPP self-assembly and were not able to inhibit IAPP amyloidogenesis even up to 5-fold excess (Figure 108).
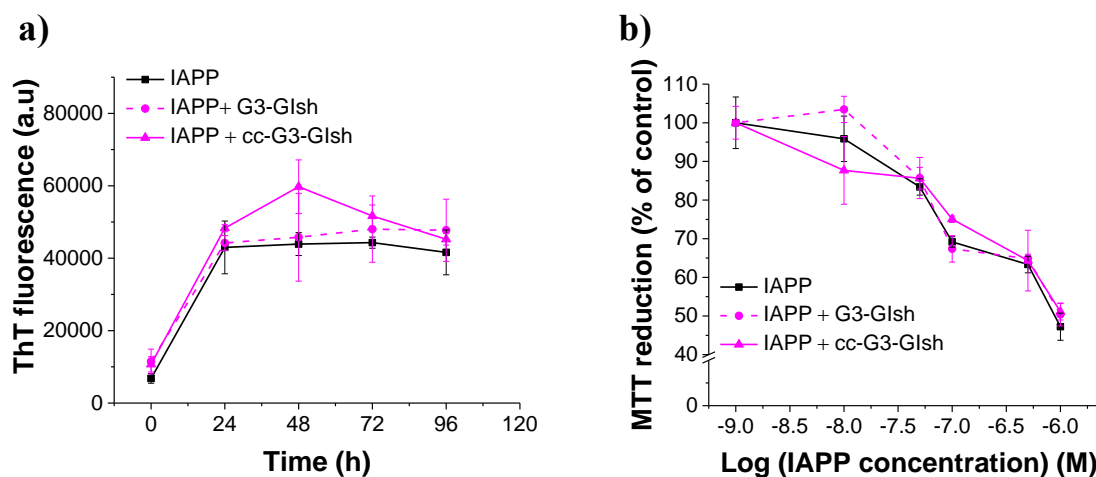
Figure 108. Effects of G3-GIsh versus cc-G3-GIsh on IAPP amyloid formation and cytotoxicity.(a) Fibrillogenesis of IAPP (6μM) alone and its mixtures (IAPP/peptide, 1/5 (G3-GIsh), 1/5 (cc-G3-GIsh)) as determined via the ThT binding assay (means (±SD), 3 assays), (b) effects on cell viability: solutions from (a) (24h-aged) were added to RIN5fm cells; cell damage was determined via the MTT reduction assay (means (±SD), 3 assays (n=3 each)).

The results revealed 1st) the importance of the linker RRR conencting the two segments IAPP(14-18) and IAPP(22-28) and 2nd) the positive effects of the S-S bridge on the ability of the peptide to inhibit Aβ40(42) and/or IAPP amyloid formation. cc-R3-GIsh could thus become a lead compound in devising potent inhibitors of amyloid self-assembly. The following tables summarize all properties of the shortened linear and cyclic peptides.

Table 53. Comparison of the inhibitory potentials of truncated linear/cyclic analogues towards Aβ40 and IAPP fibril formation and the cytotoxicity.

Peptide	Inhibition Aβ40 (1/1)[c]	IC$_{50}$ (±SD) (nM)[a]	Inhibition IAPP (1/2)[c]	IC$_{50}$ (±SD) (nM)[b]
R3-GIsh[*]	-	216 (±27)	-	n.d
cc-R3-GIsh	+	125 (±73.4)	+	47.6 (±15.5)
L3-GIsh[*]	-	458 (±142)	-	201 (±7)
cc-L3-GIsh	-	1756.66 (±721.75)	-	314 (±33.4)
G3-GIsh	-	n.d	-	n.d
cc-G3-GIsh	-	n.d	-	n.d

[a], [b] IC$_{50}$s means (±SD) from 3 titration assays (n=3 each) (Aβ40, 500nM; IAPP, 100nM); n.d, non-determined (non-inhibitory ISMs); [c] (values in paranthesis show applied Aβ40, IAPP/peptide ratio) "+" indicates inhibition and "-" indicates no inhibition; [*] IC$_{50}$s taken from Malideli et.al ref.[170].

Table 54. App.K$_d$s values of self-assembly and of interactions of peptides with Aβ40 and IAPP as determined by fluorescence binding assays.

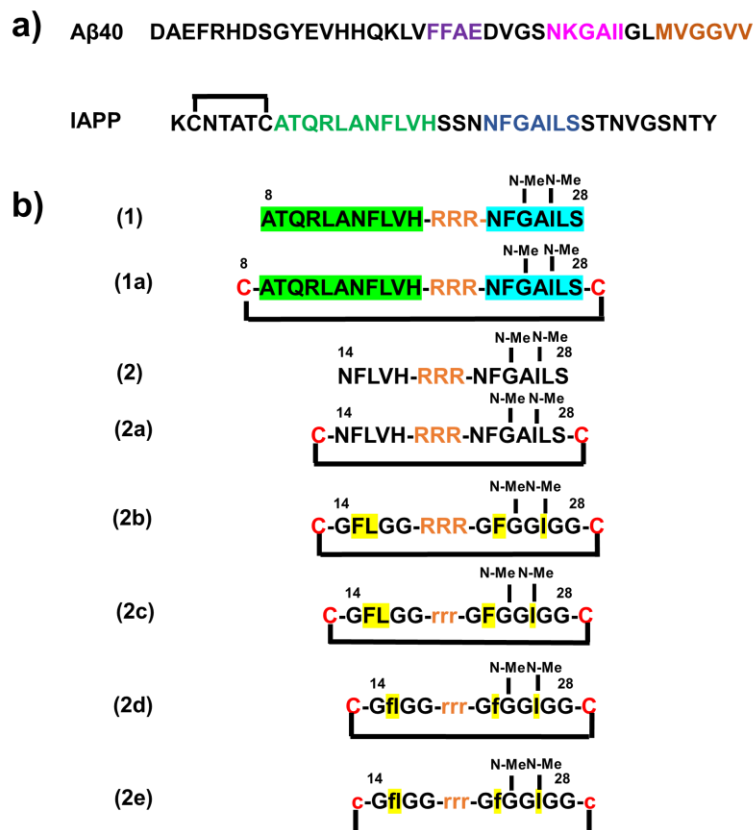| Peptide	app. K$_d$ (±SD) (nM) (self-assembly[a])	app. K$_d$ (±SD) (nM) (with Dac-Aβ40[b])	app. K$_d$ (±SD) (nM) (with Aβ40[a])	app. K$_d$ (±SD) (nM) (with Fluos-IAPP[b])	app. K$_d$ (±SD) (nM) (with IAPP[a])
R3-GIsh[*]	1900 (±217)	3133 (±404)	191	1233 (±263)	10
cc-R3-GIsh	670.33 (±57.7)	382.33 (±89.24)	171.6 (±26.10)	13.2 (±1.1)	22.6 (±1.5)
L3-GIsh[*]	1900	3000	n.d	469 (±40)	n.d
cc-L3-GIsh	808.66 (±168.82)	509.0 (±21.1.28)	1110 (±10.56)	817.66 (±115.24)	304 (±26)
G3-GIsh	NB[d]	NB[d*]	NB[d]	NB[d]	NB[d]
cc-G3-GIsh	150.33 (±592.14)	NB[d*]	NB[d]	NB5[d]	NB[d]

[a] App. K$_d$s, means (±SD) from 3 binding curves. Determined via titrations of fluorescein-labeled peptides (5nM) with non-labeled peptides, Aβ40, IAPP; [b] app. K$_d$s, means (±SD) from 3 binding curves Dac-Aβ40 (10nM) and Fluos-IAPP (5nM) were titrated with peptides; [d] NB, no binding at peptide concentrations ≤ 5μM; [d*] NB no binding at c≤10μM; n.d, not determined, (aq. buffer 1×b, pH 7.4, containing 1% HFIP); [*] Binding data taken from Malideli et al. ref.[170], where no ±SD is shown, then results were from 1 binding curve.

5.3 Role of hot spots and the linker of cISMs-sh for its inhibitory effects on Aβ40(42) and IAPP amyloid self-assembly

Recent findings have suggested that IAPP residues Phe15, Leu16, Phe 23 and Ile26 are key residues of IAPP-IAPP and IAPP-Aβ40(42) interactions[88]. Aiming at minimizing IAPP-derived elements, we next asked whether these 4 residues would be sufficient for the inhibitory activity of the above analogues. A series of cyclic analogues with different linker tripeptides (RRR, LLL, GGG and Aoc-Peg) were synthesized with 7 out of the 11 non-Gly residues of cISMS-sh substituted with Gly (except for the Cys) and abbreviated as **cALLG-sh** (Scheme 10).
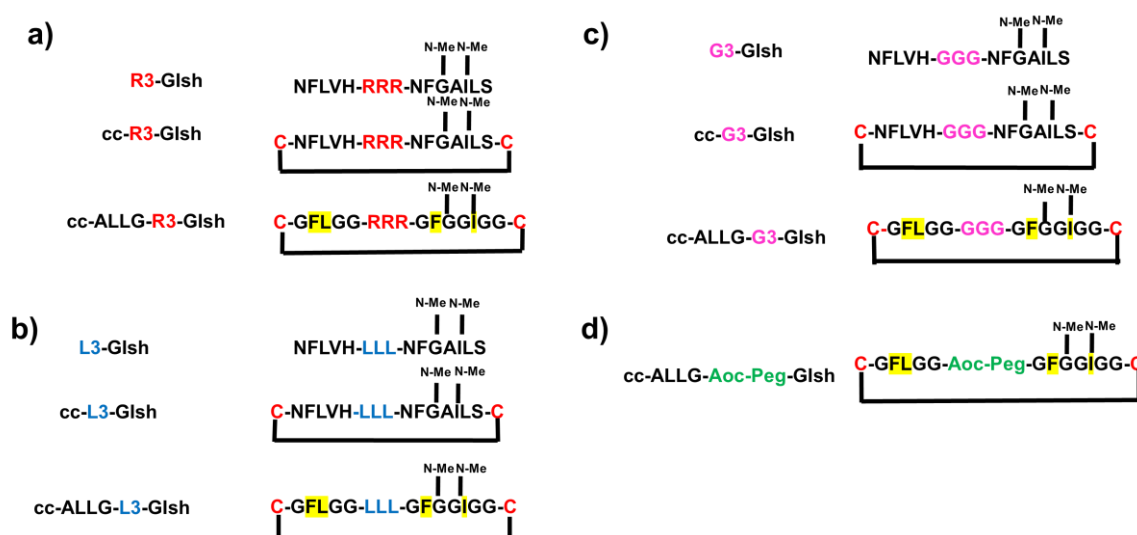
Scheme 10. Design of cyclic glycine containing analogues cALLG-sh. (a) R3-GIsh, ccR3-GIsh and cc-ALLG-R3-GIsh, (b) L3-GIsh, cc-L3-GIsh and cc-ALLG-L3-GIsh, (c) G3-GIsh, cc-G3-GIsh and cc-ALLG-G3-GIsh, (d) cc-ALLG-Aoc-Peg-GIsh. Peptides are abbreviated based on the name of the residue on the linker. "-GI indicates the presence of the N-methyl-residues at G²⁴ & I²⁶: "N-Me"; cyclization is indicated by "cc" and shortened indicated by "sh"; the 4 IAPP hot spots are highlighted with yellow[88]. (Abbrev: ISMs-sh, short ISMs; cISMs-sh, cyclic short ISMs; cALLG-sh, cyclic ISMs substituted with Gly (except for Cys); of note R3-GIsh, L3-GIsh and G3-GIsh were synthesized and studied by Malideli et al. ref.[170].

To determine the effects of Gly substitution on peptide secondary structure, I compared the CD spectra of the **cALLG-sh** with the CD spectra of their linear and cyclic precursors (Figure 109).

a)

b)

c)
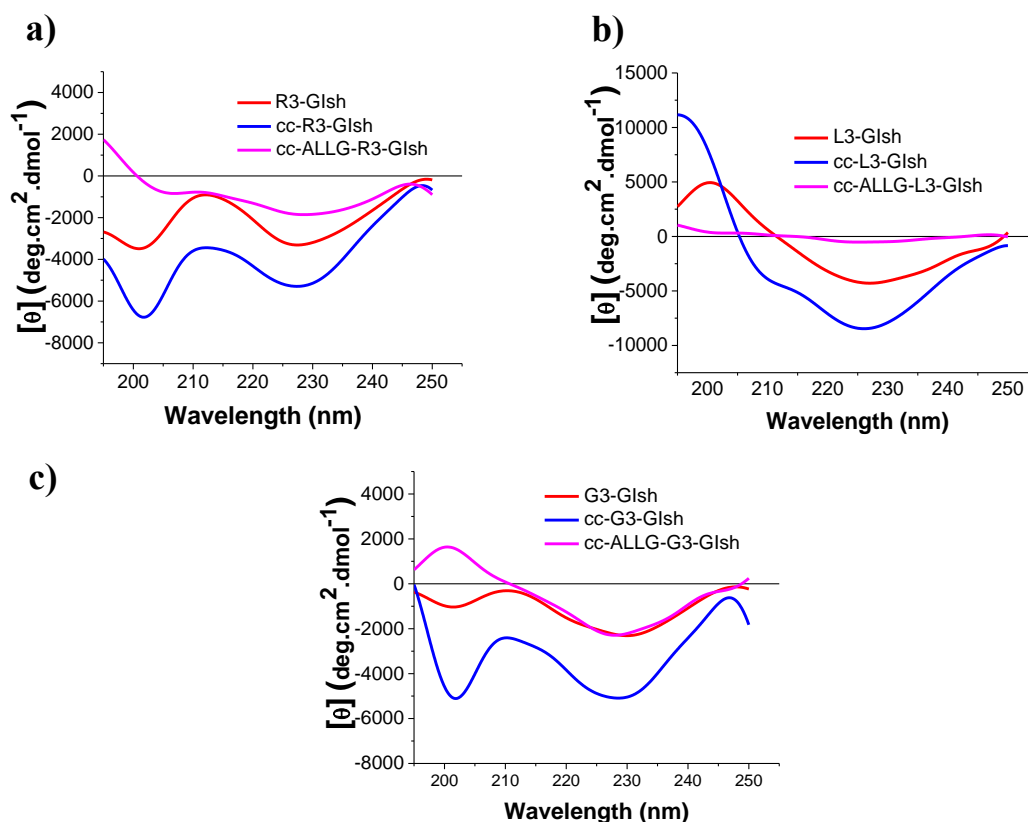
Figure 109. Conformations of peptides as determined by far-UV spectroscopy. CD spectra of (a) R3-GIsh, cc-R3-GIsh, cc-ALLG-R3-GIsh, (b) L3-GIsh, cc-L3-GIsh, cc-ALLG-L3-GIsh, (c) G3-GIsh, cc-G3-GIsh, cc-ALLG-G3-GIsh. Measurements were performed at a peptide concentration of 10μM in aq. buffer (1×b), pH 7.4, containing 1% HFIP.

The CD spectra of cc-ALLG-R3-GIsh, cc-ALLG-L3-GIsh and cc-ALLG-G3-GIsh exhibited one major minimum at 230nm, which is indicative of stabilized turn structures. As known, Gly is a very unique amino acid, in that it contains a hydrogen as side chain. This means that there is much more conformational flexibility in Gly which is often found in β-sheets/turns[147]. To investigate conformational effects of the linker, we compared the CD spectra of the four peptides at 5μM (Figure 109).
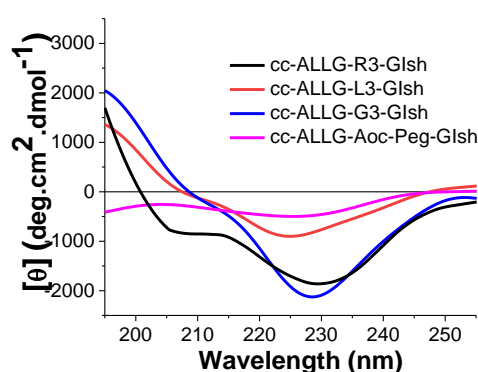
Figure 110. Comparison of CD spectra of cALLG-sh analogues. CD spectra of cc-ALLG-R3-GIsh, ccALLG-L3-GIsh, cc-ALLG-G3-GIsh and cc-ALLG-Aoc-Peg-GIsh. Measurements were performed at a peptide concentration of 5μM in aq. buffer (1×b), pH 7.4, containing 1% HFIP.

It seems that in the case of cc-ALLG-L3-GIsh and cc-ALLG-Aoc-Peg-GIsh the hydrophobic residues in the linker resulted in higher aggregation propensities, which was indicated by the reduced CD signal of β-sheet/β-turn. However, the CD spectra of cc-ALLG-R3-GIsh and cc-ALLG-G3-GIsh showed the most intense CD signal of β-sheet/β-turn, which might be due to the abundance of Gly (in the case of cc-ALLG-

G3-GIsh) or due to the positive charge of the three Arg (in the case of cc-ALLG-R3-GIsh) (Figure 110). Regarding their self-assembly properties, cc-ALLG-R3-GIsh showed 64-fold stronger self-assembly propensity than cc-R3-GIsh and 215-fold stronger self-assembly propensity than R3-GIsh. By contrast, the app. K_ds of self-assembly of cc-ALLG-L3-GIsh and cc-ALLG-G3-GIsh were very similar to the app. K_ds of self-assembly of the cc-L3-GIsh and cc-G3-GIsh (Table 56). Finally, in the case of cc-ALLG-Aoc-Peg-GIsh the app. K_d of self-assembly could not be estimated up to a concentration of 10μM (Table 56).

Next, in the chapter 4.3.3 the effects of substitution of several amino acids with Gly on inhibitory effects of cALLG-sh on Aβ40 fibrillogenesis and cytotoxicity were presented. cc-ALLG-R3-GIsh was the only cALLG-sh analogue that could inhibit Aβ40(42). An IC_{50} value of 654nM was determined, which was 5-fold weaker than the IC_{50} of cc-R3-GIsh (Table 55). Importantly, the IC_{50} value of cc-ALLG-R3-GIsh was determined against IAPP cytotoxicity and found 425nM, which was 10-fold weaker than the IC_{50} of cc-R3-GIsh. Furthermore, it was found that the reduced analogue of cc-ALLG-R3-GIsh; with cysteines in reduced form (abbreviated as cc-ALLG-R3-GIshred) was not able to inhibit IAPP fibrillogenesis (Figure 111), which indicated the importance of cyclization.
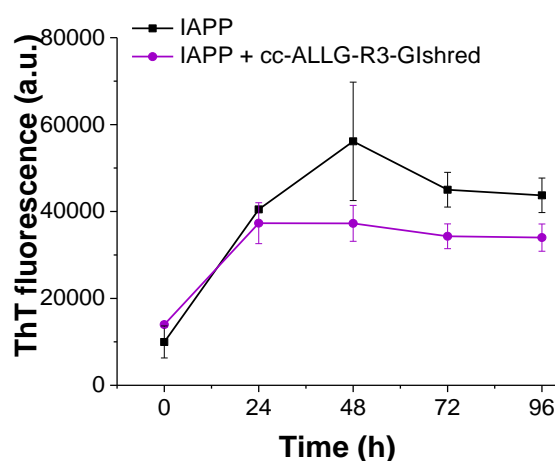
Figure 111. Effects of cc-ALLG-R3-GIshred on IAPP amyloid formation. (a) Fibrillogenesis of IAPP (6μM) alone and with cc-ALLG-R3-GIshred (10-fold excess) as determined via the ThT binding assay (means (±SD), 3 assays).

Finally, as shown in chapter 4.3.6 cc-ALLG-R3-GIsh could potently block IAPP nucleation stages, whereas, cc-ALLG-R3-GIsh could not suppress fibrillar Aβ40 mediated IAPP fibrillization.

Table 55. Comparison of the effects of truncated linear and cyclic peptides on fibril formation and cytotoxicity of Aβ40 and or IAPP.

Peptide	Inhibition of Aβ40 (1/1)[c]	IC_{50} (±SD) (nM)[a]	Inhibition of IAPP (1/2)[c]	IC_{50} (±SD) (nM)[b]
R3-GIsh[*]	+	216.0 (±27)	-	n.d
cc-R3-GIsh	+	125.1 (±73.4)	+	47.6 (±15.7)
cc-ALLG-R3-GIsh	-	654.3 (±227.8)	-	425.7 (±77.7)
L3-GIsh[*]	-	458.0 (±142)	-	201.0 (±7)
cc-L3-GIsh	-	1756.6 (±721.7)	-	314.0 (±33.4)
cc-ALLG-L3-GIsh	-	n.d	-	n.d
G3-GIsh	-	n.d	-	n.d
cc-G3-GIsh	-	n.d	-	n.d
cc-ALLG-G3-GIsh	-	n.d	-	n.d

[a], [b] IC_{50}s means (+SD) from 3 titration assays (n=3 each) (Aβ40, 500nM; IAPP, 100nM), n.d., non-determined (non-inhibitory ISMs); [c] (values in parenthesis show applied Aβ40, IAPP/peptide ratio) "+" indicates inhibition and "-" indicates no inhibition; [*] IC50 values taken from Malideli et.al ref.[170].

Thereafter, I determined the binding affinities of the cALLG-sh analogues with Aβ and/or IAPP and I compared them with the affinities of the linear or cyclic truncated peptides. The affinity of the interaction of

cc-ALLG-R3-GIsh with Dac-Aβ40 was 62-fold stronger than the affinity of the R3-GI with Dac-Aβ40 and 2-fold stronger than the affinity of cc-R3-GIsh with Dac-Aβ40 (Table 56). The affinity of the intearaction of Fluos-cc-ALLG-R3-GIsh with Aβ40 was similar to the affinities of interaction of Fluos-cc-R3-GIsh and Fluos-R3-GIsh with Aβ40 (Table 56). Moreover, the affinity of the interaction of cc-ALLG-R3-GIsh with Fluos-IAPP was 17-fold stronger than the affinity of the cc-R3-GIsh with IAPP and 2-folder stronger than the affinity of R3-GIsh with IAPP (Table 56). The affinity of the interaction of Fluos-cc-ALLG-R3-GIsh and IAPP was similar to the affinity of the interaction of Fluos-cc-R3-GIsh and Fluos-R3-GIsh with IAPP (Table56). In the case of cc-ALLG-L3-GIsh the affinity of the interation with Dac-Aβ40 was 224-fold stronger than the affinity of the interaction of L3-GIsh with Dac-Aβ40, whereas the affinity of the interaction of cc-ALLG-L3-GIsh with Fluos-IAPP was 3-fold weaker than the affinity of the interaction of L3-GIsh and 2-fold weaker of cc-L3-GIsh with Fluos-IAPP (Table 56). In the case of G3-GIsh and its cyclic peptides the affinities of the interactions either with Aβ40 or IAPP were very weak (app. $K_d \geq 5\mu M$). Similarly, in the case of cc-ALLG-Aoc-Peg-GIsh the affinities of interactions with Aβ40 or IAPP were very weak as well (app. $K_d \geq 5\mu M$) (Table 56).

Table 56. App.K_ds values of self-assembly potential and of interactions of peptides with Aβ40 and IAPP as determined by fluorescence binding assays.

Peptide	app. K_d (±SD) (nM) (self-assembly[a])	app. K_d (±SD) (nM) (with Dac-Aβ40[b])	app. K_d (±SD) (nM) (with Aβ40[a])	app. K_d (±SD) (nM)(with Fluos-IAPP[b])	app. K_d (±SD) (nM) (with IAPP[a])
R3-GIsh[*]	1900 (±217)	3133 (±404)	191	1233(±263)	10
cc-R3-Gish	670.3 (±57.7)	382.3 (±89.2)	172 (± 25)	13.2 (±11)	22.6 (±1.5)
cc-ALLG-R3-GIsh	43.3 (±3.5)	187.6 (±21.5)	130 (±36)	216.5 (±13.4)	10.7 (±1.2)
L3-GIsh[*]	1900 (±130)	3100 (±240)	n.d	469 (±40)	n.d
cc-L3-Gish	808 (±168)	509 (±12)	1110	817 (±115.24)	304 (±26)
cc-ALLG-L3-GIsh	608 (±68)	673(±61)	NB[c]	1600 (±0.2)	NB[c]
G3-Gish	NB[c]	NB[c*]	NB[c]	NB[c]	n.d
cc-G3-Gish	1503.3 (±592.14)	NB[c*]	NB[c]	NB[c]	n.d
cc-ALLG-G3-GIsh	1054 (±145)	NB[c*]	NB[c]	NB[c]	n.d
cc-ALLG-Aoc-Peg-GIsh	NB[c]	NB[c*]	297 (±122)	NB[c]	NB[c]

[a] App. K_ds, means (±SD) from 3 binding curves. Determined via titrations of fluorescein-labeled peptides (5nM) with non-labeled peptides, Aβ40, IAPP; [b] app. K_ds, means (±SD) from 3 binding curves Dac-Aβ40 (10nM) and Fluos-IAPP (5nM) were titrated with peptides; [c] NB, no binding at peptide concentrations ≤ 5μM; [c*] NB, no binding at c≤10μM; n.d, not determined (aq. buffer 1×b, pH 7.4, containing 1% HFIP); [*] Binding data taken from Malideli et. al ref.[170].

Recently, it was found that simultaneous substitution of four aromatic/hydrophobic residues by Ala dramatically impairs both IAPP amyloid self- and hetero-assembly Aβ40(42)[88]. My studies supported the importance of the above 4 residues in a specific cyclic conformation. As negative controls, 2 important analogues were synthesized and their effects on amyloid self-assembly and cell damaging on Aβ40 or IAPP amyloid self-assembly were studied[144]. 4G-2a where F15, L16, F23 and Ile26 substituted by Gly on cc-R3-GIsh (2a) cyclic peptide and the second was 4A-2b where 4AA substituted by Gly on cc-ALLG-R3-GIsh (2b). Our results showed the high impact of these 4AA on both peptides. Both 4G-2a and 4A-2b were unable to inhibit either Aβ40 or IAPP[144]. All these findings suggested a minimal motif which included the 4 amino acids (F15, L16, F23, I26), the RRR tripeptide arranged within the cyclic oligoglycine sequence that is needed for inhibition and interaction not only with Aβ40 but also with IAPP.

Further studies were performed in order to investigate the role of the Arg in the linker of cc-ALLG-R3-GIsh (2b). For that in chapter 4.4 a new series of analogues containing Gly and combinations of Arg residues in the ripeptide linker sequence were synthesized and investigated with regards to their biophysical properties and inhibition effects on Aβ and/or IAPP fibril formation (2b analogues). Comparison of the CD spectra of all seven 2b analogues showed a significant amount of β-turn around 225nm. CD spectra of cc-ALLG-G3-GI and cc-ALLG-R3-GI were also included in the comparison (Figure 112).
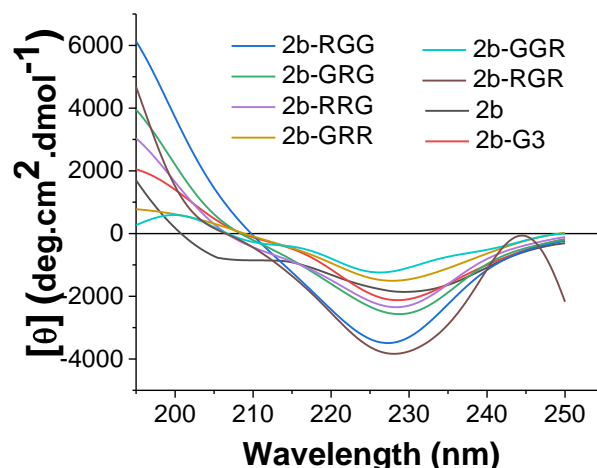
Figure 112. Comparison of secondary structure of 2b analogues by far UV spectroscopy. CD spectra of 2b-RGG, 2b-GRG, 2b-RRG, 2b-GRR, 2b-GGR, 2b-RGR, 2b and 2b-G3. Measurements were performed at peptide concentrations of 5μM in aq. buffer (1×b), pH 7.4, containing 1% HFIP.

The CD spectrum showed that most of the 2b analogues shared similar β-turn structures in comparison to CD spectra of 2b (except from 2b-RGG and 2b-RGR). All peptides showed weak binding affinities, which varied in the micromolar range (except from 2b-RGG and 2b-RGR) (Table 58). It seemed that substitution of the Arg with Gly in 2b analogues strongly affected their self-association. Comparison of the app. K_ds of the 2b analogues to the app. K_d of cc-ALLG-R3-GIsh (2b) (43nM) and the app. K_d of cc-ALLG-G3-GI (2b-G3) (1μM) suggested that all three Arg residues play an important role in the self-assembly of these peptides. Next, was investigated the importance of the position of arginines in the tripeptide linker according to their inhibition properties against Aβ40 fibril formation. As shown in chapter 4.4.3, I investigated the effects of the different analogues against Aβ40 fibrillogenesis (Table 57). As it is found presented Gly substitution of Arg with Gly in the linker of 2b resulted in a non inhibitor. Finally, as far as inhibition properties of 2b-analogues towards IAPP fibrillization and cytotoxicity is concerned, we tested only as a control (2b-GGR) (Figure 113) and it was unable to inhibit.
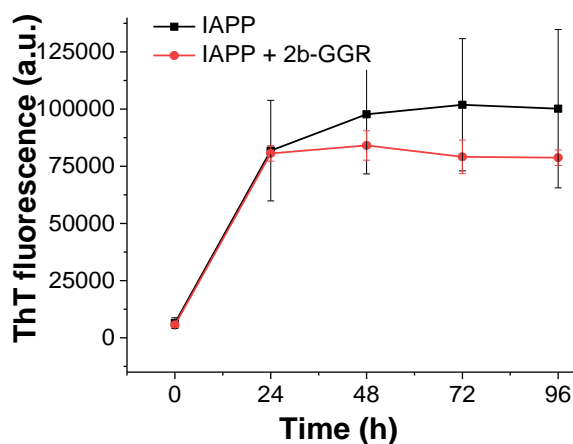
Figure 113. Effects of 2b-GGR analogue on IAPP amyloid formation. (a) Fibrillogenesis of IAPP (16.5μM) alone and its mixtures with 2b-GGR analogue (5-fold excess) was determined via the ThT binding assay (means (±SD), 3 assays).

Table 57. Comparison of the effects of linker of 2b analogues on fibril formation and cytotoxicity of Aβ40 and or IAPP.

Peptides	Inhibition Aβ40 (1/5)[a]	Inhibition IAPP (1/10)[a]
2b	+	+
2b-G3	-	-
2b-GRR	-	n.d[b]
2b-GGR	-	-
2b-RRG	-	n.d[b]
2b-RGG	-	n.d[b]
2b-GRG	-	n.d[b]
2b-RGR	-	n.d[b]

[a] (values in parenthesis show applied Aβ40, IAPP/peptide ratio) "+" indicates inhibition and "-" indicates no inhibition; [b] n.d., non-determined (as they do not inhibit IAPP).

Then I determined the affinities of interactions of 2b analogues with Aβ40. The affinities of their interaction with Dac-Aβ40 were 4-8-fold weaker than the affinity of **2b**. Only, the 2b-GRG analogue showed 6-fold stronger affinity than **2b**. Similarly, the affinities of the interactions of Fluos-2b-analogues with Aβ40 were 40-weaker than the affinity **2b**. In the case of 2b-RGR analogue the affinity of interaction with Aβ40 was 3-fold stronger (app. K_d = 44nM) than the app. K_d of **2b** (app. K_d = 130nM). Finally, as shown in Table 58 **2b** was the only analogue that could bind in low nanomolar range both monomeric/oligomeric species of Aβ40. We concluded that the three Arg of **2b** are very important for Aβ and/or IAPP inhibition. The data showed that inducing conformational flexibility due to Arg residues in the linker resulted in a compact secondary structure in which the combination of S-S bridge imposed not only a desired conformation, but also favorable charge[148],[137, 147]. Finally, the studies revealed also the importance of hot residues, which are very important for self- and hetero- association with Aβ and or IAPP[88]. All these key factors are highly important in displaying or maintaining inhibitory activity against the two polypeptides Aβ/IAPP and cc-ALLG-R3-GIsh (**2b**) was a new lead compound.

Table 58. App.K_ds values of self-assembly and of interactions of peptides with Aβ40 and IAPP as determined by fluorescence binding assays.

Peptide	app. K_d (±SD) (nM) (self-assembly[a])	app. K_d (±SD) (nM) (with Dac-Aβ40[b])	app. K_d (±SD) (nM) (with Aβ40[a])
2b	43.3 (±3.5)	187.6 (±21.5)	130 (±36)
2b-G3	1054 (±145)	NB[d]	NB[c]
2b-GRR	987 (±87)	1273 (336.20)	NB[c]
2b-GGR	2960 (±137)	741.66 (±486.01)	NB[c]
2b-RRG	NB[c]	1460 (±111.0)	NB[c]
2b-RGG	130 (±33.7)	1480 (±240.0)	NB[c]
2b-GRG	NB[c]	28.0 (±14.79)	NB[c]
2b-RGR	477 (±71)	NB[d]	44 (±28)

[a] App. K_ds, means (±SD) from 3 binding curves. Determined via titrations of fluorescein-labeled peptides (5nM) with non-labeled peptides, Aβ40; [b] app. K_ds, means (±SD) from 3 binding curves Dac-Aβ40 (10nM) was titrated with peptides; [c] NB, no binding at peptide concentrations ≤ 5μM; [d] NB, no binding at peptide concentrations ≤ 10μM, (aq. buffer 1×b, pH 7.4, containing 1% HFIP).

5.4 Effects of the incorporation of D-amino acids in cc-ALLG-R3-GI analogue

As potential therapeutics peptides offer several advantages over small molecules (increased specificity) and antibodies (small size)[52]. Nevertheless peptides have a short life, owning to rapid renal clearance and lack in vivo stability due to protease degradation[149]. A series of modifications have been developed such as

cyclization, truncation, N-methylation[150] and incorporation of D-amino acids can improve stability to proteolytic degradation[151]. Replacement of residues by D-amino acids has been successful approach to enhance half-lives of peptide drugs[152].

Previously, cc-ALLG-R3-GIsh (**2b**) bearing only 4 IAPP key residues and the RRR tripeptide arranged within the cyclic oligoglycine scaffold comprised a motif, which may be mediating in cross-amyloid inhibitory function. Moreover, exhibited inhibitory effects of cc-ALLG-R3-GIsh (**2b**) toward amyloid self-assembly of both Aβ40(42) and IAPP. However, resistance toward plasma proteases is a very important requirement for any drug candidate. Therefore, the proteolytic stability of cc-R3-GIsh (**2a**) and cc-ALLG-R3-GIsh (**2b**) in human plasma in vitro were next examined by using RP-HPLC and MALDI-TOF-MS. It should be noted that mass spectrometry (MS) alone is rarely a valid quantitative measure, while RP-HPLC analysis of peptides is directly quantitative when a UV-detector is used to quantify peptide content. However, MS of the degradation products provids insight into if or where a peptide is cleaved and/or if other modifications occurred in the plasma[153]. Unfortunately, both **2a** and **2b** were rapidly degraded, and half-life times ($t_{1/2}$) were <1h (Figure 114, Table 59). To optimize the proteolytic stability of **2b**, 3 rounds of sequence optimization were performed. First, analogue **2c** with 3 D-Arg in the linker region instead 3 L-Arg was synthesized followed by **2d** in which, in addition Phe and Leu was replaced by D-ones (Scheme 7). However, $t_{1/2}$ values were only slightly improved (1-2h) (Figure 114, Figure Appendix A26), Table 59). Therefore, **2e** in which additionally, the two L-Cys were replaced by D-Cys residues was synthesized. Of note, some studies **2d** and **2e** were performed by Luzia Heidrich and are included in her master thesis[163]. Most importantly, **2e** exhibited highly improved proteolytic stability ($t_{1/2}$>11h), being >30-fold more resistant than R3-GI (**1**) ($t_{1/2}$=20 min) and >15-fold more resistant than its L-precursor cc-ALLG-R3-GIsh (**2b**) ($t_{1/2}$= 45min) (Figure 114, Table 59). Several studies could verify that exchanging L-amino acids with D-amino acids protects from degradation[154]. For example, a beta-sheet blocker peptide (iAβ11) and a modified analogue with covalently bound putrescine (PUT-iAβ11) degraded rapidly in plasma after intravenous injection in rats. A significant protection against proteolytic degradation[155] achieved by exchanged all amino acids with their D-amino acids. Arai., et al. reported a head-to tail cyclic derivative of KLVFF and its enantiomer[45] (cyclic-(L)-KLVFF and cyclo-(D)-KLVFF). The cyclo-(D)-KLVFF was further developed to a more potent cyclic D-analogue, which had an additional phenyl group at the β-position of the Phe4 side chain. This analogue showed inhibitory potential against Aβ aggregation; most importantly this analogue had a $t_{1/2}$ of 6h, whereas its linear analogue had a $t_{1/2}$ of 10min.

a) Aβ40   DAEFRHDSGYEVHHQKLVFFAEDVGSNKGAIIGLMVGGVV

IAPP   KCNTATCATQRLANFLVHSSNNFGAILSSTNVGSNTY

b)

(1)   ATQRLANFLVH-RRR-NFGAILS

(1a)   C-ATQRLANFLVH-RRR-NFGAILS-C

(2)   NFLVH-RRR-NFGAILS

(2a)   C-NFLVH-RRR-NFGAILS-C

(2b)   C-GFLGG-RRR-GFGGIGG-C

(2c)   C-GFLGG-rrr-GFGGIGG-C

(2d)   C-GfLGG-rrr-GfGGIGG-C

(2e)   c-GfLGG-rrr-GfGGIGG-c

Scheme 11. Inhibitor design strategy. a) Aβ40 and IAPP; IAPP "hot segments" coloured[86b]. b) Template R3-GI (1) and designed peptides (C-terminal amides)[87] (red coloured residues: Cys; orange coloured residues Arg; yellow highlighted 4 important AA; D-residues: lower-case; amide bond N-methylations at G24 & I26: "N-Me".
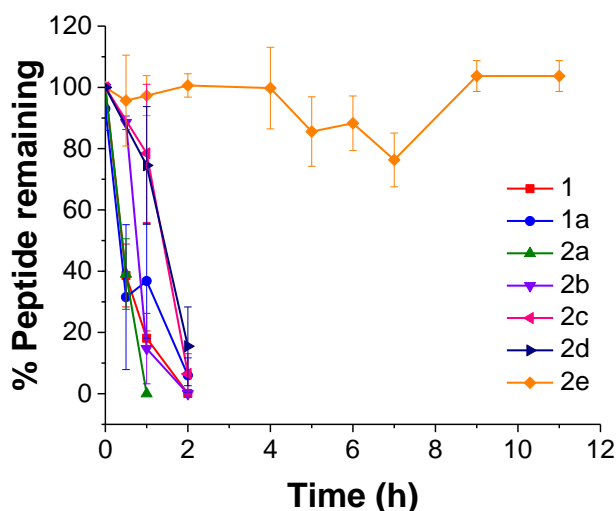
Figure 114. Proteolytic stabilities of inhibitors in human blood plasma *in vitro*. Human plasma stabilities (*in vitro*) of **1-2d** as compared to the all-D scaffold **2e**. Peptides were incubated in plasma (37°C) for the indicated time points and following separation from plasma proteins their amounts were quantified by RP-HPLC and MALDI-TOF-MS; remaining intact peptide (% of total) is plotted over incubation time. Data are means (±SD) from at least 3 experiments[144]i.

Table 59. Proteolytic stability of cyclic-R3-GI analogues in human plasma as determined by % peak height by RP-HPLC analysis.

R3-GI analogues	t$_{1/2}$ (min)[a], [b]
1	23 (±2)
1a	30 (±17)
2a	26 (±7)
2b	46 (±5)
2c	71 (±18)
2d	78 (±16)
2e	>660

[a] t$_{1/2}$ ((±SD) from at least 3 plasma degradation assays); [b] peak height: correlated with integrated peak (data not shown).

The next question that was addressed was whether the changing of specific amino-acid chirality may have affected **2b** structure and function. In fact, the shapes of the CD spectra of **2c-2e** were similar to the shape of **2b** but their minima were blue shifted, whereas the CD spectra of **2a** contained both random coil and β-sheet/β-turn elements (Figure 115. Based on fluorescence spectroscopy studies the app. K$_d$s of their self-association was determined and compared to the ones of the L-analogues **2b** and **2a**. As presented in Table 60 the app. K$_d$s of self-assembly of **2c**, **2d**, **2e** were very similar to the app. K$_d$ of **2b**, but at least 10 times stronger than the app. K$_d$ of **2a**.
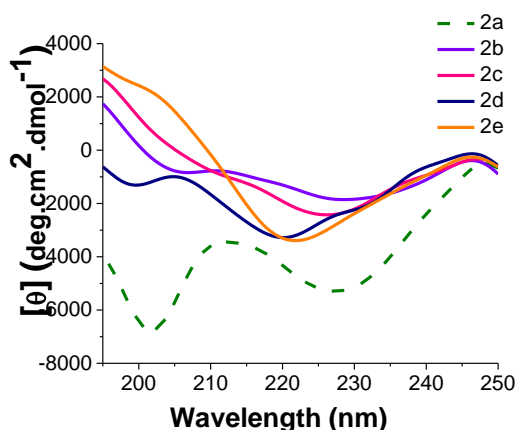
Figure 115. Conformations of 2a-2e as determined by far-UV CD spectroscopy. CD spectra shown were measured at peptide concentrations of 5μM in aq. buffer (1×b), pH 7.4, containing 1% HFIP.

Moreover, the inhibitory activities of 2c, 2d and 2e against Aβ40(42) amyloid formation and toxicity was studied and compared with the activities of 2b and 2a[163]. It was found that 2c, 2d and 2e could inhibit Aβ40(42) at five fold excess, and their IC50s values were very similar to the IC50 of the L-analogue (2b), but 6 times lower than the IC50 of 2a (Table 61). Although it has been proposed that no heterologous fibril extension occurs and therefore D-peptides might not be able to inhibit Aβ40 fibrillogenesis[156], several investigators proposed contradicting evidence. For example Tjenberg et al. have shown that KLVFF binds stereospecifically to the homologous sequence in Aβ (i.e. Aβ16-20)[33] and molecular modeling suggested that association of the two homologous sequences leads to the formation of an atypical anti-parallel beta-sheet structure stabilized primarily by interaction between the Lys, Leu, and COOH-terminal Phe. Also, Tjenberg screened combinatorial pentapeptide libraries exclusively composed of D-amino acids, and several ligands[157]. Ligands composed of D-amino acids were not only capable of binding Aβ40 but they also prevented formation of amyloid-like fibrils[157]. Chalifour et. al showed that D-enantiomers of five peptides, (KLVFFA, KKLVFFA, KFVFFA, KIVFFA, and KVVFFA), were unexpectedly more active inhibitors of

147

Aβ40 fibrillogenesis[158]. Doig and co-workers designed a peptide, D-[chGly-Tyr-chGly-chGly-mleu]-NH2 (ch=cyclohexyl, m=N-methyl), with more than 30 times the inhibitory activity towards Aβ40(42) aggregation and toxocity than KLVFF[37, 159].

Furthermore, the binding affinities of the designed peptides against monomeric/oligomeric Aβ40(42) were determined (Table 60)[162]. Concerning the interaction with Aβ40 it can be observed that **2c**, **2d** and **2e** analogues bound to Aβ40 similar app. K_ds as **2b**. In the case of the interactions of peptides with Aβ42, a trend can be observed in a way that the peptides containing more L-amino acids (**2b**, **2c**) showed weaker affinity (app. K_d ~100-200nM), whereas the peptides with more D-amino acids (**2d** and **2e**) showed stronger app. K_ds below 20nM.

Table 60. App. K_ds values of self-assembly potential and app. K_ds of interactions of peptides with Aβ40 and IAPP as determined by fluorescence titration binding assays.

Peptide	app. K_d (±SD) (nM) (self-assembly[a])	app. K_d (±SD) (nM) (with Dac-Aβ40[b])	app. K_d (±SD) (nM) (with Aβ40[a])	app. K_d (±SD) (nM) (with Aβ42[b])	app. K_d (±SD) (nM) (with Fluos-IAPP[b])	app. K_d (±SD) (nM) (with IAPP[a])
2a	670.3 (±57.7)	382.3 (±89.2)	171.6 (± 26.10)	102.6 (±2.5)	13.2 (±1.1)	22.6 (±1.5)
2b	43.3 (±3.5)	187.6 (±21.5)	130 (±36)	199.0 (±25.5)	216.5 (±13.4)	10.7 (±1.2)
2c	69.0 (±10.2)	551.0 (±42,3)	84.0 (±17)	93.6 (±65.0)	250.3 (±3.5)	1213.3 (±57)
2d	17.4 (±5.8)	107.6 (±34.5)	61.0 (±7.7)	5.7 (±0.4)	313.4 (±11.7)	3.4 (±1.7)
2e	11.6 (±1.8)	210 (±16.5)	114.0 (±1.4)	25.6 (±3.8)	245.5 (±7.3)	41.6 (±1.3)

[a] App. K_ds, means (±SD) from 3 binding curves. Determined via titrations of fluorescein-labeled peptides (Fluos-peptides 5nM) with non-labeled peptides, Aβ40, IAPP; [b] app. K_ds, means (±SD) from 3 binding curves Dac-Aβ40 (10nM), Fitc-Aβ42 (5nM) and Fluos-IAPP (5nM) were titrated with peptides; (aq. buffer 1×b, pH 7.4, containing 1% HFIP).

It seemed that although the D-amino acid containing 2b analogues (**2c**, **2d** and **2e**) could bind IAPP with strong affinities the inhibition activity was lost. A possible explanation could be a connection between the self-association of their IAPP analogs and the inhibitory capabilities. **2d** and **2e** have both very high propensities for self-association (Table 61) and high app. K_ds in their interactions with oligomeric IAPP species (Table 61).

In summary, it was found that exchanging L-amino acids with D-amino acids maintained the inhibitory capabilities concerning Aβ fibril formation and cytotoxicity. In contrast, D-amino acid substitutions showed a negative influence on the inhibitory capabilities towards IAPP fibril formation and cytotoxicity, resulting finally in **2e**, an Aβ-selective inhibitor of amyloid self-assembly. Of note, ex vivo electrophysiological studies in mouse brains showed that **2a**, **2b** and **2e** ameliorated Aβ42-mediated inhibition of hippocampal synaptic long term potentiation (LTP) which is linked to loss of memory and cognitive functions[144]. Finally, it was also shown that **Fluos-2e** was able to cross the human Blood Brain Barrier (BBB), with an apparent permeability (Papp) of 14.6×10^{-6} (±3.36)cm/s at 2h[144].

Table 61. Comparison of the inhibitory potentials of cyclic R3-GI analogues towards Aβ40 and IAPP fibril formation and the cytotoxicity.

Peptides	Inhibition Aβ40 (1/5)[c]	IC$_{50}$ (±SD) (nM)[a]	Inhibition IAPP (1/10)[c]	IC$_{50}$ (±SD) (nM)[a]
2a	+	125.1 (±73.4)	+	47.6 (±15.5)
2b	+	654.3 (±227.8)	+	425.7 (±77.7)
2c	+	204.0 (±83.6)	-	n.d[b]
2d	+	702.6 (±339.3)	-	n.d[b]
2e	+	542.5 (±240.7)	-	n.d[b]

[a] IC$_{50}$s, means (±SD) from 3-4 titration assays (n=3 each) (Aβ40,500nM; IAPP, 100nM), [b] n.d., non determined (non-inhibitor); [c] (values in parenthesis show applied Aβ40, IAPP/peptide ratio) "+" indicates inhibition and "-" indicates no inhibition.

It is known, that there is a significant interest in cyclic peptides as therapeutics[160]. The reason for this interest is founded not only on the belief that cyclic peptides have advantages over other drug modalities but also on the growing perception that they are a privileged sub-class among peptides[137]. The results of my work supported the above ideas as they yielded several cyclic peptides or analogues that have potent inhibitory effects on Aβ40(42) and/or IAPP amyloidogenesis. Soudy et al. designed and studied the effects of a cyclic peptide of the AC253 (cAC253) against Aβ42 cytotoxicity[161]. This cyclic peptide showed enhanced brain penetration after a signal intraperinotal injection and demonstrated improved proteolytic stability and pharmacokinetic behaviour compared to its linear counterpart AC253[161]. The future goal will be to study amyloid inhibitory effects in vivo and their bioavailability[144]. High oral bioavailability is one of the most important goals in drug design, as it will result in lower doses of the administered drug, fewer side effects and potentially higher patient compliance[162].

5.5 ISMs as inhibitors of insulin fibrillization and cytotoxicity

Insulin plays a major role in blood glucose homeostasis and pharmaceutical preparations of insulin are commonly used to treat diabetes[106, 163].

As the understanding of insulin aggregation mechanism and key noncovalent interactions has biochemical ramifications, there are some efforts to study potential inhibitors of this process in the form of organic fluorogens, short peptide sequences, and aromatic compounds [104, 164][158]. In partqiular, the requirement of hydrophobic and electrostatic interactions for insulin aggregation has been used for the design of prospective inhibitors[165].

The islet amyloid polypeptide (IAPP) and insulin are coproduced by the β-pancreatic cells and both peptides are able to form fibrils[166]. In vitro studies have already shown that insulin bind to IAPP and can inhibit IAPP fibrillogenesis[109a, 109c-e].
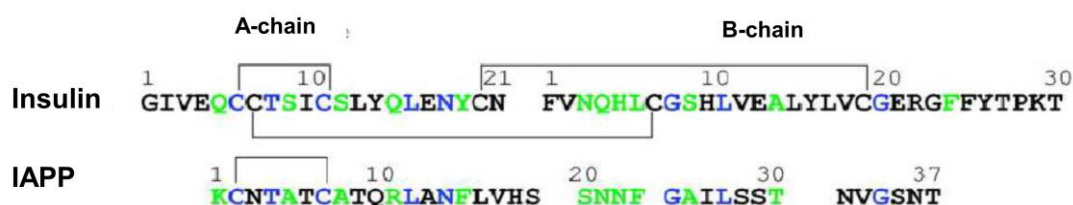
Figure 116. Primary sequence of insulin and IAPP. Residues in common to sequences are in blue and similar residues are in green[71b].

Gazit and coworkers[109a] identified a single domain within insulin that binds to IAPP and inhibits IAPP amyloid formation. This domain is located at the center of the B chain of insulin and spans residues 9-20. Recently, MD studies suggested that the stabillization of the heterodimer (B-chain-insulin) occurred between residues 11 to 19 of B-chain insulin and 8-18 of IAPP and thus inhibit IAPP amyloidogenesis[110]. It has been proposed that these two domains compose the recognition site that mediates the IAPP/insulin interaction[109a]. Finally, Velkova et al.[71b] proposed another strategy to inhibit insulin aggregation, without inhibiting insulin function. IAPP-GI, a designed peptide mimic of IAPP, has been found to inhibit amyloidogenesis and toxicity of insulin. It has been suggested that IAPP-GI could become a lead compound for development new drugs and therapeutic concepts for targeting both AD and T2D[71b].

In the last part of my PhD thesis, I investigated whether the ISMs could interact with insulin and could inhibit insulin aggregation[87]. It has been demonstrated that depending on the nature of the linker (hydrophobic, hydrophilic, polar) ISMs exhibited different structures and thus different effects on IAPP or Aβ amyloid self-assembly[87].

It was found that L3-GI and V3-GI completely blocked formation of cytotoxic species and inhibited insulin oligomerization whereas G3-GI, A3-GI were unable to do so. The results showed that the four out of five

hydrophobic linker-containing ISMs I3-GI, Nle3-GI, F3-GI, and Cha3-GI (except 2Aoc3-GI) blocked insulin fibrillogenesis, cytotoxicity and oligomerization. However, in the case of of Aoc3-GI, only insulin fibril formation and oligomerization were blocked but not cytotoxicity. Recently, Ratha et al.[106] designed a hydrophobic peptide, KR7 (KPWWPRR), which was an effective inhibitor of insulin fibrillization, but less effective inhibitor of insulin cytotoxicity. The effects of the four polar linker-containing ISMs K3-GI, Dap3-GI, R3-GI, and KAc3-GI towards insulin fibril formation and cytotoxicity were studied as well. Importantly, the two polar linker containing ISMs SpG-GI and K3-GI inhibited insulin self-assembly and cytotoxicity but the other three (R3-GI, Dap3-GI snd KAc3-GI) did not inhibit. Previously, Mishra et al.[107] started working on the design of a biocompatible short peptides that would combine hydrophobicity and polar/charged character, for the inhibition of insulin aggregation. Their results showed that such peptides inhibited insulin fibrillization and they proposed a possible model for both insulin aggregation and the mechanism of inhibition by peptide conjugates. Based on their results they predicted that the binding location of inhibitor is in the aromatic-rich region of insulin B-chain (for example, the tripeptide motif in segment B(24−26)[107]). To characterize in more detail the insulin/ISM interactions, far-UV CD spectroscopy was applied. It was found that interaction of six out of seven ISMs containing hydrophobic linkers (L3-GI, I3-GI, Nle3-GI, 2Aoc3-GI, F3-GI and Cha3-GI) with insulin resulted in a clear conformational change. In the case of A3-GI a small but clear difference was observed in the spectra of its mixture with insulin as compared to the sum of the spectra of the mixture components, indicating conformational changes upon interaction of the two peptides. By contrast, no significant conformational difference was observed in the spectrum of the mixture of G3-GI with insulin as compared to the sum of the spectra of each of the components. Importantly, clear differences between CD spectrum of the mixture and the spectra of each of the components were also observed for three out of five polar linker-containing ISMs (Dap3-GI, R3-GI and SpG-GI).

The above results identified the three ISMs L3-GI, Nle3-GI and Cha3-GI as inhibitors of self assembly of all three amyloidogenic polypeptides Aβ, IAPP and insulin, the three ISMs V3-GI, I3-GI and F3-GI as inhibitors of both Aβ and insulin (but not IAPP), the ISM 2-Aoc3-GI as inhibitor of both IAPP and insulin (but not Aβ), the two ISMs K3-GI and SpG-GI as insulin selective inhibitors, and R3-GI as an Aβ selective inhibitor (Table 62).

Table 62. Effects of ISMs on amyloidogenesis of Aβ40, IAPP and insulin.

ISMs	Aβ inhibition	IAPP inhibition	insulin inhibition
G3-GI	-	-	-
A3-GI	-	-	-
V3-GI	+	-	+
L3-GI	+	+	+
I3-GI	+	-	+
Nle3-GI	+	+	+
2-AOc3-GI	-	+	+
F3-GI	+	-	+
Cha3-GI	+	+	+
K3-GI	-	-	+
Dap3-GI	-	-	-
R3-GI	+	-	-
KAc3-GI	-	-	-
SpG-GI	-	-	+

+ indicates inhibition and – indicates no inhibition.

Previously, Susa and co-workers proposed a mechanism by which IBC (insulin B-chain) inhibits IAPP aggregation via predominantly forming helix/helix IAPP:IBC complexes[110]. Also, Luo et al. studied the molecular interactions between Aβ and insulin[167]. They reported that monomeric insulin interacts with soluble Aβ and that the two molecules reciprocally slow down the aggregation kinetics of each other[167]. Prefibrillar oligomers of Aβ that eventually formed in the presence of insulin were less cytotoxic than Aβ

oligomers formed in the absence of insulin. Moreover, mature Aβ fibrils induced fibrillation of soluble insulin, but insulin aggregates did not promote Aβ fibrillation. This study indicated that direct molecular interactions between insulin and Aβ may contribute to the strong link between T2D and AD[167]. Indeed it was reported that tripeptides WWW, WPW, WWP and PWW bind to amyloid fibrils of Aβ(9−40) at the hydrophobic groove with very high affinity. Among the tripeptides, PWW exhibited highest binding affinity towards amyloid fibrils[168]. The designed peptide, KR7, was derived with a slight modification from the known antimicrobial peptide indolicidin. It harbors a PWWP motif at the center flanked by the positively charged residues Lys and Arg at the N and C termini, respectively. Based on the hypothesis that amyloid fibrils of different proteins often share similar structural properties, the researchers were interested in testing the activity of KR7 with insulin, as the central region of the KR7 has overlapping PWW and WWP motifs. Insulin is also rich in hydrophobic amino acid residues (5.9% Phe, 5.9% Ala, 7.8% Gly, 9.8% Val, and 11.8% Leu), similar to the Aβ peptide. KR7 is an effective inhibitor of insulin aggregation with a novel inhibition modus; it seemed to arrest insulin aggregation in the later stages of fibril assembly without disassembly by binding both to monomeric insulin and to insulin fibrils[106].

6.   Appendix
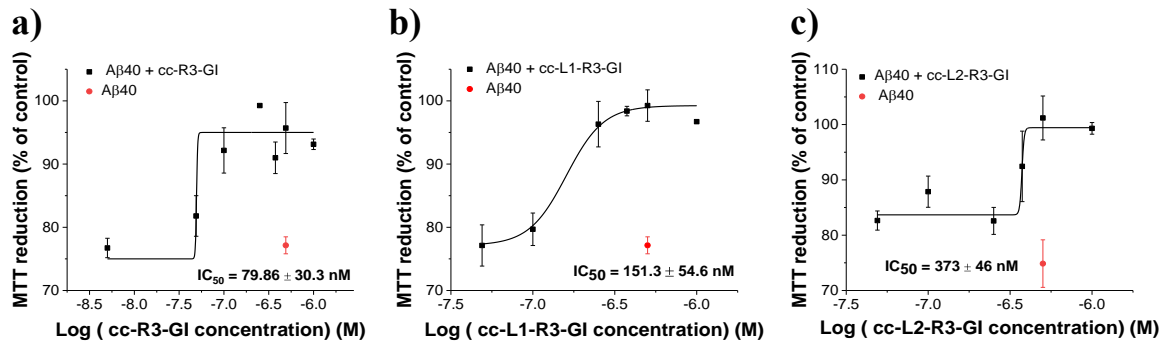
Figure A1. Effects of cISMs on Aβ40 cytotoxicity. Determination of IC$_{50}$ of inhibition of Aβ40 cytotoxicity on PC-12 cells by (a) cc-R3-GI, (b) cc-L1-R3-GI, (c) cc-L2-R3-GI. Aβ40 (16.5μM) in 50mM PB, pH 7.4, containing 100mM NaCl, 1% HFIP with different amounts of cyclic peptides and incubated for 3 days. The effect of these peptide solution on the viability of the PC-12 cells was determined by the MTT reduction assay. The final Aβ40 concentration on the cells is 500nM. The data are mean values (±SD), from 3 assays (n=3 each).
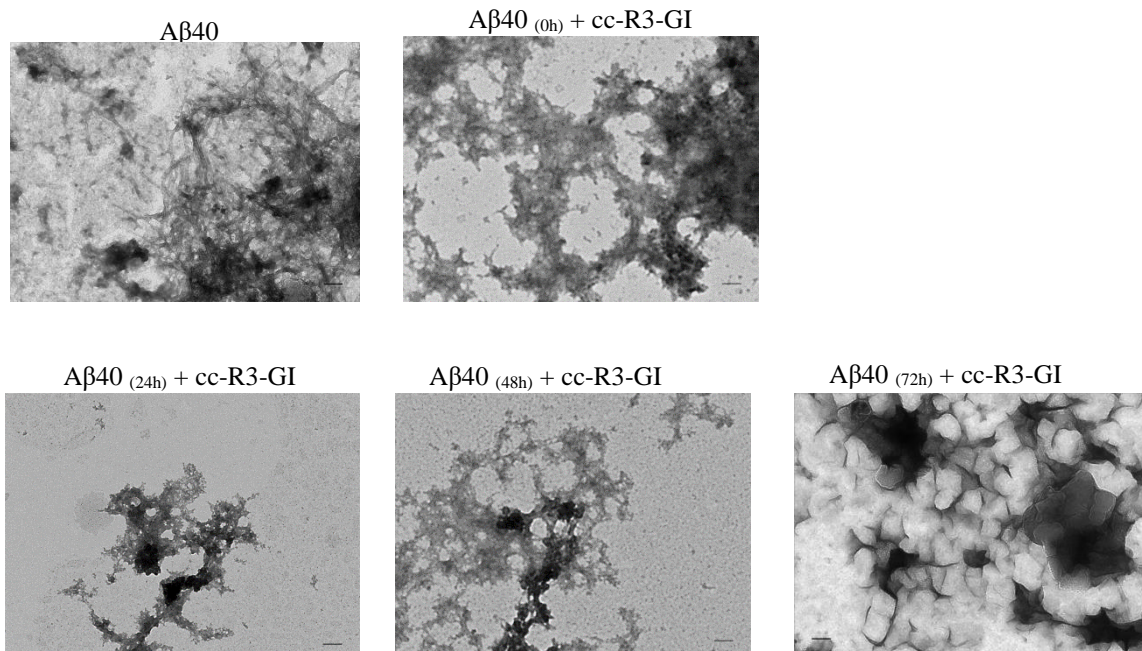
Figure A2. Effects of cc-R3-GI when added at pre-or postnucleation stages of fibrillogenesis of Aβ40. TEM images of 7 days aged mixtures of Aβ40 (16.5μM) with cc-R3-GI analogue (Aβ40/peptide, 1/1). Solutions used in the ThT binding and the MTT reduction assay shown in Figure 24 were applied for TEM examination; (bars:100nm).
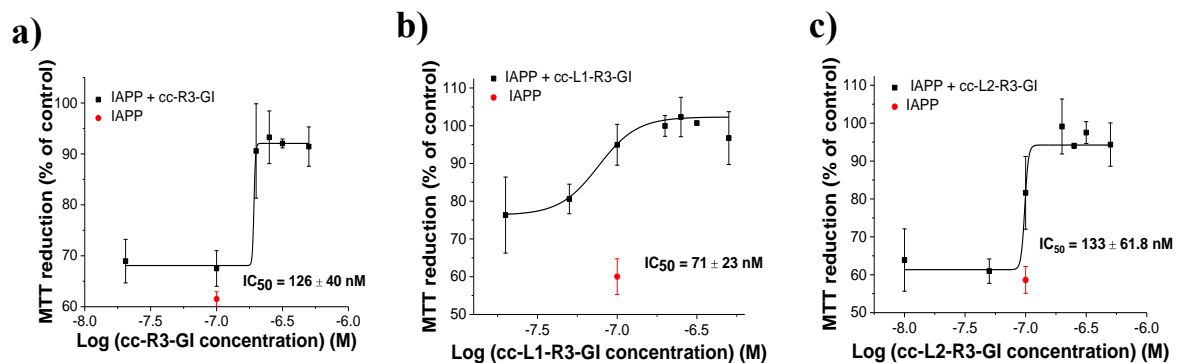
Figure A3. Effects of cISMs on IAPP cytotoxicity. Determination of IC$_{50}$ of inhibition of Aβ40 cytotoxicity on RIN5fm cells by (a) cc-R3-GI, (b) cc-L1-R3-GI, (c) cc-L2-R3-GI. IAPP (6μM) in 50mM PB, pH 7.4, containing 100mM NaCl, 0.5% HFIP with different amounts of cISMs and incubated for 24h. The effect of these peptide solution on the viability of the RIN5fm cells was determined by the MTT reduction assay. The final IAPP concentration on the cells is 100nM. The data are mean values (±SD), from 3 assays (n=3 each).
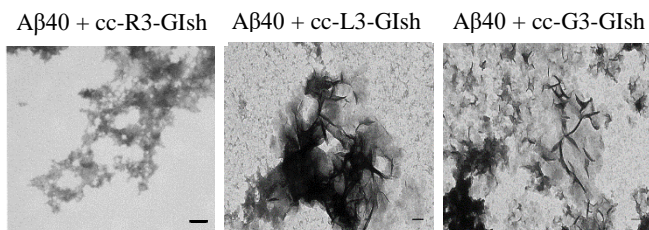
Figure A4. Effects of cISMs-sh on (1/1) Aβ40 amyloid formation via TEM. TEM images of 7 days aged mixtures of Aβ40 (16.5μM) with cc-R3-GIsh, cc-L3-GIsh. cc-G3-GIsh (Aβ40/peptide, 1/1). Solutions used in the ThT binding and the MTT reduction assay shown in Figure 39 were applied for TEM examination; (bars:100nm).
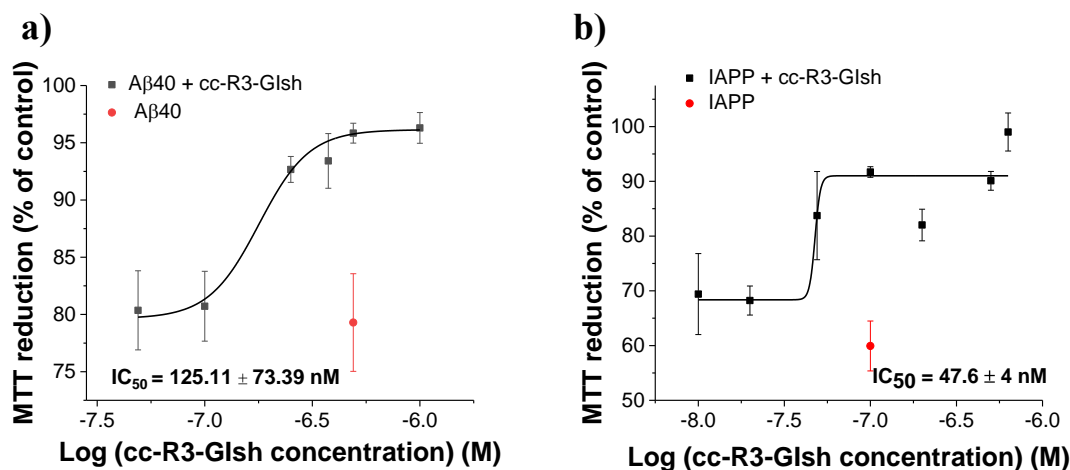
Figure A5. Effects of cc-R3-GIsh (2a) on Aβ40 and IAPP cytotoxicity. (a) Determination of IC_{50} of inhibition of Aβ40 cytotoxicity on PC-12 cells by cc-R3-GIsh (2a). (b) Determination of IC_{50} of inhibition of IAPP cytotoxicity on RIN5fm cells by cc-R3-GIsh (2a). Aβ40 (16.5μM), IAPP (6μM) in 50mM PB, pH 7.4, containing 100mM NaCl, 1% or 0.5% HFIP with different amounts of 2a and incubated for 3 days (Aβ40-related effects) or 24h (IAPP-related effects. The effect of these peptide solution on the viability of the PC-12 cells or RIN5fm cells was determined by MTT reduction. The final Aβ40 concentration on the cells is 500nM and the final IAPP concentration on the cells is 100nM. The data are mean values (±SD), from 3 assays (n=3 each).
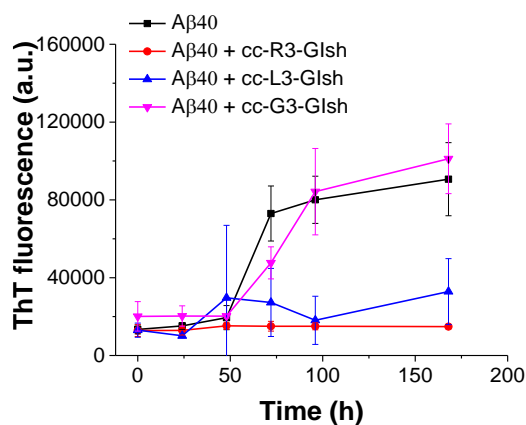
Figure A6. Effects of cISMs-sh on Aβ40 amyloid formation. Fibrillogenesis of Aβ40 (16.5μM) and its mixtures with cc-R3-GIsh (1/1) and cc-L3-GIsh (5-fold excess) or cc-G3-GIsh (10-fold excess) by the ThT binding assay (means (±SD), 3 assays).
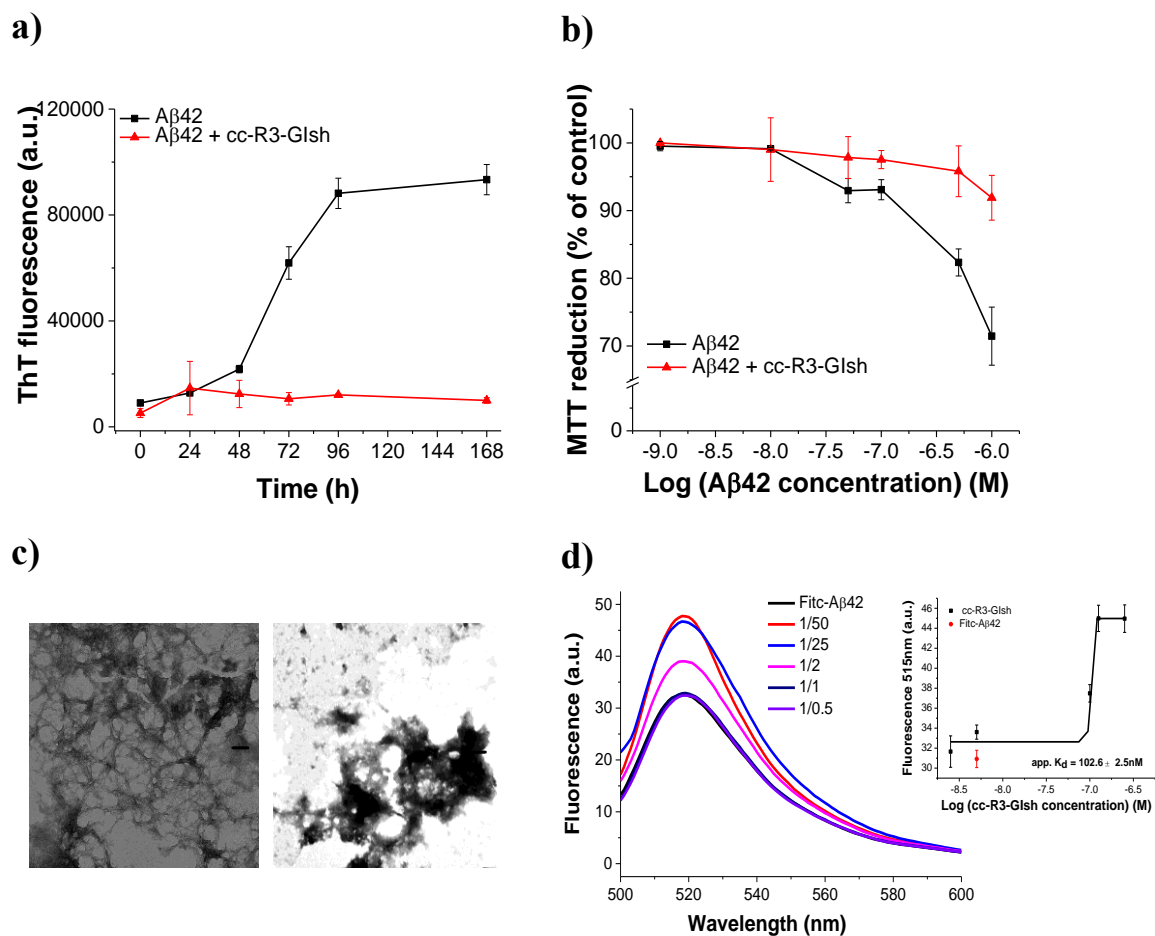
Figure A7. Effects on Aβ42 amyloid self-assembly and determination of app. K_d of interactions of cc-R3-GIsh (2a) with Fitc-Aβ42 by fluorescence spectroscopic titrations. (a) Fibrillogenesis on Aβ42 (16.5μM) and its mixture with 2a (1/1) by the ThT binding assay (means (±SD), 3 assays). (b) PC12 cell viabillity after treatment with 7 days aged solutions from (a) by the MTT reduction assay (means (±SD), 3 assays (n=3)). (c) TEM images of Aβ42 (left) and its mixture with cc-R3-GIsh (right) (7 days aged) (bars: 100nm). (d) Fluorescence spectra of Fitc-Aβ42 (5nM) and its mixtures with various amounts of 2a are shown; the molar ratios of Fitc-Aβ42/2a is as indicated (pH 7.4). In the inset, the binding curve (data are means (±SD), from 3 titration assays) is shown. Determined app. K_d =102.6 (±2.5) nM.
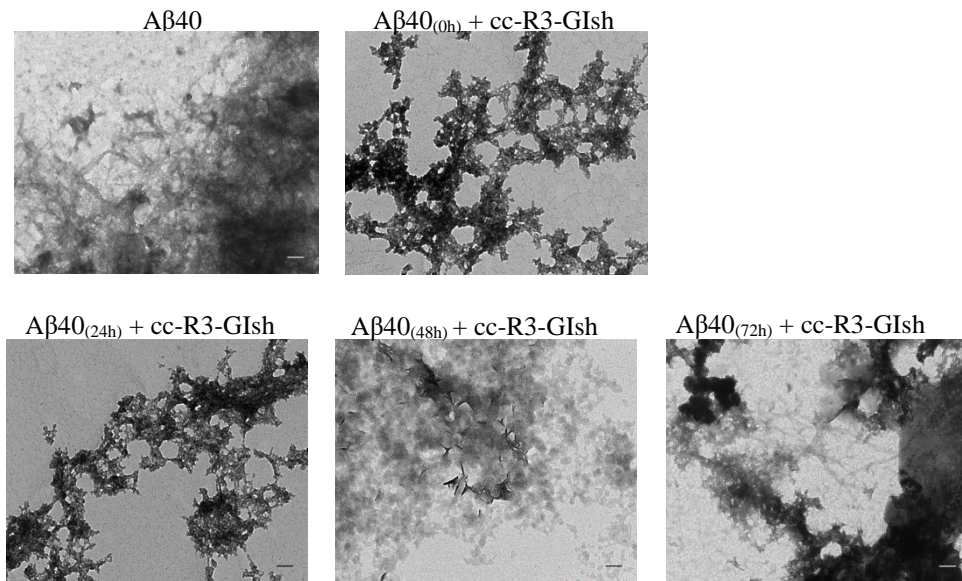
Figure A8. Inhibitory effects of cc-R3-GIsh when added at pre- or post-nucleation stages of fibrillogenesis of Aβ40. TEM images of 7 days aged mixtures of Aβ40 (16.5μM) with cc-R3-GIsh analogue (Aβ40/peptide, 1/1 Solutions used in the ThT binding and the MTT reduction assay shown in Figure 40 were applied for TEM examination; (bars:100nm).
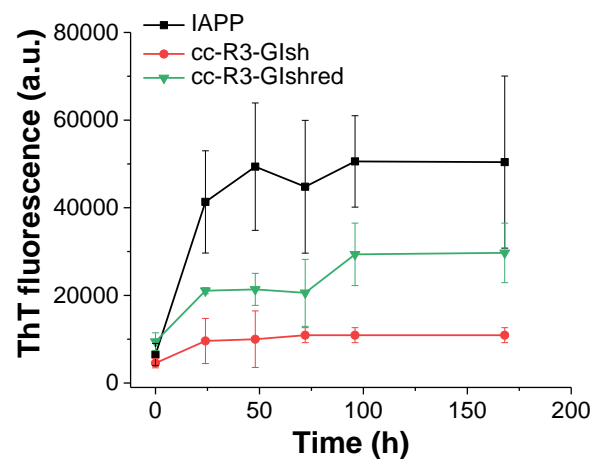
Figure A9. Effects of cc-R3-GIshred/cc-R3-GIsh analogues on IAPP amyloid formation. Fibrillogenesis of IAPP (6μM) alone or with cc-R3-GIshred (2-fold excess) and cc-R3-GIsh (2-fold excess) as determined via the ThT binding assay (means (±SD), 3 assays); (Abbrev. cc-R3-GIshred reduced form of cc-R3-GIsh).
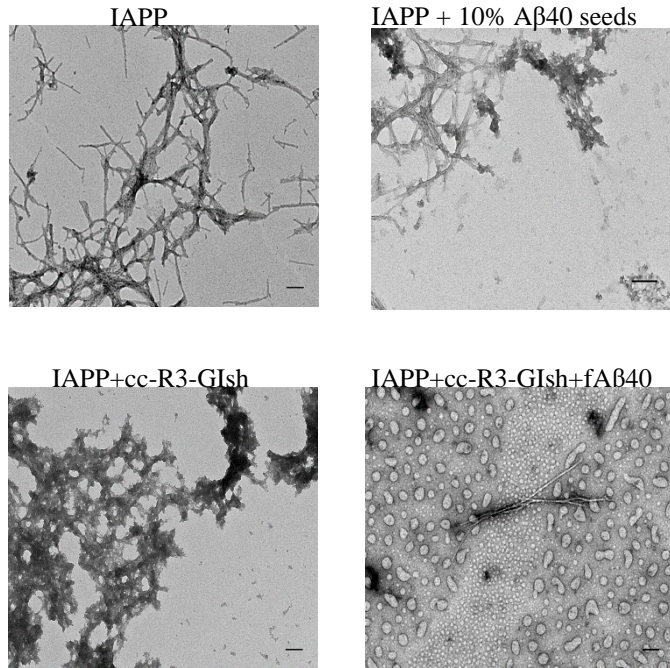
Figure A10. Inhibitory effects of cc-R3-GIsh (2a) on IAPP cross-seeding by Aβ40 fibrils (fAβ40) via TEM. TEM images of 24h-aged mixtures IAPP and its mixtures at 24h. Solutions used in the ThT binding and the MTT reduction assay shown in Figure 46 were applied for TEM examination; (bars:100nm).
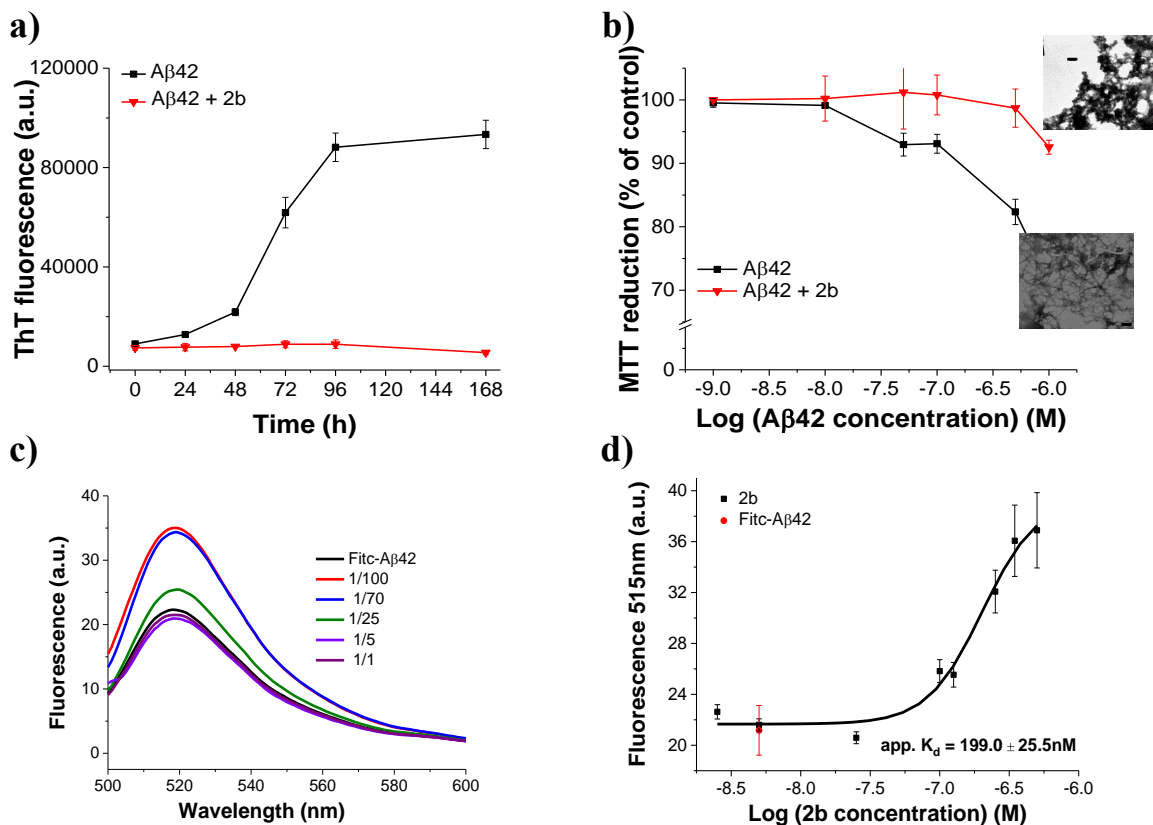
Figure A11. Effects on Aβ42 amyloid self-assembly and determination of app. K_d of interactions of cc-ALLG-R3-GIsh (2b) with Fitc-Aβ42 by fluorescence spectroscopic titrations. (a) Fibrillogenesis on Aβ42 (16.5μM) and its mixture with 2b (1/5) by the ThT binding assay (means (±SD), 3 assays). (b) PC12 cell viabillity after treatment with 7 days aged solutions from (a) by the MTT reduction assay (means (±SD), 3 assays (n=3). (c) TEM images of Aβ42 (left) and its mixture with 2b (right) (7 days aged) (bars:100nm). (d) Fluorescence spectra of Fitc-Aβ42 (5nM) and ist mixtures with various amounts of 2b are shown; the molar ratios of Fitc-Aβ42/2b is as indicated (pH 7.4). In the inset, the binding curve (data are means (±SD), from 3 titration assays) is shown. Determined app. K_d = 199.0 (±25.5) nM.
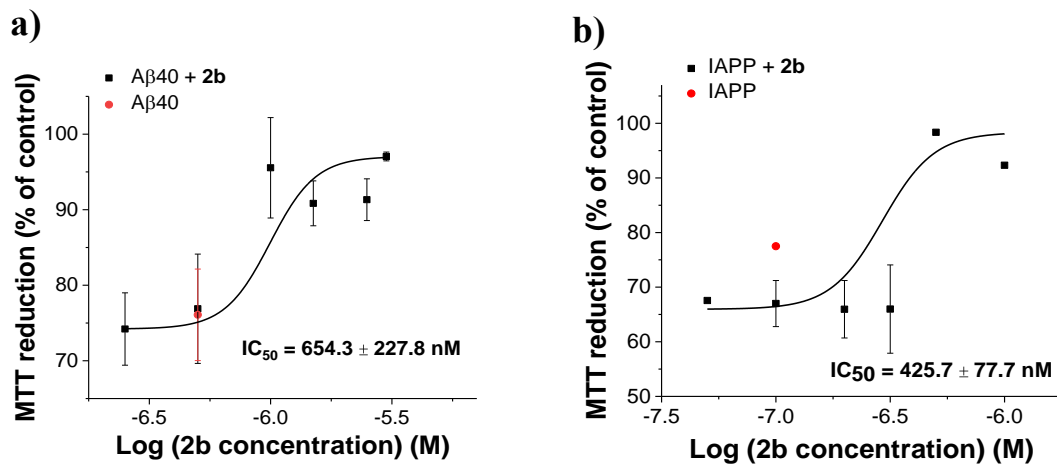
Figure A12. Effects of cc-ALLG-R3-GIsh (2b) on Aβ40 and IAPP cytotoxicity. (a) Determination of IC_{50} of inhibition of Aβ40 cytotoxicity on PC-12 cells by 2b. (b) Determination of IC_{50} of inhibition of IAPP cytotoxicity on RIN5fm cells by 2b. Aβ40 (16.5μM), IAPP (6μM), pH 7.4, containing 100mM NaCl, 1% or 0.5% HFIP with different amounts of 2b and incubated for 3days (Aβ40-related effects) or 24h (IAPP-related effects). The effect of 2b peptide on the viability of the PC-12 cells or RIN5fm cells was determined by the MTT reduction assay. The final Aβ40 concentration on the cells is 500nM and the final IAPP concentration on the cells is 100nM. The data are mean values (±SD), from 3 assays (n=3 each).
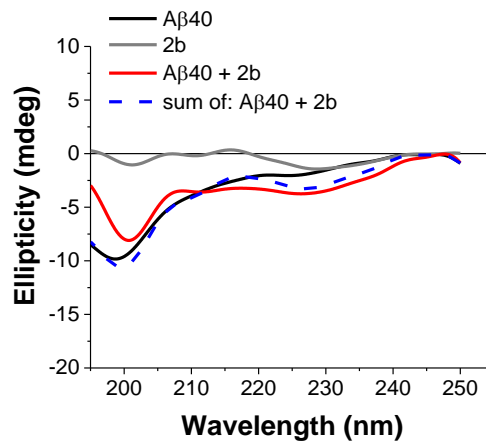
Figure A13. Interactions of inhibitory 2b with Aβ40 as studied by far-UV CD spectroscopy. (a) CD spectra and interactions of 2b (1/5) with Aβ40. Measurements were performed in aq. buffer 1×b, pH 7.4, containing 1% HFIP.
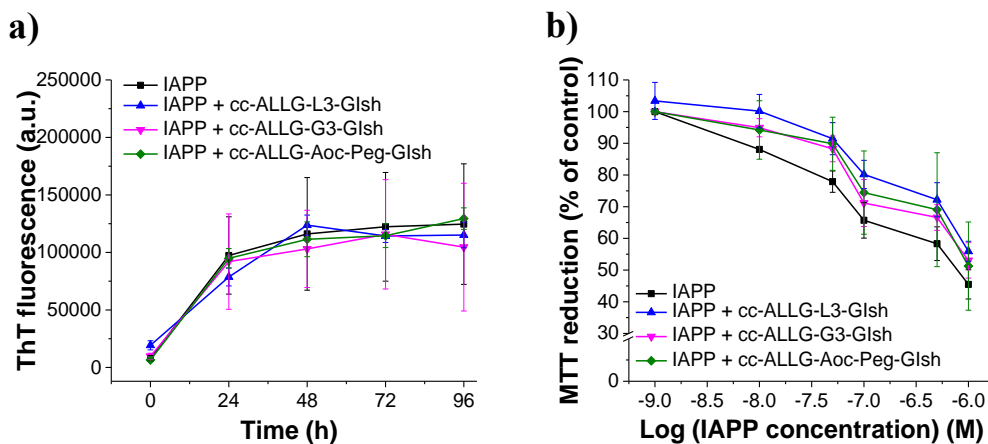
Figure A14. Effects of designed cALLG-sh analogues on IAPP amyloid formation and cytotoxicity. (a) Fibrillogenesis of IAPP (16.5μM) alone or its mixtures with cc-ALLG-R3-GIsh, cc-ALLG-L3-GIsh, cc-ALLG-G3-GIsh and cc-ALLG-Aoc-Peg-GIsh (5-fold excess) was determined via the ThT binding assay (means (±SD), 3 assays), (b) effects on IAPP cytotoxicity. Solutions from (a) aged 24h were added to RINcells. Cell damage assessed by the MTT reduction assay (means (±SD), 3 assays (n=3)).

157
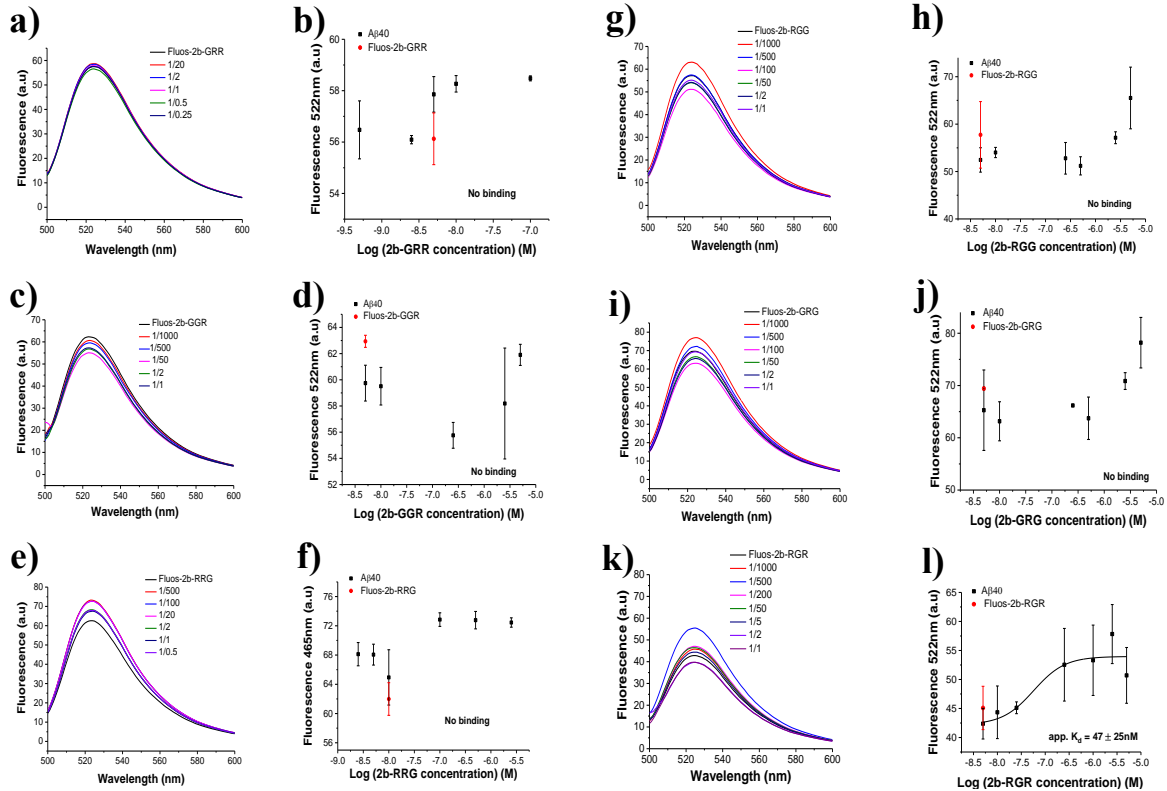
Figure A15. Determination of app. K_ds of interactions of oligomeric Aβ40 species with 2b analogues by fluorescence spectroscopy. Panels a), c), e), g), i), k) show fluorescence spectra of Fluos-2b analogues (5nM) alone and its mixtures with various amounts of Aβ40; the molar ratios of Fluos-2b analogues/Aβ40 are as indicated. Panels b), d), f), h), j), l) show the binding curves of Fluos-2b-GRR (b), Fluos-2b-RGG (d), Fluos-2b-GGR (f), Fluos-2b-GRG (h), Fluos-2b-RRG (j), Fluos-2b-RGR (l) with Aβ40; app. K_ds are means (±SD) from 3 binding curves (Fluos/2b analogues 5nM). Measurements were performed in aq. buffer 1×b, pH 7.4, containing 1% HFIP.
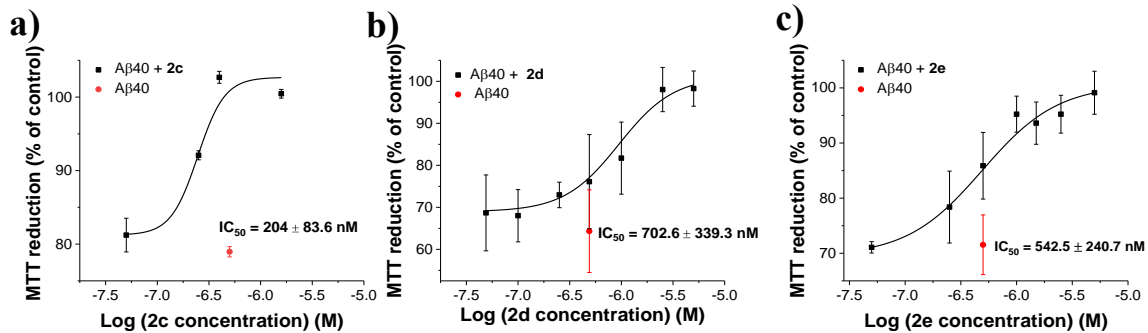
Figure A16. Effects of 2c, 2d and 2e on Aβ40 cytotoxicity. a-c) Determination of IC_{50} of inhibition of Aβ40 cytotoxicity on PC-12 cells by (a) 2c, (b) 2d and (c) 2e. Aβ40 (16.5μM), pH 7.4, containing 1% HFIP with different amounts of 2c, 2d and 2e and incubated for 3days. The effect of these peptide solutions on the viability of the PC-12 cells was determined by the MTT reduction assay. The final Aβ40 concentration on the cells is 500nM. The data are mean values (±SD), from 3 assays (n=3 each).
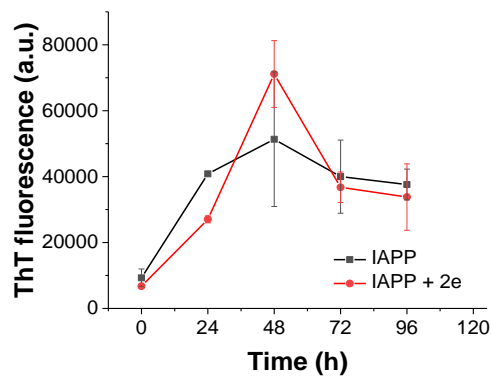
Figure A17. Effects of 2e on IAPP amyloid formation. Effects of 2e at 50-fold excess on IAPP fibril formation via the ThT binding assay.
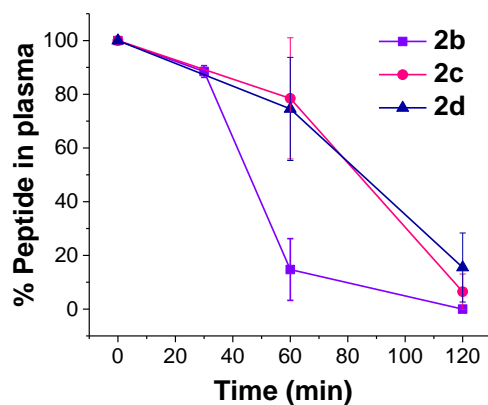
Figure A18. Human plasma stabilities (*in vitro*) of 2c and 2d as compared to the all-L scaffold 2b. Peptides were incubated in plasma (37°C) for the indicated time points and following separation from plasma proteins their amounts were quantified by RP-HPLC and MALDI-TOF; remaining intact peptide (% of total) is plotted over incubation time. Both **2c** and **2d** exhibit an ~2-fold higher proteolytic stability than **2b**. Data are means (±SD) from at least 3 experiments.

6.1 List of Tables

161

6.2 List of Figures

163

6.3   List of Schemes

6.4   List of Figures Appendix

7.   References

[1]   J. D. Sipe, A. S. Cohen, *Journal of structural biology* **2000**, *130*, 88-98.

[2]   C. A. Ross, M. A. Poirier, *Nature medicine* **2004**, *10 Suppl*, S10-17.

[3]   S. Y. Tan, M. B. Pepys, *Histopathology* **1994**, *25*, 403-414.

[4]   aM. Sunde, L. C. Serpell, M. Bartlam, P. E. Fraser, M. B. Pepys, C. C. F. Blake, *Journal of Molecular Biology* **1997**, *273*, 729-739; bC. M. Dobson, *Nature* **2003**, *426*, 884-890.

[5]   R. Riek, D. S. Eisenberg, *Nature* **2016**, *539*, 227-235.

[6]   aP. Arosio, T. P. Knowles, S. Linse, *Physical chemistry chemical physics : PCCP* **2015**, *17*, 7606-7618; bS. I. Cohen, S. Linse, L. M. Luheshi, E. Hellstrand, D. A. White, L. Rajah, D. E. Otzen, M. Vendruscolo, C. M. Dobson, T. P. Knowles, *Proceedings of the National Academy of Sciences of the United States of America* **2013**, *110*, 9758-9763; cT. P. Knowles, C. A. Waudby, G. L. Devlin, S. I. Cohen, A. Aguzzi, M. Vendruscolo, E. M. Terentjev, M. E. Welland, C. M. Dobson, *Science* **2009**, *326*, 1533-1537.

[7]   a*Alzheimer's & dementia : the journal of the Alzheimer's Association* **2016**, *12*, 459-509; bC. Reitz, R. Mayeux, *Biochemical pharmacology* **2014**, *88*, 640-651.

[8]   K. Blennow, M. J. de Leon, H. Zetterberg, *Lancet (London, England)* **2006**, *368*, 387-403.

[9]   C. Ballard, S. Gauthier, A. Corbett, C. Brayne, D. Aarsland, E. Jones, *Lancet (London, England)* **2011**, *377*, 1019-1031.

[10]   J. Raber, Y. Huang, J. W. Ashford, *Neurobiology of aging* **2004**, *25*, 641-650.

[11]   L. A. Farrer, L. A. Cupples, J. L. Haines, B. Hyman, W. A. Kukull, R. Mayeux, R. H. Myers, M. A. Pericak-Vance, N. Risch, C. M. van Duijn, *Jama* **1997**, *278*, 1349-1356.

[12]   P. Tiraboschi, L. A. Hansen, L. J. Thal, J. Corey-Bloom, *Neurology* **2004**, *62*, 1984-1989.

[13]   F. Hernandez, J. Avila, *Cellular and molecular life sciences : CMLS* **2007**, *64*, 2219-2233.

[14]   K. Iqbal, C. Alonso Adel, S. Chen, M. O. Chohan, E. El-Akkad, C. X. Gong, S. Khatoon, B. Li, F. Liu, A. Rahman, H. Tanimukai, I. Grundke-Iqbal, *Biochimica et biophysica acta* **2005**, *1739*, 198-210.

[15]   aG. G. Glenner, C. W. Wong, *Biochemical and biophysical research communications* **1984**, *120*, 885-890; bJ. Kang, H. G. Lemaire, A. Unterbeck, J. M. Salbaum, C. L. Masters, K. H. Grzeschik, G. Multhaup, K. Beyreuther, B. Muller-Hill, *Nature* **1987**, *325*, 733-736; cC. L. Masters, G. Simms, N. A. Weinman, G. Multhaup, B. L. McDonald, K. Beyreuther, *Proceedings of the National Academy of Sciences of the United States of America* **1985**, *82*, 4245-4249.

[16]   R. G. Canter, J. Penney, L.-H. Tsai, *Nature* **2016**, *539*, 187-196.

[17]   H. S. Nhan, K. Chiang, E. H. Koo, *Acta neuropathologica* **2015**, *129*, 1-19.

[18]   S. Lammich, E. Kojro, R. Postina, S. Gilbert, R. Pfeiffer, M. Jasionowski, C. Haass, F. Fahrenholz, *Proceedings of the National Academy of Sciences of the United States of America* **1999**, *96*, 3922-3927.

[19]   R. G. Canter, J. Penney, L. H. Tsai, *Nature* **2016**, *539*, 187-196.

[20]   M. M. Murray, S. L. Bernstein, V. Nyugen, M. M. Condron, D. B. Teplow, M. T. Bowers, *Journal of the American Chemical Society* **2009**, *131*, 6316-6317.

[21]   B. De Strooper, E. Karran, *Cell* **2016**, *164*, 603-615.

[22]   aE. Abramov, I. Dolev, H. Fogel, G. D. Ciccotosto, E. Ruff, I. Slutsky, *Nature neuroscience* **2009**, *12*, 1567-1576; bJ. J. Dougherty, J. Wu, R. A. Nichols, *The Journal of neuroscience : the official journal of the Society for Neuroscience* **2003**, *23*, 6740-6747.

[23]   D. M. Walsh, I. Klyubin, J. V. Fadeeva, W. K. Cullen, R. Anwyl, M. S. Wolfe, M. J. Rowan, D. J. Selkoe, *Nature* **2002**, *416*, 535-539.

[24]   W. Wei, L. N. Nguyen, H. W. Kessels, H. Hagiwara, S. Sisodia, R. Malinow, *Nature neuroscience* **2010**, *13*, 190-196.

[25]   L. Verret, E. O. Mann, G. B. Hang, A. M. Barth, I. Cobos, K. Ho, N. Devidze, E. Masliah, A. C. Kreitzer, I. Mody, L. Mucke, J. J. Palop, *Cell* **2012**, *149*, 708-721.

[26]   R. Kayed, C. A. Lasagna-Reeves, *Journal of Alzheimer's disease : JAD* **2013**, *33 Suppl 1*, S67-78.

[27]   A. T. Petkova, Y. Ishii, J. J. Balbach, O. N. Antzutkin, R. D. Leapman, F. Delaglio, R. Tycko, *Proceedings of the National Academy of Sciences of the United States of America* **2002**, *99*, 16742-16747.

[28]   aI. Bertini, L. Gonnelli, C. Luchinat, J. Mao, A. Nesi, *Journal of the American Chemical Society* **2011**, *133*, 16013-16022; bA. K. Paravastu, R. D. Leapman, W. M. Yau, R. Tycko, *Proceedings of the National Academy of Sciences of the United States of America* **2008**, *105*, 18349-18354; cA. T. Petkova, W. M. Yau, R. Tycko, *Biochemistry* **2006**, *45*, 498-512.

[29]   T. Luhrs, C. Ritter, M. Adrian, D. Riek-Loher, B. Bohrmann, H. Dobeli, D. Schubert, R. Riek, *Proceedings of the National Academy of Sciences of the United States of America* **2005**, *102*, 17342-17347.

[30] Y. Xiao, B. Ma, D. McElheny, S. Parthasarathy, F. Long, M. Hoshi, R. Nussinov, Y. Ishii, *Nature structural & molecular biology* **2015**, *22*, 499-505.

[31] J. Cummings, P. S. Aisen, B. DuBois, L. Frolich, C. R. Jack, Jr., R. W. Jones, J. C. Morris, J. Raskin, S. A. Dowsett, P. Scheltens, *Alzheimer's research & therapy* **2016**, *8*, 39.

[32] aE. Angelopoulou, C. Piperi, *Annals of Translational Medicine* **2018**, *6*; bT. Hard, C. Lendel, *J Mol Biol* **2012**, *421*, 441-465; cK. L. Sciarretta, D. J. Gordon, S. C. Meredith, *Methods in enzymology* **2006**, *413*, 273-312.

[33] L. O. Tjernberg, J. Naslund, F. Lindqvist, J. Johansson, A. R. Karlstrom, J. Thyberg, L. Terenius, C. Nordstedt, *The Journal of biological chemistry* **1996**, *271*, 8545-8548.

[34] aD. J. Gordon, K. L. Sciarretta, S. C. Meredith, *Biochemistry* **2001**, *40*, 8237-8245; bD. J. Gordon, R. Tappe, S. C. Meredith, *The journal of peptide research : official journal of the American Peptide Society* **2002**, *60*, 37-55; cD. J. Gordon, S. C. Meredith, *Biochemistry* **2003**, *42*, 475-485.

[35] Z. Datki, R. Papp, D. Zadori, K. Soos, L. Fulop, A. Juhasz, G. Laskay, C. Hetenyi, E. Mihalik, M. Zarandi, B. Penke, *Neurobiology of disease* **2004**, *17*, 507-515.

[36] V. Minicozzi, R. Chiaraluce, V. Consalvi, C. Giordano, C. Narcisi, P. Punzi, G. C. Rossi, S. Morante, *The Journal of biological chemistry* **2014**, *289*, 11242-11252.

[37] N. Kokkoni, K. Stott, H. Amijee, J. M. Mason, A. J. Doig, *Biochemistry* **2006**, *45*, 9906-9918.

[38] A. Kapurniotu, A. Schmauder, K. Tenidis, *J Mol Biol* **2002**, *315*, 339-350.

[39] M. Cruz, J. M. Tusell, D. Grillo-Bosch, F. Albericio, J. Serratosa, F. Rabanal, E. Giralt, *The journal of peptide research : official journal of the American Peptide Society* **2004**, *63*, 324-328.

[40] D. Grillo-Bosch, N. Carulla, M. Cruz, L. Sanchez, R. Pujol-Pina, S. Madurga, F. Rabanal, E. Giralt, *ChemMedChem* **2009**, *4*, 1488-1494.

[41] M. A. Findeis, *Current topics in medicinal chemistry* **2002**, *2*, 417-423.

[42] W. Hoyer, C. Gronwall, A. Jonsson, S. Stahl, T. Hard, *Proceedings of the National Academy of Sciences of the United States of America* **2008**, *105*, 5099-5104.

[43] H. Shaykhalishahi, A. Gauhar, M. M. Wordehoff, C. S. Gruning, A. N. Klein, O. Bannach, M. Stoldt, D. Willbold, T. Hard, W. Hoyer, *Angewandte Chemie (International ed. in English)* **2015**, *54*, 8837-8840.

[44] aP. N. Cheng, C. Liu, M. Zhao, D. Eisenberg, J. S. Nowick, *Nature chemistry* **2012**, *4*, 927-933; bJ. Zheng, A. M. Baghkhanian, J. S. Nowick, *Journal of the American Chemical Society* **2013**, *135*, 6846-6852; cC. Liu, M. Zhao, L. Jiang, P. N. Cheng, J. Park, M. R. Sawaya, A. Pensalfini, D. Gou, A. J. Berk, C. G. Glabe, J. Nowick, D. Eisenberg, *Proceedings of the National Academy of Sciences of the United States of America* **2012**, *109*, 20913-20918.

[45] T. Arai, T. Araya, D. Sasaki, A. Taniguchi, T. Sato, Y. Sohma, M. Kanai, *Angewandte Chemie (International ed. in English)* **2014**, *53*, 8236-8239.

[46] T. Arai, D. Sasaki, T. Araya, T. Sato, Y. Sohma, M. Kanai, *Chembiochem : a European journal of chemical biology* **2014**, *15*, 2577-2583.

[47] G. Yamin, P. Ruchala, D. B. Teplow, *Biochemistry* **2009**, *48*, 11329-11331.

[48] M. Richman, S. Wilk, M. Chemerovski, S. K. Warmlander, A. Wahlstrom, A. Graslund, S. Rahimipour, *Journal of the American Chemical Society* **2013**, *135*, 3474-3484.

[49] A. Kapurniotu, A. Buck, M. Weber, A. Schmauder, T. Hirsch, J. Bernhagen, M. Tatarek-Nossol, *Chemistry & biology* **2003**, *10*, 149-159.

[50] aM. D. Griffin, L. Yeung, A. Hung, N. Todorova, Y. F. Mok, J. A. Karas, P. R. Gooley, I. Yarovsky, G. J. Howlett, *J Mol Biol* **2012**, *416*, 642-655; bN. Todorova, L. Yeung, A. Hung, I. Yarovsky, *PloS one* **2013**, *8*, e57437.

[51] P. Y. Cho, G. Joshi, J. A. Johnson, R. M. Murphy, *ACS chemical neuroscience* **2014**, *5*, 542-551.

[52] P. Y. Cho, G. Joshi, M. D. Boersma, J. A. Johnson, R. M. Murphy, *ACS chemical neuroscience* **2015**, *6*, 778-789.

[53] X. Lu, C. R. Brickson, R. M. Murphy, *ACS chemical neuroscience* **2016**, *7*, 1264-1274.

[54] G. Roglic, *Diabetes Research and Clinical Practice* **2015**, *108*, 367-368.

[55] C. Herder, M. Roden, *European journal of clinical investigation* **2011**, *41*, 679-692.

[56] K. J. Chang-Chen, R. Mullur, E. Bernal-Mizrachi, *Reviews in endocrine & metabolic disorders* **2008**, *9*, 329-343.

[57] P. Sonksen, J. Sonksen, *British journal of anaesthesia* **2000**, *85*, 69-79.

[58] aA. Abedini, A. M. Schmidt, *FEBS letters* **2013**, *587*, 1119-1127; bJ. N. Fawver, Y. Ghiwot, C. Koola, W. Carrera, J. Rodriguez-Rivera, C. Hernandez, K. T. Dineley, Y. Kong, J. Li, J. Jhamandas, G. Perry, I. V. Murray, *Current Alzheimer research* **2014**, *11*, 928-940; cP. Westermark, A. Andersson, G. T. Westermark, *Physiological reviews* **2011**, *91*, 795-826.

[59] R. Akter, P. Cao, H. Noor, Z. Ridgway, L. H. Tu, H. Wang, A. G. Wong, X. Zhang, A. Abedini, A. M. Schmidt, D. P. Raleigh, *Journal of diabetes research* **2016**, *2016*, 2798269.

[60]   S. Mosselman, J. W. Hoppener, C. J. Lips, H. S. Jansz, *FEBS letters* **1989**, *247*, 154-158.

[61]   P. Cao, A. Abedini, D. P. Raleigh, *Current opinion in structural biology* **2013**, *23*, 82-89.

[62]   L. Marzban, G. Trigo-Gonzalez, X. Zhu, C. J. Rhodes, P. A. Halban, D. F. Steiner, C. B. Verchere, *Diabetes* **2004**, *53*, 141-148.

[63]   A. V. Kajava, U. Aebi, A. C. Steven, *J Mol Biol* **2005**, *348*, 247-252.

[64]   C. Goldsbury, K. Goldie, J. Pellaud, J. Seelig, P. Frey, S. A. Muller, J. Kistler, G. J. Cooper, U. Aebi, *Journal of structural biology* **2000**, *130*, 352-362.

[65]   aM. R. Nilsson, D. P. Raleigh, *J Mol Biol* **1999**, *294*, 1375-1385; bP. Westermark, U. Engstrom, K. H. Johnson, G. T. Westermark, C. Betsholtz, *Proceedings of the National Academy of Sciences of the United States of America* **1990**, *87*, 5036-5040.

[66]   J. J. Wiltzius, S. A. Sievers, M. R. Sawaya, D. Cascio, D. Popov, C. Riekel, D. Eisenberg, *Protein science : a publication of the Protein Society* **2008**, *17*, 1467-1474.

[67]   K. Tenidis, M. Waldner, J. Bernhagen, W. Fischle, M. Bergmann, M. Weber, M. L. Merkle, W. Voelter, H. Brunner, A. Kapurniotu, *J Mol Biol* **2000**, *295*, 1055-1071.

[68]   L. M. Yan, M. Tatarek-Nossol, A. Velkova, A. Kazantzis, A. Kapurniotu, *Proceedings of the National Academy of Sciences of the United States of America* **2006**, *103*, 2046-2051.

[69]   J. M. Griffiths, T. T. Ashburn, M. Auger, P. R. Costa, R. G. Griffin, P. T. Lansbury, *Journal of the American Chemical Society* **1995**, *117*, 3539-3546.

[70]   L. M. Yan, A. Velkova, M. Tatarek-Nossol, E. Andreetto, A. Kapurniotu, *Angewandte Chemie (International ed. in English)* **2007**, *46*, 1246-1252.

[71]   aJ. Brange, L. Langkjoer, *Pharmaceutical biotechnology* **1993**, *5*, 315-350; bA. Velkova, M. Tatarek-Nossol, E. Andreetto, A. Kapurniotu, *Angewandte Chemie (International ed. in English)* **2008**, *47*, 7114-7118.

[72]   L. M. Yan, A. Velkova, M. Tatarek-Nossol, G. Rammes, A. Sibaev, E. Andreetto, M. Kracklauer, M. Bakou, E. Malideli, B. Goke, J. Schirra, M. Storr, A. Kapurniotu, *Angewandte Chemie (International ed. in English)* **2013**, *52*, 10378-10383.

[73]   E. A. Mirecka, S. Feuerstein, L. Gremer, G. F. Schroder, M. Stoldt, D. Willbold, W. Hoyer, *Scientific reports* **2016**, *6*, 33474.

[74]   K. N. Huggins, M. Bisaglia, L. Bubacco, M. Tatarek-Nossol, A. Kapurniotu, N. H. Andersen, *Biochemistry* **2011**, *50*, 8202-8212.

[75]   K. Sivanesam, I. Shu, K. N. Huggins, M. Tatarek-Nossol, A. Kapurniotu, N. H. Andersen, *FEBS letters* **2016**, *590*, 2575-2583.

[76]   D. F. Kruger, M. A. Gloster, *Drugs* **2004**, *64*, 1419-1432.

[77]   P. Cao, F. Meng, A. Abedini, D. P. Raleigh, *Biochemistry* **2010**, *49*, 872-881.

[78]   H. Wang, Z. Ridgway, P. Cao, B. Ruzsicska, D. P. Raleigh, *Biochemistry* **2015**, *54*, 6704-6711.

[79]   aK. Gudala, D. Bansal, F. Schifano, A. Bhansali, *Journal of diabetes investigation* **2013**, *4*, 640-650; bG. J. Biessels, S. Staekenborg, E. Brunner, C. Brayne, P. Scheltens, *The Lancet. Neurology* **2006**, *5*, 64-74.

[80]   aJ. A. Luchsinger, M. X. Tang, S. Shea, R. Mayeux, *Neurology* **2004**, *63*, 1187-1192; bW. Q. Qiu, M. F. Folstein, *Neurobiology of aging* **2006**, *27*, 190-198.

[81]   A. R. Cole, A. Astell, C. Green, C. Sutherland, *Neuroscience and biobehavioral reviews* **2007**, *31*, 1046-1063.

[82]   R. A. Shiurba, K. Ishiguro, M. Takahashi, K. Sato, E. T. Spooner, M. Mercken, R. Yoshida, T. R. Wheelock, H. Yanagawa, K. Imahori, R. A. Nixon, *Brain research* **1996**, *737*, 119-132.

[83]   J. J. Lucas, F. Hernandez, P. Gomez-Ramos, M. A. Moran, R. Hen, J. Avila, *The EMBO journal* **2001**, *20*, 27-39.

[84]   W. Noble, E. Planel, C. Zehr, V. Olm, J. Meyerson, F. Suleman, K. Gaynor, L. Wang, J. LaFrancois, B. Feinstein, M. Burns, P. Krishnamurthy, Y. Wen, R. Bhat, J. Lewis, D. Dickson, K. Duff, *Proceedings of the National Academy of Sciences of the United States of America* **2005**, *102*, 6990-6995.

[85]   V. N. Uversky, A. L. Fink, *Biochimica et biophysica acta* **2004**, *1698*, 131-153.

[86]   aM. Zhang, R. Hu, H. Chen, Y. Chang, J. Ma, G. Liang, J. Mi, Y. Wang, J. Zheng, *Physical chemistry chemical physics : PCCP* **2015**, *17*, 23245-23256; bE. Andreetto, L. M. Yan, M. Tatarek-Nossol, A. Velkova, R. Frank, A. Kapurniotu, *Angewandte Chemie (International ed. in English)* **2010**, *49*, 3081-3085.

[87]   E. Andreetto, E. Malideli, L. M. Yan, M. Kracklauer, K. Farbiarz, M. Tatarek-Nossol, G. Rammes, E. Prade, T. Neumuller, A. Caporale, A. Spanopoulou, M. Bakou, B. Reif, A. Kapurniotu, *Angewandte Chemie (International ed. in English)* **2015**, *54*, 13095-13100.

[88]   M. Bakou, K. Hille, M. Kracklauer, A. Spanopoulou, C. V. Frost, E. Malideli, L. M. Yan, A. Caporale, M. Zacharias, A. Kapurniotu, *The Journal of biological chemistry* **2017**.

[89]   G. Alberti, P. Zimmet, J. Shaw, Z. Bloomgarden, F. Kaufman, M. Silink, *The International Diabetes Federation Consensus Workshop* **2004**, *27*, 1798-1811.

[90]   D. Cheng, *Nutrition & metabolism* **2005**, *2*, 29.

[91]   I. Zundorf, T. Dingermann, *Pharmazie in unserer Zeit* **2001**, *30*, 27-32.

[92]   J. Brange, A. Volund, *Advanced drug delivery reviews* **1999**, *35*, 307-335.

[93]   M. B. Davidson, *Diabetologia* **1982**, *22*, 494-495.

[94]   aE. Y. Chi, S. Krishnan, T. W. Randolph, J. F. Carpenter, *Pharmaceutical research* **2003**, *20*, 1325-1336; bJ. Owens, *Drug discovery today* **2002**, *7*, 8-9.

[95]   M. A. Weiss, *The Journal of biological chemistry* **2009**, *284*, 19159-19163.

[96]   M. Correia, M. T. Neves-Petersen, P. B. Jeppesen, S. Gregersen, S. B. Petersen, *PloS one* **2012**, *7*.

[97]   X. Chang, A. M. Jorgensen, P. Bardrum, J. J. Led, *Biochemistry* **1997**, *36*, 9409-9422.

[98]   N. B. Phillips, Z. L. Wan, L. Whittaker, S. Q. Hu, K. Huang, Q. X. Hua, J. Whittaker, F. Ismail-Beigi, M. A. Weiss, *The Journal of biological chemistry* **2010**, *285*, 11755-11759.

[99]   M. J. Burke, M. A. Rougvie, *Biochemistry* **1972**, *11*, 2435-2439.

[100]   F. E. Dische, C. Wernstedt, G. T. Westermark, P. Westermark, M. B. Pepys, J. A. Rennie, S. G. Gilbey, P. J. Watkins, *Diabetologia* **1988**, *31*, 158-161.

[101]   aM. I. Ivanova, S. A. Sievers, M. R. Sawaya, J. S. Wall, D. Eisenberg, *Proceedings of the National Academy of Sciences of the United States of America* **2009**, *106*, 18990-18995; bS. Tzotzos, A. J. Doig, *Protein science : a publication of the Protein Society* **2010**, *19*, 327-348.

[102]   J. L. Jiménez, E. J. Nettleton, M. Bouchard, C. V. Robinson, C. M. Dobson, H. R. Saibil, *Proceedings of the National Academy of Sciences* **2002**, *99*, 9196.

[103]   A. Arora, C. Ha, C. B. Park, *FEBS letters* **2004**, *564*, 121-125.

[104]   T. J. Gibson, R. M. Murphy, *Protein science : a publication of the Protein Society* **2006**, *15*, 1133-1141.

[105]   V. Banerjee, R. K. Kar, A. Datta, K. Parthasarathi, S. Chatterjee, K. P. Das, A. Bhunia, *PloS one* **2013**, *8*, e72318.

[106]   B. N. Ratha, A. Ghosh, J. R. Brender, N. Gayen, H. Ilyas, C. Neeraja, K. P. Das, A. K. Mandal, A. Bhunia, *The Journal of biological chemistry* **2016**, *291*, 23545-23556.

[107]   N. K. Mishra, K. B. Joshi, S. Verma, *Molecular pharmaceutics* **2013**, *10*, 3903-3912.

[108]   N. K. Mishra, R. N. Krishna Deepak, R. Sankararamakrishnan, S. Verma, *The journal of physical chemistry. B* **2015**, *119*, 15395-15406.

[109]   aS. Gilead, H. Wolfenson, E. Gazit, *Angewandte Chemie (International ed. in English)* **2006**, *45*, 6476-6480; bE. T. Jaikaran, M. R. Nilsson, A. Clark, *The Biochemical journal* **2004**, *377*, 709-716; cS. Janciauskiene, S. Eriksson, E. Carlemalm, B. Ahren, *Biochemical and biophysical research communications* **1997**, *236*, 580-585; dJ. L. Larson, A. D. Miranker, *J Mol Biol* **2004**, *335*, 221-231; eP. Westermark, Z. C. Li, G. T. Westermark, A. Leckstrom, D. F. Steiner, *FEBS letters* **1996**, *379*, 203-206.

[110]   A. C. Susa, C. Wu, S. L. Bernstein, N. F. Dupuis, H. Wang, D. P. Raleigh, J. E. Shea, M. T. Bowers, *Journal of the American Chemical Society* **2014**, *136*, 12912-12919.

[111]   D. P. Fairlie, A. Dantas de Araujo, *Biopolymers* **2016**, *106*, 843-852.

[112]   T. Vojkovsky, *Peptide research* **1995**, *8*, 236-237.

[113]   E. Kaiser, R. L. Colescott, C. D. Bossinger, P. I. Cook, *Analytical biochemistry* **1970**, *34*, 595-598.

[114]   Y. Han, F. Albericio, G. Barany, *The Journal of organic chemistry* **1997**, *62*, 4307-4312.

[115]   M. Friedman, *Journal of agricultural and food chemistry* **2004**, *52*, 385-406.

[116]   J. Howl, *Peptide synthesis and applications, Vol. 298*, Springer Science & Business Media, **2005**.

[117]   T. Kimura, T. Fukui, S. Tanaka, K. Akaji, Y. Kiso, *Chemical & pharmaceutical bulletin* **1997**, *45*, 18-26.

[118]   S. Sivaramakrishnan, A. H. Cummings, K. S. Gates, *Bioorganic & medicinal chemistry letters* **2010**, *20*, 444-447.

[119]   aA. Glas, D. Bier, G. Hahne, C. Rademacher, C. Ottmann, T. N. Grossmann, *Angewandte Chemie (International ed. in English)* **2014**, *53*, 2489-2493; bS. H. Joo, *Biomolecules & therapeutics* **2012**, *20*, 19-26; cM. Pelay-Gimeno, A. Glas, O. Koch, T. N. Grossmann, *Angewandte Chemie (International ed. in English)* **2015**, *54*, 8896-8927.

[120]   E. Andreetto, L. M. Yan, A. Caporale, A. Kapurniotu, *Chembiochem : a European journal of chemical biology* **2011**, *12*, 1313-1322.

[121]   B. J. Olson, *Current protocols in pharmacology* **2016**, *73*, A.3a.1-a.3a.32.

[122]   M. Biancalana, S. Koide, *Biochimica et biophysica acta* **2010**, *1804*, 1405-1412.

[123]   T. Mosmann, *Journal of immunological methods* **1983**, *65*, 55-63.

[124]   R. H. Westerink, A. G. Ewing, *Acta physiologica (Oxford, England)* **2008**, *192*, 273-285.

[125] K. Muthusamy, P. I. Arvidsson, P. Govender, H. G. Kruger, G. E. Maguire, T. Govender, *Bioorganic & medicinal chemistry letters* **2010**, *20*, 1360-1362.

[126] A. Kazantzis, M. Waldner, J. W. Taylor, A. Kapurniotu, *European journal of biochemistry* **2002**, *269*, 780-791.

[127] S. M. Kelly, T. J. Jess, N. C. Price, *Biochimica et biophysica acta* **2005**, *1751*, 119-139.

[128] D. J. Craik, D. P. Fairlie, S. Liras, D. Price, *Chemical biology & drug design* **2013**, *81*, 136-147.

[129] aJ. D. Knight, J. A. Williamson, A. D. Miranker, *Protein science : a publication of the Protein Society* **2008**, *17*, 1850-1856; bJ. J. Wiltzius, S. A. Sievers, M. R. Sawaya, D. Eisenberg, *Protein science : a publication of the Protein Society* **2009**, *18*, 1521-1530; cP. Nedumpully-Govindan, F. Ding, *Scientific reports* **2015**, *5*, 8240.

[130] aQ. X. Hua, M. A. Weiss, *The Journal of biological chemistry* **2004**, *279*, 21449-21460; bR. Jansen, W. Dzwolak, R. Winter, *Biophysical Journal* **2005**, *88*, 1344-1353.

[131] A. A. Zompra, A. S. Galanis, O. Werbitzky, F. Albericio, *Future medicinal chemistry* **2009**, *1*, 361-377.

[132] A. Tapeinou, M. T. Matsoukas, C. Simal, T. Tselios, *Biopolymers* **2015**, *104*, 453-461.

[133] aS. E. Northfield, C. K. Wang, C. I. Schroeder, T. Durek, M. W. Kan, J. E. Swedberg, D. J. Craik, *European journal of medicinal chemistry* **2014**, *77*, 248-257; bA. F. Haag, B. Kerscher, S. Dall'Angelo, M. Sani, R. Longhi, M. Baloban, H. M. Wilson, P. Mergaert, M. Zanda, G. P. Ferguson, *The Journal of biological chemistry* **2012**, *287*, 10791-10798.

[134] O. Ovadia, S. Greenberg, J. Chatterjee, B. Laufer, F. Opperer, H. Kessler, C. Gilon, A. Hoffman, *Molecular pharmaceutics* **2011**, *8*, 479-487.

[135] D. Laimou, T. Katsila, J. Matsoukas, A. Schally, K. Gkountelias, G. Liapakis, C. Tamvakopoulos, T. Tselios, *European journal of medicinal chemistry* **2012**, *58*, 237-247.

[136] V. Gaillard, M. Galloux, D. Garcin, J. F. Eleouet, R. Le Goffic, T. Larcher, M. A. Rameix-Welti, A. Boukadiri, J. Heritier, J. M. Segura, E. Baechler, M. Arrell, G. Mottet-Osman, O. Nyanguile, *Antimicrobial agents and chemotherapy* **2017**, *61*.

[137] C. K. Wang, D. J. Craik, *Biopolymers* **2016**, *106*, 901-909.

[138] M. R. Nicolls, *Current Alzheimer research* **2004**, *1*, 47-54.

[139] D. Goyal, S. Shuaib, S. Mann, B. Goyal, *ACS combinatorial science* **2017**, *19*, 55-80.

[140] aS. Gilead, E. Gazit, *Angewandte Chemie (International ed. in English)* **2004**, *43*, 4041-4044; bL. A. Scrocchi, Y. Chen, S. Waschuk, F. Wang, S. Cheung, A. A. Darabie, J. McLaurin, P. E. Fraser, *J Mol Biol* **2002**, *318*, 697-706.

[141] H. Jo, N. Meinhardt, Y. Wu, S. Kulkarni, X. Hu, K. E. Low, P. L. Davies, W. F. DeGrado, D. C. Greenbaum, *Journal of the American Chemical Society* **2012**, *134*, 17704-17713.

[142] V. Celentano, D. Diana, L. De Rosa, A. Romanelli, R. Fattorusso, L. D. D'Andrea, *Chemical Communications* **2012**, *48*, 762-764.

[143] aE. S. Lovelace, C. J. Armishaw, M. L. Colgrave, M. E. Wahlstrom, P. F. Alewood, N. L. Daly, D. J. Craik, *Journal of medicinal chemistry* **2006**, *49*, 6561-6568; bD. Boldbaatar, S. Gunasekera, H. R. El-Seedi, U. Goransson, *Journal of natural products* **2015**, *78*, 2545-2551.

[144] A. Spanopoulou, L. Heidrich, H. R. Chen, C. Frost, D. Hrle, E. Malideli, K. Hille, A. Grammatikopoulos, J. Bernhagen, M. Zacharias, G. Rammes, A. Kapurniotu, *Angewandte Chemie (International ed. in English)* **2018**.

[145] O. V. Maltsev, U. K. Marelli, T. G. Kapp, F. S. Di Leva, S. Di Maro, M. Nieberler, U. Reuning, M. Schwaiger, E. Novellino, L. Marinelli, H. Kessler, *Angewandte Chemie (International ed. in English)* **2016**, *55*, 1535-1539.

[146] A. Muppidi, H. Zhang, F. Curreli, N. Li, A. K. Debnath, Q. Lin, *Bioorganic & medicinal chemistry letters* **2014**, *24*, 1748-1751.

[147] S. Ohnishi, H. Kamikubo, M. Onitsuka, M. Kataoka, D. Shortle, *Journal of the American Chemical Society* **2006**, *128*, 16338-16344.

[148] aC. El Amri, F. Bruston, P. Joanne, C. Lacombe, P. Nicolas, *European biophysics journal : EBJ* **2007**, *36*, 901-909; bJ. K. Kim, S. A. Lee, S. Shin, J. Y. Lee, K. W. Jeong, Y. H. Nan, Y. S. Park, S. Y. Shin, Y. Kim, *Biochimica et biophysica acta* **2010**, *1798*, 1913-1925; cK. K. Morishetti, S. Huang Bde, J. M. Yates, J. Ren, *Journal of the American Society for Mass Spectrometry* **2010**, *21*, 603-614; dB. X. Yan, Y. Q. Sun, *The Journal of biological chemistry* **1997**, *272*, 3190-3194.

[149] A. K. Sato, M. Viswanathan, R. B. Kent, C. R. Wood, *Current opinion in biotechnology* **2006**, *17*, 638-642.

[150] A. F. B. Rader, F. Reichart, M. Weinmuller, H. Kessler, *Bioorganic & medicinal chemistry* **2017**.

[151] D. J. Craik, D. J. Adams, *ACS chemical biology* **2007**, *2*, 457-468.

[152]   aM. Werle, A. Bernkop-Schnurch, *Amino acids* **2006**, *30*, 351-367; bM. Muttenthaler, A. Andersson, A. D. de Araujo, Z. Dekan, R. J. Lewis, P. F. Alewood, *Journal of medicinal chemistry* **2010**, *53*, 8585-8596.

[153]   S. A. Fuchs, R. Berger, L. W. Klomp, T. J. de Koning, *Molecular genetics and metabolism* **2005**, *85*, 168-180.

[154]   aJ. B. Mitchell, J. Smith, *Proteins* **2003**, *50*, 563-571; bR. Prades, B. Oller-Salvia, S. M. Schwarzmaier, J. Selva, M. Moros, M. Balbi, V. Grazu, J. M. de La Fuente, G. Egea, N. Plesnila, M. Teixido, E. Giralt, *Angewandte Chemie (International ed. in English)* **2015**, *54*, 3967-3972; cX. Wei, C. Zhan, Q. Shen, W. Fu, C. Xie, J. Gao, C. Peng, P. Zheng, W. Lu, *Angewandte Chemie (International ed. in English)* **2015**, *54*, 3023-3027.

[155]   J. F. Poduslo, G. L. Curran, A. Kumar, B. Frangione, C. Soto, *Journal of neurobiology* **1999**, *39*, 371-382.

[156]   aW. P. Esler, E. R. Stimson, J. B. Fishman, J. R. Ghilardi, H. V. Vinters, P. W. Mantyh, J. E. Maggio, *Biopolymers* **1999**, *49*, 505-514; bT. Ban, M. Hoshino, S. Takahashi, D. Hamada, K. Hasegawa, H. Naiki, Y. Goto, *J Mol Biol* **2004**, *344*, 757-767.

[157]   L. O. Tjernberg, C. Lilliehook, D. J. Callaway, J. Naslund, S. Hahne, J. Thyberg, L. Terenius, C. Nordstedt, *The Journal of biological chemistry* **1997**, *272*, 12601-12605.

[158]   R. J. Chalifour, R. W. McLaughlin, L. Lavoie, C. Morissette, N. Tremblay, M. Boule, P. Sarazin, D. Stea, D. Lacombe, P. Tremblay, F. Gervais, *The Journal of biological chemistry* **2003**, *278*, 34874-34881.

[159]   H. Amijee, C. Bate, A. Williams, J. Virdee, R. Jeggo, D. Spanswick, D. I. Scopes, J. M. Treherne, S. Mazzitelli, R. Chawner, C. E. Eyers, A. J. Doig, *Biochemistry* **2012**, *51*, 8338-8352.

[160]   aD. J. Craik, Y. Young Shim, U. Goransson, G. P. Moss, N. Tan, P. D. Jadhav, J. Shen, M. J. Reaney, *Biopolymers* **2016**, *106*, 917-924; bE. Melander, C. Eriksson, B. Jansson, U. Goransson, M. Hammarlund-Udenaes, *Biopolymers* **2016**, *106*, 910-916.

[161]   R. Soudy, A. Patel, W. Fu, K. Kaur, D. MacTavish, D. Westaway, R. Davey, J. Zajac, J. Jhamandas, *Alzheimer's & dementia (New York, N. Y.)* **2017**, *3*, 44-56.

[162]   H. Wen, H. Jung, X. Li, *The AAPS journal* **2015**, *17*, 1327-1340.

[163]   aJ. Brange, G. G. Dodson, D. J. Edwards, P. H. Holden, J. L. Whittingham, *Proteins* **1997**, *27*, 507-516; bG. Walsh, *Applied microbiology and biotechnology* **2005**, *67*, 151-159.

[164]   aK. Giger, R. P. Vanam, E. Seyrek, P. L. Dubin, *Biomacromolecules* **2008**, *9*, 2338-2344; bY. Hong, L. Meng, S. Chen, C. W. Leung, L. T. Da, M. Faisal, D. A. Silva, J. Liu, J. W. Lam, X. Huang, B. Z. Tang, *Journal of the American Chemical Society* **2012**, *134*, 1680-1689; cM. M. Varughese, J. Newman, *Journal of biophysics (Hindawi Publishing Corporation : Online)* **2012**, *2012*, 434289.

[165]   S. Grudzielanek, V. Smirnovas, R. Winter, *J Mol Biol* **2006**, *356*, 497-509.

[166]   aR. L. Hull, G. T. Westermark, P. Westermark, S. E. Kahn, *The Journal of clinical endocrinology and metabolism* **2004**, *89*, 3629-3643; bA. Kapurniotu, *Biopolymers* **2001**, *60*, 438-459; cS. J. Wimalawansa, *Critical reviews in neurobiology* **1997**, *11*, 167-239.

[167]   J. Luo, S. K. Warmlander, A. Graslund, J. P. Abrahams, *ACS chemical neuroscience* **2016**, *7*, 269-274.

[168]   M. H. Viet, K. Siposova, Z. Bednarikova, A. Antosova, T. T. Nguyen, Z. Gazova, M. S. Li, *The Journal of Physical Chemistry B* **2015**, *119*, 5145-5155.

[169]   L. Heidrich, Master Thesis, Technische Universität München, **2016**.

[170]   Malideli E., Kapurniotu A., et al, unpublished results.

8.   Curriculum vitae

Personal information

Name: Anna Spanopoulou
Date of birth: 17 November 1987
Place of birth: Patra
Citizenship: Greek

Education

- **3/2013-today: PhD studies,** Wissenschaftszentrum Weihenstephan für Ernährung, Landnutzung und Umwelt, Division of Peptidebiochemistry, Technische Universität München
Title of PhD thesis: 'Synthesis and Study of conformationally constrained peptides as inhibitors of self-assembly' under supervision of Prof. Dr. Kapurniotu
- Co-inventor on a European patent application on the macrocyclic peptides reported in Spanopoulou et al., 2018 manuscript
- **10/2010-7/2012: Master studies,** Pharmacochemistry-Design & Synthesis of Natural Products, Department of Pharmacognosy & Chemistry of Natural Products, University of Patras, Greece, (grade 9.8/10, Excellent)
Title of Master thesis: 'Synthesis of Conotoxins analogues of species Conus consors', under supervision Prof. Dr. Kordopatis, (grade 10/10 Excellent)
- **03-05/2012**, **Erasmus Practical training**: Department of Biochemistry & Organic chemistry, University of Uppsala**,** Sweden
- **LLP Erasmus scholarship Master Project**: 'Design and synthesis of polypeptide conjugates for therapeutically applications', under supervision Prof. Dr. Baltzer
- **9/2005-3/2010 Diploma in Chemistry**, University of Ioannina, Greece, (grade 6.93/10 Very good)
Title of Diploma Thesis: 'Chemotherapeutic actions of Cu complexes', under supervision of Prof. Dr. Hadjikakou, (grade 10/10 Excellent)
- **2002-2005**: 11th Lyceum Patras. Greece, (grade 17.8/20, Very good)
- **1999-2002**: 1st Gymnasium Patras, Greece (grade 18.7 /20, Excellent)
- **1993-1999**: Elementary school, Arsakeia-Tositseia schools Patras, Greece

Freising,…...January 2019
Anna Spanopoulou

9. Acknowledgements

10. Declaration

I, Anna Spanopoulou, declare that I have written this thesis independently, exclusively based on the literature and tools mentioned in the thesis. This document has not previously been submitted for a degree at any other institution than the Technical University of Munich.

Freising, den ....Januar 2019 ....
<div align="center">Unterschrift</div>